

INAUGURAL-DISSERTATION

zur

Erlangung der Doktorwürde

der
Naturwissenschaftlich-Mathematischen Gesamtfakultät
der
Ruprecht-Karls-Universität Heidelberg

vorgelegt von

AUNG MOE, B.Sc., M.Sc.
aus TAUNGDWINGYI, MYANMAR

Heidelberg, 2000

**STRUCTURAL DEVELOPMENT OF A VOLCANIC SEQUENCE
OF THE LAHN AREA DURING THE VARISCAN OROGENY
IN THE RHENOHERCYNIAN BELT (GERMANY)**

Gutachter: Prof. Dr. Heiner Flick
Prof. Dr. Reinhard O. Greiling

Heidelberg, 2000

**This thesis is dedicated to my beloved mother & sister
and to the memory of my father & daughter.**

CONTENTS

CHAPTER 1

Introduction	1
1.1 Location.....	1
1.2 Previous studies	1
1.3 The input of the Variscan orogeny on the study area	3
1.4 Aim of the study	5

CHAPTER 2

Regional setting.....	6
2.1 Tectonic setting.....	6
Variscan tectonic models	8
2.2 Structural setting.....	12
Alpine tectonic effect on the Rheinische Schiefergebirge	13
2.3 The setting of the study area.....	15

CHAPTER 3

Field structural data analysis	16
3.1 Folding.....	16
3.1.1 Regional structures	16
3.1.2 Structural types of small-scale folds.....	19
3.1.3 Discussion	19
3.2 Faulting.....	22
3.2.1 Regional structures	22
3.2.2 Discussion	26
3.3 Jointing.....	26
3.3.1 Regional structures	26
3.3.2 Discussion	26
3.4 Cleavage.....	29
3.4.1 Regional structures	29
3.4.2 Discussion	31
3.5 Lineation.....	31
3.5.1 Regional structures	31
3.5.2 Discussion	33
3.6 Age relationship between the structures	33
3.7 Other structures	35

CHAPTER 4

Strain analysis	37
4.1 Determination of 2-dimensional strain.....	39
4.1.1 R_f/ϕ strain analysis.....	39
4.1.2 Fry strain analysis	41
4.1.3 Strain ellipse (R_f/ϕ) in XZ-section	43
4.2 Determination of 3-dimensional strain	53
4.2.1 Results	53
4.2.2 Strain ratio plot	57
4.2.3 Plotting in Flinn-diagrams	59
4.2.4 Strain intensity.....	62
4.2.5 Strain path in Flinn-diagram.....	64
4.3 Correlation between strain and AMS	68
4.4 Strain-vorticity analysis.....	68
4.5 Discussion.....	71

CHAPTER 5	
Re-analysis of previous investigations	73
5.1 Rhenohercynian basin.....	73
5.2 Central Lahn basin.....	76
5.2.1 Basin structure.....	76
5.2.2 Volcaniturbiditic facies study.....	78
5.2.2.1 Freienfels-Ernsthausen sub-area.....	78
5.2.2.2 Guntersau-Freienfels sub-area	79
5.2.3 Extension model correlation	80
5.2.3.1 Red Sea Type continental extension basin	80
5.2.3.2 Japan Sea Type back-arc continental extension basin	81
5.3 Structural features	82
5.3.1 Joint development model	82
5.3.2 Drag fold model	84
CHAPTER 6	
Orogenic compression	86
6.1 Inversion involved tectonic history	86
6.2 Inversion in the Weilburg area	89
6.2.1 Synthetic half-grabens	91
6.2.2 Antithetic half-grabens	91
6.2.3 Full-graben.....	94
6.3 Discussion.....	97
CHAPTER 7	
Magnetofabric analysis	99
7.1 Magnetic susceptibility.....	99
7.2 Analysis of data.....	103
7.3 Study of AMS	107
7.3.1 AMS applied to regional structures	107
7.3.2 AMS applied to sheet flow lava	107
7.3.3 AMS applied to lapillituff.....	118
7.3.4 AMS applied to mafic dyke	125
7.3.5 AMS applied to pillow lava	131
7.3.6 AMS applied to limestone.....	135
7.3.7 AMS applied to strain	139
7.4 Natural Remanent Magnetization (NRM)	146
CHAPTER 8	
Discussion and conclusions.....	153
REFERENCES	157
APPENDIX (APPENDIX A-C)	
PLATES (PLATE 1-17)	

LIST OF FIGURES

Fig. 1-1. Location map of the study area in the Lahn syncline, <i>Rheinische Schiefergebirge</i> , Germany.....	2
Fig. 1-2. Previous structural studies of the Lahn syncline.....	4
Fig. 2-1. Generalized tectonic evolution model of the Variscan orogen in Central Europe.....	7
Fig. 2-2. Geological map of the <i>Rheinische Schiefergebirge</i> east of the Rhine river (after KÖNIGSWALD & MEYER 1994).....	9
Fig. 2-3. Geological map of the Weilburg area (after KEGEL 1922).....	10
Fig. 2-4. The scope of the tectonic position of the Weilburg area.....	11
Fig. 3-1. Sketch showing the structural profile of the Zeppelinfels near Weilburg (Kirschhofen syncline) with fold development in the Adorf- <i>Plattenkalk</i> and <i>Kalkknotenschiefer</i>	18
Fig. 3-2. Diagrams of minor fold study in the Weilburg area (bedding as great circles).....	20
Fig. 3-3. Relationships between s ₀ , s ₁ and s ₂ on stereoplot, and sketch and photo at the long limb of the NW vergent fold in the Ahausen syncline.....	21
Fig. 3-4. Contour in stereoplots of faults (thrust, normal and reverse) in the Weilburg area.....	23
Fig. 3-5. Fault plane and slickenside striation analysis (A) and corresponding stress field (B) for the Freienfels-Ernsthausen sub-area in the Weilburg area.....	24
Fig. 3-6. Syndepositional faulting and folding in hand specimens (B and C), development in the Freienfels-Ernsthausen sub-area. A: Location map, B: Thrusting with related movement and C: Normal faults overprinted by subsequent inversion.....	25
Fig. 3-7. Relationship between joint-study and regional structures of the Weilburg area.....	27
Fig. 3-8. Pole-contour and rose diagrams of joints of the Weilburg area.....	28
Fig. 3-9. Pole diagrams of s ₁ -cleavage of the Weilburg area.....	30
Fig. 3-10. Linear diagrams of $\delta = s_0/s_1$ (intersection of bedding s ₀ and s ₁ -cleavage) of the Weilburg area.....	32
Fig. 3-11. Stereoplot showing the relation of the thrust and conjugated <i>en-echelon</i> vein array with correlated movement in terms of σ_1 (horizontal compression).....	34
Fig. 3-12. A : Basin and dome refolding in the Lahn syncline, B: 3-dimensional refold pattern referring to the attitudes of axial plane cleavage and s ₂ -cleavage (without scale).....	36
Fig. 4-1. A: Straining of an elliptical marker (after LISLE 1985), B: co-ordinate reference frame in the different stages of deformation (Y-axis parallel to the fold axis), (after MAZZOLI & CARNEMOLLA 1993).....	38
Fig. 4-2. Rf/ ϕ 2-D strain analysis diagrams of the Weilburg area.	
A. Diagram of <i>Kalkknotenschiefer</i> of the Ahausen syncline: measurement on XZ plane at s ₁ -cleavage on long limb of fold.....	44
B. Diagram of <i>Kalkknotenschiefer</i> of the Ahausen syncline: measurement on XZ plane at s ₁ -cleavage on short limb of fold.....	45
C. Diagram of <i>Kalkknotenschiefer</i> of the Ahausen syncline: measurement on XZ plane with s ₂ -cleavage at s ₁ -cleavage on long limb of fold.....	46
D. Diagram of <i>Kalkknotenschiefer</i> of the Ahausen syncline: measurement on XZ plane with s ₂ -cleavage (kink folding) at s ₁ -cleavage on long limb of fold.....	47
E. Diagram of <i>Kalkknotenschiefer</i> of the Kirschhofen syncline: measurement on XZ plane at bedding.....	48
F. Diagram of lapillituff of the Kanapee anticline: measurement on bedding (s ₀) at lineation (L ₁ = intersection lineation), (XY plane at bedding).....	49
G. Diagram of lapillituff of the Freienfels-Ernsthausen sub-area: measurement on XZ plane at s ₁ -cleavage.....	50
H. Diagram of amygdaloidal lava (<i>Mandelstein</i>) of the Freienfels-Ernsthausen sub-area: measurement on XZ plane at s ₁ -cleavage.....	51
Fig. 4-3. Index map for orientation of sections and localities of determined strain ellipsoids. Profiles are referred to road-cut section.....	54
Fig. 4-4. Strain axes orientation in stereoplots (lower hemisphere) for the Weilburg area.....	56
Fig. 4-5. A: Plot of the length of major (X) and minor (Z) axes of the deformed objects, {slope of the line (the best fits the cluster of points) gives the average strain ratio}, B: Plot on the Flinn-diagram (X/Y versus Y/Z) with strain path on k-values.....	58

Fig. 4-6. Comparison of strain ellipsoid formation with different observations of Deformation (A) and conversion of strain axes rotation (B) plotting on the Flinn-diagram (C) with strain path indicated.....	60
Fig. 4-7. Sketch showing the relationship of the strain ellipse with the structures of bedding (A), cleavage (B) and lineation in a fold (C) of the Weilburg area.....	61
Fig. 4-8. Three-axes plot (after OWENS 1974 and HSU 1966), (A), and ϵ_s and its θ angle in isometric three-axes plot diagram (B).....	63
Fig. 4-9. Deformation process for the Weilburg area with corresponding strain path in Flinn-diagram (after FLINN 1962).....	65
Fig. 4-10. Relationship between initial ellipse alignment and their final shapes.....	67
Fig. 4-11. Strain ellipse rotation and corresponding kinematic vorticity number (W_k), (A), W_k development in steady-state flow deformation (B), (after TIKOFF & FOSSEN 1995).....	69
Fig. 4-12. Deformation phases in the Weilburg area according to the strain determination on XZ plane. D2-phase gives two types of strain ellipse.....	70
Fig. 4-13. Strain development in half-graben basins in the Weilburg area, Lahn syncline. A: Location map of half-grabens and section X-Y, B: Strain position in antithetic half-grabens. Strain in lapilli and pillow lavas indicates s1-cleavage plane, thrust plane and strike-slip plane near the boundary between two antithetic half-graben basins.....	71
Fig. 5-1. Model for the Rhenohercynian basin during Silurian to Middle Devonian time. A: Rift development in simple shear Wernicke model, (after WERNICKE 1981 and LISTER et al. 1986), B: Block diagram of the Rhenohercynian basin through Lahn, Dill, Wittgenstein and Ostsauerland areas, C: Synthetic and antithetic half-graben and full-graben depositional basins at the Weilburg area.....	74
Fig. 5-2. Map: position of rift development in the Weilburg area, cross-section (vertically exaggerated): half-graben basin position and volcanic filling during Middle Devonian. This section is restored to a pre-strained length (calculated shortening of the Weilburg area about 52 % by present study).....	77
Fig. 5-3. Facies model of a submarine volcano of the Givetian/Adorfian volcanic episode in the Lahn-Dill area (after FLICK et al. 1990).....	78
Fig. 5-4. Sketch comparing the Rhenohercynian back-arc basin development (present author, compare with Fig. 2-1), (A), and the block diagram of Japan Sea type back-arc margin (after TWISS & MOORES 1993), (B).....	81
Fig. 5-5. Comparison of nomenclature of joints in a NW vergent fold (after RIETSCHEL & STRIBRNY 1979), (A), the structural development of Lahn syncline (after KEGEL 1922), (B), and present joint-study of the Weilburg area (C).....	83
Fig. 5-6. A: A five-layer complex consisting of three relatively competent layers (black) and two relatively incompetent layers (white) sandwiched between two thick slabs of incompetent uniform material which impose a uniform compression upon the multilayer and adjacent material (after RAMBERG 1963), B: Drag folds in a banded incompetent layer sandwiched between competent beds under shear movement (after BILLINGS 1972).....	84
Fig. 6-1. Development of folding with variable strain patterns in different sub-basins with implication to the pre-rift and syn-rift basin position in the Weilburg area. (block diagram based on the geological map Fig. 1C, modified after RIETSCHEL 1966).....	88
Fig. 6-2. Synthetic half-graben basin deformation at the Ahausen syncline by inversion tectonics during Variscan orogenic movement from SE to NW. A: Road-cut level profile (after SCHLEUNIGER 1989), B: Interpretative sub-profile, arrows in the brackets mark the movement during the extensional period.....	90
Fig. 6-3. Accretionary prism type deformation in the antithetic type half-graben of the Guntersau-Freienfels sub-area. A: Profile of the Guntersau-Freienfels sub-area (after BEHNISCH 1988), B: Interpretative accretionary prism of the Guntersau-Freienfels sub-area.....	92
Fig. 6-4. Structural profile of the Zeppelinfeld near Weilburg (Kirschhofen syncline) exhibiting the fold development in the Upper Devonian Adorf- <i>Plattenkalk</i> and <i>Kalkknotenschiefer</i> . A: Profile of the Kirschhofen syncline, B: Interpretation of the full-graben basin of the Kirschhofen syncline.....	95
Fig. 6-5. Sketch showing the style of inversion tectonics with the development of fold style and fault system in the Weilburg area, Lahn syncline, Rhenohercynian zone, from extension (A) to compression period (B).....	96

Fig. 6-6. Structural development of inversion tectonics as revealed along the long profile of the Weilburg area: comparison of the structural characters of the different half-grabens.....	98
Fig. 7-1. Circuit diagram of Kappabridge KLY-2 (after GEOFYZIKA Brno, CZ).....	102
Fig. 7-2. A: Geometry of measurement setting of Anisotropy of Magnetic Susceptibility (AMS), (after JELINEK 1977), B: The AMS ellipsoid (after De WALL 1991).....	104
Fig. 7-3A. Comparison of magnetic lineation (K_1) of AMS (A) and intersection lineation (B) between each sub-area in the Weilburg area.....	108
Fig. 7-3B. Contour in stereoplots of the magnetic foliation of the Weilburg area.....	109
Fig. 7-4. Magnetofabrics (AMS values of K_1 , K_2 , K_3 stereoplot) of the Weilburg area.....	110
Fig. 7-5. L-F diagrams (after FLINN 1962 and KHAN 1962) of dyke, sheet flow lava and lapillituff of the Guntersau-Freienfels basin in the Weilburg area, A: dyke, B: sheet flow lava and lapillituff.....	111
Fig. 7-6. T-P' diagrams (after JELINEK 1981) of dyke, sheet flow lava and lapillituff of the Guntersau-Freienfels sub-area in the Weilburg area, A: dyke, B: sheet flow lava and lapillituff.....	112
Fig. 7-7. Sketch showing the interpretation of flow direction in sheet flow lava and current direction in hydroclastics and epiclastics in the Weilburg area.	113
Fig. 7-8. AMS fabrics distributions of sheet flow lava at Guntersau-Freienfels sub-area, in the Weilburg area. (Profile along the Weital-road by BEHNISCH 1987).....	114
Fig. 7-9. AMS distribution of sheet flow lava and lapillituff at the Freienfels-Ernsthausen sub-area, in the Weilburg area.....	115
Fig. 7-10. K_m vs P' diagrams of dyke (A), sheet flow lava (B) and lapillituff (C) of the Weilburg area.....	116
Fig. 7-11. T vs Samples diagrams of dyke (A), sheet flow lava (B) and lapillituff (C) of the Guntersau-Freienfels sub-area, in the Weilburg area.....	117
Fig. 7-12. AMS stereoplot (lower hemisphere) of lapillituff (hydroclastics and epiclastics) of the Weilburg area. A: Hydroclastic lapillituff of Guntersau-Freienfels sub-area, B: bedding rotation of A, C: Epiclastics lapillituff of Guntersau-Freienfels sub-area, D: bedding rotation of C, E: Hydroclastics and epiclastics of Freienfels-Ernsthausen sub-area and F: bedding rotation of E.....	119
Fig. 7-13. AMS fabrics distribution of lapillituff (hydroclastics and epiclastics) of the Guntersau-Freienfels sub-area in the Weilburg area.	120
Fig. 7-14. Showing high anisotropy degree related to the accretionary prism-type deformation in the local half-graben basin as exemplified in T-P ^I diagrams of lapillituff (A) and sheet flow lava (B) from the Guntersau-Freienfels sub-area.....	121
Fig. 7-15. Different AMS distribution between lapillituff and sheet flow lava exemplified in L-F and T-P ^I diagrams of the Freienfels-Ernsthausen sub-area.....	122
Fig. 7-16. P ^I vs Samples diagram of dyke (A), sheet flow lava (B) and lapillituff (C) of the Guntersau-Freienfels sub-area in the Weilburg area.....	123
Fig. 7-17. Showing high anisotropy degree related to the accretionary prism-type deformation in the local half-graben basin as exemplified in T-P ^I diagrams of lapillituff (A) and sheet flow lava (B) from the Freienfels-Ernsthausen sub-area and the same average anisotropy degree in lapillituff and sheet flow lava.....	124
Fig. 7-18. AMS fabrics of dykes (metabasaltic composition) distribution at the Guntersau-Freienfels sub-area in the Weilburg area.	126
Fig. 7-19. T-P ^I diagrams of dyke (D1), chilled zone (D1.1) and host rock (D1.2) in the Guntersau-Freienfels sub-area in the Weilburg area.....	128
Fig. 7-20. A: Reconstruction of the pattern of dyke system in the Guntersau-Freienfels sub-area (half-graben basin), based on the inclinations (I) of K_1 and K_3 , and field observations, B: Stereoplots of all dykes from the Guntersau-Freienfels sub-area in the Weilburg area.....	129
Fig. 7-21. AMS fabrics distribution in miscellaneous rocks of the Weilburg area.	130
Fig. 7-22. P ^I vs K_m mean AMS diagram of pillow lava of the Weilburg area (diagram: after FULLER 1963 and BORRADAILE & SARVAS 1990). Arrow indicates progressive deformation (after BORRADAILE & HENRY 1997) in the Freienfels-Ernsthausen sub-area.....	132
Fig. 7-23. Spatial distribution of pillow lavas with corresponding AMS fabrics in the Weilburg area.....	133
Fig. 7-24. T-P ^I diagrams of pillow lava of the Weilburg area (A) and exclusively the Freienfels-Ernsthausen sub-area with arrow to high anisotropy (B).....	134

Fig. 7-25. L-F diagrams of pillow lava of the Weilburg area (A) and specifically the Freienfels-Ernsthausen sub-area showing high anisotropy direction (B).	135
Fig. 7-26. P^I vs K_m mean AMS diagrams of dyke (A), sheet flow lava (B) and lapillituff (C) in the Guntersau-Freienfels sub-area in the Weilburg area.....	136
Fig. 7-27. A: Magnetic intensity vs Temperature diagram for the magnetic minerals to determine the Curie temperature in °C by the demagnetization in TRM (Thermal Remanent Magnetization) method. Data from limestone epiclastics near Freienfels in the Weilburg area. B: The AMS fabrics of limestone fragments.....	137
Fig. 7-28. AMS characteristics in L-F, T- P^I and P^I - K_m diagrams of limestone (massive and epiclastic) in the Weilburg area.....	138
Fig. 7-29A. Correlation between AMS and strain in the Weilburg area.....	140
Fig. 7-29B. Correlation between AMS and strain in the Weilburg area.....	141
Fig. 7-30. Diagrams for correlation between AMS and strain by L-F and X/Y vs Y/Z (Flinn diagram), and X-Z (strain ratio) diagrams of the Weilburg area.....	142
Fig. 7-31. Correlation of normalized principal magnetic susceptibilities M_i and logarithmic strain ϵ_i in volcanic rocks from the Weilburg area.....	144
Fig. 7-32. Comparison of the fabric diagrams between pole of s1-cleavage and pole of magnetic foliation (K_3) in each sub-area in the Weilburg area.....	145
Fig. 7-33. Instrumentation diagram of Minispin Magnetometer (after MOLSPIN Newcastle, NE).....	147
Fig. 7-34A. Magnetic intensity vs Temperature diagrams for the magnetic minerals to determine the Curie temperature in °C by the demagnetization in TRM (Thermal Remanent Magnetization) method. Data from lapillituff of the Guntersau-Freienfels sub-area in the Weilburg area.....	148
Fig. 7-34B. Magnetic intensity vs Temperature diagrams for the magnetic minerals to determine the Curie temperature in °C by the demagnetisation in TRM (Thermal Remanent Magnetization) method. Data from sheet flow lava of the Guntersau-Freienfels sub-area in the Weilburg area.....	149
Fig. 7-35A. Magnetic intensity vs Temperature diagrams for the magnetic minerals to determine the Curie temperature in °C by the demagnetization in TRM (Thermal Remanent Magnetization) method. Data from lapillituff of the Freienfels-Ernsthausen sub-area in the Weilburg area.....	150
Fig. 7-35B. Magnetic intensity vs Temperature diagrams for the magnetic minerals to determine the Curie temperature in °C by the demagnetization in TRM (Thermal Remanent Magnetization) method. Data from sheet flow lava of the Freienfels-Ernsthausen sub-area in the Weilburg area.....	151
Fig. 7-36. Mean Magnetic Susceptibility (K_m) and Natural Remanent Magnetization (NRM) vs sample number (locality) in different sub-areas of the Weilburg area.....	152
Fig. 8-1. Sketch showing the mechanism of folding in the <i>Rheinische Schiefergebirge</i> during the Variscan Tectonic movement.....	155

LIST OF TABLES

Table 2-1. Stratigraphic sequence of the Lahn-Dill area in the Upper Palaeozoic (after FLICK et al. 1998).	14
Table 4-1. R_f/ϕ analysis in the different rock types.....	40
Table 4-2. Measured normalised strain ratios on three studied sections through different rock types.....	42
Table. 4-3. Finite strain data from strain markers of <i>Kalkknoten</i> and lapilli. $X>Y>Z$ are the principal axes of the finite strain ellipsoid.	55
Table. 4-4. Strain intensity k , d and ϵ_s (θ) of Weilburg area.	62
Table 7-1. (Volume-) Susceptibility and anisotropy (crystal or grain shape controlled) of the most common metamorphic minerals (after JUCKENACK 1990).....	100
Table 7-2. Finite strain and magnetic susceptibility principal values used in the correlation diagram in Fig. 7-38.....	143

LIST OF PLATES

- Plate 1. Fold development in the Kirschhofen syncline with vertical bedding in *Adorf-Plattenkalk* at the Zeppelinfels, south-eastern part of the syncline.
- Plate 2. Fold development in the Kirschhofen syncline continuation from Plate 1. disharmonic folding from SE to NW direction at the Zeppelinfels.
- Plate 3. The Kirschhofen syncline, continuation of Plate 2., A: Upright fold (SW plunging) in *Kalkknotenschiefer* in the disharmonic fold at the road-cut of the Zeppelinfels. (arrow indicates upright fold axis), B: Twisted fold in sandstone layer intercalating in slate at the road-cut of the Zeppelinfels (Both are looking NE).
- Plate 4. A: Relationship of bedding and s1-cleavage in lapillituff (*Schalstein*) at road-cut between Guntersau and Freienfels (looking NE). B: Pillow lava and s1-cleavage relationship at the road-cut between Freienfels and Weinbach (looking NE).
- Plate 5. Undeformed pillow lava and its typical joint development at the road-cut near the Laimbach junction, Weital road (looking NE).
- Plate 6. s2-cleavage development (kink folding) in lapillituff (*Schalstein*) near Freienfels (looking NE), (arrow indicates s2-cleavage), (A), and in *Kalkknotenschiefer* at the road-cut opposite of Ahausen in the Ahausen syncline (looking SW), (B).
- Plate 7. A: Non-sigmoidal right-stepped shear fracture in sheet flow lava near Freienfels (looking NE). B: Sigmoidal tension gashes in conjugate alignments in sheet flow lava between Freienfels and Weinbach (looking SE), (Both exposures in the Freienfels-Ernsthausen sub-area).
- Plate 8. A: Overthrust fault at Guntersau: Lapillituff (*Schalstein*) thrust over *Adorf-Plattenkalk* at the road-cut section (looking NE). B: Overthrust fault at Freienfels: Lapillituff (*Schalstein*) thrust over reef limestone at the road-cut section (looking NE). Both exposures indicate to thrust front (deformation toe) of a local accretionary wedge with respect to the Guntersau-Freienfels half-graben basin (A) and the Freienfels-Ernsthausen half-graben basin (B).
- Plate 9. Thrust related folding with axial cleavage development at the old railroad-cut between Essershausen and Ernsthausen. Showing a small scale in-sequence thrust model with backlimb and forelimb thrust development. General lithology: lapillituff and ashtuff alternations with intercalated calcareous laminations (after JÄGER 1996).
- Plate 10. *Kalknoten* expose in *Adorf-Plattenkalk* at the Zeppelinfels in the Kirschhofen syncline (looking NE).
- Plate 11. Bedding and s1-cleavage development in *Kalkknotenschiefer* (A) and *Kalkknoten* lying in the s1-cleavage (B) at the road-cut opposite of Ahausen in the Ahausen syncline (looking SW).
- Plate 12. A: Progressive deformation as revealed in *Kalkknotenschiefer* at the road-cut, opposite of Ahausen in the Ahausen syncline (looking SW). B: Deetail of *Kalkknotenschiefer* showing *Kalkknoten*: rotation by simple shear and preferred orientation by progressive simple shear movement (looking SW).
- Plate 13. Individual *Kalkknoten* for strain analysis of *Kalkknotenschiefer* from the Ahausen syncline.
- Plate 14. A: Lapillus as a strain marker embedded in lapillituff at the Guntersau-Freienfels sub-area. B: Individual lapilli for strain analysis of the lapillituff at the Freienfels-Ernsthausen sub-area.
- Plate 15. Metabasaltic conglomerate (JÄGER 1993): epiclastic lapillituff at the road-cut near Edelsberg junction in the Freienfels-Ernsthausen sub-area (looking NE).
- Plate 16. Metabasaltic dyke exposures at the road-cut between Guntersau and Freienfels (A) dyke D5 and (B) dyke D6. Both exposures are looking NE.
- Plate 17. Metabasaltic dyke exposures at the road-cut between Guntersau and Freienfels (A) dyke D8a and (B) dyke D7. Both exposures are looking NE.

ABSTRACT

Structural analysis has been carried out on a sequence of mainly meta-volcanic rocks of Devonian age in the southern Rhenish Massif. The area investigated is situated at Weilburg on the Lahn river, a part of the Lahn synclinorium in the *Rheinische Schiefergebirge*. It belongs to the Rhenish Massif, itself part of the Rhenohercynian zone of the Variscan orogen. The area is occupied by a succession of Middle to Upper Devonian sedimentary and volcanic rocks. This succession continues into the Lower Carboniferous on the edge of the investigated area. It was affected by very low- to low-grade metamorphism during the Variscan orogeny.

The present study focuses on the structural development of these Palaeozoic volcanic rocks using field structural data analysis, strain analysis, magnetofabric analysis (Anisotropy of Magnetic Susceptibility: AMS) and re-analysis of previous investigations on the Lahn syncline area.

The **field structural data analysis** uses bedding, cleavage, lineations, folds, faults, and joints. Stereoplot analyses are interpreted together with the geological map to evaluate the deformation processes. Bedding in volcanics is rare, but common in ashtuff alternations. Small scale (cm-scale) syndepositional structures (fold and fault) are often in this alternation sediments. Bedding and s1-cleavage relationships show a clear NW vergence, in which s1-cleavage is steeper than bedding except for two outcrops. s2-cleavage as well s1-cleavage folding occurs as kinking and buckling. Lineations are not common, however, calculated intersection lineations are dispersed in a form of girdle on stereoplots. Folds plunge to NE as well as to SW. Drag folds developed only in incompetent beds, e.g. ashtuff layers and sedimentary rocks. Faults in terms of thrusts are NW facing boundary thrust and imbricate thrust systems. NW-SE trending cross faults and tension joints are pronounced. NNE-SSW and WNW-ESE trending faults and joints are overprinted as X and Y minor Riedel shear planes suggesting neotectonics. Following the field structural data, three deformation phases (D1 – D3) are marked. Consequently, superposed folding (basin and dome) structure is constructed on the Weilburg area in the Lahn syncline.

The **strain analysis** is carried out using *Kalkknoten* (lime nodules), lapilli and amygdales as strain markers in both, 2-D and 3-D. The 2-D analysis is based on the Rf/ϕ measurement, and 3-D analysis is applied by the direct measurement of the principal finite strain axes. The 2-D analysis used mostly the XZ planes of strain ellipse and plotted Rf/ϕ diagrams. $R_i = 2$ values are exactly the same in all sedimentary rocks, e.g. *Kalkknotenschiefer*. The strain ratio diagram also shows a regionally homogeneous deformation except epiclasts. In the 3-D strain analysis, the long (X) axis of principal finite strain ellipsoid parallels to s1-cleavage as well as to bedding. The strain intensity (\mathcal{E}_s) of sedimentary rocks (0.45 - 0.69) is higher than that of lapillituff (0.24 - 0.34), and k-values also show more flattening in sedimentary rocks. The strain path demonstrate the shapes to become oblate with a volume change, then to prolate and back to oblate by different route which is agreed with the strain intensity. Following the strain analysis, the deformation phases can be divided into D1 - D4 which are well consistent with strain path and field data analysis. Strain partitioning distinguishes in the local basin, e.g. in the antithetic half-graben basin observations of almost undeformed in the rear prism to

highly deformed in the thrust front and later dextral shear strain in a contact zone of neighbouring basins.

Re-analysis of previous investigations used to interpret a simple shear continental extensional basin model for the Rhenohercynian basin, to be compared with the present Japan Sea and Red Sea, and the extensional depositional basin for the Lahn syncline before deformation. The volcanic suite (acidic to basic type volcanism) of the study area suggests partial melting at the detachment fault by a simple shear continental extension of Rhenohercynian zone. By classifying central, proximal and distal facies in the facies study of volcanoclastic rocks, source areas (volcanic centres) has been used to define the inferred flow directions of volcanic rocks. Sheet flow lava moved without folding, but drag folds are developed in incompetent beds which is observed in the multilayers of meta-ashtuff. Joint development is useful to find out for superposed fractures on the study area and the *Rheinische Schiefergebirge*.

Orogenic compression was implied on the study area as a part of continental extension zone during the Variscan orogeny. With it, inversion tectonics can be observed by short-cut thrusts through pre-rift (Lower Devonian), syn-rift (Middle to upper Lower Carboniferous) sequences by reactivation of extensional boundary faults in the synthetic half-grabens, accretionary prism-type deformation with developing imbricate thrusting in the antithetic half-graben basins and a transition (flexural-slip folding) from vertical tight fold with vertical reverse faults in the SE to overturned fold in the NW in the full-graben basin. During orogenic compression, different types of deformation, e.g. folding types (asymmetrical folding, disharmonic folding and thrust related folding) and fault systems (short-cut thrusts, transition of vertical reverse faults to thrusts, imbricate thrusts), affected these different types of graben basins. As a result, in the study area full-graben and half-graben basins can be recognized as a full-graben at the Kirschhofen syncline, antithetic half-grabens at the Guntersau-Freienfels and the Freienfels-Ernsthausen sub-areas and synthetic half-grabens at the Ahausen syncline and the Kanapee anticline.

The **magnetofabric analysis** with respect to AMS is carried out for the different rock types with various data analyses for separate sub-areas. The AMS fabrics is used to interpret the flow direction of sheet flow lavas which agrees with its inferred flow direction; the current direction of turbiditic lapillituff which is parallel along a half-graben basin, and also, the current direction of epiclastic lapillituff which crosses the basin, like debris flows. And T-P¹ diagram (Jelinik-diagram) is used to confirm the accretionary prism-type deformation as anisotropy degree in thrust front is higher than that of rear prism. Furthermore, high-level intrusions recognized as dykes and sills by their inferred emplacement. Pillow lavas are useful for deformation indicator by field and magnetic studies. And inverse fabrics (changes of K₁ and K₃ positions) are very common in limestone. P¹-K_m diagrams manifest the low-grade facies deformation in the study area. L-F and T-P¹ diagrams show the magnetic strain ellipsoids and strain path including deformation phases. T-Samples and P¹-Samples diagrams are useful to compare the degree of deformation in neighbouring rocks. AMS and strain correlation coincides well, especially for K₃ axes to Z axes, except in limestone. However, K₁ and K₂ axes do not correlate regularly to strain axes X and Y. No linear quantitative relationship in the correlation of normalized principal magnetic susceptibility M_i and logarithmic strain ϵ_i , suggests no influence of the

strain deformation on the magnetization. Thermal Remanent Magnetization is carried out for different rock types to get magnetic minerals, e.g. Magnetite, hematite, pyrrhotite. The Natural Remanent Magnetization and Mean susceptibility vs Sample Localities plots exhibit the different group of anomaly, suggested the different sources of volcanics.

Discussion and conclusions: By the present investigation the tectonic movement deduced as northwards, then oroclinal bending in the Rhenish Massif around the SE front of London-Brabant Massif and then the northward movement continued is obliquely superposed on the oroclinal bending. Thus, a dextral shear sense of strain ellipse rotation into the s₁-cleavage (axial plane cleavage) and preferred orientation of strain ellipse in the s₁-cleavage was developed due to dextral transpression, succeeded by dextral transtension in the late orogenic period. Neotectonic faults and joints are observed as superposed fractures by the NW-SE oriented maximum horizontal stress (S_{Hmax}) during Alpine orogeny.

ACKNOWLEDGEMENT

The author is very grateful to Prof. H. Flick and Prof. R. O. Greiling who supervised this work, for their kind encouragement, guidance and aid throughout the study. He is indebted to Frau K. Riedelsberger for her support and continuous encouragement. Thanks are also due to Frau Dr. H. de Wall for teaching theory and practical knowledge of magnetic study. Special thanks are extended to Jens Seeling for his encouragement and sharing of computer knowledge and to Frank Schobel for his enormous help in the magnetic measurements. Appreciation is also extended to his colleagues and the staff of Geology and Palaeontology Institute of Heidelberg University for their help in many ways.

CHAPTER 1
INTRODUCTION

CHAPTER 1

INTRODUCTION

The Lahn area (Lahn syncline) is a part of the Rhenohercynian basin in the Variscan realm that exhibits widespread volcanic sequences. These accompanied clastic and carbonate sedimentation from the onset of late Lower Devonian to middle Lower Carboniferous times reaching a climax during the Middle Devonian (Givetian) in the middle Lahn area. Thus, volcanism was characterized as typical of submarine condition by the volcaniturbiditic rocks and pillow lavas. The present study investigates the structural development of this volcanic sequence specifically at the Weilburg area in the middle Lahn area by using field structural data analysis, strain analysis, re-analysis of previous investigations and magnetofabric analysis (Anisotropy of Magnetic Susceptibility: AMS).

1.1 LOCATION

The study area is situated within the Lahn syncline in the southeast of the *Rheinische Schiefergebirge* in Germany (Fig. 1-1). The Lahn syncline is 65 km long and 35 km wide, trends NE-SW, and is paralleled by the Dill syncline. In the literature on Variscan geology in Central Europe the usage of the terms Lahn-Dill synclines/area (Lahn syncline and Dill syncline) is quite familiar, and these two great synclinal structures are separated by the Hörre zone. The Lahn-Dill area borders the Siegen anticlinorium to the north, the Taunus anticlinorium to the south, and the Hessen depression in the east. The Dill syncline can be continued into the Mosel syncline in the western *Rheinische Schiefergebirge* whereas the Lahn syncline terminates at its south-western rim.

1.2 PREVIOUS STUDIES

Previous geological investigations in the Lahn area go back as far as BECHER (1789) and mostly emphasize general geology, petrology, geochemistry, mineral deposits, stratigraphy and facies studies. Structural studies, however, including structural maps (Fig. 1-2), are comparatively rare.

Important studies on the Lahn area with respect to the present study in chronological order are as follows:

AHLBURG (1918A, B and C) published geological maps (GK 25) of the middle Lahn area which are still more or less valid today, in particular the maps of Weilburg and Weilmünster.

KEGEL (1922) outlined the geology of the whole Lahn syncline area, presenting a geological map and cross sections including the structural zones prepared by the late AHLBURG (Fig. 1-2E).

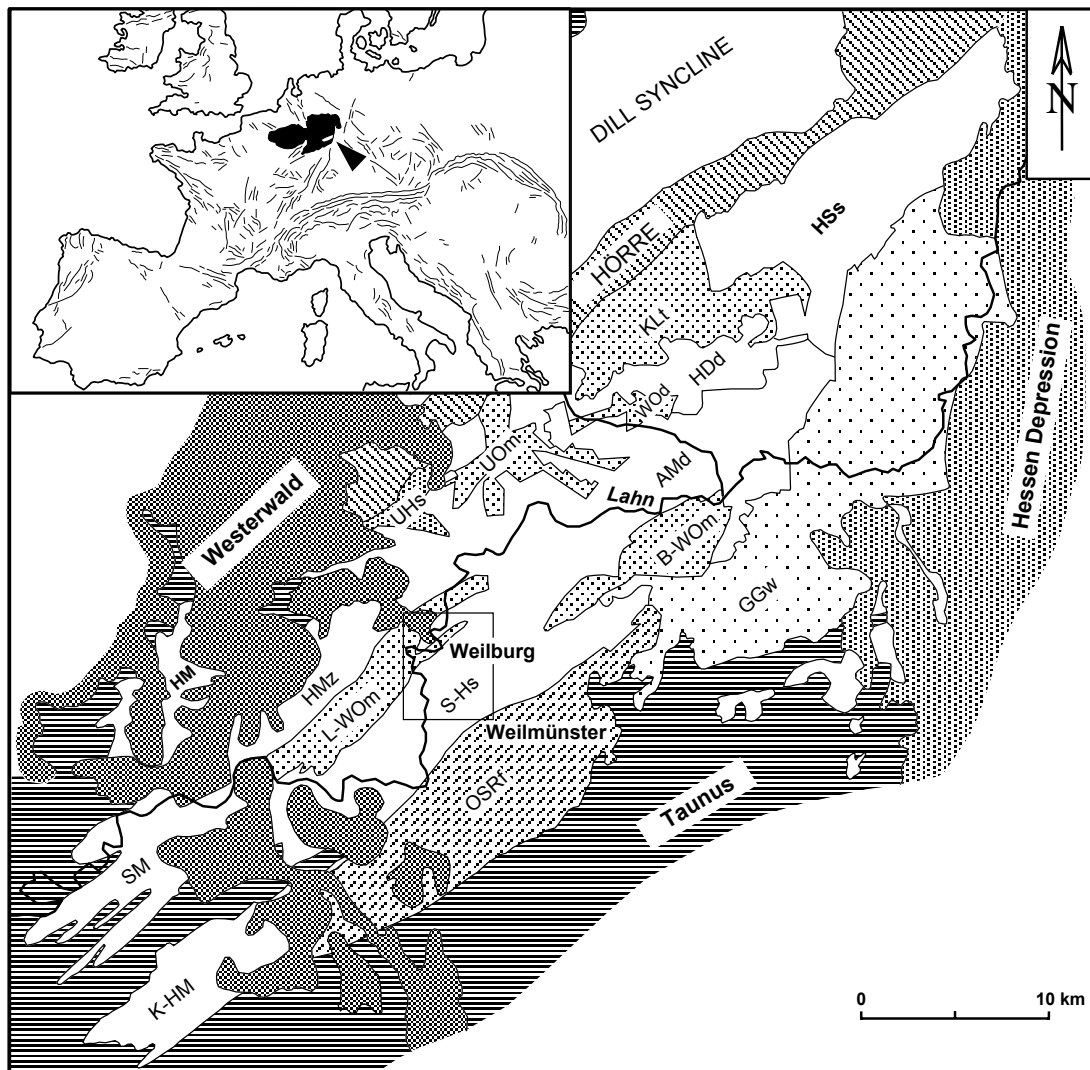


Fig. 1-1. Location map of the study area in the Lahn syncline, *Rheinische Schiefergebirge*, Germany.

K-HM = Katzenelnbogen-Hahnstättener Mulde; SM = Schaumburger Mulde; OSRF = Oberdevon der Südlichen Randfazies; S-Hs = Schalsstein-Hauptsattel; L-WOm = Limburg-Weilburger Oberdevonmulde; HMz = Hadamarer Mitteldevonzug; U-Hs = Unterdevon-Hauptsattel; UOm = Ulmer Oberdevonmulde; WOd = Werdorfer Oberdevondecke; HDd = Hohensolmsener Diabasdecke; GGw = Giessener Grauwacke; B-WOm = Braunfels-Wetzlarer Oberdevonmulde; AMd = Asslarer Mitteldevondecke; KLI = Kulmtafel des Lemptales; Hs = Hessische Schieferserie.
Structural units: according to AHLBURG (see KEGEL 1922), map compiled by NESBOR (1987).

PAULY (1958) investigated the geology of a part of the south-western end of the Lahn syncline and prepared a tectonic map with detailed fold identification. He stated that orogenic and epirogenic movements in the Rhenohercynian occurred at the boundary of Lower to upper Middle Devonian caused by the Brandenburg folding phase.

BENDER (1965) provided a tectonic map of the north-eastern part of the Lahn syncline which demonstrates faulting as boundary thrust as well as folding with their plunge axes to SW and NE (double plunging), (Fig. 1-2A).

RIETSCHEL (1966) studied the stratigraphy and facies of the middle Lahn trough in the *Schalstein-Hauptsattel* (anticline), (defined in KEGEL 1922) providing a tectonic map of the Weilburg area (Fig. 1-2C). He stated tectonic activities in terms of Brandenburg folding and transgression in the upper Middle Devonian.

FLICK (1977) investigated the silicic volcanics (keratophyres and quartz-keratophyres) of the whole Lahn-Dill area and consecutively worked on these in 1978 and 1979. Furthermore, FLICK & NESBOR (1988) summarized the volcanic activities of the Lahn syncline in time and episodes. Also FLICK et al. (1998) upgraded the results and new interpretations of the Lahn- and Dill synclines presenting the stratigraphic sequence as shown in Table 2-1.

NESBOR (1987 and 1988) examined the doleritic spilites of the Lahn area with discussion of regional geology and geotectonic setting using major and trace element chemistry. In addition, he defined the continental intra-plate magmatism in the Lahn area. NESBOR & FLICK (1987A, 1987B and 1988) pointed out the facies development of pyroclastics, thrust tectonics and Devonian intrusions in the Lahn area. NESBOR et al. (1993) worked on an integrated approach to facies and paleogeography of the volcanism during the Devonian time in the Lahn-Dill area.

REQUADT (1990), by making the geological map of Schaumburg in the south-western Lahn syncline for the geological survey of Rheinland-Pfalz came to different conclusions for the structural interpretation of PAULY'S (1958) ideas, (Fig. 1-2D). He deduced that the transgression conglomerate of the Brandenburg folding is obsolete.

BEHNISCH (1993) investigated the depositional processes of Devonian volcanoclastics, and recognized the characteristic of volcanoclastics as turbidites in the *Schalstein-Hauptsattel* (anticline) in the middle Lahn area.

The study area is documented in some detail by M.Sc theses by JÄGER (1996), SCHLEUNIGER (1991) and BEHNISCH (1990) from the Geology and Palaeontology Institute of Heidelberg University.

1.3 THE INPUT OF THE VARISCAN OROGENY ON THE STUDY AREA

The study area is part of the *Rheinische Schiefergebirge* which is itself part of the Rhenohercynian zone according to the classification of KOSSMAT (1927) of the Variscan orogen (Fig. 2-1).

Variscan/Hercynian: Variscan in German literature is a synonym for Hercynian, the latter being used frequently in the English and French literature. Both terms are used to name an orogeny. The term Variscan was introduced by EDUARD SUESS (1888) to describe the mountains between the Ardennes and Vosges in the west and Sudetes in the east.

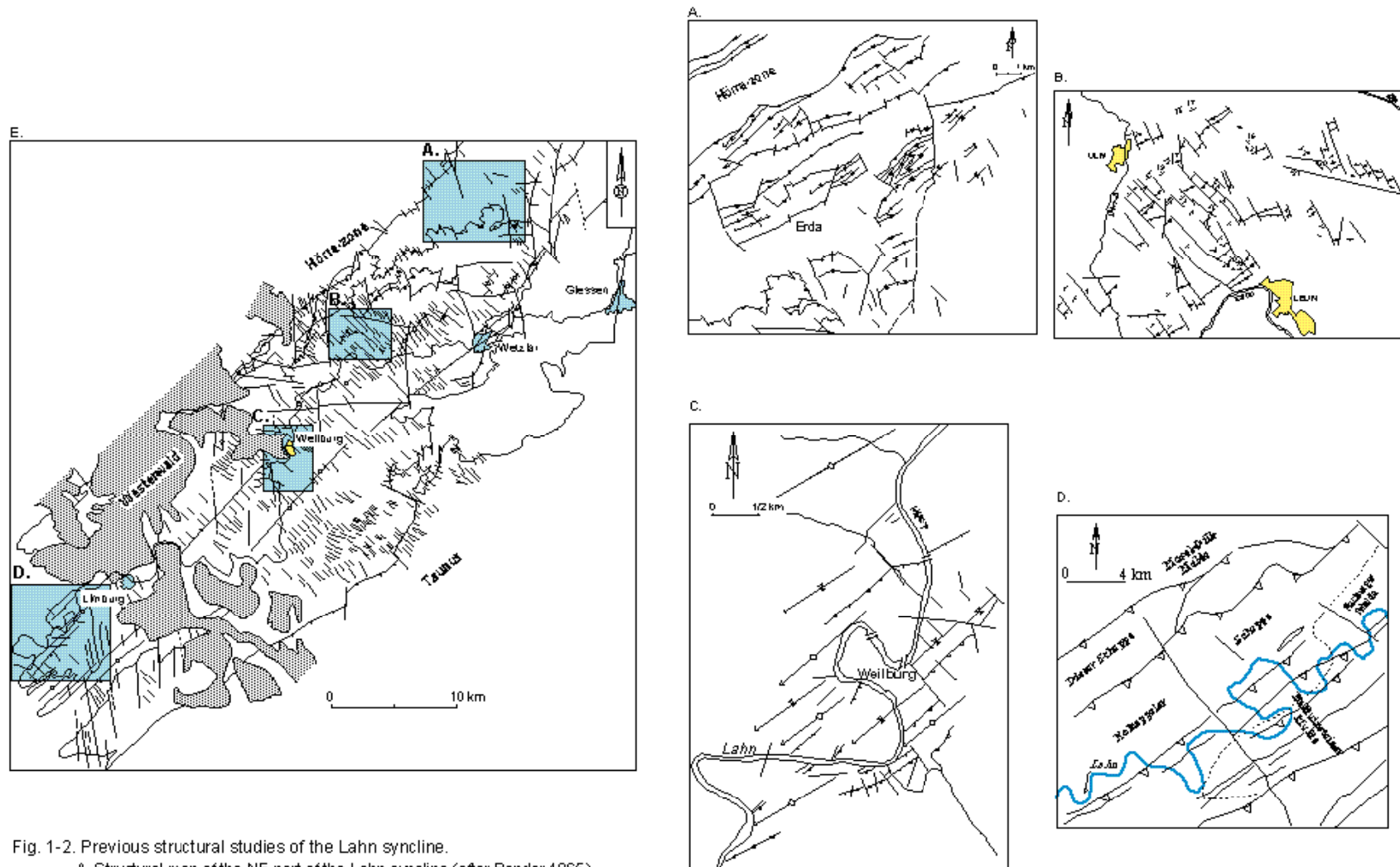


Fig. 1-2. Previous structural studies of the Lahn syncline.

- A. Structural map of the NE part of the Lahn syncline (after Bender 1965)
- B. Structural map of between Ulm and Leun of the Lahn syncline (after Ahlburg 1918A & B)
- C. Structural map of the middle part of the Lahn syncline (after Rietschel 1966)
- D. Structural map of the SW part of the Lahn syncline (after Requardt 1990)
- E. Structural map of the whole Lahn syncline (after Kegel 1922)

A French geologist (1892) working in the Belgian Coalfields, created the term Hercynian. LEOPOLD VON BUCH (1849) had already introduced the term Hercynian with reference to the WNW-ESE tectonic direction running parallel to the northern margin of the Harz mountains in Germany. In this sense, it is still commonly used in German literature. Both terms are equally frequently used in the literature, but Variscan is becoming preferable. HANS STILLE (1924) changed and widened the sense of the term Variscan to encompass the chronology of tectonic events within a late Palaeozoic time span throughout the world. Now it is used to describe the collision of Laurussia with Gondwana during Devonian and Carboniferous times. Following BAILEY (1935), the Variscan orogeny in Europe has been correlated to events in the south and central Appalachians (Alleghenian orogeny). Thus, America and Europe were sites of a single orogenic belt prior to the Mesozoic drift (RAST 1988).

1.4 AIM OF THE STUDY

The present study focuses on the structural development of Palaeozoic volcanic rocks of the Weilburg area in the middle Lahn syncline:

1. Field data analysis: measuring the bedding, cleavage, lineations, folds, faults and joints, in the study area and analyzing them with stereoplots and roseplots to determine the deformation phases during the tectonic episodes.
2. Strain analysis: evaluating the strain deformation (2-D and 3-D) in the *Kalkknoten* (lime nodules) of the *Kalkknotenschiefer* and lapilli of the lapillituff to calculate the deformation in mesoscopic scale in the rocks.
3. Magnetofabric analysis: measuring AMS with a Kappabridge KLY-2, using the ANISO 10 - 14 programs for calculations, for structural interpretations of the deformation and regional reconstruction of its pre-deformation stage.
4. Re-analysis of previous investigations: including the depositional setting by detailed facies analyses in the present study area compiled by a Ph.D. thesis, Heidelberg University, as an indication of the continental extensional tectonics; also interpreting the structural style of profiles in the present study area given in previous M.Sc theses, Heidelberg University, as a form of the inversion tectonics in the study area, part of the Variscan orogen.
5. Final structural development: constructing the development of structures in the study area with reference to the field data, strain analysis data and the re-analysis of previous investigations resulting the deformation from compression tectonics (Variscan tectonic collision).

CHAPTER 2
REGIONAL SETTING

CHAPTER 2

REGIONAL SETTING

The study area is part of the *Rheinische Schiefergebirge* in the Late Palaeozoic Variscan orogenic zone. Bearing this in mind, the regional setting of the area has been approached using tectonic, regional geological and structural viewpoints. Tectonically, the area exemplified continental extension on ensialic crust in a possible back-arc margin environment (see below) and was subsequently deformed by the Variscan orogeny. Regionally, the area as part of the *Rheinische Schiefergebirge* belongs to the Rhenohercynian zone, which developed accretionary tectonics with thrusts and related folding.

2.1 TECTONIC SETTING

Opinions vary as to whether the area (Fig. 1-1) developed a back-arc extensional basin, a view held by SMITH (1996), FLOYD (1995), BERTHELSEN (1992), ZIEGLER (1989), FRANKE (1989B), FLICK & NESBOR (1988), ENGEL et al. (1983), or as a passive continental margin as postulated by ONCKEN et al. (1999), ONCKEN (1997) and FRANKE & ONCKEN (1990). The present study agrees with the interpretation that the Rhenohercynian basin was a back-arc continental extensional basin during the Silurian to the Middle Devonian (see Chapter 5).

The Lahn-Dill area is characterized by clastic and subordinate carbonate sedimentation in a pelagic shelf environment together with widespread bimodal volcanism, which accompanied the extensional tectonics (FLICK et al. 1998, FLICK et al. 1990, FLICK & NESBOR 1988). Volcanic activity occurred during four episodes: (1) Emsian/Eifelian, (2) Givetian/Adorfian, (3) Nehdenian-Wocklumian and (4) Dinantian II, (Table 2-1), (FLICK et al. 1990, FLICK & NESBOR 1988, FLICK et al. 1998). Mafic volcanism is the most widespread with a peak in the Givetian/Adorfian episode (FLICK & NESBOR 1988, PEREKALINA 1981, WALLISER 1981).

Variscan Orogeny: During the Variscan time, the Rheic ocean was situated between Northern Gondwana and a continent comprising Laurussia and Avalonia (OCZLON 1992, LORENZ & NICHOLLS 1984, LORENZ 1976, BURRETT 1972, MCKERROW & ZIEGLER 1971). The closure of this ocean led to the development of the Variscan Orogen in Central and Western Europe. The southward extension of the Rheic, known as the Theic ocean, separated North America and Africa (Gondwana), (HATCHER 1988, RODGERS 1988, RAST & SKEHAN 1983, MCKERROW & ZIEGLER 1971).

The Variscan orogeny was active throughout from South Portugal in the west to Moravia and Silesia in the east during early to Middle Carboniferous time. The Variscan orogen is divided into several zones: the Subvariscan, Rhenohercynian, Saxothuringian and Moldanubian as defined in Central Europe, (Fig. 1-1) according to their sedimentary and tectonic environment (KOSSMAT 1927), but equivalent zones extend throughout the main part of Europe.

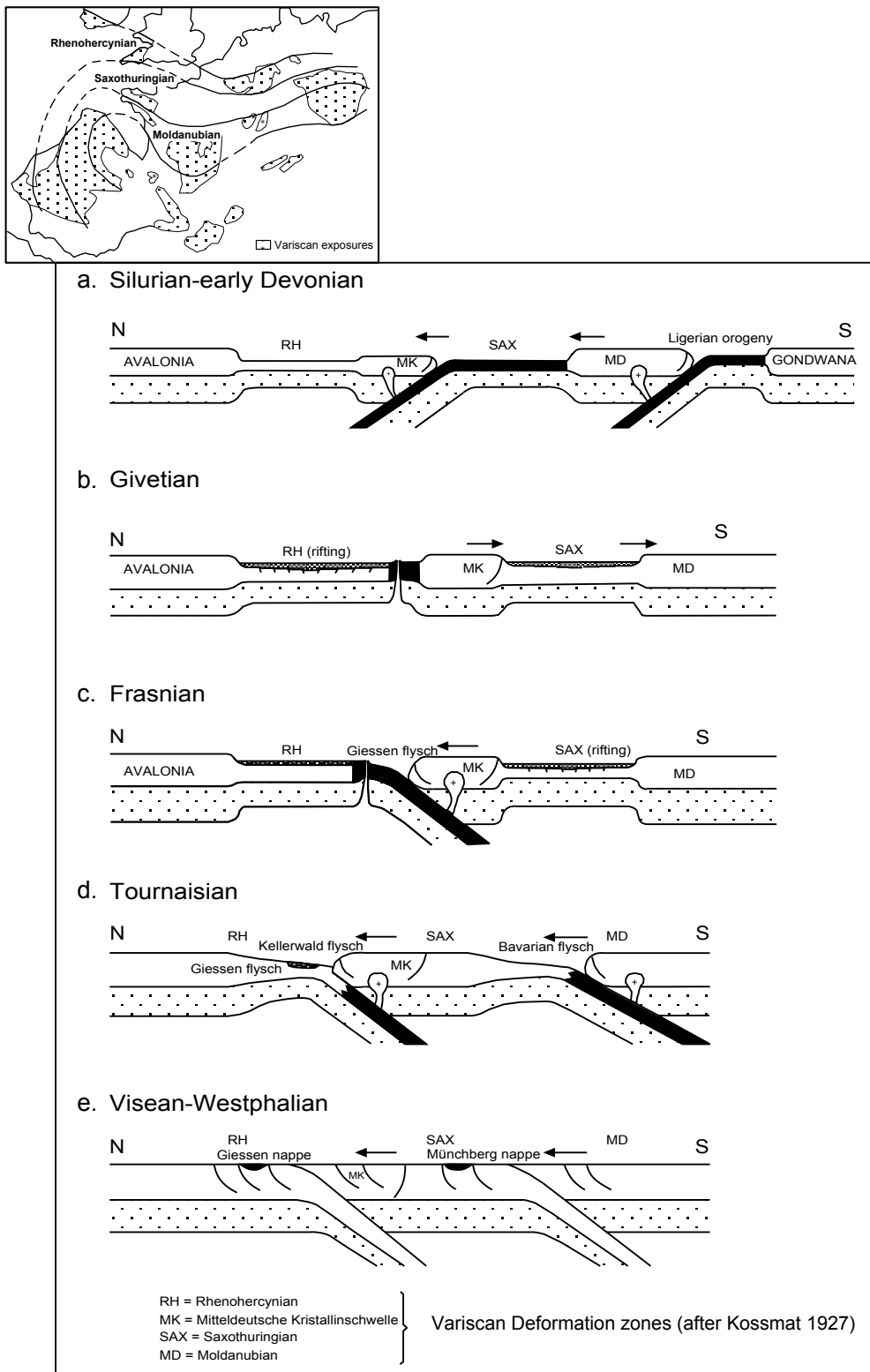


Fig. 2-1. Generalized tectonic evolution model of the Variscan orogen in Central Europe.

white color = continental crust; black = oceanic crust; spotted = subcrustal lithosphere.
 (compiled using models of BERTHELSEN 1992, OCZLON 1992, FRANKE & ONCKEN 1990 and FRANKE 1989B)

The Rhenohercynian zone includes the Rhenish Massif (*Ardennes* and *Rheinische Schiefergebirge*), the Harz Mountains, SW-England and S-Portugal and continues eastwards into the Moravo-Silesian zone. The Saxothuringian zone comprises the *Mitteldeutsche Kristallinschwelle*, Saxony, Thuringia, and the northern part of the Vosges and Schwarzwald. The SW continuation of this zone passes through the central and north Armorican Massif and is inferred to continue to the Ossa-Morena zone in the Iberian Massif using the evidence of type and environment of volcanism (FLOYD 1982). The Moldanubian zone ranges from the Bohemian Massif, across most of Vosges and Schwarzwald, to the Massif Central, the southern Armorican Massif and the central Iberian Massif. By using similarities in tectonic and deformation phases these zones have been correlated across the Atlantic Ocean to the Appalachian regions by RAST (1988, 1983), e.g. Valley and Ridge Province with Rhenohercynian (non-metamorphic extensional zone), Blue Ridge with Saxothuringian (metamorphic external zone), and Piedmont with Moldanubian (internal zone).

Variscan tectonic models (Fig. 2-1):

A. During Silurian and early Devonian in the Caledonian orogenic period the continents of Laurentia and Baltica fused to form Laurussia with Avalonia being accreted as a pericontinental area. In the northern part of Central Europe, a marine shelf still existed in southern Avalonia (OCZLON 1992) enclosing the Rhenohercynian basin. This large-scale shelf (OCZLON 1992, FRANKE 1989B) is perhaps similar to the present Japan Sea tectonic model. For that time, the *Mitteldeutsche Kristallinschwelle* is considered as a continuation of a pericontinental shelf prior to the opening of the Rhenohercynian basin (FRANKE 1989B).

During the Caledonian orogeny, the southern Avalonia margin (BERTHELSEN 1992) developed an active margin and a volcanic island arc (MEISL 1990). On the other side, the northern Gondwana margin was deformed by the Ligerian orogeny (OCZLON 1993), and the shelf area developed into a pericontinental back-arc rift basin which included the Saxothuringian basin (OCZLON 1992, COCKS & FORTEY 1982). During late Silurian, the Rheic ocean widened after the collision of Avalonia and Laurussia. Thus, the area between Laurussia and Gondwana formed a passive environment towards the south (OCZLON 1992, FRANKE 1989B). This is accompanied by intra-continental rifting especially in the Rhenohercynian basin. This may have led to the Giessen Ocean in an environment similar to Red Sea-type rifting (OCZLON 1992, present study) between the Caledonian Massif (Old Red Continent) and the *Mitteldeutsche Kristallinschwelle*.

B. During Middle Devonian, the Rhenohercynian basin was still an extensional environment (LEEDER 1988, FLICK & NESBOR 1988) developing a rift-related volcanism (FLICK & NESBOR 1988, NESBOR 1987). The onset of the ocean spreading centre was beginning in the south (BERTHELSEN 1992, FRANKE & ONCKEN 1990, FRANKE 1989B). In early Upper Devonian, the Rheic ocean comprising the Rhenohercynian and the Saxothuringian oceans was caused to close.

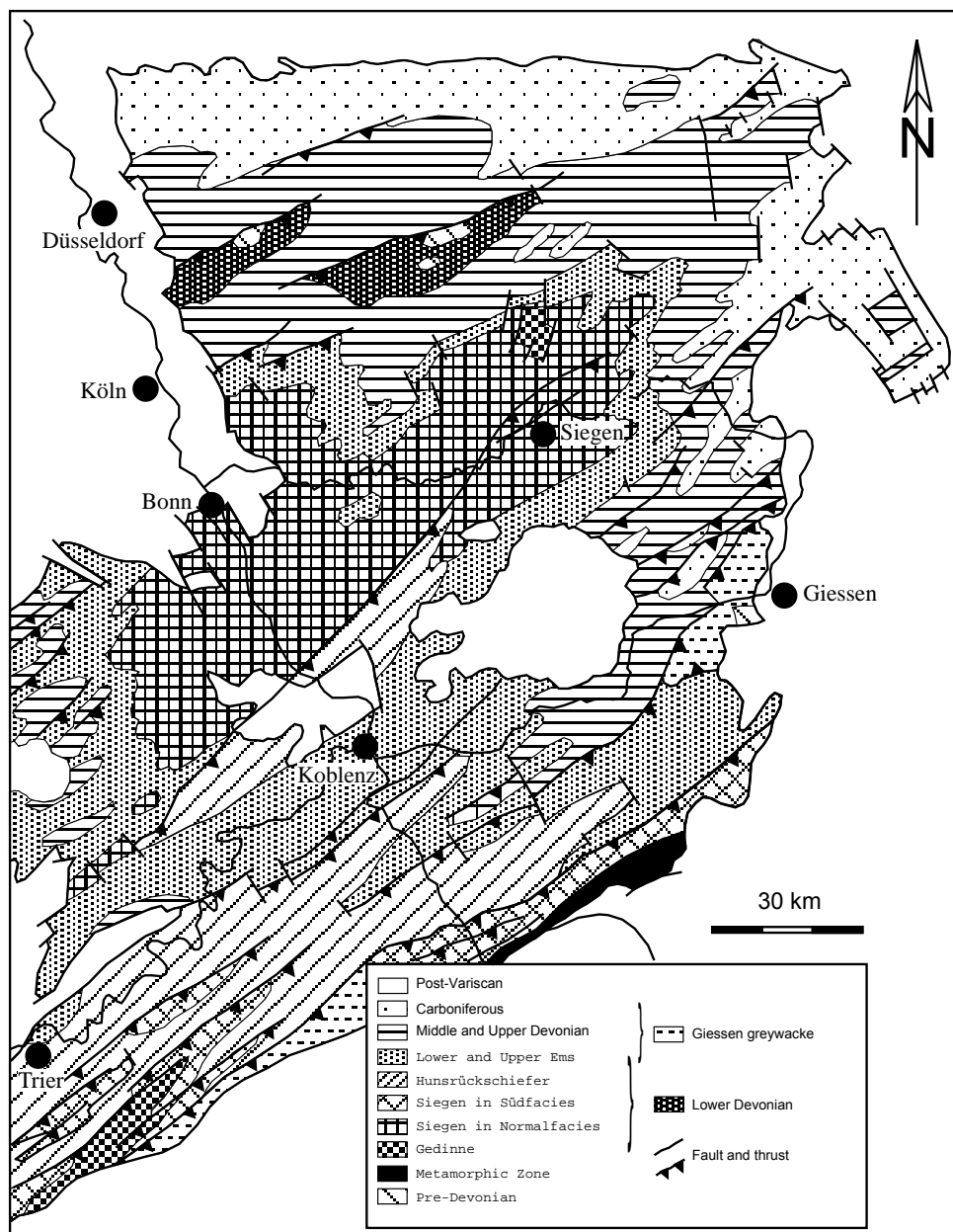


Fig. 2-2. Geological map of the *Rheinische Schiefergebirge* east of the Rhine river (after KÖNIGSWALD & MEYER 1994)

During this time, the Rhenohercynian ocean was subducted under the *Mitteldeutsche Kristallinschwelle*, which later became a midland micro-plate (FRANKE 1989B). During the southward extension marginal movement of the Rheic ocean, the Saxothuringian ocean had extended onwards during late Devonian. By the closure of the Saxothuringian ocean the *Mitteldeutsche Kristallinschwelle* was backthrust over the Palaeozoic rift sequences of the Saxothuringian zone (BERTHELSEN 1992, FRANKE 1989B). These were welded together before the final Variscan collision (BERTHELSEN 1992, FRANKE 1989A, 1989B). In late Upper Devonian the Saxothuringian ocean subducted under the Moldanubian zone.

C. During late Devonian, the subduction of the Rhenohercynian under the Saxothuringian was directed towards the south. The Saxothuringian ocean still continued its extensional stage. The Giessen flysch was developed at the subduction zone to the south of the Rhenohercynian. In the late Namurian time there was a transition from flysch-type sedimentation to coal-bearing molasse as the orogeny spread across the basin, e.g. Tournaisian subduction-related flysch of the Hörre-Kellerwald-Acker area to Carboniferous molasse of the Ruhr Coalfield.

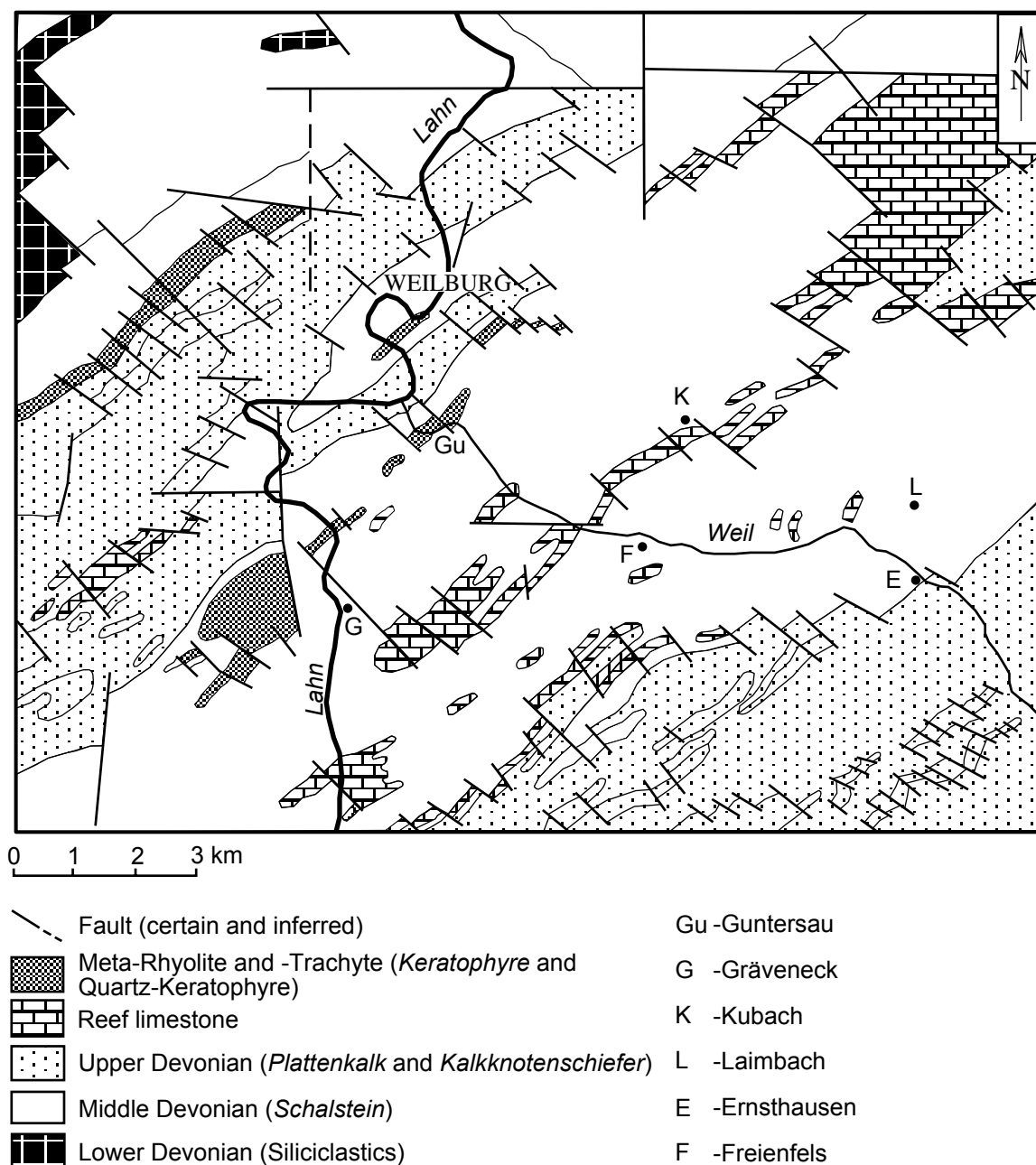


Fig. 2-3. Geological map of the Weilburg area (after KEGEL 1922).

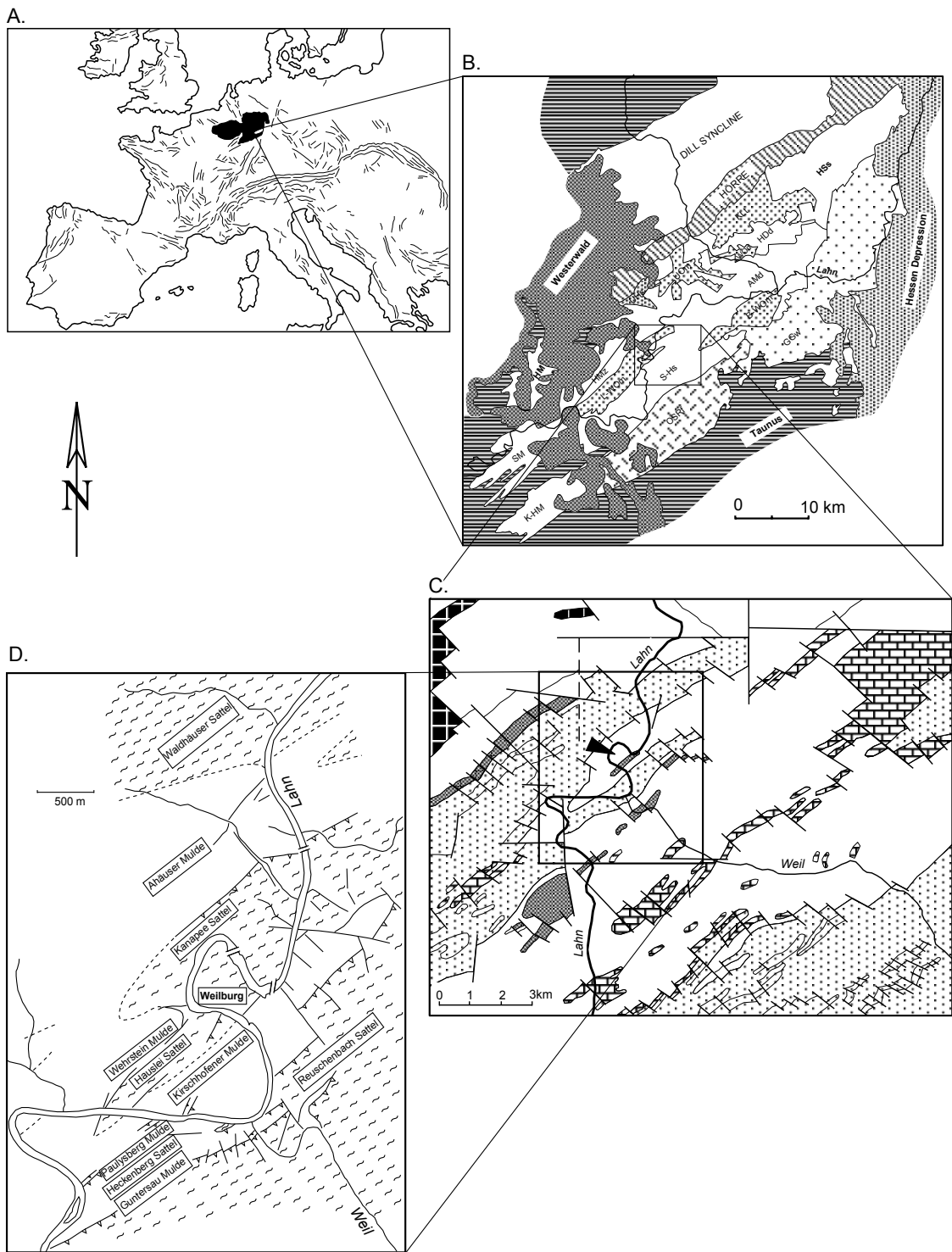


Fig. 2-4. The scope of the tectonic position of the Weilburg area.

- A. Present position of the Rhenish Massif in Europe.
- B. Sub-structures in the Lahn syncline (after KEGEL 1922, NESBOR 1987, explanation in Fig. 1-1)
- C. Geological map of the Weilburg area (after KEGEL 1922, explanation in Fig. 2-3)
- D. Structural map of the Weilburg area (after RIETSCHEL 1966)

D. During late Carboniferous, the subduction of the Saxothuringian under the Moldanubian was accompanied by the Bavarian flysch. Along the sutures between the Rhenohercynian and the Saxothuringian, and also between the Saxothuringian and the Moldanubian, nappe tectonics developed as Giessen (*Rheinische Schiefergebirge*) and South Harz/Selke nappes (Harz) in the Rhenohercynian zone and as Münchberg nappe in the Saxothuringian zone.

E. During the orogenic stage in the Rhenohercynian zone, the orogenic development shows a NW directed polarity, which is demonstrated by the migration of folding and thrusting (strong NW vergent tight folding to normal folding), flysch sedimentation (late Devonian to Carboniferous), metamorphic grade (400 - 450 °C to 300 °C) and the age of metamorphism and deformation (330 Ma to 300 Ma) from south to north (AHRENDT et al 1983).

The Variscan orogeny was caused by the closure of the Rheic ocean or the opening of the proto-Tethys (LORENZ & NICHOLLS 1984). In these oceans, the South European Plate, which was a jigsaw puzzle of sub-plates (LORENZ 1976), included the Saxothuringian and the Moldanubian. The sub-plates of the Variscan orogen (LORENZ & NICHOLLS 1984, LORENZ 1976, BADHAM & HALLS 1975, DEWEY et al. 1973), moved northwards to fuse with Laurussia. According to NICOLAS (1972) and MCKERROW & ZIEGLER (1971) the type of Variscan orogenic style resembles the present Andean-type orogen (terms: MITCHELL & READING 1969). However, this is hardly compatible with the position of the Variscan chain between Gondwana in the south and Laurussia in the north. These two orogens are compared in illustrations by NICOLAS (1972), i.e. the subduction of the proto-Tethys ocean underwent to the South European Plate (WURSTER 1988, LORENZ & NICHOLLS 1984, LORENZ 1976, BADHAM & HALLS 1975, DEWEY et al. 1973).

2.2 STRUCTURAL SETTING

During the Variscan orogeny, the *Rheinische Schiefergebirge* (Rhenish Massif) represents a part of the Rhenohercynian zone as a fold-and-thrust belt. The intra-crustal deformation of the Rhenohercynian zone marks the transition from thin-skinned to thick-skinned tectonics to the east and southeast which controls the different deformation style of the Rhenish Massif and its foreland. Thin-skinned tectonics is exemplified by frontal thrusts, comparable to the Faille du Midi – Aachen Thrust, e.g. by the great Ennepe fault to the east of the Rhine river (MURAWSKI et al. 1983). The regional structures are generally trending NE-SW with NW-facing (NW-vergence) folds and overthrusts. These contractional structures branch off from a mid-crustal décollement, which is clearly seen in the seismic section of the DECORP 2-N (FRANKE et al. 1990). Section balancing of imbricate sheets of the foreland propagating shuppen and fold structures (DITTMAR et al. 1994, BEHRMANN et al. 1991, ONCKEN 1989) suggests that the crustal scale décollement at its actual depth of roughly 13 - 18 km is located within the basement below the Devonian basin filling (BEHRMANN et al. 1991).

An important ramp structure delineates the north-western rim of the Mosel syncline west of the Rhine

river and its continuation, the Dill syncline east of the Rhine river. The structure of the Mosel syncline has been interpreted as a large fold and cleavage fan, south of the Siegen thrust (MEYER & STETS 1975).

The Siegen thrust may branch off from a gently south-dipping master décollement in the middle crust which splits into several thrusts east of the Rhine river. The Boppard thrust (ONCKEN 1989) forms the southern boundary of the Mosel syncline and, together with its continuation east of the Rhine river, presumably forms the basal thrust of the strongly folded and highly imbricated Hunsrück and Taunus Nappe (see DITTMAR & ONCKEN 1992). These thrusts and the Taunuskamm thrust (ONCKEN 1988) of the southern Rhenish Massif are examples of such wedge-shaped foreland propagating fold and thrust systems in the roof of gently SE dipping master detachments.

The southernmost thrust sheet is the metamorphic zone of the southern Hunsrück and Taunus (Northern Phyllite Zone). It forms a multiply folded imbricate belt of partly mylonitic metasediments and metavolcanics. This thrust sheet is cut by the Southern Hunsrück Boundary Fault.

Major thrusts east of the Rhine river are listed from north to south as follows (Fig. 2-2): Ennepe-fault, Ebbe-thrust, Siegen main-thrust, Sackpfeifen thrust, Boppard thrust, Taunuskamm thrust, and Giessen Nappe (WALTER et al. 1995). The Lahn-Dill synclinoria are separated by the Hörre zone, which lies in the continuation of the Boppard thrust.

Alpine tectonic effect on the Rheinische Schiefergebirge

During the Alpine orogeny, along the perimeter of the Alpine collision front, the Rhenish Massif was tectonically unstable. In the vicinity of the collision front, intra-plate tectonics were active in different degree of intensity. With regard to the intensity, the horizontal NW-SE directed compressive stress trajectories from the Alps to the lower Rhine embayment were deduced by fault plane solutions (AHORNER et al. 1972). The consolidated Variscan orogen of Central Europe formed a rigid abutment to the Alpine orogeny. Only the upper Rhinegraben was formed into a zone of weakness. Bundle of lineaments were active as an extensional graben striking in the direction of the sinistral shear component of the recent stress field. The earthquake fault plane solutions show that the upper Rhinegraben reacts as a sinistral shear track (BONJER 1981, ILLIES & GREINER 1978, AHORNER 1975).

MÜLLERRIED (1921) noticed that originally normal faults at the rim of the Rhinegraben became strike-slip faults. Between the active tectonics of the Alps and the passive foreland block of the Rhenish Massif, the upper Rhinegraben came into being with sinistral shear movement during Pliocene. Since that time it has remained seismotectonically active (AHORNER 1975). However, according to FLÖTTMANN & ONCKEN (1992), the Rhinegraben was predisposed by NS-sinistral movement during the Variscan orogenic period. According to a belt of earthquake epicentres and mild neotectonic transverses through the *Rheinische Schiefergebirge* from Frankfurt to Bonn a massive horizontal compressive stress axis in a direction of 135°N azimuth was formed (AHORNER 1975).

Near Bonn, active graben-tectonics is obvious again (MEYER et al. 1983) and corresponds to the new direction (approximately NW-SE) of the axis under tension. Thus, only near the surface did the active rift belt of the lower Rhinegraben appear to be interrupted by the Rhenish Massif. The lower Rhinegraben separated the Rhenish Massif to the east and west of Rhine river by rupture deformation.

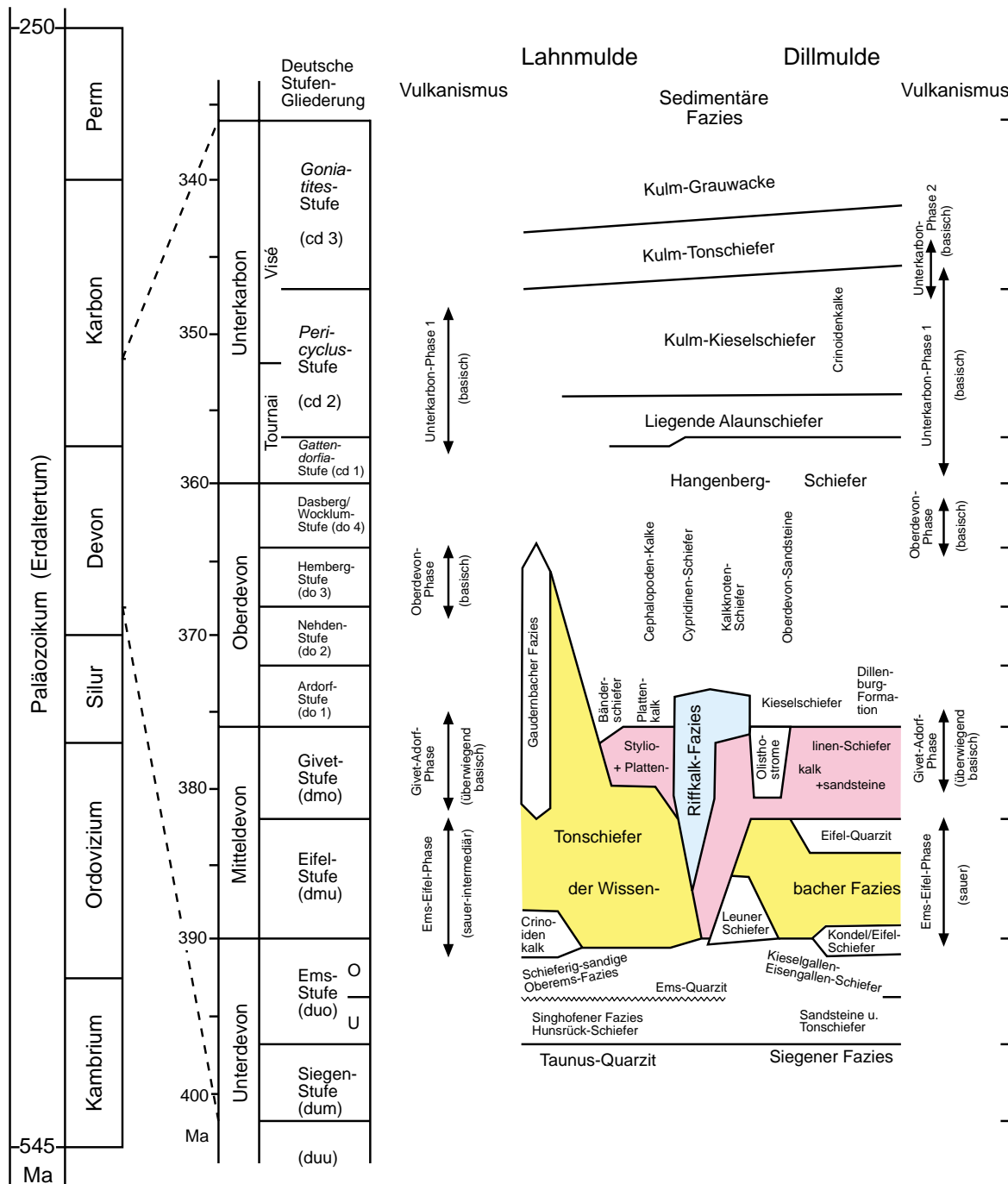


Table 2-1. Stratigraphic sequence of the Lahn-Dill area in the Upper Palaeozoic. (after FLICK et al. 1998)

ILLIES & FUCHS (1983) noticed that during Pliocene the stress pattern and motion changes of the Rhenish Massif at the southern rim were caused by two different kinematic responses: (1) the whole block yielded to an anti-clockwise rotation which is supported by extensional faulting at and parallel to the southern rim; (2) the Massif responded to internal brittle fracturing and deformation caused by a wedging of the apex of the block east of the Rhinegraben into the southern rim of the Rhenish Massif.

2.3 THE SETTING OF THE STUDY AREA

The study area (Weilburg area), part of the middle Lahn synclinorium, is occupied by Middle Devonian volcanic rocks and minor reef limestones, by Upper Devonian Adorf-*Plattenkalk* (thin-bedded limestone) and *Kalkknotenschiefer* (lime nodular slate) with basaltic intrusions and by Lower Carboniferous *Alaunschiefer* (black alum slate), (Table 2-1, Fig. 2-3). The structural setting in the area follows the regional trend of NE-SW. The area covers a north-eastern part of the *Limburg-Weilburger Oberdevonmulde* (LWO-syncline) and a south-western part of the *Schalstein-Hauptsattel* (SH-anticline), (Fig. 2-4). The north-eastern part of the LWO-syncline mainly exposes Adorf-*Plattenkalk*, *Kalkknotenschiefer* and *Alaunschiefer* in a SW plunging structure. On the other hand, the south-western part of the SH-anticline exposes mostly *Schalstein* (mainly lapillituff), sheet flow as well as pillow lavas in a NE plunging structure. This indicates that the LWO-syncline and the SH-anticline are presumably double plunging folds within the Lahn synclinorium which is generally a NE plunging structure.

During the Middle Devonian, the Weilburg area was dominated by extensive bimodal submarine volcanism (Chapter 2.1) producing mainly basaltic lavas and tuffs. The tuffs regionally known as *Schalstein* (lapillituff) dominate the volcanic edifices (for the volcanic facies cf. NESBOR et al. 1993). At the same time reef limestones developed interlocking with the volcanics as is demonstrated by its microfauna (BUGGISCH & FLÜGEL 1992, RIETSCHEL 1966). The reef limestones reflect volcanic ridge position, however, reef debris is prominent as epiclastics in volcanoclastic sediments. Iron ore beds are developed predominantly at the termination of the volcanic activity around the Givetian/Adorfian boundary by alteration processes (NESBOR et al. 1993, FLICK et al. 1990). In the Upper Devonian, thin-bedded limestones are common, for which conodont faunas show to be of the Adorfian age. They are followed by red-buff coloured slates and red *Kalkknotenschiefer* (lime nodular slates) representing the Nehdenian and Hembergian stage. In the NE part of LWO-syncline these are followed by the Cypridina slates which indicate a change in the facies by their light grey colour and belong to the Dasbergian and Wocklumian stage. Siliceous *Alaunschiefer* on top containing silicic phosphate concretions represent an oxygen deficient facies. Their stratigraphic position in the Lower Carboniferous was clarified by conodont faunas (RIETSCHEL 1966), (see Table 2-1). Doleritic intrusions and submarine basaltic flows accompanied the Lower Carboniferous sediments.

CHAPTER 3

FIELD STRUCTURAL DATA ANALYSIS

CHAPTER 3

FIELD STRUCTURAL DATA ANALYSIS

Field data are collected from road-cut profiles, these being nearly perpendicular to the regional structural trend (Fig. 2-3). The structural data are quoted by direction and dip notation and stereoplots of the lower hemisphere (equal-area projection method).

In this investigation the whole profile is divided into three sub-areas where the volcanic rocks are exposed, namely Weilburg-Ahausen (representing the Kanapee anticline), Guntersau-Freienfels and Freienfels-Ernsthausen (see details in chapter 5) by referring to the exposures of reef limestone, iron formation and turbiditic volcanoclastics and volcanic centres as well (NESBOR et al. 1993, FLICK & NESBOR 1988).

The investigated area belongs to the *Schalstein-Hauptsattel* (SH-anticline) and the *Limburg-Weilburger Oberdevonmulde* (LWO-syncline), (defined in KEGEL 1922), located in the Weilburg area. The investigation is partly based on the geological map by RIETSCHER (1966), covering the Ahausen syncline, Kanapee anticline, Wehrstein syncline, Hauslei anticline, Kirschhofen syncline, Reuschenbach anticline, Guntersau syncline, Paulysberg syncline and the Heckenberg anticline, which define the LWO-syncline (Fig. 2-4D), and partly based on the geological map by KEGEL (1922) for the area between Guntersau and Ernsthausen, part of the SH-anticline (Fig. 2-3).

Along the section between Weilburg and Ernsthausen JÄGER (1993) and BEHNISCH (1988) have documented the lithology for about 10 km along the road-cut profile which is the eastern flank of the Weil stream valley (Fig. 2-3). The lithology of the section on both sides of the Lahn river between Weilburg and Ahausen was compiled by SCHLEUNIGER (1989).

3.1 FOLDING

3.1.1 Regional structures

The study area belongs to the very low- to low-grade metamorphic area of the Renohercynian zone, whereby the ages of metamorphism and deformation coincide (AHRENDT et al. 1983, WEBER 1981B, PHILLIPS 1962). Although the Lahn synclinorium is generally NE plunging, sub-structures plunge not only to the NE but also to the SW which is documented in the geological map by BENDER (1965) showing the Lahn synclinorium as a double plunging fold (Fig. 1-2A). Sub-structures of the LWO-syncline are plunging to the SW, whereas those of the SH-anticline are plunging to the NE being revealed by the morphological characters of folded structures in the geological map by RIETSCHER (1966) and by KEGEL (1922), (Fig. 2-4D & E), (cf. WILSON 1982 and THORNBURY 1980). These fold structures are mostly bounded by SE dipping boundary thrust faults (Fig. 2-4) and generally exhibit a transition from subvertical tight upright to overturned folds (terms of folds: GHOSH 1993, TWISS &

MOORES 1992, BILLINGS 1972, FLEUTY 1964). Most anticlines are occupied by volcanic rocks of Middle Devonian age and synclines by Upper Devonian and Lower Carboniferous sedimentary rocks.

The northeastern part of Limburg-Weilburger Oberdevonmulde (Fig. 2-4D):

The **Ahausen syncline** is occupied by Upper Devonian rocks, mainly red *Kalkknotenschiefer* and red *Tonschiefer*, and by Lower Carboniferous rocks, *Alaunschiefer* and grey-buff *Tonschiefer*. Lower Carboniferous basaltic intrusion exposes at NW. NW vergent asymmetrical folds are well developed in the *Kalkknotenschiefer*, the fold axes plunging about 15° NE.

The **Kanapee anticline** is occupied by volcanic rocks of Givetian age. In the NW part of this anticline, the bedding dip is very gentle about 5 - 15° towards NW forming open fold. In the SE part of this anticline, near a rhyolite body, the dip gets steeper forming tight fold.

The **Kirschhofen syncline** exposes Upper Devonian rocks constituted by well bedded Adorf-*Plattenkalk* (thin-bedded limestone), thinly laminated *Kalkknotenschiefer* (pelite and limestone alternations or lime nodular slate) and metabasalt in a transition from a nearly vertical tight fold to an overturned fold. Especially near the SE contact, which is a fault zone, the bedding becomes vertical, e.g. at the Zeppelinfels (cliff) near Weilburg (Plate 1). A nearly symmetrical upright fold with an interlimb angle of about 35° is observed within the *Kalkknotenschiefer* (Plate 3A). The syncline is characterized by disharmonic folding (see Plates 1 & 2 & Fig. 3-1). Overturned folding is exposed at the NW part of the Kirschhofen syncline, noticeable by the position of the intersection of bedding plane s_0 (045°/90°) and s_1 -cleavage (125°/80°), (Plates 1 & 10). The attitude of the s_1 -cleavage changes at the Zeppelinfels, (Plates 1 & 11). The NW-facing s_1 -cleavage was rotated from NW into subvertical position at the Zeppelinfels road-cut.

The **Reuschenbach anticline** is constituted by the *Schalstein* (lapillituff), best exposed at the Gänsberg cliff, where the bedding is dipping only to the SE. Bedding is well developed in the ashtuff, showing attitudes of bedding (s_0) by 35°/160° and of s_1 -cleavage by 45°/140°, for more details about Gänsberg geology see FLICK et al. (1990) and NESBOR & FLICK (1988).

The **Guntersau syncline** is a fault-bounded structure which exposes Upper Devonian Adorf-*Plattenkalk* and *Kalkknotenschiefer* dipping to the SE. Crenulation cleavage (s_2) can be observed in the *Kalkknotenschiefer*.

The Schalstein-Hauptsattel (Fig. 2-4D):

Between Guntersau and Ernsthausen covering of the SH-anticline, two sub-areas namely the Guntersau-Freienfels sub-area and the Freienfels-Ernsthausen sub-area, can be distinguished. The beddings are generally SE dipping about 30 - 40° (Plate 4A). Fold axes of recognizable microfolds plunge NE with NW vergence (Fig. 3-2).

The microfolds can be well observed in the ashtuff and fine grained lapillituff (Plate 9) interbedded in sheet flow lavas. Since the sheet flow lavas are compact and homogeneous, they have not developed any fold structures. This can be correlated with the drag fold model of RAMBERG (1987), valid for incompetent layers interbedded between competent beds (see Chapter 5).

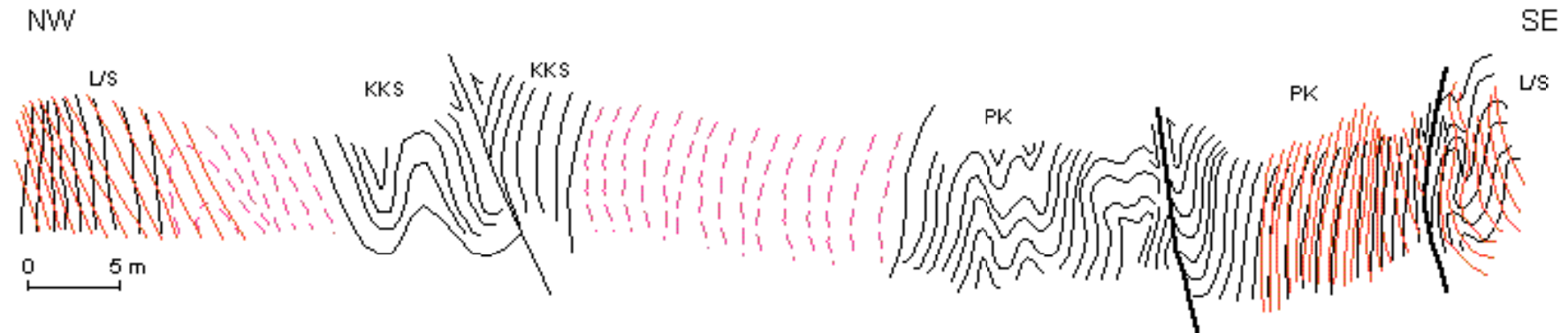


Fig. 3-1. Sketch showing the structural profile of the Zeppelinfeld near Weilburg (Kirschhofen syncline) with fold development in the Adorf-Plattenkalk and Kalkknotenschiefer.

L/S=lappili tuff and slate interbedded, KKS=Kalkknotenschiefer, PK=Plattenkalk
Thin lines = cleavage, medium lines = bedding, thick lines = fault.

3.1.2 Structural types of small-scale folds

Crenulation folds (s2-cleavage): Crenulation folds can be observed in the *Kalkknotenschiefer* of the Guntersau and the Ahausen synclines and in the lapillituff of the Guntersau-Freienfels and the Freienfels-Ernsthausen sub-areas respectively (Plates 6 & 12), however, they are not common in lapillituff. They generally plunge to the SW (Fig. 3-3), which might be related to the SW plunging folds in the LWO-syncline (Fig. 2-4D) as superposed folding (F2) in the study area.

Drag folds: Drag folds are developed in incompetent beds that in turn are sandwiched between thick competent beds. They may indicate the position of anticlinal crests or synclinal troughs of the major folds in the area (RAMBERG 1987). They are formed by layer parallel shear (cf. GHOSH 1993) where the gliding of an approximately horizontally stratified rock-mass has taken place (WILSON 1982, BILLINGS 1972).

Thus, the drag fold setting (attitude of fold-axial plane: $130^{\circ}/43^{\circ}$) shows about 1 cm thick intercalated calcareous layer in about 2 cm thick meta-ashtuff (JÄGER 1996), (Plate 9).

3.1.3 Discussion

In the study area, fold-style partitioning is characteristic for the different structural sub-units: e.g., Ahausen syncline: NW vergent asymmetrical fold, Kanapee anticline: very gentle buckle fold, Kirschhofen syncline: disharmonic fold, Reuschenbach anticline: inclination of bedding plane (thrust-related fold at the NW contact), Guntersau syncline: inclination of bedding plane, Guntersau-Ernsthausen: thrust-related fold or drag fold type on a minor scale. At the Kirschhofen syncline the SW-plunging upright fold exhibits a transition from subvertical tight upright folds in the SE to overturned folds in the NW.

Generally in the study area, the LWO-syncline is characterized by SW plunging folds whereas the SH-anticline has NE plunging folds. Thus, both structures can be expected to be parts of double plunging folds due to secondary folding in NW-SE direction. The fold axis of the LWO-syncline is located about midway between Limburg and Weilburg.

Folds generally exhibit NW vergence, some are just upright (Plate 3A) as a consequence of the basement controlling the folding (see Chapter 6).

Crenulation folds are systematically developed as kink-type crenulation on the long limbs and buckle-type crenulation on the short limbs of the asymmetrical minor folds of the Ahausen syncline (Plate 12A). These folds developed axial plane cleavage (s1-cleavage) and were affected by progressive layer-parallel shear resulting in kink-type folding of the s1-cleavage on the long limb (Plate 12A & Fig. 3-9), and buckling of the s1-cleavage on the short limb (Fig. 3-3).

The study area is mostly occupied by volcanic rocks, which are more rigid than the sedimentary rocks e.g. Adorf-*Plattenkalk* and *Kalkknotenschiefer*. Thus, volcanic rocks respond to the deformation with brittle failure as fractures (NESBOR & FLICK 1987B), faults (normal and reverse) and thrusts as well. Accordingly the SH-anticline (documented by the Guntersau-Freienfels and the Freienfels-Ernsthausen sub-areas) demonstrates that folding is rare in the volcanics.

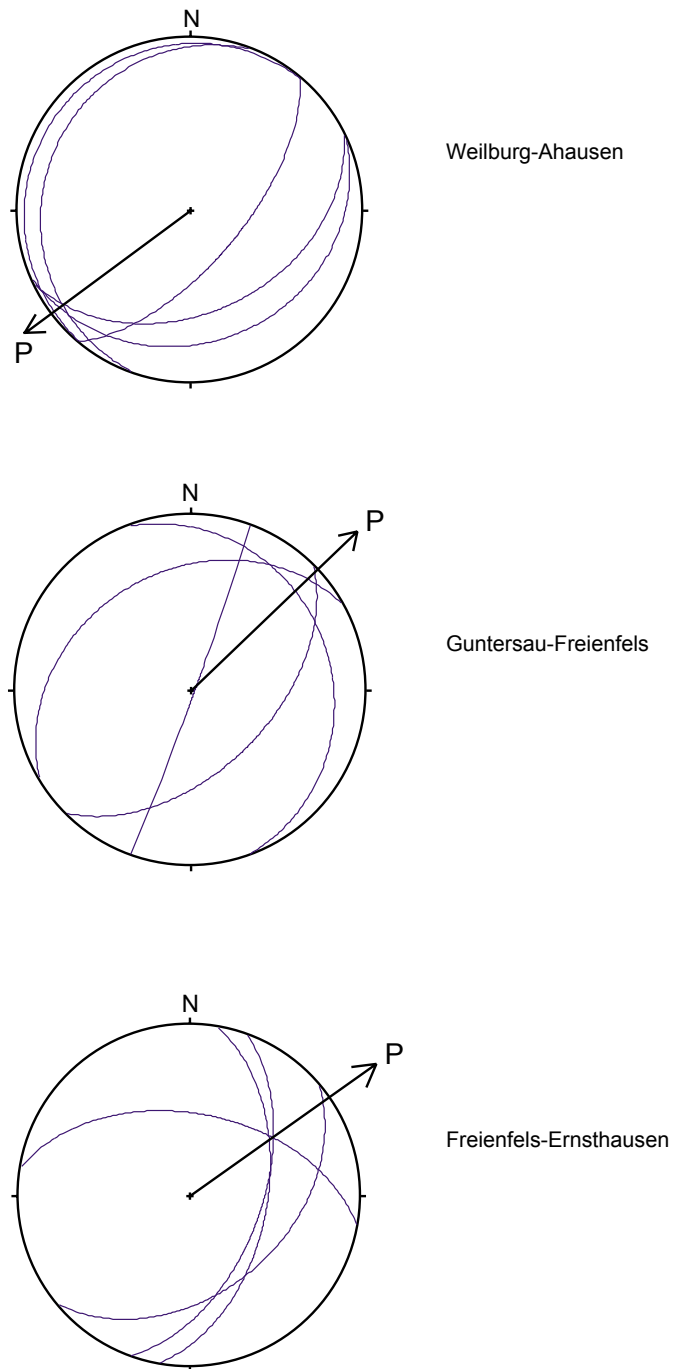


Fig. 3-2. Diagrams of minor fold study in the Weilburg area (bedding as great circles).
P = direction of plunge.

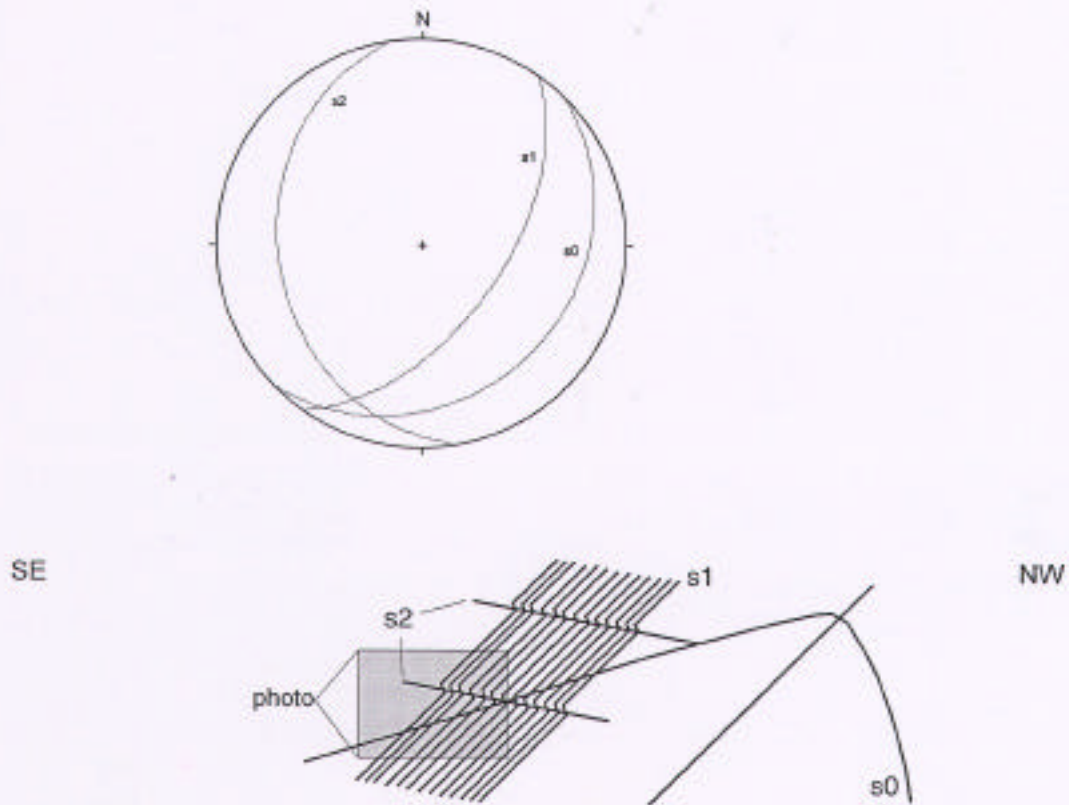


Fig. 3-3. Relationships between s0, s1 and s2 on stereoplot, and sketch and photo at the long limb of the NW vergent fold in the Ahausen syncline.

Only small-scale folds can be observed, in the ashtuff and fine-grained lapillituff alternations (Plate 9), (see Chapter 5). Further details on the deformation of the volcanic rocks, i.e. lavas and volcanoclastics alike, will be given in Chapter 7.

3.2 FAULTING

3.2.1 Regional structures

Whereas generally NW vergent asymmetrical folds are typical over the entire area of the Lahn syncline, almost no folds are developed in volcanic units, especially those dominated by sheet flow lavas with many thrust faults (cf. NESBOR & FLICK 1987). These are very commonly observed in the field (cf. pole-diagram in Fig. 3-4), however, they are not noted in the geological map by KEGEL (1922), (Fig. 1-2E & 2-3) where NW-SE trending faults are pronounced.

For the study area, the geological map by RIETSCHER (1966), (Fig. 2-3) shows thrust faults as boundary between two structural units, e.g. Kanapee anticline and Kirschhofen syncline, known as boundary thrust fault (Fig. 2-4D). Additionally, in the Kanapee anticline, Kirschhofen syncline and the Guntersau syncline off-sets by obviously younger faults with nearly N-S and E-W trends, indicated with shear movements.

Fault plane and slickenside study shows the type of faults, normal, reverse and strike-slip faults respectively (Fig. 3-5). Furthermore, it demonstrates an orientation of extension in NE-SW and an orientation of compression in NW-SE direction which coincide with the structures on a regional scale.

Thrusts in terms of boundary thrusts are relatively pronounced where separating different structural units. In contrast, thrusts within more or less homogeneous volcanic units are not easy to recognize. The boundary thrusts (Plate 8A & B) were formed by reactivation of the older faults, e.g. extensional border faults, due to basin inversion during the Variscan orogeny.

Syn depositional faults can also be observed as mesoscopic structures (cm scale) on polished sections (hand specimens) of fine ashtuff and ashtuff alternations (Fig. 3-6). There are two types: normal faults and reverse faults. Following COWARD (1994) syn depositional faults are now being recognized in many orogenic belts, and it is understood that much intra-continental deformation is accommodated by the reactivation of pre-existing structures.

The northeastern part of Limburg-Weilburger Oberdevonmulde (Fig. 2-4D):

The Kanapee anticline is bordered by NW facing overthrusts to the Ahausen syncline on its NW and to the Kirschhofen syncline on its SE. At both junctions, short-cut thrust faults related to the boundary thrusts cut across the sequences of the adjacent syncline or anticline respectively (cf. Chapter 6). On the other hand the Kirschhofen syncline, Reuschenbach anticline, and Guntersau syncline are all bordered by NW facing boundary thrusts.

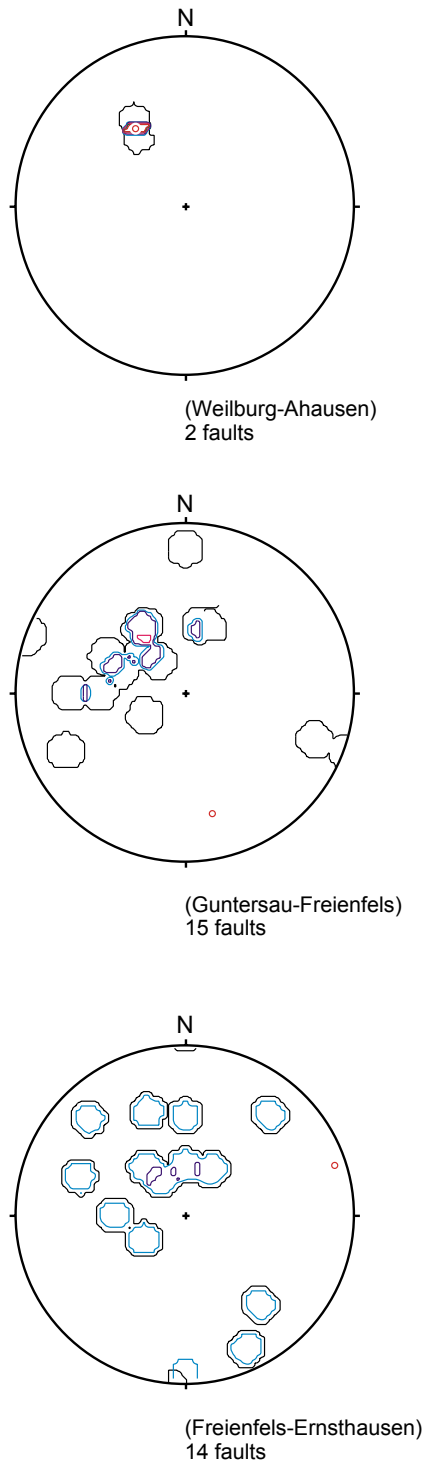


Fig. 3-4. Contour in stereoplots of faults (thrust, normal and reverse) in the Weilburg area.

The Schalstein-Hauptsattel (Fig. 2-4D):

The study area covers the SH-anticline between Guntersau and Ernsthausen, in which the Guntersau-Freienfels sub-area borders the Guntersau syncline to the NW and the Freienfels-Ernsthausen sub-area to the SE by overthrusts (Plate 8A & B). These overthrusts are moved on the detachment faults at the local décollement zone (see Chapter 6). Within their sub-areas low to medium angle imbricate thrusts occur.

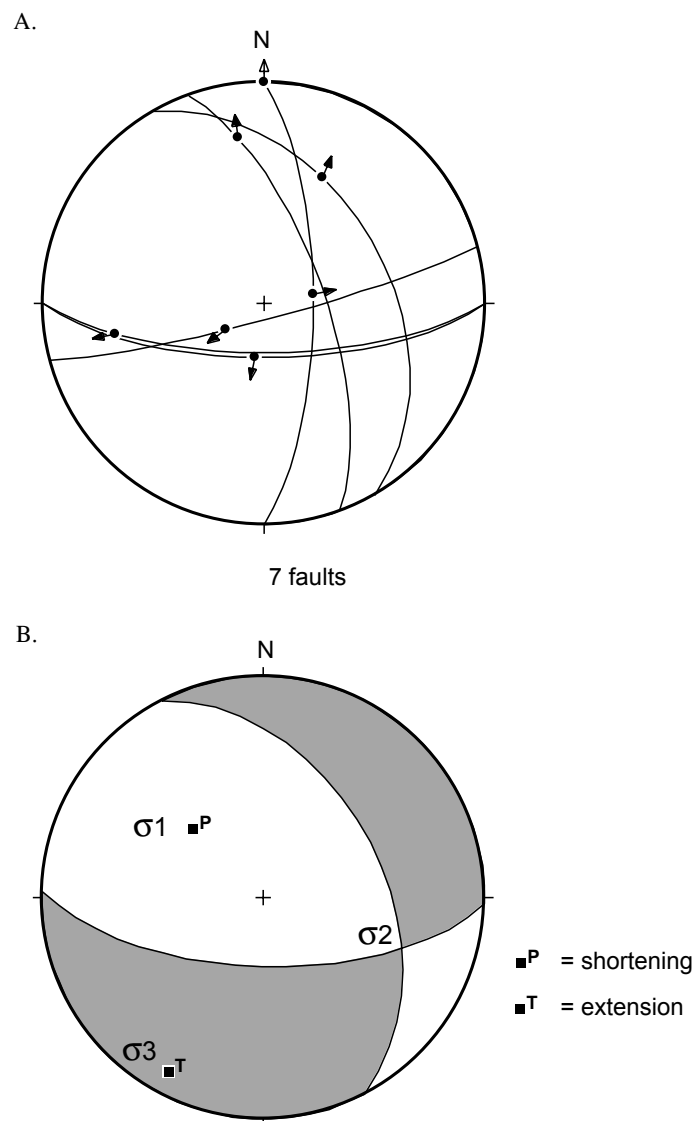


Fig. 3-5. Fault plane and slickenside striation analysis (A) and corresponding stress field (B) for the Freienfels-Ernsthausen sub-area in the Weilburg area.

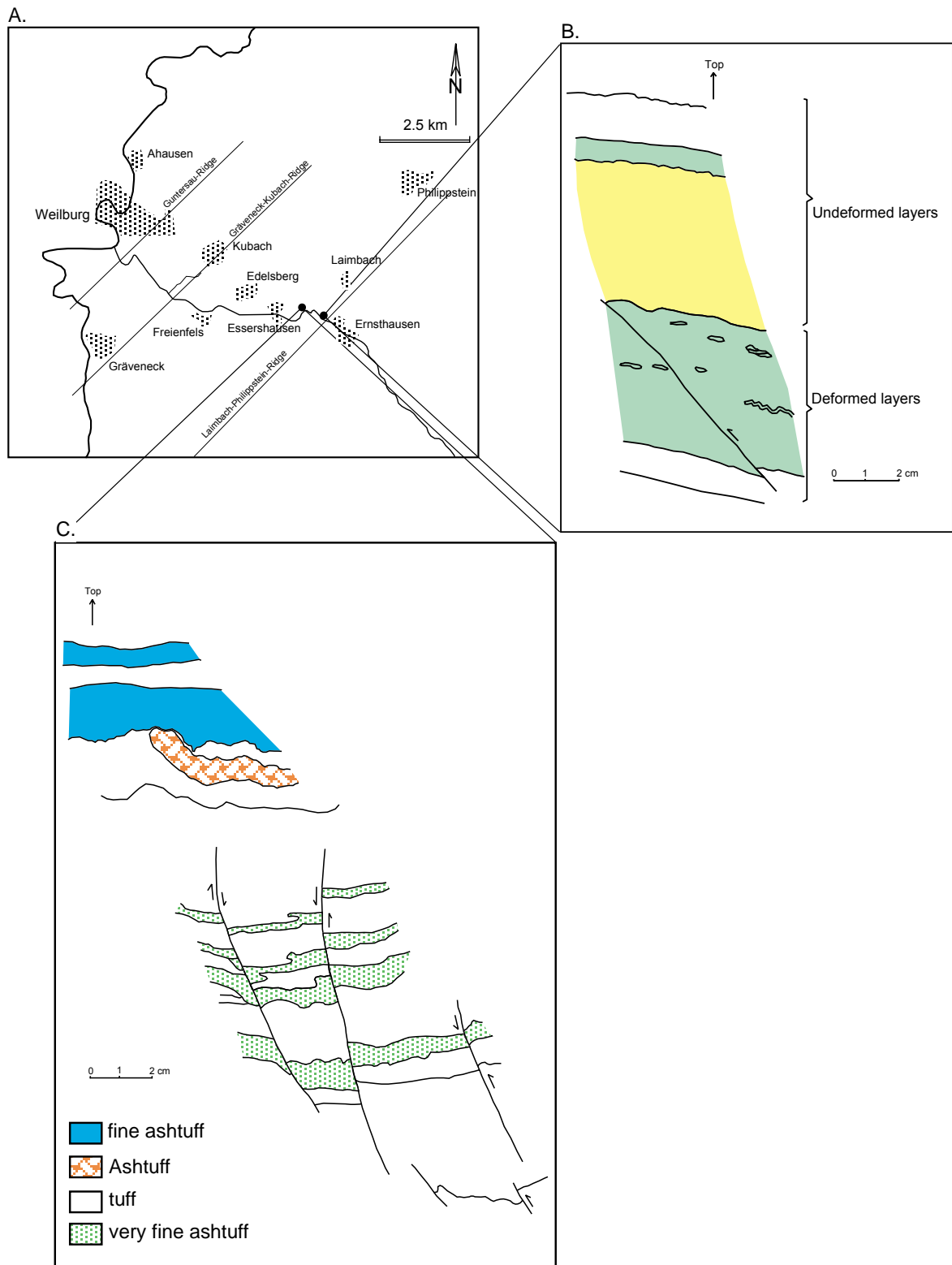


Fig. 3-6. Syndepositional faulting and folding in hand specimens (B and C), development in the Freienfels-Ernsthausen sub-area.
 A: Location map, B: Thrusting with related movement and C: Normal faults overprinted by subsequent inversion.

3.2.2 Discussion

In the long profile throughout the study area between Ahausen and Ernsthausen via Weilburg (Fig. 6-1), thrust faults showing NW-vergence are generally frequent. Boundary thrusts as low angle overthrusts, which are only observed in the SH-anticline and its NE border, reflect the pre-compressive basin development as well as the response of the basin fill to the compressive stress (cf. Chapter 5 and 6). However, the boundary thrust in the LWO-syncline is generally distinguished in thrust faults.

The fault system partitioning can be explained for local areas as follows: e.g. in the SH-anticline, faults are developed in two imbricate thrust systems as an accretionary prism deformation (see Chapter 6); the Kirschhofen syncline has developed a transition from vertical reverse faults to NW facing thrusts, which can be correlated with flexural-slip folding on the detachment fault which was nearly horizontal (see Chapter 6), and the Ahausen syncline has developed the NW facing thrusts together with genetically related short-cut thrusts on an extensional boundary fault (see Chapter 6).

3.3 JOINTING

3.3.1 Regional structures

Joints are formed synchronously with folding in an orogenic belt. The regional structural trend of the investigated area, as in the whole *Rheinische Schiefergebirge*, is NE-SW. Regarding this trend longitudinal joints in NE-SW direction, diagonal joints in NNW-SSE and WNW-ESE directions and cross joints in NW-SE direction reflect the stress geometry of the Variscan fold belt. Superposed neotectonic structures are formed by horizontal compression about 135° N azimuth (AHORNER 1975) which is similar to the old orogenic compression of Variscan.

Joint development corresponds with the formation of faults, e.g. the trends of NW-SE, N-S and E-W (Fig. 3-7). In addition, the NE-SW direction of prominent longitudinal-joints can be correlated with boundary thrusts (Fig. 3-7).

3.3.2 Discussion

Joint data are represented by contour- and rose-diagrams for the different sub-areas. The mechanical conditions for the genesis of the fundamental joint system can be modelled as follows: tension fractures are well pronounced during the tectonic period which are parallel to the simple compressional force that means being normal to the axes of folds or regional strike. Sometimes the tension joints are filled by quartz and/or calcite. In addition, two inclined shear planes are developed at angles less than 45° according to the joint-rose (Fig. 3-8).

In the sub-areas of Weilburg-Ahausen and Guntersau-Freienfels, nearly N-S and E-W trending joints are systematically developed, coinciding with the N-S and E-W trending faults, that are dominant structures on the geological map of that areas. In the Freienfels-Ernsthausen sub-area, these N-S and

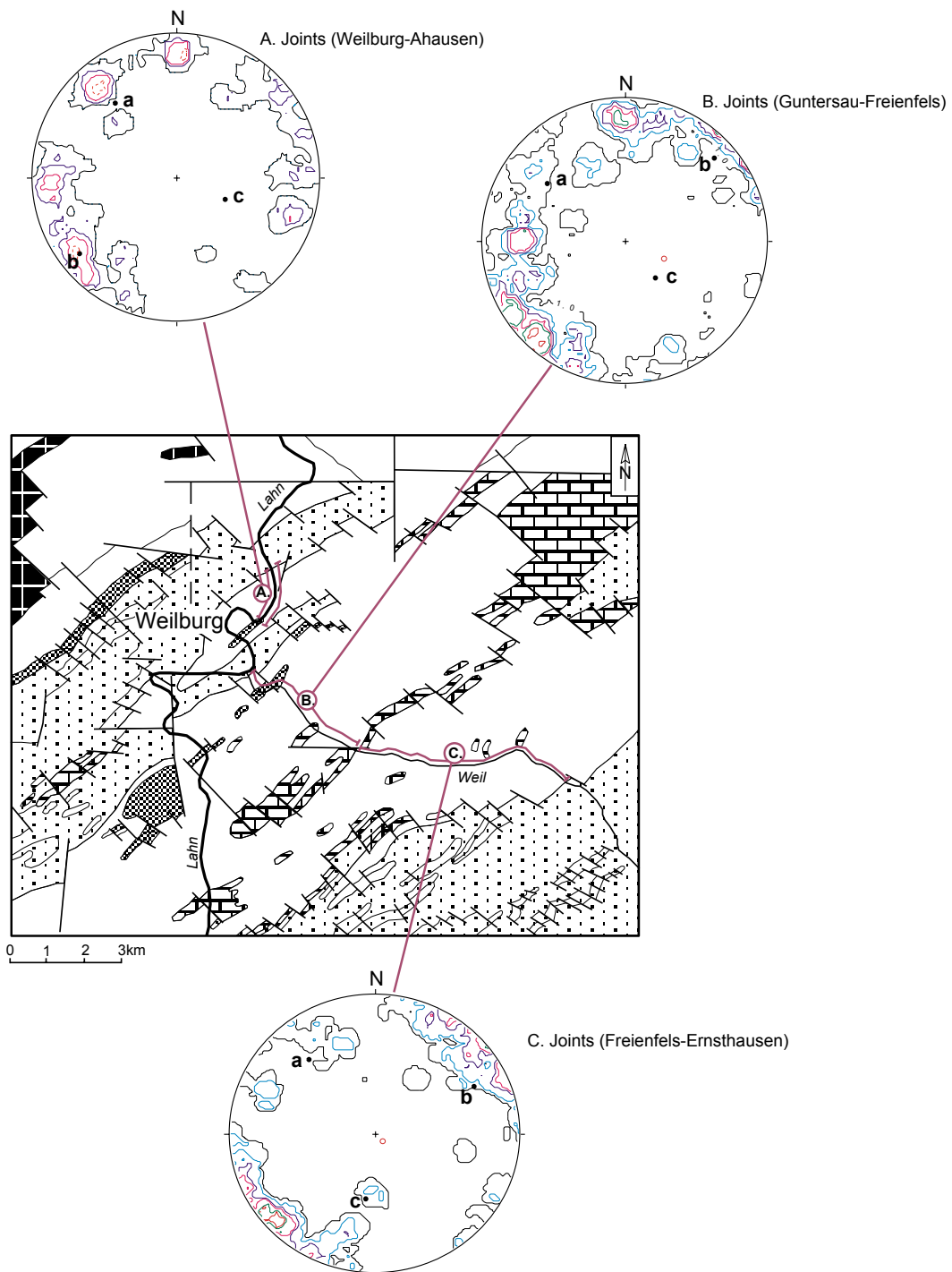


Fig. 3-7. Relationship between joint-study and regional structures of the Weilburg area.

- A. Profile of the Weilburg-Ahausen sub-area.
 - B. Profile of the Weilburg-Freienfels sub-area.
 - C. Profile of the Freienfels-Ernsthausen sub-area.
- (Symbols description of geol. map in Fig. 2.3)

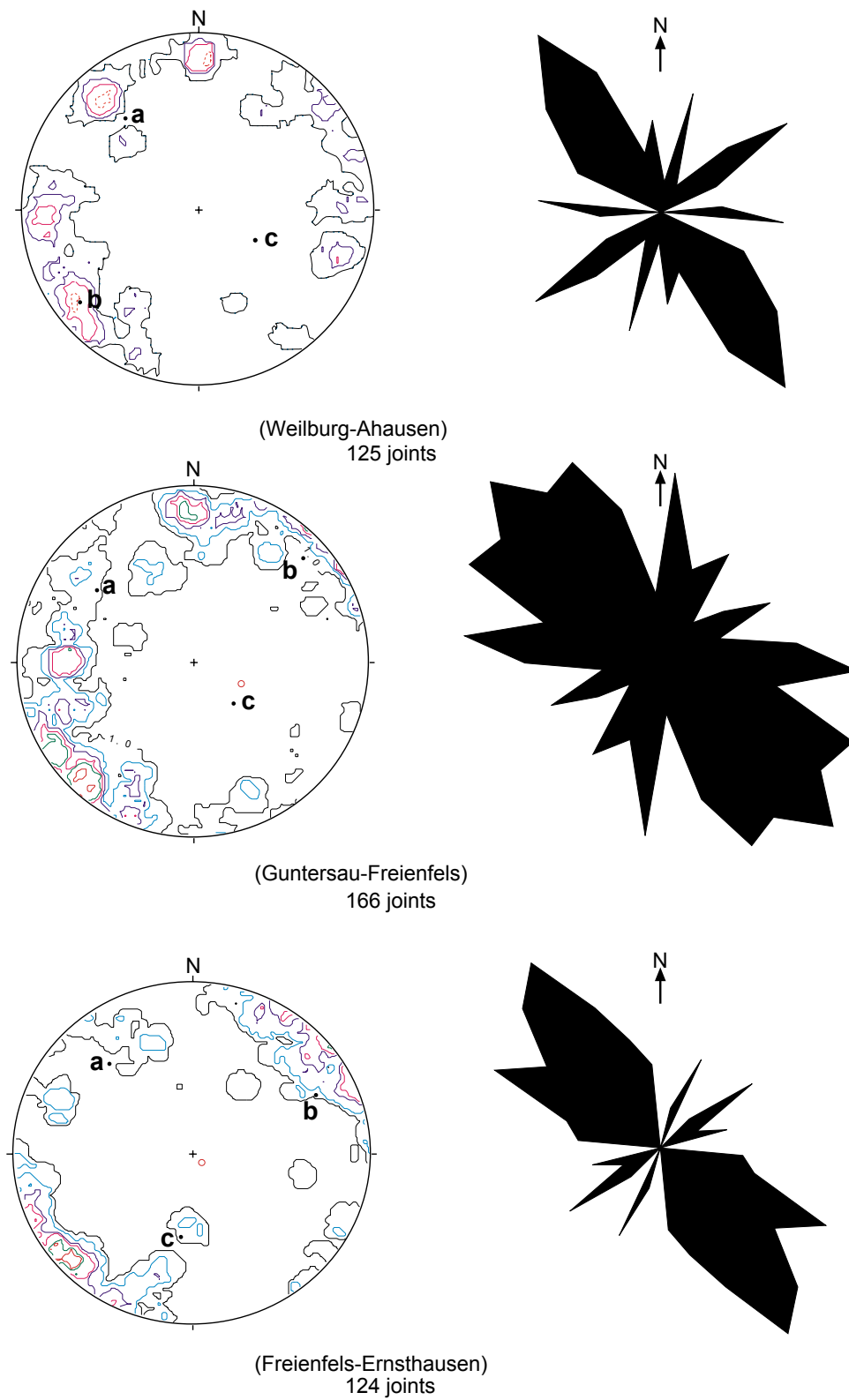


Fig. 3-8. Pole-contour and rose diagrams of joints of the Weilburg area. a, b & c are axes of co-ordinates (see text).

E-W trends are absent.

A summary of the major joints is as follows:

Trend of joints and faults	NW-SE	N-S and E-W	Diagonal (WSW-ENE/NNW-SSE)
Weilburg-Ahausen	x	x	-
Guntersau-Freienfels	x	x	x
Freienfels-Ernsthausen	x	-	-

Joints are more likely to indicate the orientation of a stress field at one instant in geological time (cf. BANKWITZ 1966). By comparison with the geological map of the Lahn area by KEGEL (1922) the N-S and E-W trending joints can be correlated with corresponding faults (Fig. 3-7 & 3-8), suggesting a younger generation, possibly neotectonics of the Alpine age {see the model of ENGELDER & GEISER (1980), or the trajectory stress upon the *Rheinische Schiefergebirge* during Pliocene by AHORNER et al. (1972)}.

The NW-SE trend of the joints (Fig. 3-8) coincides with the most prominent fault direction in the Lahn syncline (see KEGEL 1922). Structurally the NW-SE trend represents cross joints and cross faults, or mechanically tension joints and tension faults. According to WILSON (1982) rocks fail when compressed, either by tension or by shear. Although rocks are much weaker when subjected to tensional stress than to shearing stress, in the field they have failed as often by shearing as by tension (indicating to quartz and calcite fillings). Both styles of rupture are found together, tensional fractures being supplementary to zones of shearing and *vice versa* (cf. WILSON 1982).

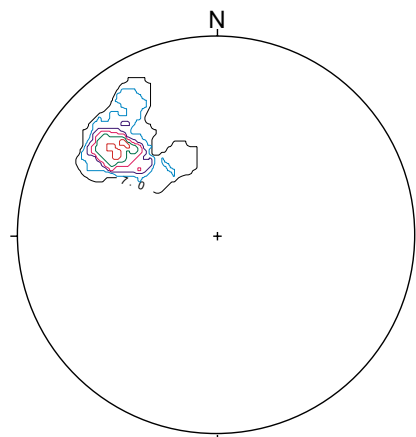
3.4 CLEAVAGE

3.4.1 Regional structures

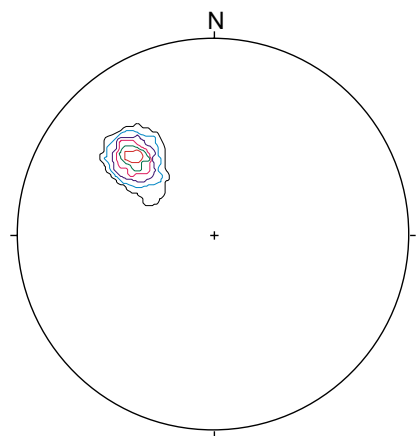
In the study area cleavage is developed in sedimentary rocks as well as in volcanic rocks generally dipping about 40 - 50° to the SE (120 - 140° N azimuth). It shows an anastomosing array in the preferred orientation of the lapilli in the lapillituff and of the *Kalkknoten* in the *Kalkknotenschiefer*. Subsequently, stretching lineations can be observed on the cleavage surface.

Cleavage strike has a more easterly trend than that of the bedding. Occasionally (localities: road-cuts near junction of Edelsberg on the Weiltal road and Zeppelinfels) dip direction is 200 - 250° (Fig. 3-9). Cleavage is well developed in both, laminated and massive lapillituff, whereas it is very poor in lavas. Pillows, however, may be well cleaved as in the Guntersau-Freienfels sub-area and at the exposure near the Lackfabrik, Weilburg (Kanapee anticline). In addition, the deformed elongated pillows lie in the s1-cleavage (Plate 4B).

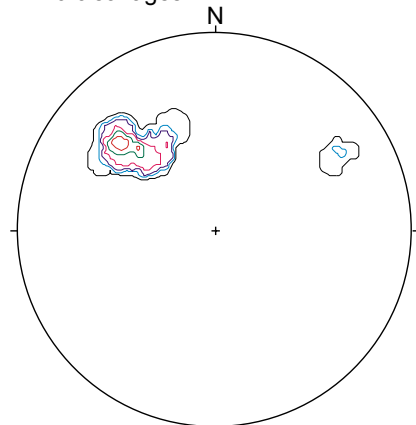
Cleavage refraction (RAMSAY 1967, GHOSH 1966) of the s1-cleavage orientation, is demonstrated e.g. in the alternations of meta-ashtuff and fine-grained meta-ashtuff at the exposure (a very minor fold) between Essershausen and Ernsthausen.



s1-cleavage (Weilburg-Ahausen)
20 cleavages



s1-cleavage (Guntersau-Freienfels)
20 cleavages



s1-cleavage (Freienfels-Ernsthausen)
25 cleavages

Fig. 3-9. Pole diagrams of the s1-cleavage of the Weilburg area.

The s1-cleavage is generally perfectly axial planar as demonstrated in minor folds (meter scale, Plate 9). Therefore, the regional fold structures can be reconstructed by means of the axial planes. Occasionally s1-cleavage fans around the very minor folds (cm-scale), e.g. again between Essershausen and Ernsthausen.

In the study area, the s1-cleavage is generally steeper than the bedding ($s_0 = 110^\circ/35^\circ$; $s_1 = 135^\circ/45^\circ$), and the angle between s_0 and s_1 ranges mostly about $25 - 30^\circ$ (Plate 4A).

Different relationships can be quoted from the following localities:

Localities	s0	s1
Kanapee	290/15	130/65
Near railway station	135/50	130/65
Kubach limestone	062/15	130/25

Exceptions exist at the Zeppelinfels in the Kirschhofen syncline where the bedding is subvertical (Plates 1 & 2) and steeper than the s1-cleavage (indicating overturned fold).

3.4.2 Discussion

The study area (as a part of Lahn syncline) is characterized by strongly NW-facing folds with SE-dipping fold-axial planes and cleavage planes. The cleavage orientation (s1-cleavage) being rather constant can be used as a tectonic marker (PHILLIPS 1962), whereby deformation of the cleavage suggests later phases of tectonic movements.

The cleavage attitude has changed in some parts of the study area, i.e. the Zeppelinfels and the Freienfels-Ernsthausen sub-area. The effect of the late- or post-orogenic movements resulted in a change of the s1-cleavage orientation near Edelsberg ($242^\circ/62^\circ$) and ($205^\circ/72^\circ$), (Fig. 3-9). At the Zeppelinfels profile, on the road-cut, the dip angle of the s1-cleavage is nearly vertical (about 85° to SE). Thus, this case could be clear rotation of the s1-cleavage (Fig. 3-9), (cf. WEBER 1981A).

3.5 LINEATION

3.5.1 Regional structures

In the study area lineations are developed as intersection lineation, slip lineation or stretching lineation. On the cleavage surface bedding-cleavage intersection is shown and stretched grains are at a high angle to the intersection lineation (cf. GHOSH 1993, RAMSAY & HUBER 1983B and WILSON 1982). Intersection lineations throughout the area form a great circle girdle (Fig. 3-10) which indicates the superposition of later upon earlier folds (TURNER & WEISS 1963).

Slip lineations can be found as striations on slickensides indicating the direction of fault movement during the last phase of deformation (determination according to RAMSAY 1967 and GHOSH 1993). The

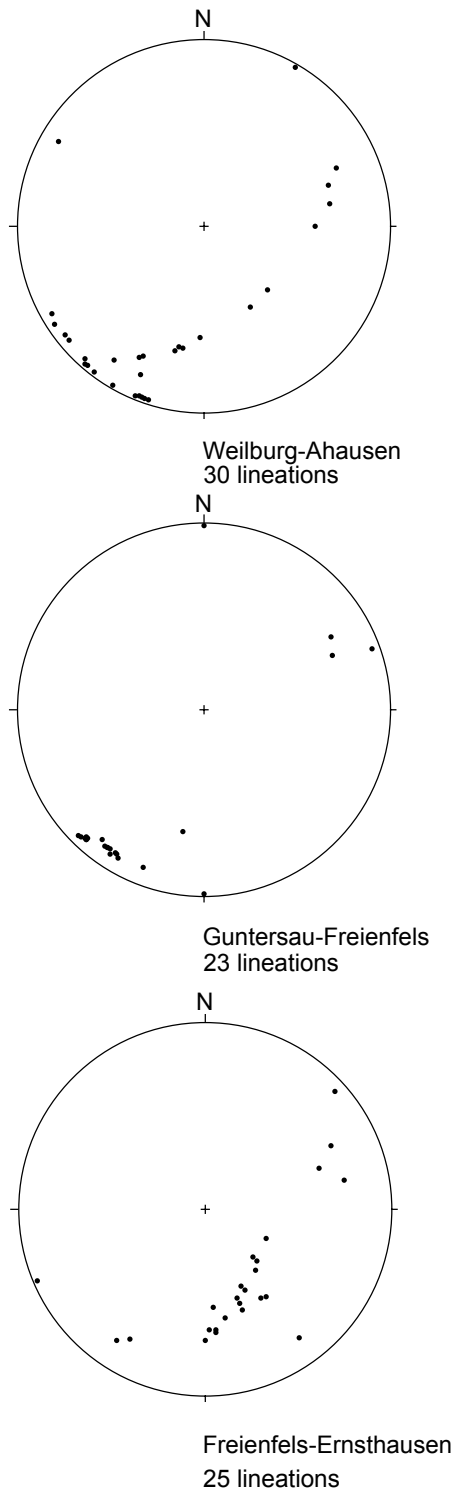


Fig. 3-10. Linear diagrams of $\delta = s_0/s_1$ (intersection of bedding s_0 and s_1 -cleavage) of the Weilburg area.

paleostress analysis from fault plane and slickenside striations shows an inclined compressive stress, more or less normal to the s1-cleavage (Fig. 3-5).

Near Freienfels junction of two sub-areas, limestone fragments in the epiclastic lapillituff are aligned defining a lineation in the regional trend suggesting a stretching along the strike.

3.5.2 Discussion

Lineations are excellent indicators of tectonic movements. The intersection lineations in the Freienfels-Ernsthausen profiles (Fig. 3-10) are parallel to the fold axes trending NE-SW, the extension direction. This is also valid for the alignment of epiclastic fragments near Freienfels which indicates a stretching due to shear movement along this extensional direction.

Slip lineation on the s1-cleavage surfaces were developed by progressive shear movement. At the same time *Kalkknoten* were reoriented with their long axes into the s1-cleavage by layer parallel shear.

3.6 AGE RELATIONSHIP BETWEEN THE STRUCTURES

In accordance with structural maps in the Lahn syncline area by REQUADT (1990), RIETSCHEL (1966), BENDER (1965) and KEGEL (1922), (Fig. 1-2) the deformational structures caused by faulting can be arranged according to their relative age as follows:

- | | |
|--|----------|
| 1. N-S faults (diagonal/shear faults) | youngest |
| 2. E-W faults (diagonal/shear faults) | ↓ |
| 3. NW-SE faults (cross/tension faults) | ↓ |
| 4. NE-SW faults (thrust faults/probably longitudinal faults) | oldest |

NNW-SSE (N-S) and WSW-ENE (E-W) oriented faulting near Limburg could be dated between Upper Miocene and Pleistocene in relation to the lower Rhinegraben tectonics (MEYER et al. 1983). The shear and tension faults that are developed between a couple of shear zones in the study area will therefore probably be contemporaneous to the Rhinegraben tectonics (cf. BILLINGS 1972).

Thus, the sequence of structures show the following age relationships:

- | | |
|--|----------|
| 1. N-S faults (Variscan and reactivated later) | youngest |
| 2. E-W faults (Variscan and reactivated later) | ↓ |
| 3. NW-SE faults (Variscan and reactivated later) | ↓ |
| 4. Thrusting (Variscan orogeny) | ↓ |
| 5. Folding (Variscan orogeny) | oldest |

Tectonic deformation phases: Field structural study suggests the following deformation phases:

D1: Variscan orogenic period: folding, thrusting, faulting, s1-cleavage, stretching lineation, metamorphism.

D2: Late Variscan orogenic period: lateral shear faulting, crenulation folding (s2-cleavage), intersection lineation.

D3: Post-orogenic period: shear faulting, jointing.

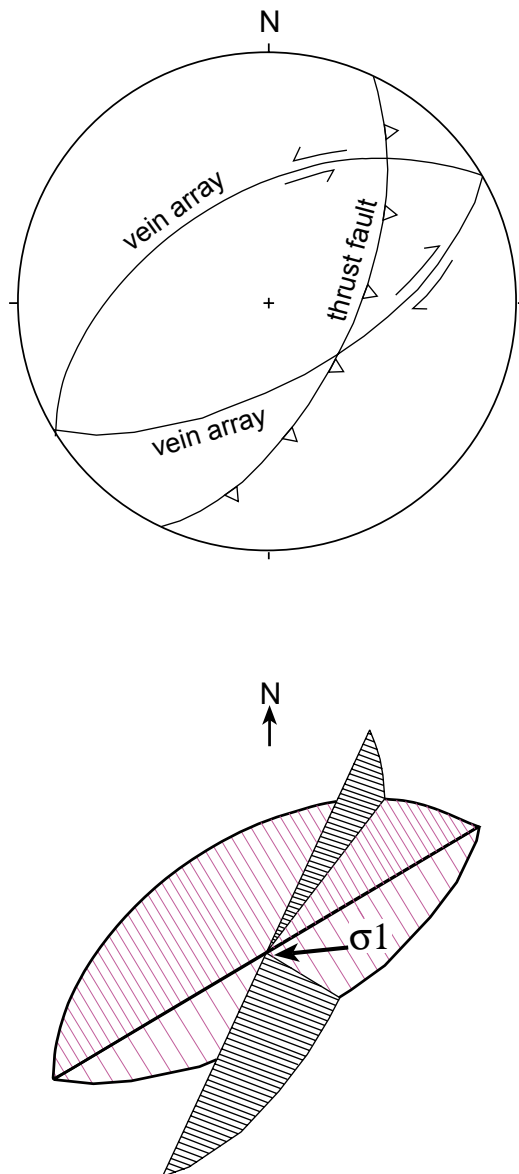


Fig. 3-11. Stereoplot showing the relation of the thrust and conjugated *en-echelon* vein array (see Plate 7B) with correlated movement in terms of σ_1 (horizontal compression).

3.7 OTHER STRUCTURES

Conjugate shear En-echelon veins: The *en-echelon* veins are developed in the lapillituff which crops out at the Freienfels-Weinbach road-cut near Freienfels, being part of the Freienfels-Ernsthausen sub-area. These *en-echelon* veins represent *hk0* shears (cf. Fig. 5-5A), (terminology: HANCOCK et al. 1983) their (tension gashes) long axes lying at 45° N and short axes lying at 135° N to the shearing surface (Plate 7B), (cf. RAMSAY 1967). These *hk0* shears are related to a thrust fault with the attitude $070^\circ/65^\circ$. Conclusively, the orientation of the shear in relation to the thrust fault (Fig. 3-11) suggests dextral shear movement along the junction trending NE-SW between Freienfels-Ernsthausen and Guntersau-Freienfels sub-areas .

Non-sigmoidal right-stepped tension gashes (cf. BEACH 1975) in sub-vertical position occur on a road-cut near Freienfels, Freienfels-Ernsthausen sub-area (Plate 7A) which suggest dextral shear movements along this profile.

Superposed folding: Generally in the study area, the LWO-syncline is characterized by SW plunging folds whereas the SH-anticline by NE plunging folds. Thus, both structures can be expected to be part of double plunging folds due to secondary folding in NW-SE direction. For example, in the LWO-syncline, SW plunging characteristics for the NE part (Weilburg area) whereas the SW part (Limburg area) shows NE plunging (Fig. 3-12). Thus, the fold axis at its lowest point in the midway between Limburg and Weilburg areas.

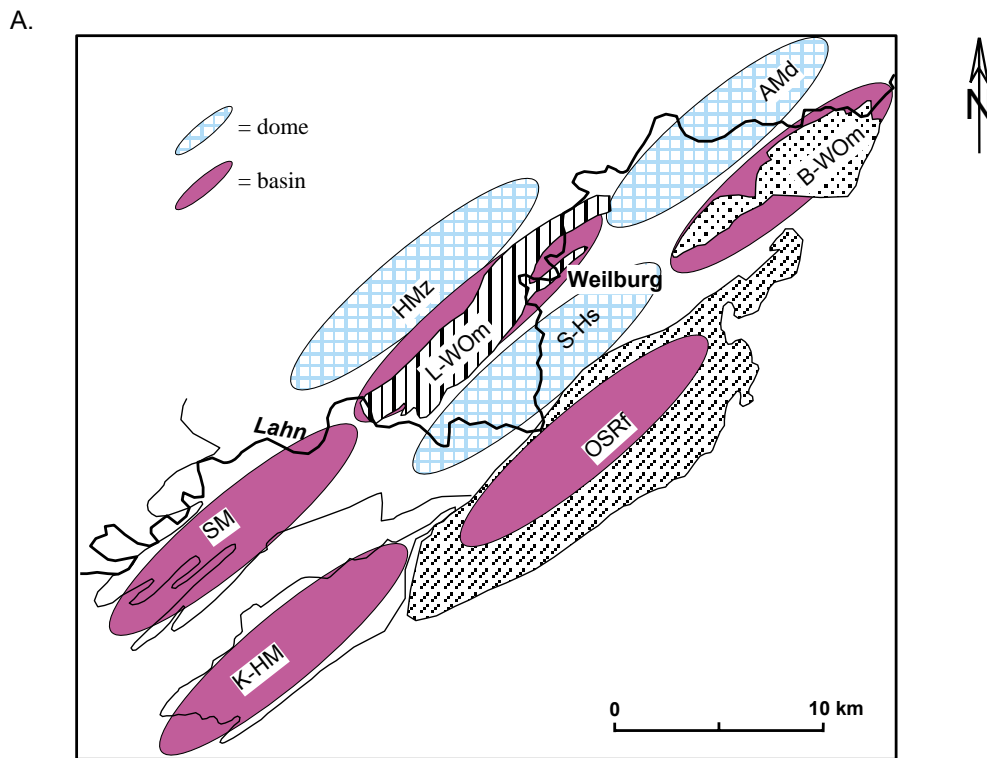
On the other hand, the SH-anticline shows NE plunging at the NE part (Weilburg area). Consequently, the LWO-syncline is a regionally double plunging syncline, likewise SH-anticline is a regionally double plunging anticline (cf. Fig. 3-12).

Consequently, mesoscopic superimposed structures are listed as following:

Intersection lineations measured within the different sub-areas of the study area form a great circle coinciding with the mean orientation of the *s1*-cleavage plane (Fig. 3-10). The noncylindrical condition of the fold system as indicated by the intersection lineations is due to the superposition of later upon earlier folds (TURNER & WEISS 1963).

Superposed folding (F2) indicating *s2*-cleavage as well as crenulation folds (*s1*-cleavage folding) is in a sub-horizontal position (about $230^\circ/25^\circ$).

The outcrop (Plate 3B) at the Zeppelifels, shows rigid folding in a rather thick sandstone layer in slates. The origin of this fold can be deduced as follows: after a first folding (F1) the crest (nearest one) of this fold was flattened (inter-limb angle was zero) together with thrust movements (indicating extensional border faults, Plate 1) at the trend of the regional structures being E-W. Later, the fold limb was shifted to NE (present: the offset crest), due to the northward ongoing tectonic movement (cf. Fig. 8-1). Thus, this is a determinant of the northward tectonic movement on the development of the oroclinal bending in the Rhenish Massif around the London-Brabant Massif after the colliding of the Rhenohercynian with the London-Brabant Massif during the Variscan orogeny, whereby the regional trend was changed over from E-W to NE-SW (present position).



K-HM = Katzenelnbogen-Hahnstättener Mulde; SM = Schaumburger Mulde; OSRF = Oberdevon der Südlichen Randfazies; S-Hs = Schalstein-Hauptsattel; L-WOm = Limburg-Weilburger Oberdevonmulde; HMZ = Hadamarer Mitteldevonzug; B-WOm = Braunfels-Wetzlarer Oberdevonmulde; AMd = Asslarer Mitteldevondecke;

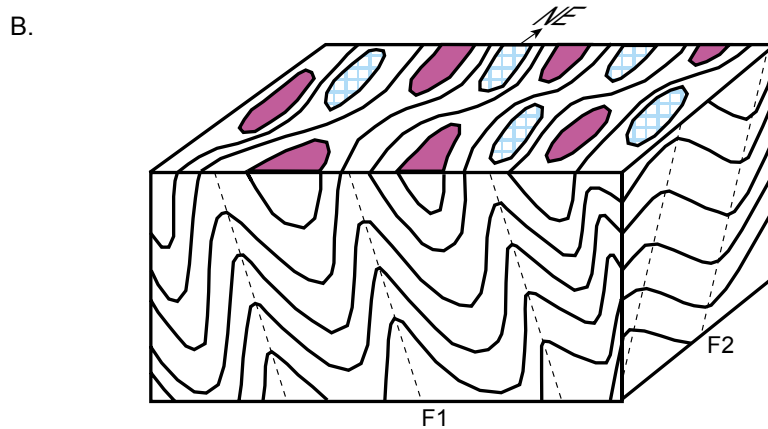


Fig. 3-12. A: Basin and dome refolding in the Lahn syncline, B: 3-dimensional refold pattern referring to the attitudes of axial plane cleavage and s2-cleavage (without scale).

CHAPTER 4
STRAIN ANALYSIS

CHAPTER 4

STRAIN ANALYSIS

Strain analysis deals with the quantification of the geological deformation. Strain can be determined by measuring the changes in the shape of objects with a known initial shape. The strain has four components: (1) principal longitudinal strains: e_1 , e_2 and e_3 , (2) orientation of the original strain ellipse axis: θ , (3) orientation of the final strain ellipse axis: ϕ (see Fig. 4-1) and (4) the rotation: W . The principal longitudinal strain, $e = (L_f - L_o)/L_o$, where L_f and L_o are the final and the original lengths of the strain objects. The finite strain ellipsoid has three orthogonal principal axes with semi-axes length $1+e_1 \geq 1+e_2 \geq 1+e_3$ ($L_f/L_o = 1+e$). In the geometric properties of the strain ellipsoid the reference co-ordinate frame is often reoriented to coincide with the principal strain axes. The co-ordinate frame has X, Y and Z, parallel to the principal strains of values e_1 , e_2 and e_3 respectively. The three planes XY, YZ and XZ are known as the principal planes of finite strain. The strain ellipses on these planes are defined as the principal strain ellipses with the strain ratios $R_{xy} = (1+e_1)/(1+e_2)$, R_{yz} and R_{xz} . In practice not all of these strain components can be determined. Although it is often possible to measure directly the strain ellipse derived from an initial circle, the initial size of the circle is generally not known, therefore it is not always possible to measure e_1 and e_2 but only the ellipticity or aspect ratio defined as $R = k(1+e_1)/(1+e_2)$ where k is a constant depending on the diameter of the initial circle. The determination of the ellipse orientation is generally straightforward, but the rotation of the initial orientation of strain ellipse axis has to be calculated. In the study area, excellent strain markers, e.g. *Kalkknoten* (lime nodules), lapilli, and epiclastic fragments are well preserved. The arithmetic mean of the strain ratios R_{xy} , R_{yz} and R_{xz} derived from a number of *Kalkknoten* in each locality had to be calculated. It gives the shape expressed in the form of $1+e_1: 1+e_2: 1+e_3$ as a: b: 1.

The XY plane contains the long and the intermediate axes, the YZ plane contains the intermediate and the short axes, and the XZ plane contains the long and the short axes. These principal planes are normal to each others.

In the uniaxial compaction stage, the oblate spheroid is represented as $X = Y$, X and Y parallel to the layering and Z vertical, however in the folding stage, Y axes parallel the fold axis (Fig. 4-1B), (MAZZOLI 1995, MAZZOLI & CARNEMOLLA 1993, RAMSAY 1967).

A prominent s_1 -cleavage is usually taken to be parallel to the XY plane and lineation parallel to the X axes in terms of stretching lineation (cf. GHOSH 1993 and RAMSAY 1967). The alignment of ellipsoidal shapes is oriented along both, bedding and s_1 -cleavage.

The three orthogonal sections are cut through the rock specimens making one section parallel to the s_1 -cleavage (XY plane), a second section normal to the s_1 -cleavage (XZ plane), and a third section perpendicular to both, s_1 -cleavage and lineation or the other two sections (YZ plane). The XZ plane always corresponds to the plane experienced in tectonic strain (MAZZOLI 1995).

In this study, a mathematical construction of the strain ellipsoid (cf. RAMSAY & HUBER 1983A) is also applied to measurements of deformed *Kalkknoten* and lapilli.

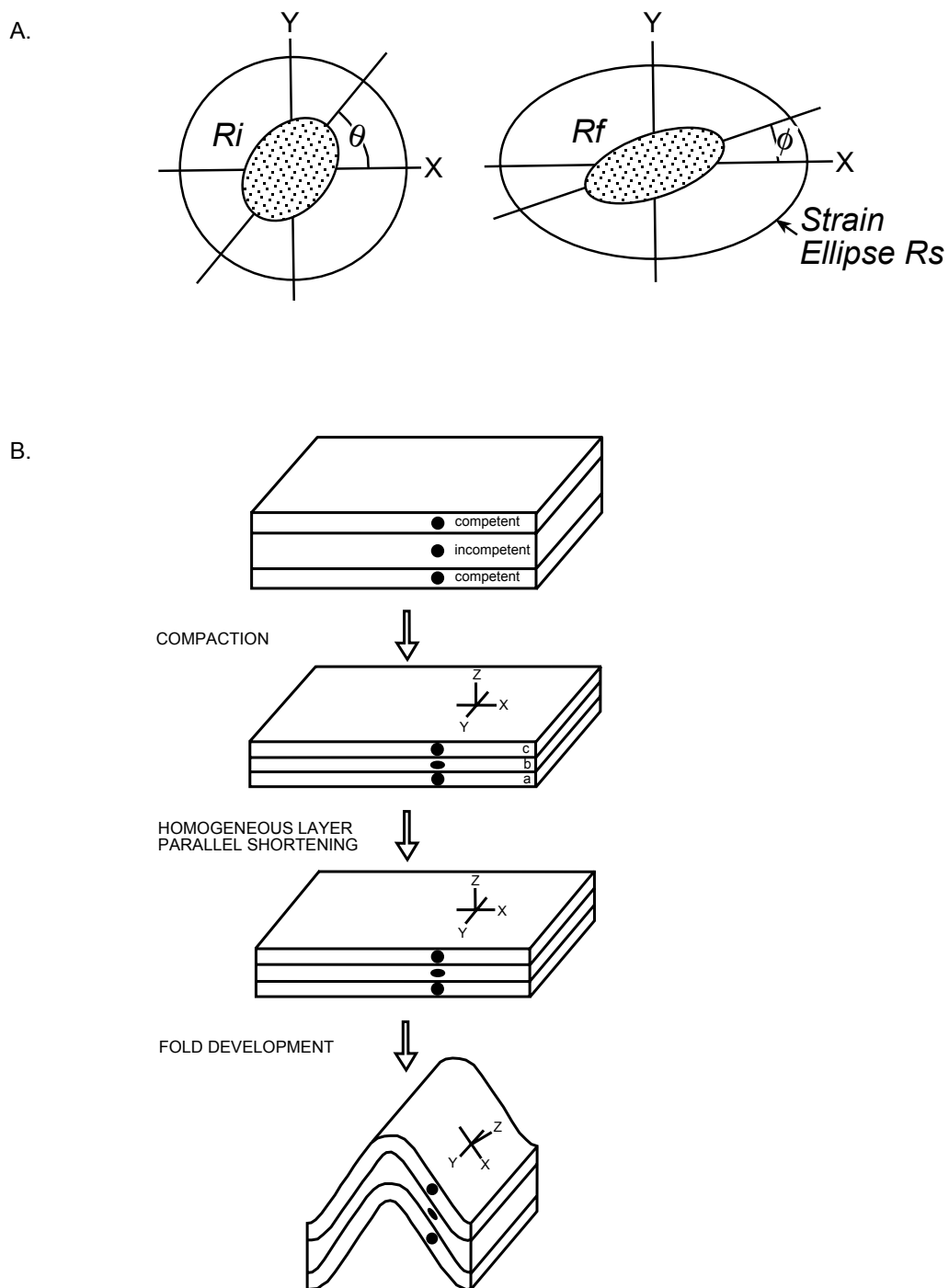


Fig. 4-1. A: Straining of an elliptical marker (after LISLE 1985), B: co-ordinate reference frame in the different stages of deformation (Y-axis parallel to the fold axis), (after MAZZOLI & CARNEMOLLA 1993)

4.1 DETERMINATION OF 2-DIMENSIONAL STRAIN

The 2-D strain is determined by using Rf/ϕ and Fry methods in the *Kalkknotenschiefer*, lapillituff and Mandelstein from the road-cut profiles of the Lahn and Weil valleys. In particular, the detailed 2-D strain is worked out in the Rf/ϕ method in different structural units, whereas the Fry method is used for the correlation between strain and Anisotropy of Magnetic Susceptibility (AMS).

4.1.1 Rf/ϕ strain analysis

The Rf/ϕ analysis can provide useful information on initial fabrics, and on the relative orientation of strain in bedding or s1-cleavage, in addition to giving strain values. These parameters depend on five variables (DUNNET 1969): (1) initial particle shape, (2) initial particle orientation, (3) strain intensity, (4) strain orientation, and (5) degree of ductility contrast between particles and the entire particle/matrix system. The Rf/ϕ method is one of the best of those tested as information is directly available about relationships of the strain to other features (HANNA & FRY 1979).

The XZ plane gives the greatest initial shape, which is consistent with its orientation at a high angle to bedding. Following DUNNET (1969), the XZ section shows the high density plot and symmetric distribution, but the YZ and XY sections are less specific. The XY plane obtains the maximum and minimum values scattering across the centre which also suggests an initial fabric. In addition, the lack of points around the centre of the XY section is commonly encountered as an absence of initially circular particles.

Method: The Rf/ϕ method is a technique to determine the strain from objects that had initially circular, sub-circular, sub-elliptical or elliptical shapes. It involves measurements of the elliptical shape Rf (ratio of long axis and short axis) and the orientation ϕ of deformed objects, and the construction of a Rf/ϕ diagram (RAMSAY & HUBER 1983A). The Rf/ϕ diagram is then compared with standard strain curves developed by LISLE (1985). The deformation characteristics (Rf, ϕ) with initial ratio (Ri, θ) can be read off (Fig. 4-1). The grid can be placed on a Rf/ϕ data set, and the axial ratios and orientations read off to obtain the destraining of the rock by an amount corresponding to the R_s value of the grid. The essential feature of the Rf/ϕ method is to allow the markers (by using the standard nets by LISLE 1985) to be graphically destrained repeatedly until the group of restored markers shows Ri and θ distributions which most closely match those assumed to have existed in the rock by measuring the long and short axes to determine the ratios. For a primary shape which deviates from perfect ellipses, HOLST (1982) took the longest dimension as major axis measurements and the longest dimension perpendicular to the minor axis as the shortest axis. The Rf/ϕ technique has been applied on the *Kalkknoten* and lapilli in the present study. This method used a plot of $\log. Rf$, the final ellipse ratio against ϕ , the final long axis orientation of each ellipse.

Analysis: The study area is mainly occupied by the lapillituff (*Schalstein*: pyroclastics, hydroclastics and epiclastics) which shows up as turbidites (BEHNISCH 1993). Sedimentary rocks: *Kalkknotenschiefer* and *Adorf-Plattenkalk*, and lapillituff are deformed with a s1-cleavage which was developed as an axial cleavage in a fold. And, the s1-cleavage was folded later.

Table 4-1. Rf/φ analysis in the different rock types.

No.	Rock type-locality	Rs	Ri	θ
1	<i>Kalkknotenschiefer</i> : Ahausen (long limb)	3.4	2.0	54
2	<i>Kalkknotenschiefer</i> : Ahausen (short limb)	2.2	2.0	54
3	<i>Kalkknotenschiefer</i> : Ahausen (1 st phase)	3.4	2.0	54
	<i>Kalkknotenschiefer</i> : Ahausen (2 nd phase)		3.0	63
4	<i>Kalkknotenschiefer</i> : Ahausen (buckling)	3.2	2.0	54
5	<i>Kalkknotenschiefer</i> : Kirschhofen	4.4	2.0	54
6	Lapillituff: Kanapee	2.0	1.5	36
7	Lapillituff: Freienfels-Ernsthausen sub-area	2.7	1.75	36
8	<i>Mandelstein</i> : Freienfels-Ernsthausen sub-area	1.9	1.75	45

The results are shown in Table 4-1, in which the Ri/θ values are read off using the methods of TWISS & MOORES (1992) and LISLE (1985).

The Rf/φ analysis of lapillituff from the Freienfels-Ernsthausen sub-area, using lapilli as strain markers lying in the s1-cleavage, shows the strain ellipticity Rs = 2.7 and initial ellipticity Ri = 1.75, θ = 36°. The lapilli are primarily embedded in the fine ashtuff parallel to the bedding.

However, the Rf/φ analysis of lapillituff from the Kanapee anticline using lapilli as strain marker found lying in the bedding shows the same distribution as the lapillituff of the Freienfels-Ernsthausen sub-area, but the strain ellipticity Rs = 2.0 and its initial ellipticity Ri = 1.5 indicate less deformation than that of the Freienfels-Ernsthausen sub-area. In addition, sub-horizontal bedding with very faint cleavage indicating weak tectonic deformation is observed. In addition, lapilli showing the anastomosing boundary suggest prior compaction.

The Rf/φ analysis of Mandelstein (amygdaloidal basalt) of the Freienfels-Ernsthausen sub-area shows a strain ellipticity Rs = 1.9 and an initial ellipticity Ri = 1.75. Comparison of the Rs and Ri shows an almost undeformed state except the observation of pressure shadows around the *Mandels* (amygdales).

The Rf/φ analyses of the *Kalkknotenschiefer* from the Ahausen syncline show various fabrics in different structural positions of strain markers, e.g. *Kalkknoten*. The *Kalkknoten* are observed lying in the s1-cleavage, which are reoriented by s1-cleavage kinking, s1-cleavage wavy folding and the s1-cleavage buckling, respectively. In which, the Ri/θ values from different structural positions show the same, e.g. Ri = 2.0 and θ = 54°, and superimposed deformation, e.g. s1-cleavage kinking (s2-

cleavage), shows the $R_{i(D1)} = 3$ and $\theta_{(D1)} = 63^\circ$ (after D1-deformation). The R_s values range from 3.2 to 3.4, however, the strain from the short limb is about 2.2 (R_s).

The R_f/ϕ analysis on the *Kalkknotenschiefer* of the Kirschhofen syncline shows symmetrical fabrics in which the strain markers (*Kalkknoten*) are still lying in the bedding. Respecting the high R_s value of 4.4, the strain ellipse could be deformed by progressive pure shear conditions (cf. DUNNET & SIDDANS 1971), however, the R_i/θ value is the same as for the strain markers lying in the s1-cleavage of the Ahausen syncline.

The finite strain is oblate. Nevertheless, the R_i/θ values among the *Kalkknotenschiefer* of the different sub-areas are the same in the initial ellipticity $R_i = 2$ and $\theta = 54^\circ$ which indicates the same origin before s1-cleavage formation. Besides, the R_s values of the *Kalkknotenschiefer* indicate the different levels of deformation depending on their structural situations.

The asymmetrical distribution of the R_f/ϕ fabrics indicate the preferred orientation of the strain marker with respect to the *Kalkknoten* lying in the s1-cleavage (RAMSAY 1967), (see the R_f/ϕ diagrams of *Kalkknotenschiefer* of the Ahausen syncline and that of lapillituff of the Freienfels-Ernsthausen sub-area).

The R_f/ϕ diagrams of the Ahausen syncline show superimposed deformation with strain path which shows the combination of pure shear and simple shear (cf. LE THEOFF 1979, DUNNET & SIDDANS 1971, DUNNET 1969).

The orientation of strain ellipses of lapilli and *Kalkknoten* not only parallel with the s1-cleavage but also with the bedding shows the different deformation levels depending on pure shear and simple shear. The strain markers lying in the bedding plane show higher R_s value ($R_s = 4.4$) which indicates high strain. Suggestion can be done that the strain markers lying in the s1-cleavage plane were deformed by progressive simple shear, likewise the strain markers lying in the bedding were deformed by progressive pure shear (flattening strain).

4.1.2 Fry strain analysis

Method: The Fry method of strain determination is a graphical solution of the centre to centre point method which is both rapid and accurate and a clear answer of sufficient accuracy for the strain investigation, which can be seen from the developing graph. The centre to centre point method measures the distances between a centre point of a chosen object and the centre point of the nearest neighbouring object. By considering a rock with statistically uniformly distributed rounded objects, the type of packing will set up certain characteristic distances of the centres of neighbouring objects from any one chosen object. If the objects have identical radii, and the packing is perfect, this zonal repetition of the distances of the centres from any one centre will show regular periodic variations. The distances between object centres become modified in proportion to the value of the longitudinal strain along that direction, that is in proportion to strain ellipse diameters. Because the values of the periodic distance spacing change according to the strain ellipse shape, this geometry can be used to establish

the shape and orientation of this ellipse. For a series of redistributed originally anti-clustered points the Fry construction is as follows (FRY 1979, HANNA & FRY 1979):

1. On a sheet of paper mark the centres of all objects. Number these points.
2. Take a transparent overlay and mark a central reference point. Place this reference point over one of the central points in (1). Trace the position of all other points (2,3,4,---etc.) on the overlay.
3. Move overlay keeping a constant azimuth so that the overlay reference point lies over point (2). Trace the positions of all other points (2,3,4,5,----etc.) on the overlay.
4. Repeat for all other points on the base sheet. The points that accumulate on the overlay are not uniformly distributed.

Around the central overlay reference point there is a point vacancy, or a region which shows a very low point concentration. This can have a circular or elliptical form. The vacancy arises from the fact that any two original particles cannot come to lie closer than the sum of their radii. A circular vacancy field implies no strain, an elliptical vacancy field implies that the rock suffered strain. The shape and orientation of the strain ellipse are directly recorded by the elliptical form of the field. If no vacancy field is seen after a plot of some 50 separate moves of the overlay have been made this implies that the initial aggregate of points possessed a completely random arrangement. Under these circumstances no final solution can be found. The rock could be either unstrained or strained if its initial geometric configuration was controlled by a Poission distribution. This technique enables the bulk rock strain to be calculated using the redistribution of points in the deformed rock and the distances between these points as extended line elements.

The Fry method is applied in the present study area to quantify the strain from the deformed *Kalkknotenschiefer* and lapillituff.

Modified Fry methods can also be used in addition to the Fry method and are known as the normalized Fry method, enhanced Fry method, enhanced normalized Fry method, which are compatible with the computer program for FRY ANALYSIS, INSTRAIN (BRECHT 1995, ERSLEV & GE 1990, ERSLEV 1988).

Table 4-2. Measured normalized strain ratios on three studied sections through different rock types.

No.	Rock type and sample No.	X axis orientation	X axis	Y axis orientation	Y axis	Z axis orientation	Z axis
1	Limestone (Fe2)	060/40	3.7	330/5	1.3	240/50	1
2	Pillow fragments (Fe6)	145/45	2.0	210/15	1.2	304/15	1
3	Lapillituff (Fg10)	152/35	2.8	225/10	2.0	306/60	1
4	Lapillituff (Fe7)	144/43	2.0	060/5	1.6	314/50	1
5	Mandelstein (Fe3)	170/40	1.6	350/40	1.3	260/10	1
6	Pillow Lava (P3)	150/55	3.6	230/5	2.0	330/40	1

Analysis: Measurements are made at three sections: XZ, XY and YZ which are prepared by thin-sections. All the section-planes are measured by Fry-method for R_s and ϕ . Then, using the TRISEC program (MILTON 1980) the shape and attitude of ellipsoids in terms of principal axes: X, Y and Z can be calculated (Table 4-2). Those results are used in the correlation between the strain and the AMS (Table 7-3), (see Chapter 7).

4.1.3 STRAIN ELLIPSE (R_f/ϕ) IN XZ-SECTION

The R_f/ϕ strain analysis in different structural units, using the XZ plane for the greatest initial shape and tectonic strain, is related to the style of folding indicating the different phases which are experienced in the tectonic movement. The strain path in the R_f/ϕ diagrams is observed from pure shear to simple shear or simple shear to pure shear.

(A) **Ahausen syncline** (see Fig. 4-3): The Ahausen syncline is occupied by Upper Devonian *Kalkknotenschiefer* mainly, which are deformed to asymmetrical folds. The R_f/ϕ analysis is done in the XZ plane by using *Kalkknoten*. The long axis of the principal finite strain ellipse is parallel to the s1-cleavage. In addition, the s1-cleavage was folded to be formed s2-cleavage (crenulation fold).

The R_f/ϕ diagram of Fig. 4-2A shows that points are dispersed, which is from the long limb of a fold without s2-cleavage. In that the R_f/ϕ fabrics shows the asymmetry, indicating the further increment of simple shear during s1-cleavage formation. The ellipsoids are generated from the boudins which are primarily formed lying in the bedding plane.

Fig. 4-2. R_f/ϕ 2-D strain analysis diagrams of the Weilburg area.

A. Diagram of <i>Kalkknotenschiefer</i> of the Ahausen syncline: measurement on XZ plane at the s1-cleavage on long limb of fold.	page 44
B. Diagram of <i>Kalkknotenschiefer</i> of the Ahausen syncline: measurement on XZ plane at the s1-cleavage on short limb of fold.	page 45
C. Diagram of <i>Kalkknotenschiefer</i> of the Ahausen syncline: measurement on XZ plane with s2-cleavage at the s1-cleavage on long limb of fold.	page 46
D. Diagram of <i>Kalkknotenschiefer</i> of the Ahausen syncline: measurement on XZ plane with s2-cleavage (kink folding) at the s1-cleavage on long limb of fold.	page 47
E. Diagram of <i>Kalkknotenschiefer</i> of the Kirschhofen syncline: measurement on XZ plane at the bedding (s0).	page 48
F. Diagram of lapillituff of the Kanapee anticline: measurement on bedding (s0) at lineation (l1), (XY plane at bedding).	page 49
G. Diagram of lapillituff of the Freienfels-Ernsthausen sub-area: measurement on XZ plane at the s1-cleavage.	page 50
H. Diagram of <i>Mandelstein</i> (amygdaloidal lava) of the Freienfels-Ernsthausen sub-area: measurement on XZ plane at the s1-cleavage.	page 51

Fig. 4-2A.

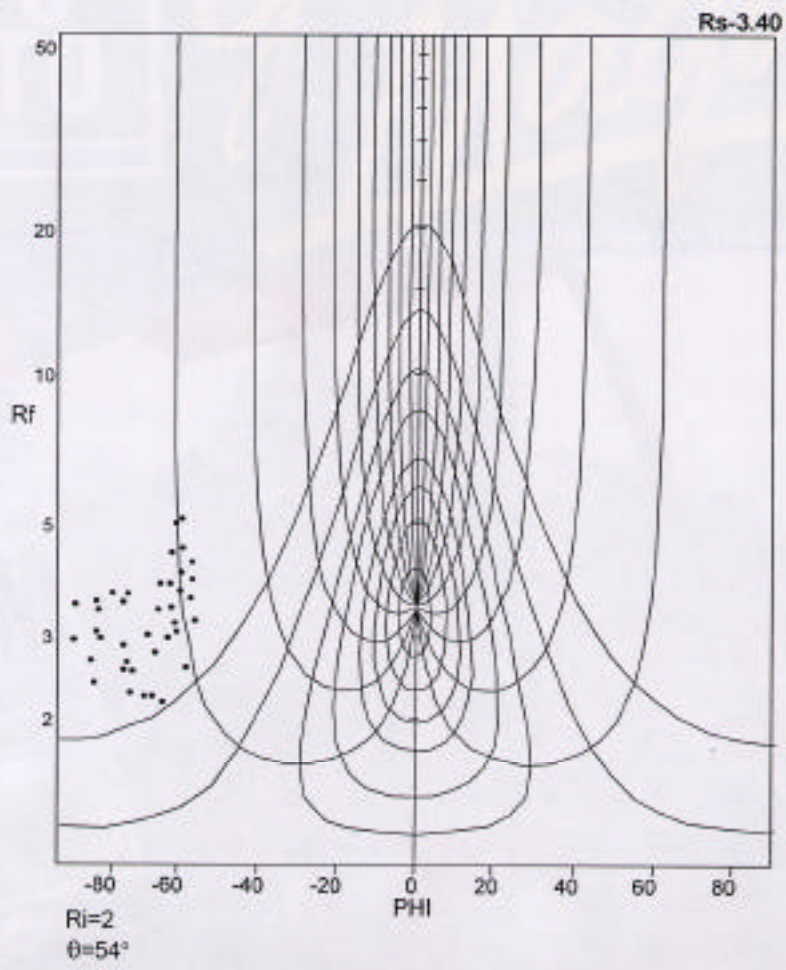


Fig. 4-2B.

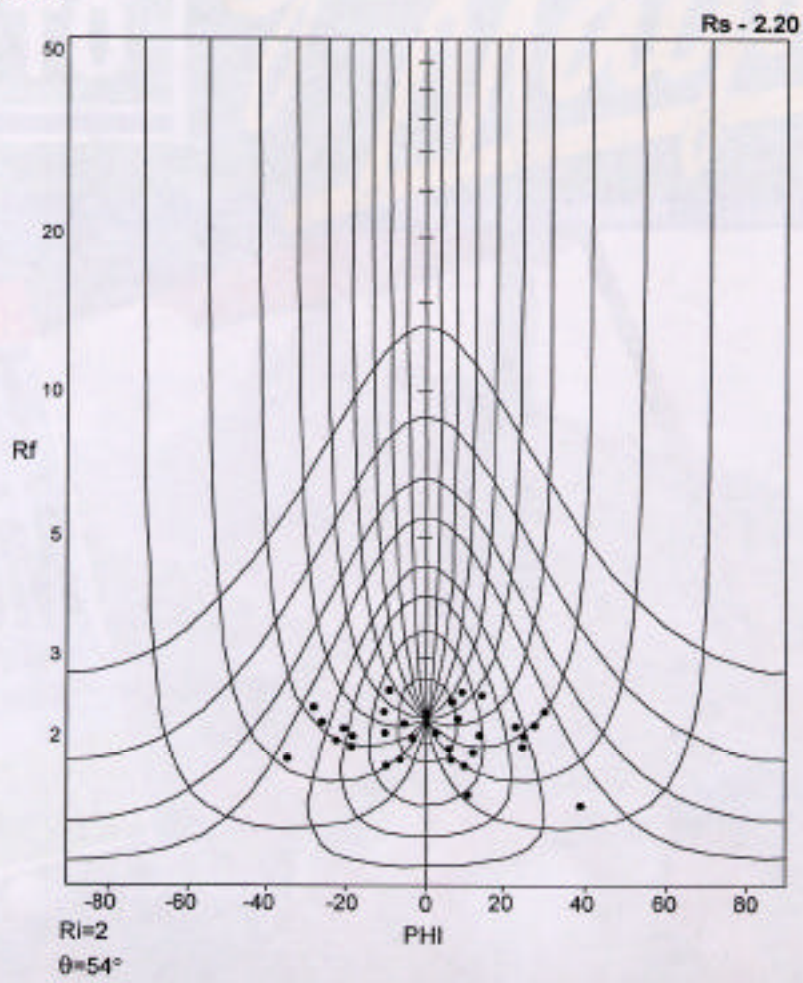


Fig. 4-2C.

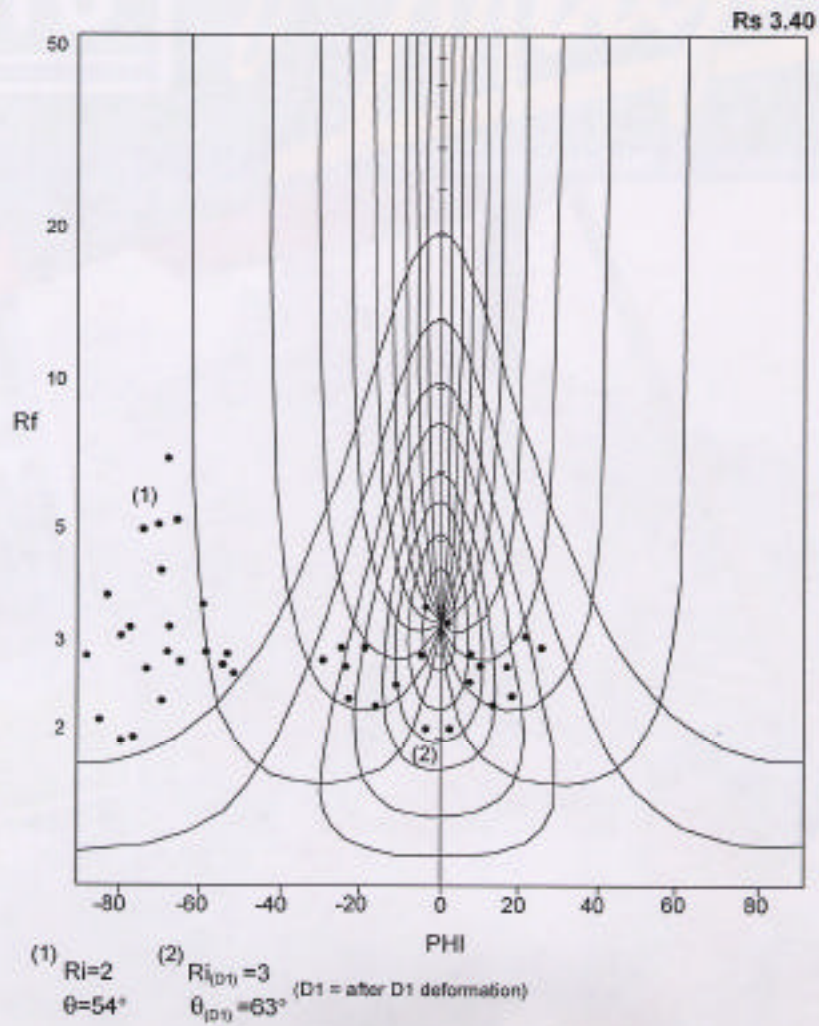
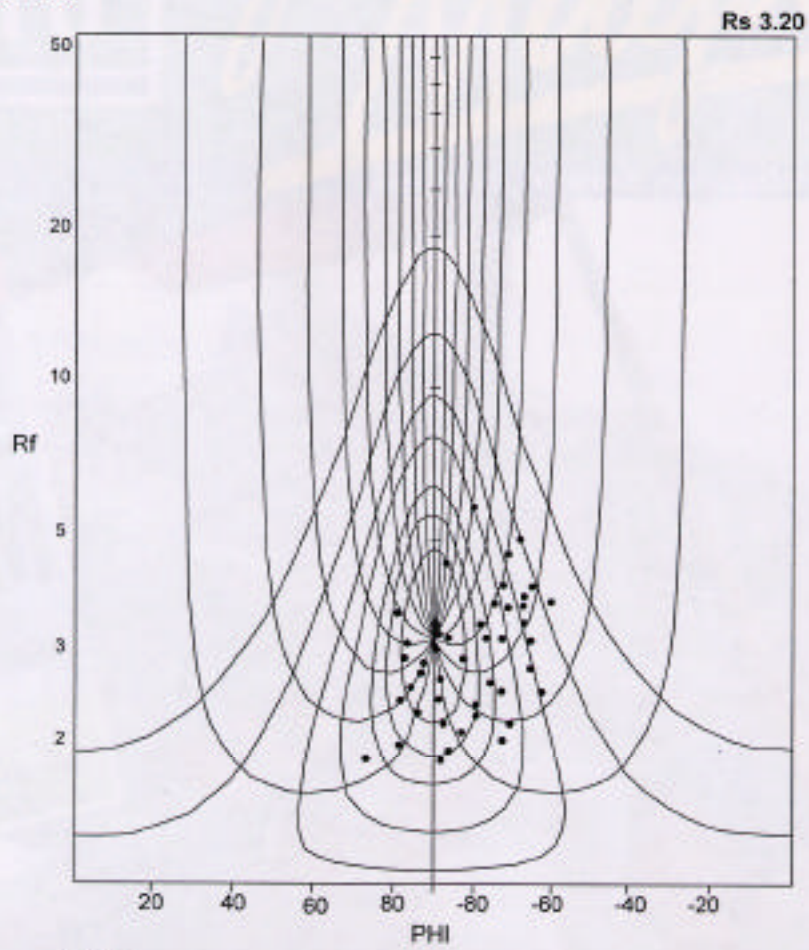


Fig. 4-2D.



$R_i=2$
 $\theta=54^\circ$

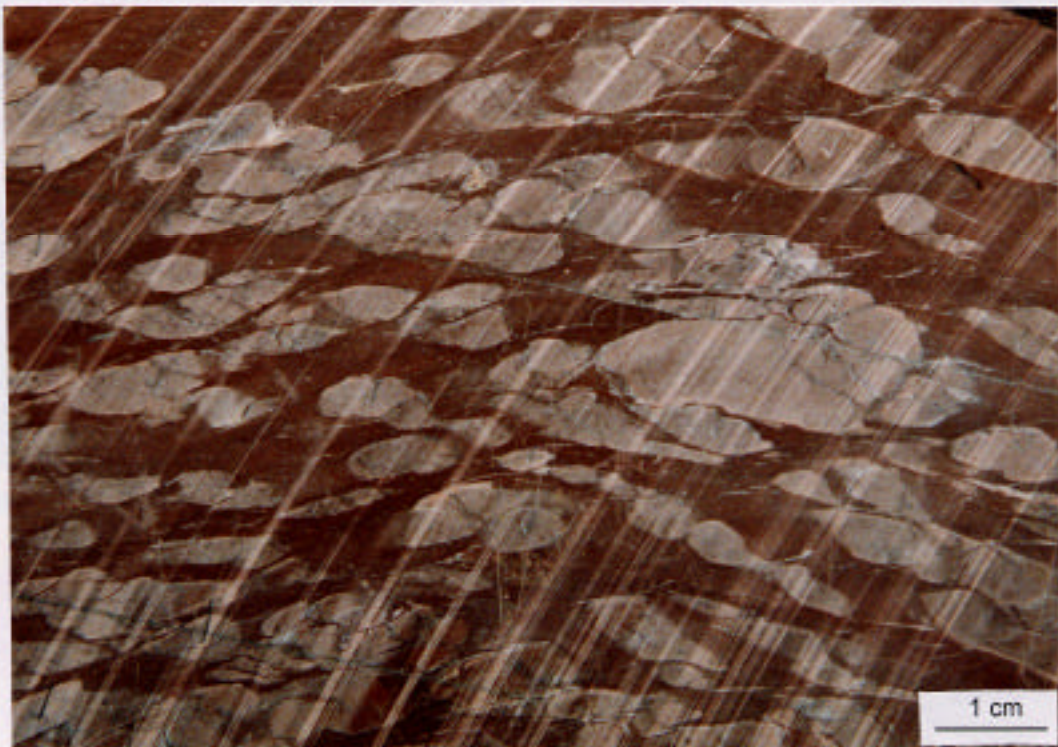


Fig. 4-2E.

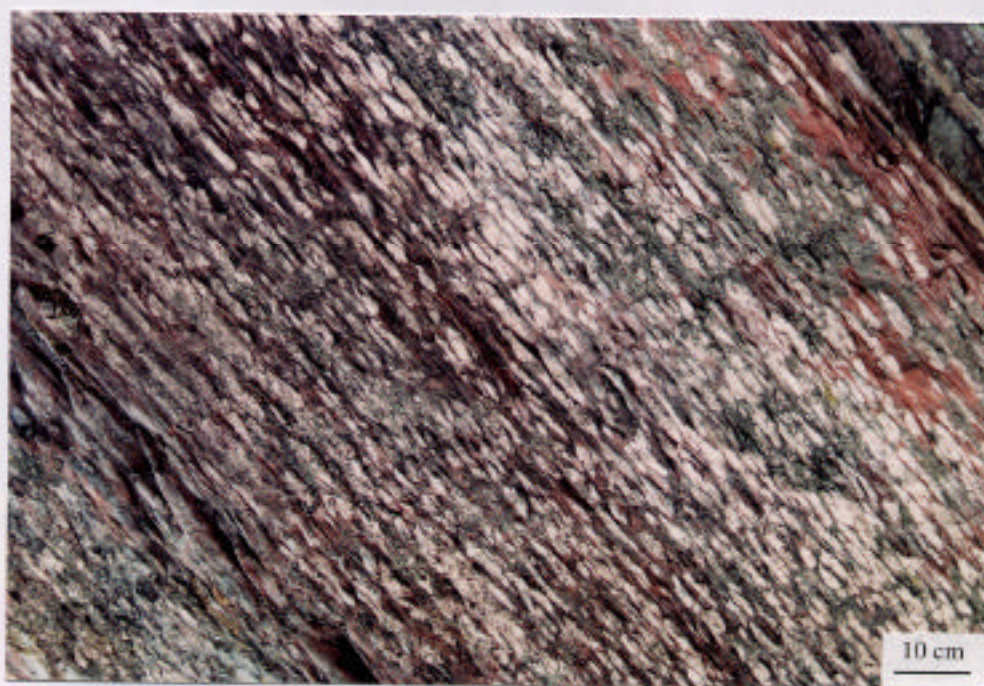
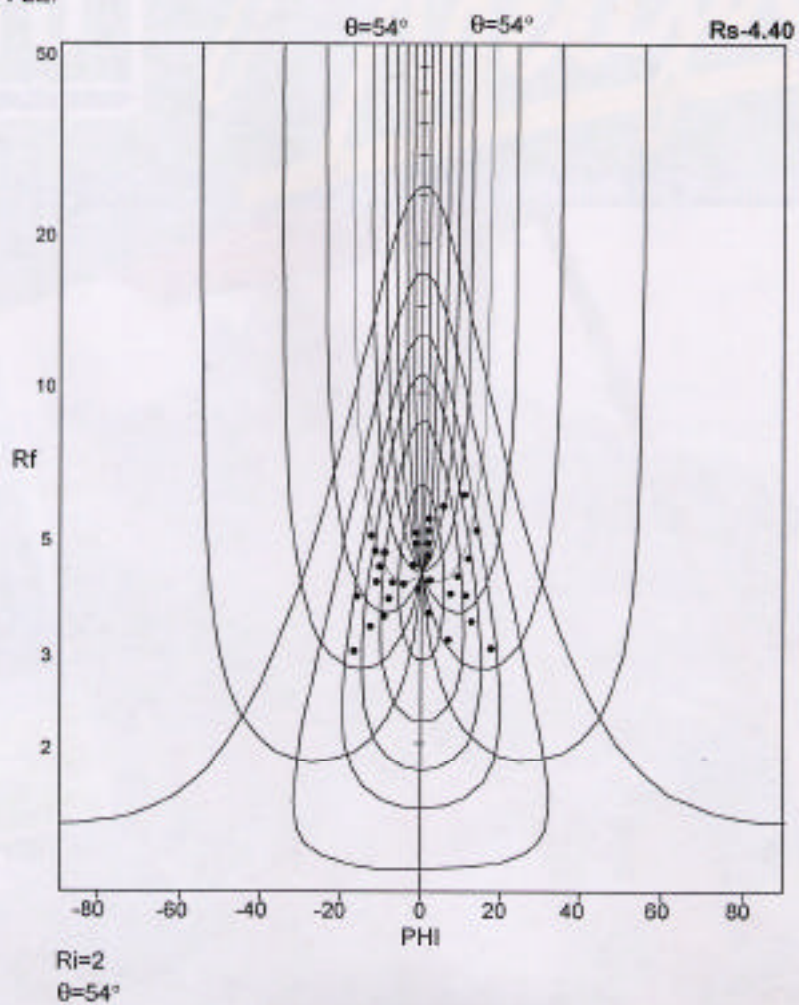


Fig. 4-2F.

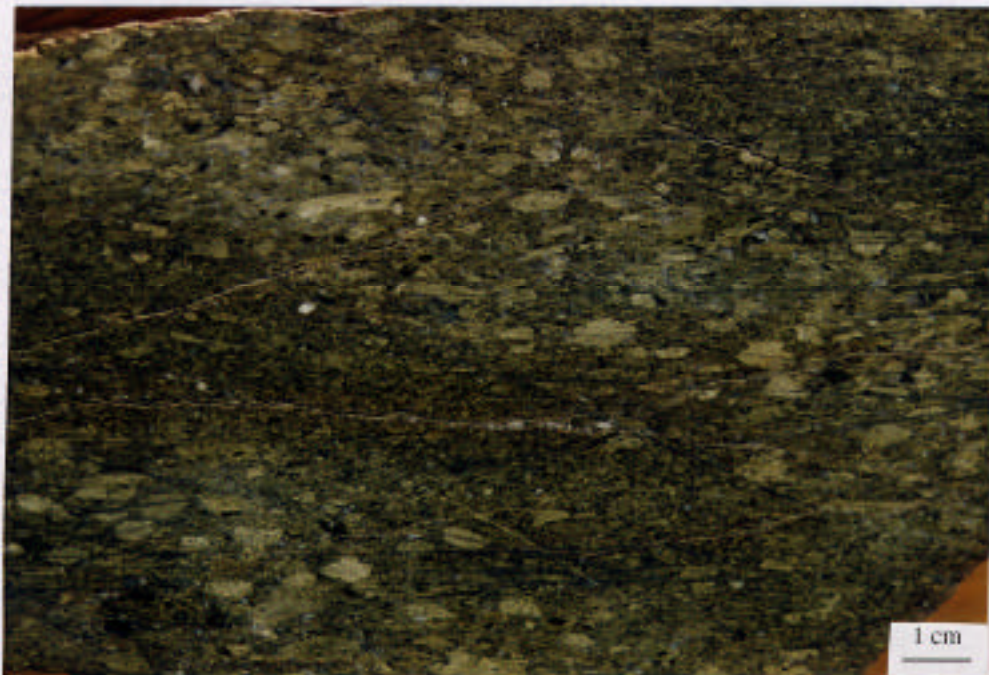
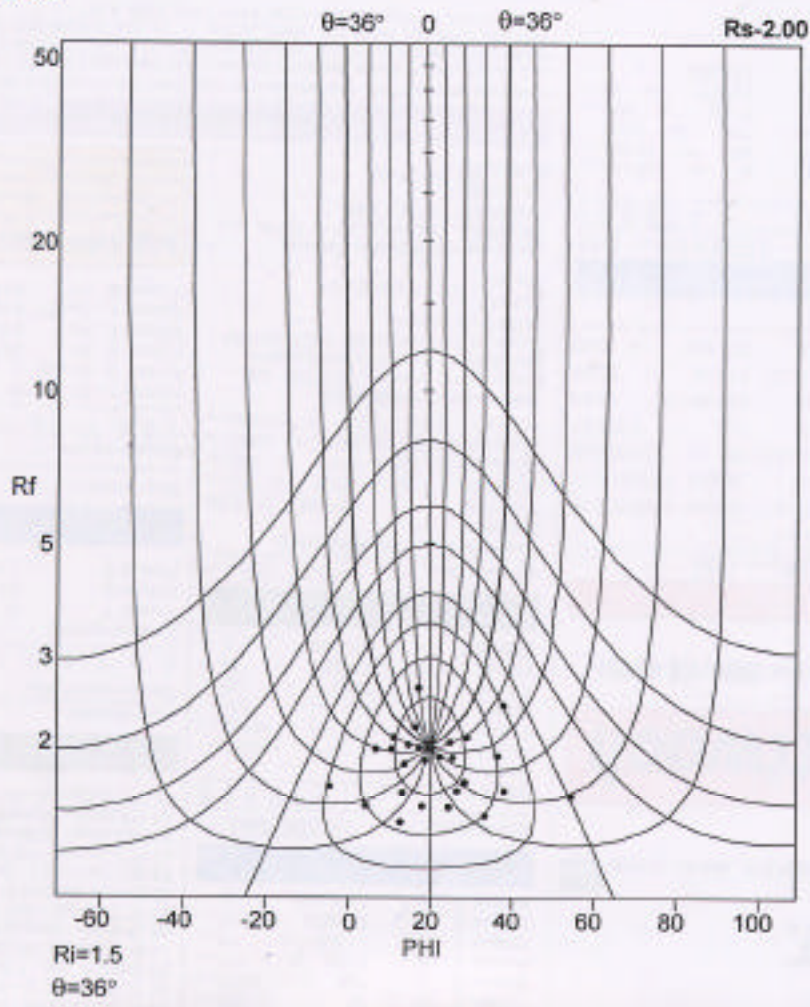


Fig. 4-2G.

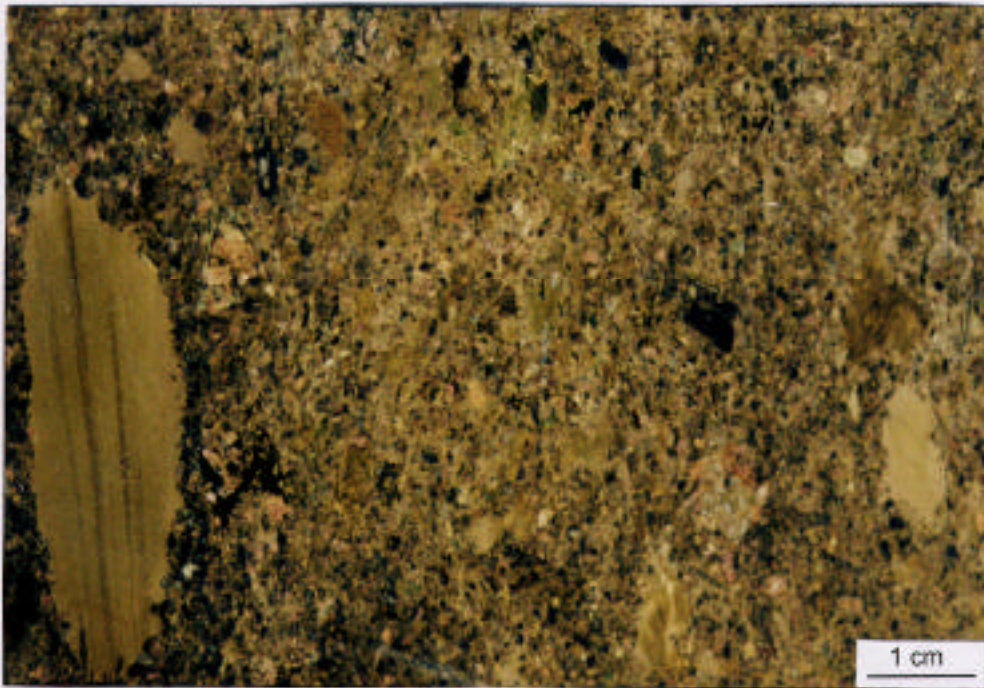
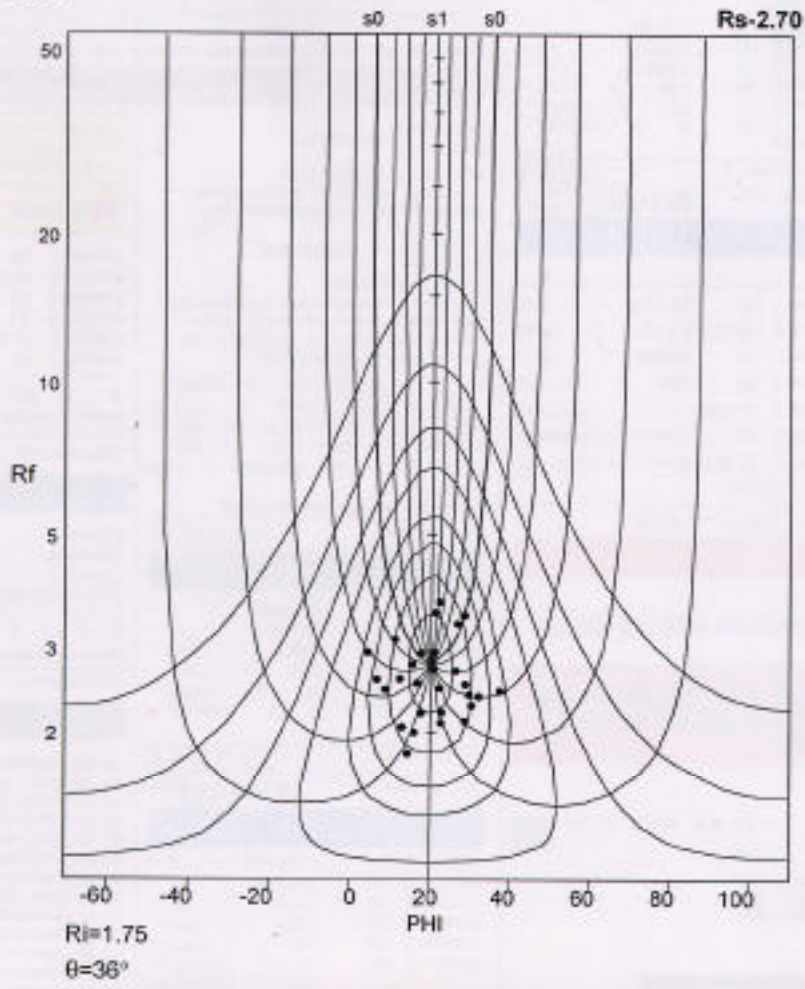
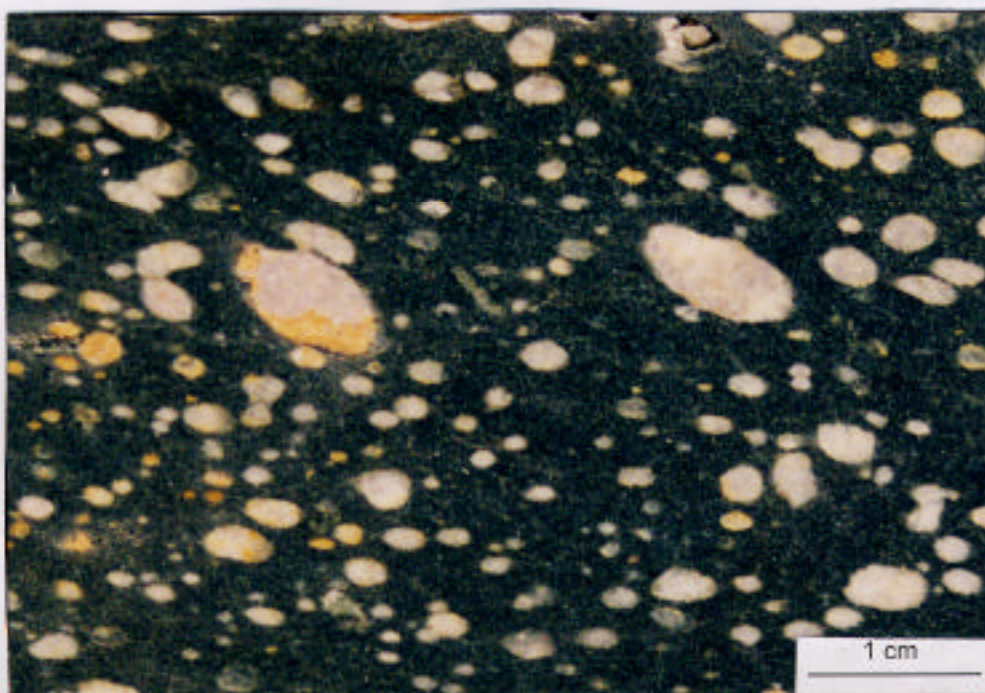
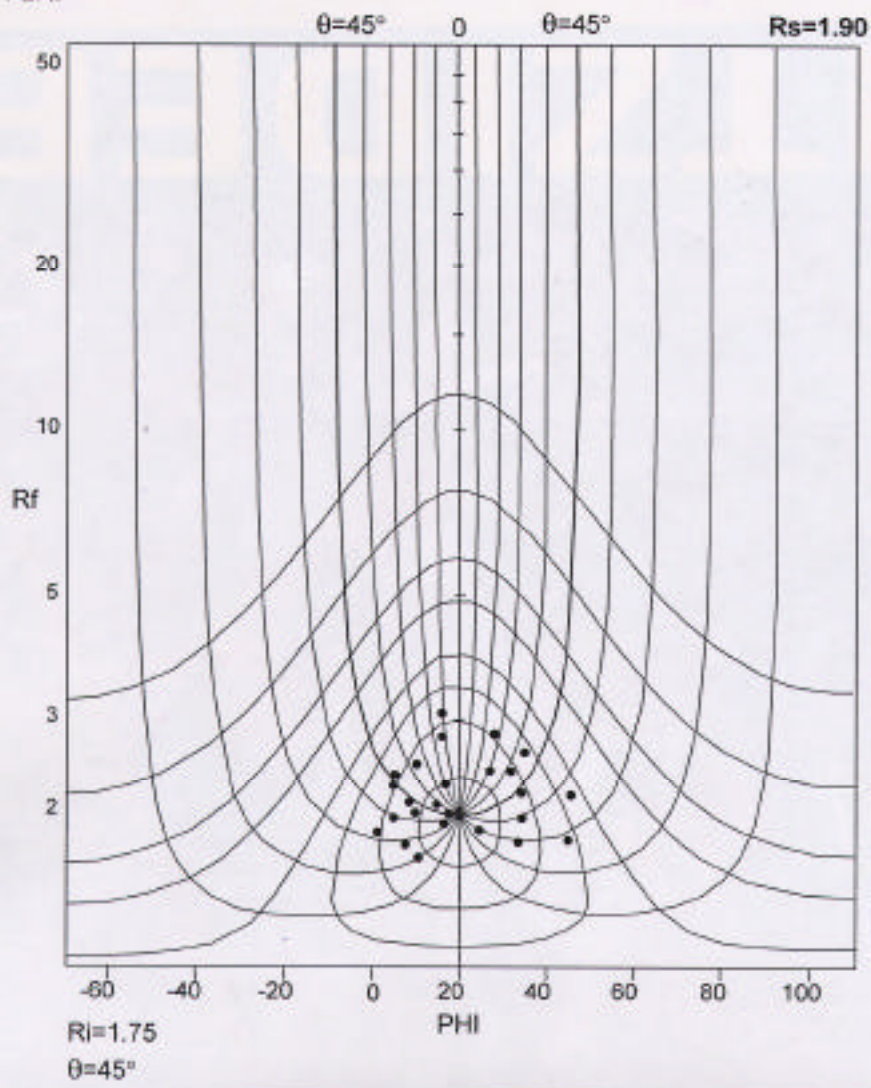


Fig. 4-2H.



The Rf/ϕ diagram of Fig. 4-2B shows symmetry fabrics which represent the short limb of an asymmetrical fold. The s1-cleavage plane is wavy folding because of its small local folds on the short limb (cf. GHOSH 1993). The long axis of strain ellipses on the XZ plane follow the s1-cleavage trace. The cluster of points lying on the θ applies the orientation (RAMSAY 1967). The Rf/ϕ fabric shows the symmetry suggesting the homogeneity of the strain ellipse, however, points are randomly orientated (cf. RAMSAY 1967). In this case, X and Y axes are nearly the same ($X = Y$).

The Rf/ϕ diagram of Fig. 4-2C which represents the s1-cleavage and the s2-cleavage (s1-cleavage kinking) shows two clusters of points (cf. superposed deformation by LE THEOFF 1979): one is totally dispersed which indicates the further increment of simple shear during the s1-cleavage formation; the other one is symmetrically distributed, which indicates the s2-cleavage in the embryonic stage of kinking (superposed strain deformation).

The Rf/ϕ diagram of Fig. 4-2D represents the folded s1-cleavage on the long fold limb and shows high dispersion which indicates the same as figure (4-2B), however, it is only a folding of the s1-cleavage, which is not as tight as in Fig. 4-2B.

These results can be concluded as: (1) 50 % shortening normal to the axial plane of fold (cf. TWISS & MOORES 1992), (2) layer-parallel shear with s1-cleavage formation, and (3) progressive simple shear with s1-cleavage folding by the further increment of deformation (Plate 12A). The deformation in the Ahausen syncline can be interpreted as representing two phases: (1) Variscan deformation together with the s1-cleavage formation, and (2) s1-cleavage folding (s2-cleavage: indicating F2) by the tectonic movement during the late Variscan.

(B) **Kanapee anticline** (Fig. 4-3): The Kanapee anticline consists of a tight fold in the SE and an open anticline in the NW, in which the s1-cleavage is well developed in incompetent beds. The strain ellipse (lapilli) was determined in the XY plane. The strain ellipses lie in the bedding plane and parallel to the fold axis. The same case is observed near the Freienfels at the junction of two sub-areas in the Freienfels-Ernsthausen sub-area where epiclastics (limestone fragments) parallel to the regional trend (Fig. 4-6).

The Rf/ϕ diagram shows an asymmetrical distribution (Fig. 4-2E). According to the field observation, the area was not highly deformed during the s1-cleavage formation. Perhaps, the area was shielded by its basin condition constituting a synthetic half-graben (see Chapter 6), (Fig. 6-4). Microscopically, no deformations can be observed, however, the rock just shows evidence of compaction (Fig. 4-2E) by the anastomosing boundary on clastics. In the corresponding AMS study, (see Chapter 7) L-F diagram (Flinn-diagram) shows plain strain ($k = 0$).

(C) **Kirschhofen syncline** (Fig. 4-3): The Kirschhofen syncline is occupied by Adorf-*Plattenkalk* and *Kalkknotenschiefer* in which the principal strain ellipses parallel to the bedding. The Rf/ϕ diagram shows symmetrical fabrics (Fig. 4-2F) which indicate pure shear deformation. This syncline (Fig. 4-3) shows a transition from vertical tight folds in the SE to overturned folds in the NW (flexural-slip folding). The R_s value shows relatively high strain among the *Kalkknotenschiefer* of the Weilburg area, perhaps indicating superposed flattening deformation on strain ellipses. Thus, the strain ellipses lying in the bedding indicate to be primarily generated in the bedding.

(D) **Guntersau syncline** (Fig. 4-3): The Guntersau syncline is made up of *Kalkknotenschiefer* in which the strain ellipses lie in the bedding. Shearing along the s_1 -cleavage plane (cf. BURG et al. 1981) is shown by the asymmetrical augen structures as a rigid body rotation (cf. NICOLAS 1987), which could mark an embryonic stage of the rotational strain deformation.

(E1 and E2) **Guntersau-Freienfels-Ernsthausen sub-area** (Fig. 4-3): The Guntersau-Freienfels-Ernsthausen sub-area is mainly composed by lapillituff and sheet flow lava, mostly *Mandelstein*. Generally, the principal strain ellipses in the XZ plane are found lying in the s_1 -cleavage. The Rf/ϕ diagrams of both lapillituff and sheet flow lava show a dispersion, lying asymmetrical in the s_1 -cleavage (Fig. 4-2G). The Rf/ϕ diagram of the sheet flow lava, using *Mandels* (amygdales) as strain markers shows asymmetrical distribution in the s_1 -cleavage as well (Fig. 4-2H). Thus, both lapillituff and sheet flow lava have a preferred orientation (Ramsay 1967) by the s_1 -cleavage formation.

4.2 DETERMINATION OF 3- DIMENSIONAL STRAIN

Three-dimensional (3-D) strain analysis was carried out at road-cut profiles along the Weil and Lahn valleys (Fig. 4-3), using ellipsoid-shaped *Kalkknoten* and lapilli (Plates 13 and 14) as strain markers which are lying in the s_1 -cleavage and in the bedding, an irregular anastomosing planar fabric. In most instances, the s_1 -cleavage lies at a low angle of about 30° to the bedding on a fold limb, almost irrespective of fold tightness.

4.2.1 Results

Three-dimensional finite strain data determined from different sites in terms of local sub-areas in the Weilburg area (Fig. 4-3) are shown in stereoplots (Fig. 4-4) and Table 4-3, (the parameters of individual ellipsoids directly measured). The measured strains appear not to be influenced by the later deformation, however, s_2 -cleavage fabric was observed as s_1 -cleavage folding (crenulation fold). The XY plane of the principal finite strain ellipsoid is generally parallel to the s_1 -cleavage, but in the s_2 -cleavage (crenulation fold) the ellipsoids change their orientation.

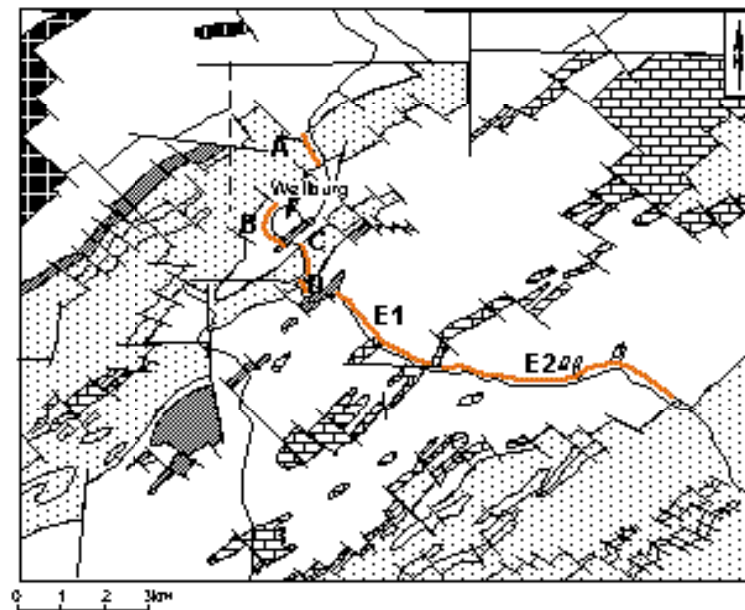
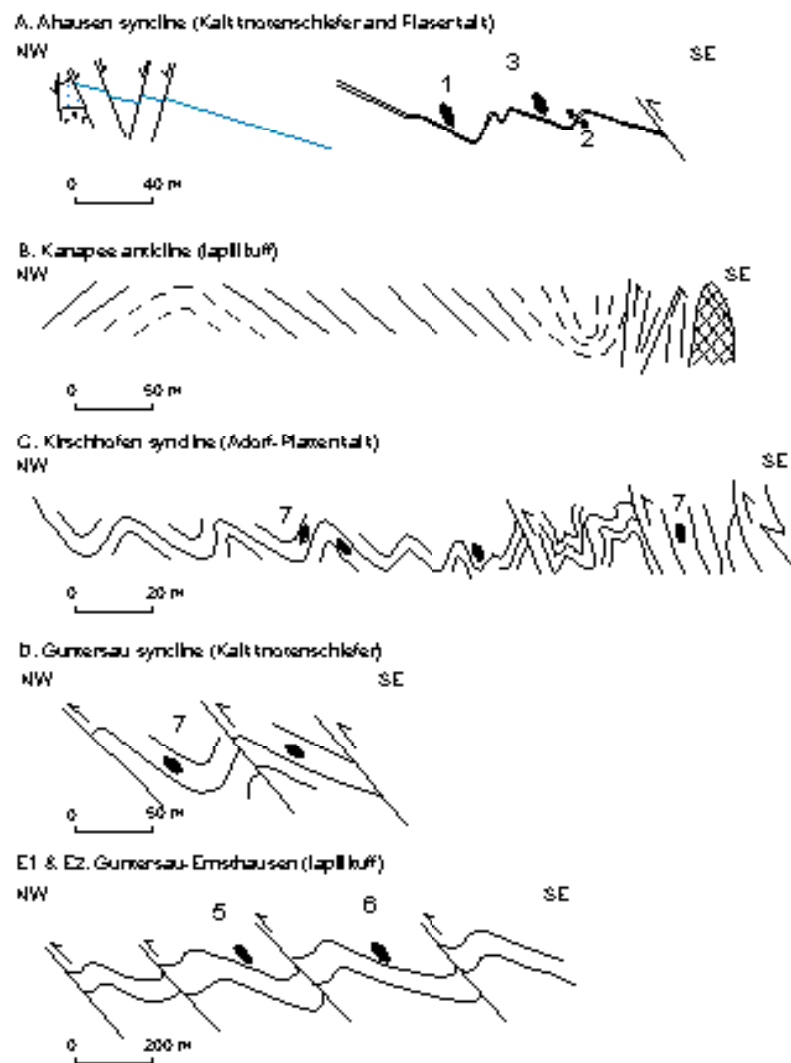


Fig. 4-3. Index map for orientation of sections and localities of determined strain ellipsoids. P profiles are referred to road-cut section. *Ellipse Numbers* in table 4.3. (Symbol descriptions of geol. map in Fig. 2.3)

Table 4-3. Finite strain data from strain markers of Kalkknoten and lapilli. $X>Y>Z$ are the principal axes of the finite strain ellipsoid.

No.	s0	s1	Orientation of axes			Length of axes (cm)			XY	YZ	Position of ellipsoid (XZ-plane)	Location and rock type
			X	Y	Z	X	Y	Z				
1	030, 23	122, 57	122, 57	033, 3	305, 33	4.3	2.5	1.0	1.72	2.5	s1	Ahausen (Kalkknotenschiefer)
2	310, 45	156, 55	156, 55	045, 10	315, 35	2.5	2.5	0.6	1.0	4.1	s1	Ahausen (Kalkknotenschiefer)
3	140, 26	165, 65	165, 65	264, 2	345, 25	2.0	1.5	0.5	1.3	3.0	s1	Ahausen (Kalkknotenschiefer)
4	-	140, 45	140, 45	210, 15	304, 15	22.0	14.0	11.0	1.6	1.2	s1	Edeberg (epiclastics)
5	-	144, 43	144, 43	060, 5	314, 50	17.0	12.0	5.6	1.4	2.1	s1	Essershausen (lapillituff)
						9.0	5.5	2.5	1.6	2.2	s1	Essershausen (lapillituff)
6	-	152, 35	152, 35	225, 10	306, 60	2.8	2.8	1.5	1.0	1.8	s1	Guntersau (lapillituff)
						8.0	5.5	3.5	1.4	1.5	s1	Guntersau (lapillituff)
7	120, 54	160, 82	160, 82	208, 3	300, 35	3.5	3.5	0.5	1.0	7.0	s0	Kirschhofen syncline (Kalkknotenschiefer)
									0.01	1.0	s1	Kirschhofen syncline (Kalkknotenschiefer)
8	-	150, 42	060, 40	330, 5	240, 50	37.1	12.2	9.5	2.9	1.1	l1	Freienfels (epiclastics) (see Fig. 47)
									0.3	3.4	s1	Freienfels (epiclastics)

N.B.
s0 = bedding, s1 = cleavage, l1 = lineation

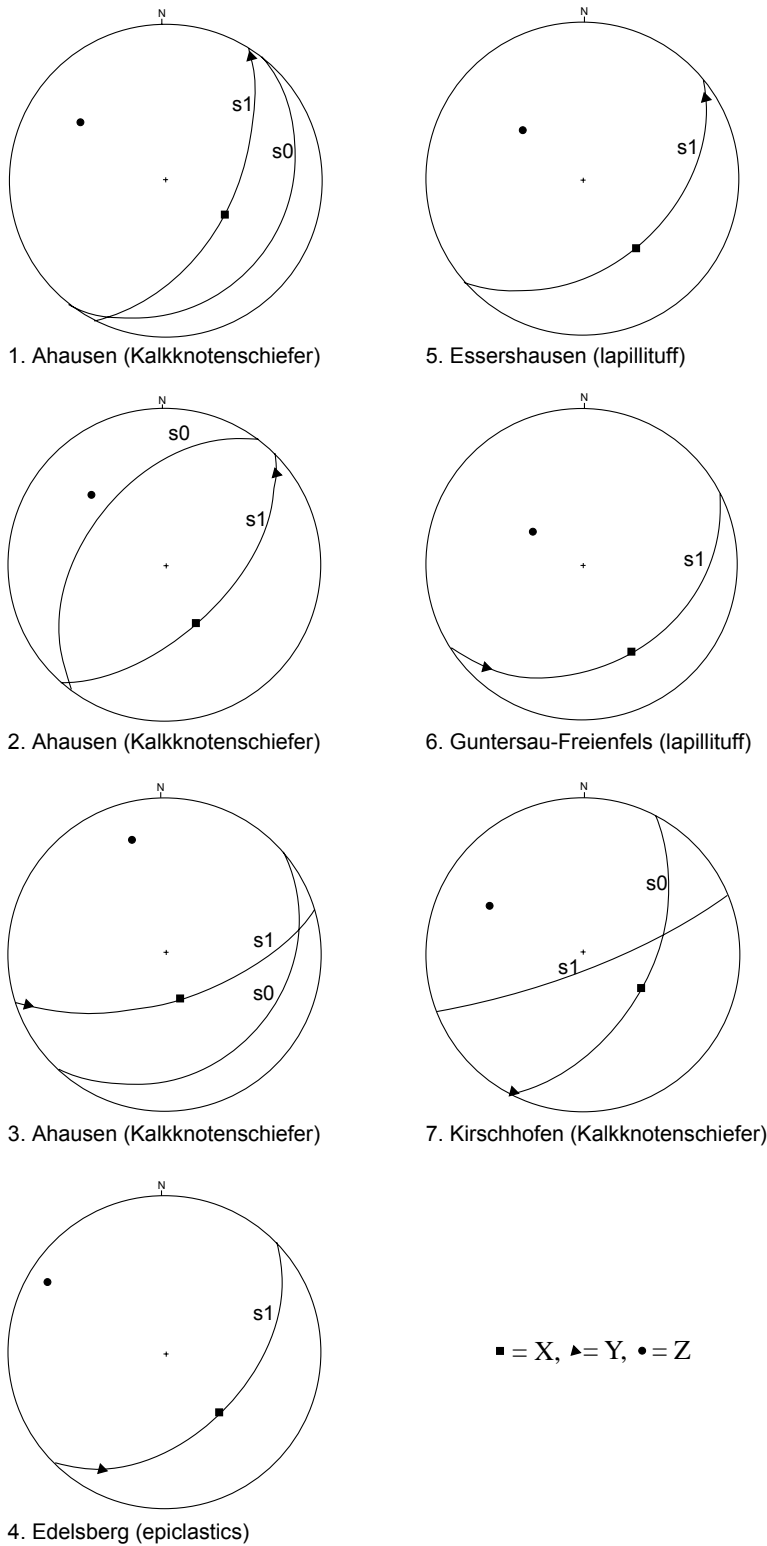


Fig. 4-4. Strain axes orientation in stereoplots (lower hemisphere) for the Weilburg area (see details in Table 4-3 and Fig. 4-3).

In the Flinn-diagram, the strain ellipsoids come to lie almost all in the flattening field (Fig. 4-5B). The angle of plunge (see Table 4-3) of the maximum elongation direction (X axes) varies from 55 - 65°. The intermediate Y axes show an average plunge about 3 - 15°, i.e. almost horizontal, whereas the minimum elongation Z axes are generally moderate plunge about 15 - 60°.

The finite strain is presented graphically by drawing the shape of XY-principal plane of strain ellipses on the map (Fig. 4-3). In the Figure 4-3, there is a tendency for the maximum elongation direction, the X axes, to align sub-perpendicular with the regional structural trends (fold axis traces). The intermediate Y axes are generally sub-horizontal with a variable plunge as the angle of plunge is shown beside the corresponding ellipse. The shapes of the XZ-principal plane of strain ellipses are presented in cross section, depending on the orientation of the X axes (sub-parallel to the profile).

The maximum elongation X axes of strain markers from the Kirschhofen syncline are lying in the bedding sub-perpendicular to the regional trend. Also that of epiclastic strain markers near Freienfels lying in the intersection lineation are parallel to the regional trend. In addition, the *Kalkknotenschiefer* (finite strain ellipsoids) show two orientations: parallel to the bedding plane and parallel to the s1-cleavage plane.

Discussion: In the *Kalkknotenschiefer*, *Kalkknoten* were rotated from the bedding to the s1-cleavage, first acting as rigid strain markers. Later, they were plastically deformed, reflecting a passive strain, undergoing stretching along the s1-cleavage by progressive simple shear (dextral shear sense: Plate 12).

In the lapilituff, lapilli are deformed constituting a passive strain ellipsoid (passive marker), (e.g. INGLES 1983). The original shape of lapilli have been elliptical or circular or irregular being deformed within the shear zone with respect to layer-parallel shear (Plate 14A), simultaneously undergoing either contractions or extensions perpendicular to the walls (cf. INGLES 1983 and RAMBERG 1975) by sub-horizontal position of the Y axis (Table 4-3).

Thus, rotational strain may generally have taken place in both coaxial and non-coaxial bulk deformations under pure shear, simple shear, and combined pure and simple shear (Plate 12).

4.2.2 Strain ratio plot (Long-short axes plot)

The strain ratio plots on the long X-axis and short Z-axis are shown in a diagram (GHOSH 1993, LISLE 1985, LANGHEINRICH 1976, ELLIOTT 1970, RAMSAY 1967, CLOOS 1947), (Fig. 4-5A), using the 3-D analysis data for the whole area including the *Kalkknotenschiefer* and the lapilituff.

In the Figure 4-5A, all points (Table 4-3) from the different sub-areas of the whole area are plotted. The best-fit for the cluster of points is represented by a line through the origin. The slope represents a strain ratio of about 3.7 indicating plastic deformation (cf. LISLE 1985, WOOD & HOLM 1980 and BOUCHEZ 1977).

Thus, the deformation of the whole area is generally homogeneous except for cobble sized epiclastic fragments (pillow lava), (Plate 15) which are out of the best-fit line (Fig. 4-5A) to be heterogeneous deformation (cf. WOOD & HOLM 1980 and BOUCHEZ 1977).

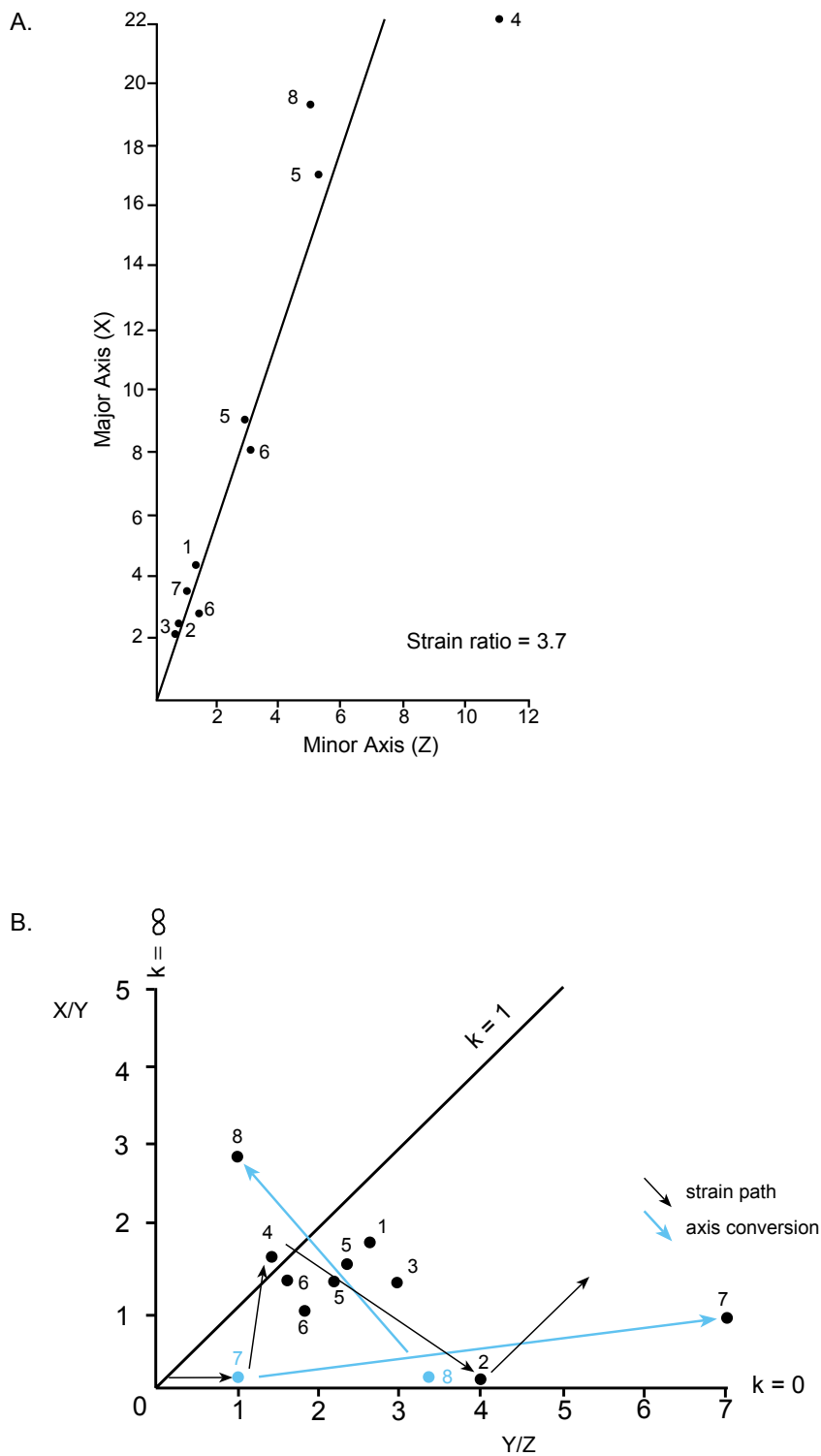


Fig. 4-5. A: Plot of the length of major (X) and minor (Z) axes of the deformed objects, (slope of the line (the best-fit line of cluster points) gives the average strain ratio), B: Plot on the Flinn-diagram (X/Y vs Y/Z) with strain path on k-values. (Plot-numbers: see Table 4-3 or 4-4)

The cobble sized epiclastic fragments show constrictional strain (Fig. 4-5B) which is comparable to the cobbles deformation of MOSHER (1987): regarding the orientation of the original long X axes rotated toward parallel to the fold axes to become final X axes, the strain of the bulk conglomerate is constrictional.

4.2.3 Plotting in Flinn-diagrams

Method: The method of representing ellipsoidal shapes in graphs was first suggested by ZINGG (1935) as a way of analyzing the shapes of *Kalkknoten* in the *Kalkknotenschiefer*. Its full potential as a tool for structural analysis was realized by FLINN (1962, 1978), and the method has since become known as the Flinn method. It is achieved by plotting the ratios of the major axes to the intermediate ellipsoid axes R_{xy} as ordinate against the ratios of the intermediate to the minor axes R_{yz} abscissa. The origin of the graph is not the point (0, 0) but the point (1, 1) because R_{xy} and R_{yz} values less than unity cannot exist, by definition. The plot arranges ellipsoids according to their shape. The origin represents a spherical shape. the ellipsoids are sorted into a range of shapes varying continuously from oblate along the ordinate to prolate along the abscissa and at the same time according to increasing distance from spherical shape with increasing distance from origin. Flinn suggested the parameter k to describe the general position of the ellipsoid in plot. The k value is defined as $k = R_{xy} - 1 / R_{yz} - 1$. This represents the tangent of the angle θ between the abscissa axis and the line joining a point P in the graph and the point (1, 1). Ellipsoids with k values lying between zero and unity have more or less pancake forms (oblate ellipsoids), and where $k = 0$ the form becomes uniaxial parallel to the pancake shape. Those ellipsoid plots with k values lying between unity and infinity have general elongated, cigar-like forms (prolate ellipsoids), which, where $k = \infty$, are uniaxial, parallel with the cigar axis. In this case, the parameter k divides the constant volume ellipsoid into five types:

$k = 0$	Uniaxial oblate type
$1 > k > 0$	Flattening type
$k = 1$	Plain strain type
$\infty > k > 1$	Constriction type
$k = \infty$	Uniaxial prolate type.

The Flinn method is applied on the deformed *Kalkknotenschiefer* and lapillituff of the Weilburg area, Lahn syncline.

Axis conversion for plotting in the Flinn-diagram: The maximum long X-axis of the strain marker may lie in the s_1 -cleavage, on the other hand, it may lie in the bedding or in the lineation (parallel fold axis). If the strain marker is oriented in the s_1 -cleavage, it has to be considered that its original position had been more or less in the bedding plane due to the compaction. During the s_1 -cleavage formation, it was rotated or reoriented into the s_1 -cleavage, thus, it should be considered as a part of the rotational phenomena. In the study area, the strain ellipsoids are mostly lying in the s_1 -cleavage but the strain markers lying in the bedding plane are used as a reference. Thus, the strain markers in the s_1 -cleavage must have changed their strain axes in their plotting. There are two cases:

Case (1) changes from X-axis to Z-axis, and also Z-axis to X-axis (lying in the s1-cleavage): In other words, the X-axis became Z-axis position, and also the Z-axis became X-axis position (cf. see detailed in Fig. 4-6) during the rotation of the strain markers (SANDERSON 1976, RAMSAY & WOOD 1973, RAMSAY 1967) figured out by the rotation mechanism of SCHWERDTNER (1973), (Fig. 4-6B).

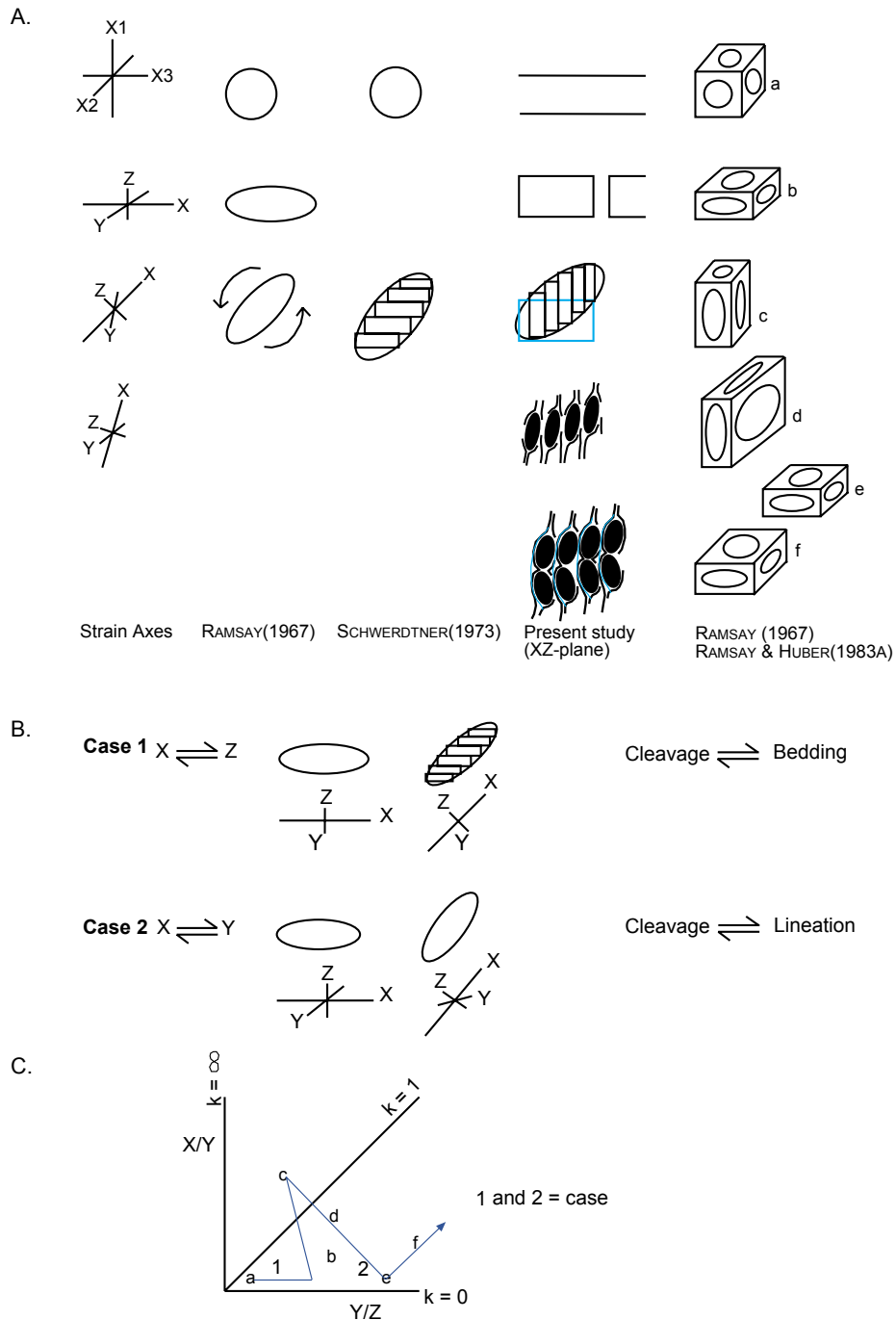


Fig. 4-6. Comparison of strain ellipsoid formation with different observations of deformation (A) and conversion of strain axes rotation (B) plotting on the Flinn-diagram (C) with strain path indicated.

Case (2) changes from X-axis to Y-axis, and also Y-axis to X-axis (parallel to the fold axis): It approximately seems to be a pencil-cleavage formation (GHOSH 1993, RAMSAY & HUBER 1983A), (Fig. 4-6 & 4-7). The pencil cleavage results from a planar fabric (MAZZOLI 1995, GHOSH 1993, RAMSAY & HUBER 1983A) giving way to a linear pencil structure, also sub-parallel to the fold axis. According to RAMSAY & HUBER (1983A) the pencil cleavage represents a linear fabric element associated with a prolate finite strain in the material, whereas this pencil cleavage is resulting from the combination of diagenetic compaction and related tectonic strain (cf. MAZZOLI & CARNEMOLLA 1993).

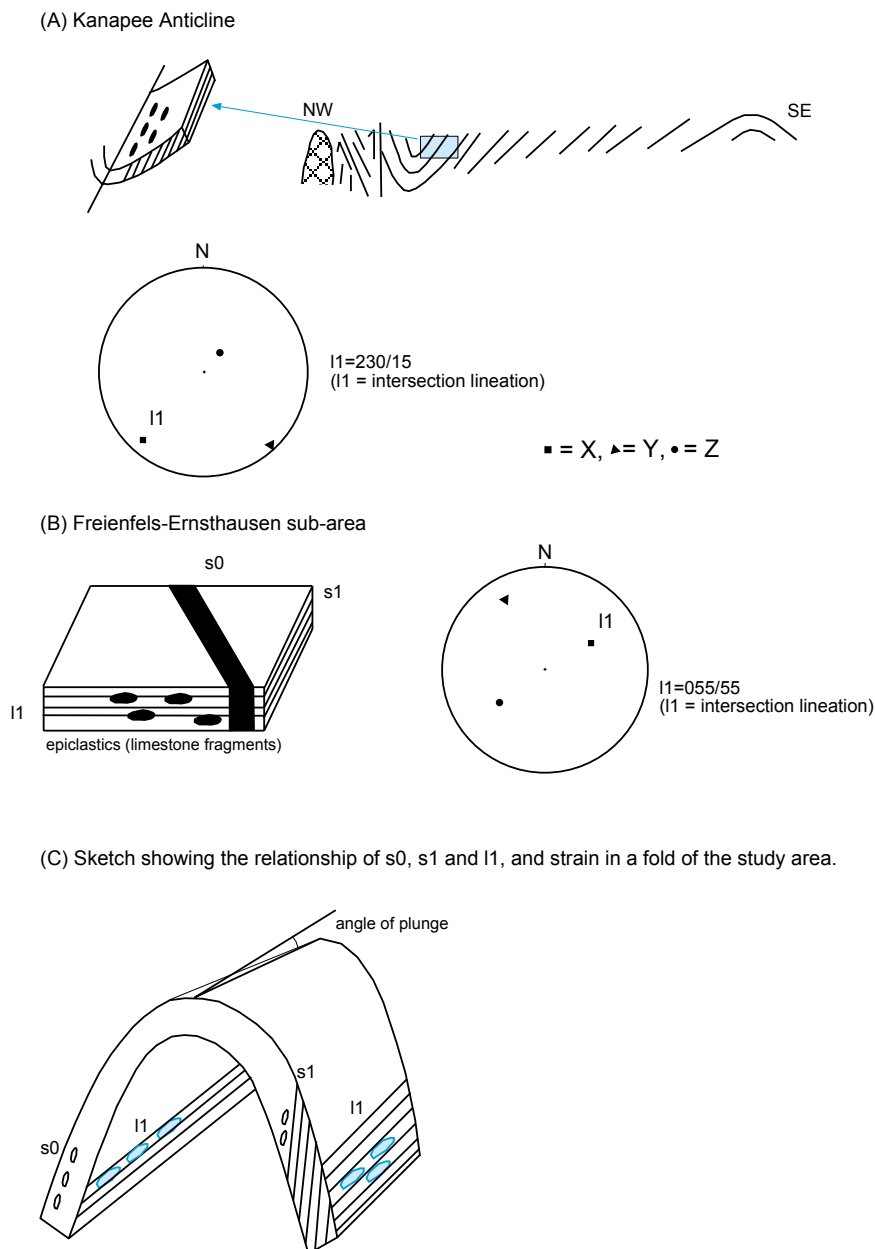


Fig. 4-7. Sketch showing the relationship of the strain ellipse with the structures of bedding (A), s1-cleavage (B) and lineation in a fold (C) of the Weilburg area.

The co-ordinate positions in terms of X, Y and Z show the deformation stages in the sense of RAMSAY & HUBER (1983A), (Fig. 4-6). Thus, the pencil-cleavage lies in the planar fabrics field, whereby the strain ellipsoid takes in a prolate shape (GHOSH 1993, RAMSAY & HUBER 1983A), sub-parallel to the fold axis (Fig. 4-7).

4.2.4 Strain intensity

The strain intensity can be calculated by the 3-D measurement, derived as follows:

Flinn values $k = \ln R_{xy} / \ln R_{yz}$ (RAMSAY 1967),

Intensity of deformation $d = [(\ln R_{xy}-1)^2 + (\ln R_{yz}-1)^2]^{1/2}$ (GIESE et al. 1997) and

Strain magnitude parameter $\epsilon_s = 1/\sqrt{3} \{(\ln R_{xy})^2 + (\ln R_{yz})^2 + (\ln R_{xz})^2\}^{1/2}$ (NADAI 1963).

As a whole, the finite strain appears in different characters, which is noticed as different style of deformation depending on their basin position. The values of k, d and ϵ_s show the deformation (Table 4-4), e.g. Kirschhofen syncline shows $k = 0.04$, $d = 6.0$ and $\epsilon_s = 0.69$ for *Kalkknoten*. In this case, the ellipsoids parallel to the bedding plane (Fig. 4-1) show a higher intensity of deformation than the ellipsoids parallel to the s1-cleavage plane. Likewise, the ϵ_s -values with θ angles envisage the shape differentiation of ellipsoids (see Table 4-4 and Fig. 4-8).

The ellipsoids lying in the s1-cleavage could be a second generation because these ellipsoids have slipped out from the original ellipsoids lying in the bedding, and the intensity values of these are less than those of the ellipsoids lying in the bedding.

Table 4-4. Strain intensity k, d and ϵ_s (θ) of the Weilburg area.

No.	Location and rock type	k	d	ϵ_s (θ)
1	Ahausen (<i>Kalkknotenschiefer</i>)	0.59	1.66	0.45 (52°)
2	Ahausen (<i>Kalkknotenschiefer</i>)	0.06	3.1	0.51 (71°)
3	Ahausen (<i>Kalkknotenschiefer</i>)	0.23	2.02	0.44 (61°)
4	Edelsberg (epiclastics)	2.58	0.63	0.25 (25°)
5	Essershausen (lapillituff)	0.45	1.17	0.34 (50°)
		0.59	1.34	0.39 (49°)
6	Guntersau (lapillituff)	0.16	0.8	0.22 (52°)
		0.17	0.64	0.24 (35°)
7	Kirschhofen (<i>Kalkknotenschiefer</i>)	0.04	6.0	0.69 (78°)
8	Freienfels (epiclastics)	11.1	1.9	0.46 (6°)

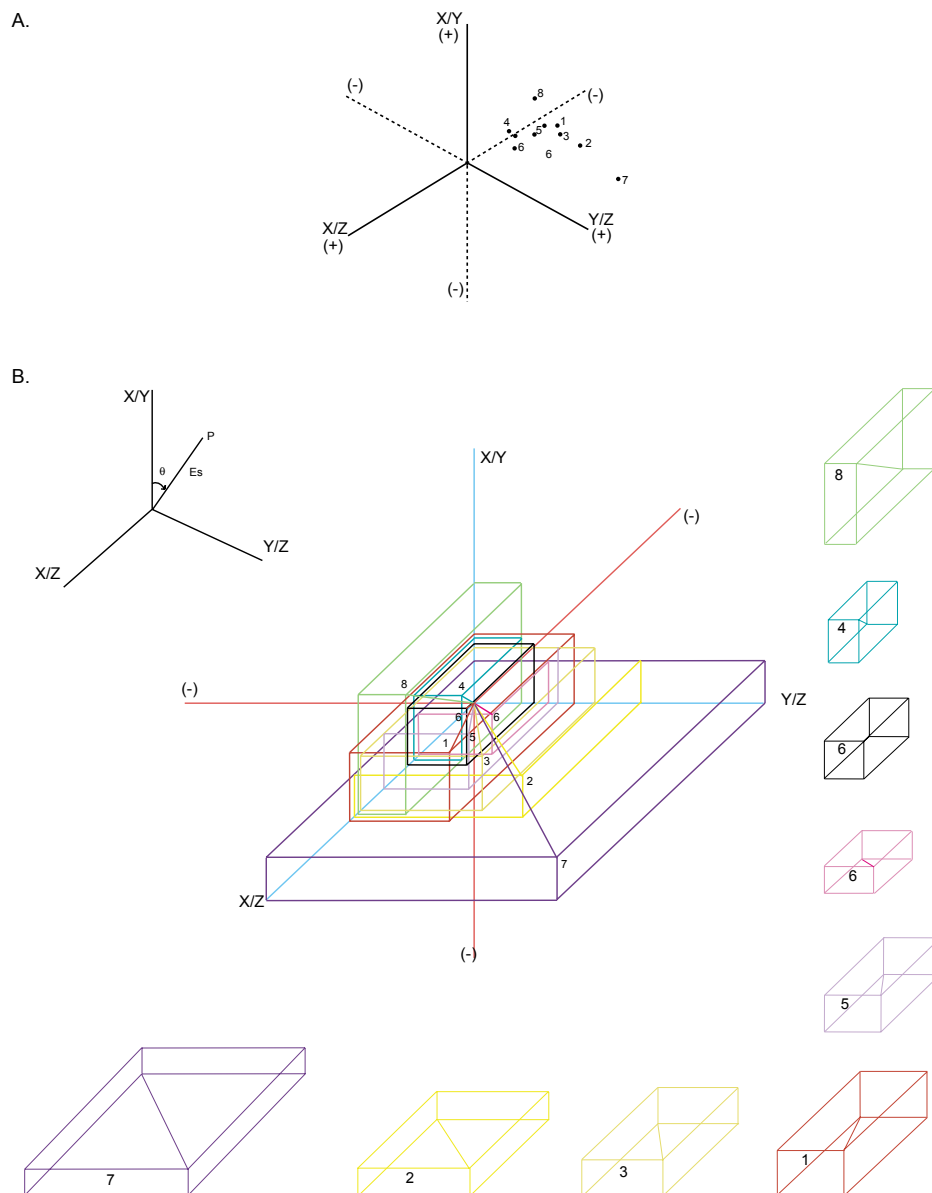


Fig. 4-8. Three-axes plot (after OWENS 1974B and HSU 1966), (A), and ϵ_s and its θ angle in isometric three-axes plot diagram (B). (Plot-numbers: see Tables 4-3 and 4-4)

Exceptionally, the No. 2 example shows the highest deformation from the Ahausen syncline with the values of $k = 0.06$, $d = 3.10$ and $\epsilon_s = 0.51$, and which was superposed by the second deformation, e.g. strain ellipsoid is lying in the s_1 -cleavage wavy folding (s_2) on the short limb of a fold and shows the last stage of deformation in the Flinn-diagram (Fig. 4-3). The majority of points are in the oblate field (Fig. 4-4B & 4-5), in which the strain intensity (ϵ_s) values (cf. LISLE 1984) of sedimentary rocks, e.g. *Kalkknotenschiefer* are generally higher than that of lapillituff (Fig. 4-6).

4.2.5 Strain path in Flinn-diagram

Finite strain can be found in naturally deformed rocks of sedimentary origin and may result from the superposition of the tectonic strain on pre-tectonic (diagenetic) compaction. The pre-tectonic compaction will have a major influence on the degree of preferred orientation of platy minerals in pelitic rocks. In the study area, the 3-dimensional fabric of weakly deformed rocks may be related either to sedimentary structures (bedding), or to vertical compaction or to the regional strain. The results of the analysis are discussed considering the possible deformation paths which may have produced the strain features. Most of the determined finite strain ellipsoids are of oblate type and show a peculiar distribution of the maximum elongation (Fig. 4-5).

In the Flinn-diagram, the strain path starting from the initial position moves along the uniaxial compaction or layer-normal shortening field, which could be the chocolate-bar type boudinage structures of *Kalkknoten* whereby strain ellipsoids lie in the bedding plane in the Kirschhofen syncline (Plate 10). These *Kalkknoten* were coaxially superposed by vertical uniaxial compaction in the pelitic sediments due to tectonic strain. In addition, the R_s value shows the highest strain in the area. Thus, volume loss (Δ_0) has been produced under the layer-parallel shortening, there (Fig. 4-5 & 4-9).

The strain path continues along a straight line with sub-vertical slopes towards the prolate field. During this stage, the maximum principal strain is parallel to the fold axis, and the minimum principal strain axis is vertical. For this stage, examples are formed in the epiclastic fragments of the lapillituff exposed near the Freienfels village. This fragments could be due to maximum stretching by dextral movement parallel to the regional strike. An equivalent prolate strain ellipsoid is obtained from the pillow lava epiclastics (Plate 15) which lie nearly sub-parallel to the cleavage. Following MOSHER (1987), cobbles have commonly a more prolate shape because of the orientation of their original X-axis which rotated during the deformation, as mentioned before (Page 59), cobbles are comparable to epiclastics.

Later, the strain path returns towards the apparent flattening field (without following the same path because of the effects of the incremental volume change during the tectonic deformation). The maximum principal strain changes into vertical and intermediate principal strain and becomes parallel to the Y-axis (cf. Fig. 4-1). The minimum principal strain however turns horizontal, becoming parallel to the tectonic shortening. This apparent flattening field is very common for the strain in the Weilburg area, where most of the strain ellipsoids lying in the s1-cleavage are oblate in any structural position.

The strain path eventually reaches an uniaxial oblate state, the maximum principal strain axes are horizontal, intermediate axes parallel to Y axis and minimum axes become vertical, normal to the tectonic shortening. On continuing deformation the maximum principal strain will become vertical and the intermediate parallel to Y axis and the minimum parallel to the tectonic shortening (cf. MAZZOLI 1995 and GHOSH 1993). For this stage, the strain ellipsoids from the short limb in the s1-cleavage wavy folding (s2-cleavage) and from the long limb in the s1-cleavage kinking (s2-cleavage) represent the uniaxial oblate state.

Thus, the strain deformation can be discussed within the development of finite strain states, recorded in the strain path which consists of vertical uniaxial compaction of the *Kalkknotenschiefer* with volume loss, followed by tectonic deformation. Volume changes during tectonic deformation can result from:

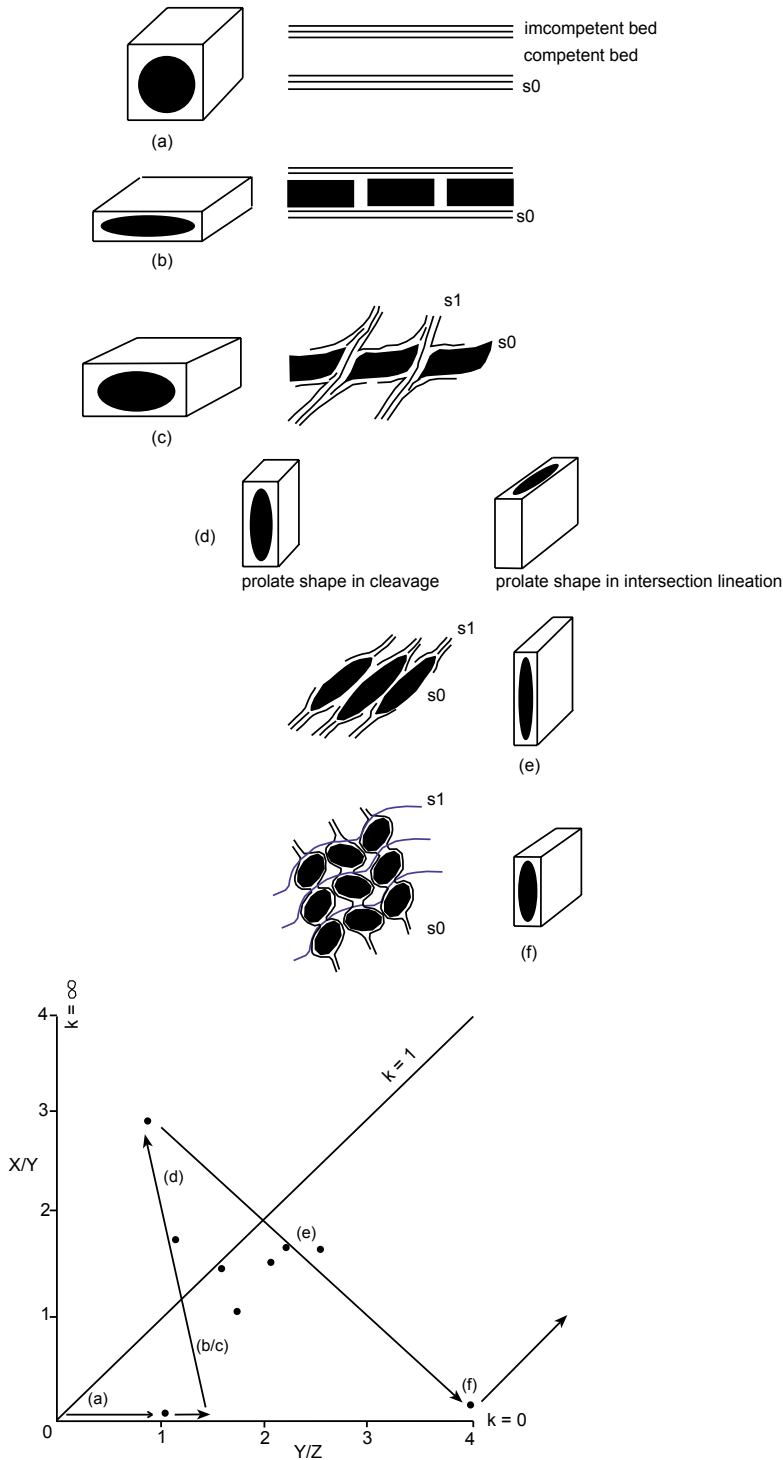


Fig. 4-9. Deformation process for the Weilburg area with corresponding strain path in Flinn-diagram (after FLINN 1962)

(1) The volume loss takes place during the initial stage of tectonic deformation, whereby horizontal shortening consists of a reduction in volume, e.g. strain path of strain ellipsoids lying in the bedding plane moves to that of apparent constriction field, and

(2) during the onset of tectonic deformation, the rate of volume loss will equal the rate of horizontal shortening but decreases as deformation proceeds (cf. MAZZOLI 1995), e.g. resulting in the strain ellipsoid lying in the s₁-cleavage.

According to co-ordinate system, the XZ plane corresponds to the plane in which tectonic strain occurred. Within this reference frame, the total deformation tensor for the stages of the progressive deformation, indicating progressive simple shear, can be obtained from the sequential incremental strain. The strain analysis in this type of deformation sequence produces a deformation path where the total strain moves from the oblate to the prolate strain field and back to the oblate field (Fig. 4-9).

Along the strain path, there is a change in the intensity of k values, e.g. k-values (sample No.): 0.04 (7) → 2.58 (4) → 11.1 (8) → 0.59 (1 & 5) → 0.23 (3) → 0.17 (6) → 0.06 (2) (see Table 4.4, cf. Fig. 4-5B). The k-values show the different intensities of deformation suggesting different deformation phases, e.g. 0.04 (7), pure shear to 0.06 (2), simple shear (cf. Fig. 4-5B), by a superposition of flattening shear strain on primary fabrics (second phase of deformation).

A strain history can be seen involving the superposition of uniaxial flattening (compaction) and initial layer-parallel shortening followed by tectonic strain and with a layer-parallel shearing mechanism, e.g. in the Kirschhofen syncline, the principal strain ellipsoids are lying in the bedding.

A roughly coaxial strain history is envisaged only for local areas where the shear component is negligible. In these areas, prolate finite strain may be observed where tectonic strain has not been large enough to reverse pre-tectonic flattening by volume loss, or new strain path for the late deformation, e.g. epiclastic fragments parallel to fold axes near the Freienfels in the Freienfels-Ernsthausen sub-area (cf. MOSHER 1987).

For most of the determined finite strains, from fold limb regions where the s₁-cleavage is developed, layer-parallel shear during folding most probably played in a primary part. The deformation path for these areas is likely to be within the oblate strain field of the deformation plot due to the shear component during folding. Observed finite strain ellipsoids are generally of oblate type, oriented parallel to the fold axial plane (s₁-cleavage). Thus, the whole area generally exhibits oblate ellipsoids.

The uniaxial oblate state is reached again while the s₁-cleavage was folded. In the finite strain ellipsoids, the intermediate principal strain becomes parallel to the Y-axis, e.g. strain ellipsoids lying in the s₁-cleavage wavy folding on the short limb of the fold in the Ahausen syncline.

The strain path demonstrates the different phases of deformation. Thus, according to strain analysis, deformation depends on the properties of strained materials, conditions of the deformation effect, and structural position of strained materials. Regarding the nature of deformation, the strain can never be homogeneous, depending on the scale, e.g. a homogeneous strain in the macroscopic scale, is not known in megascopic scale (Fig. 4-10), (cf. SCHWERDTNER 1973).

The superposition of compaction, initial layer-parallel shortening and layer-parallel shear indicating progressive simple shear may represent a general deformation sequence for the pelitic rock in different structural settings. By this type of strain superposition, a change-over from a maximum extension approximately parallel to the bedding, to the axial plane (s1-cleavage), to the intersection lineation, and to uniaxial oblate state can be envisaged.

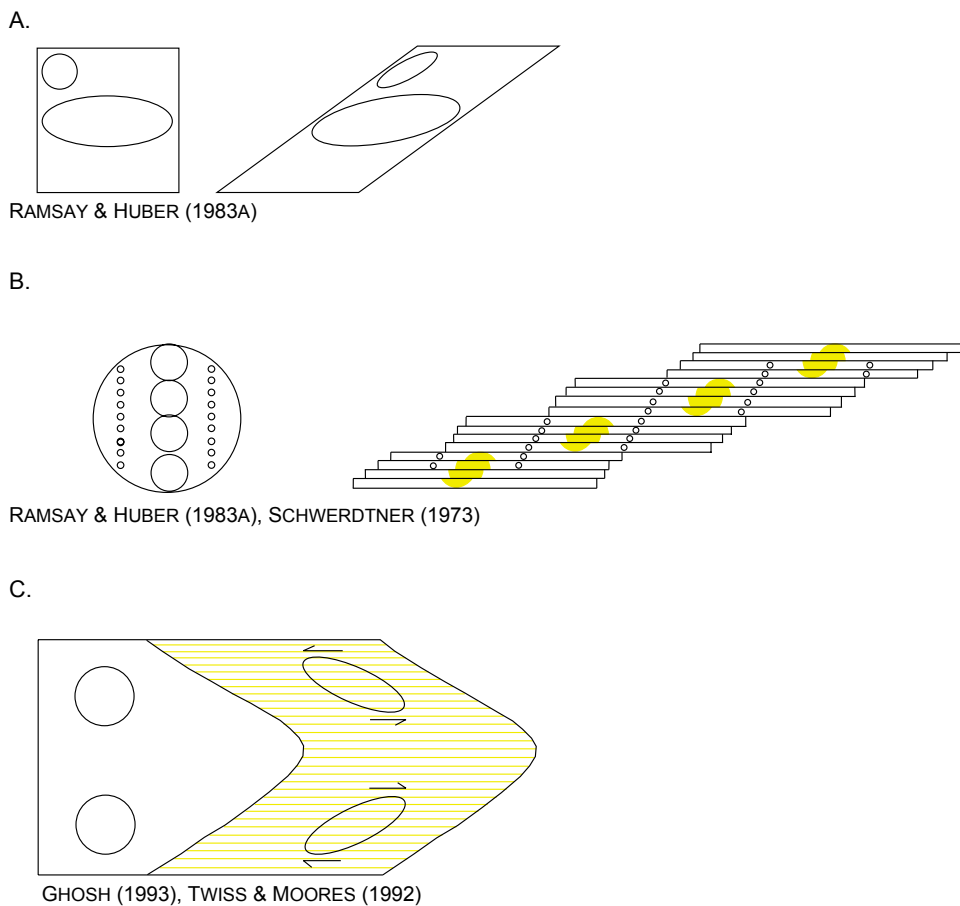


Fig. 4-10. Relationship between initial ellipse alignment and their final shapes.

The volume loss depends on the volume changes which are possible during both, the diagenetic compaction and the tectonic deformation. The compaction occurs during the burial of a sedimentary sequence consisting of alternating competent beds (lime bed) and incompetent beds (argillaceous bed). The tectonic deformation also occurs in processes (1) which cause an increase in rock density with respect to the dehydration mineral transformation (clay minerals to micas); (2) which cause pressure-solution transfer with evidence such as 40–60 % volume loss, associated with pressure solution accompanying slaty cleavage formation.

4.3 CORRELATION BETWEEN STRAIN AND AMS (Anisotropy of Magnetic Susceptibility)

Early studies noted a correspondence between the strain and magnetofabric ellipsoids in sedimentary rocks (e.g. GRAHAM 1966). On a continuous basis, AMS was successfully correlated quantitatively with finite strain in shales, slates, limestones and red beds (TARLING & HROUDA 1993).

Here, just a brief comparison of the finite strain with the AMS analysis in volcanic rocks is given, a detailed correlation follows in Chapter 7. The maximum and intermediate axes of the AMS magnitude ellipsoid define a magnetic foliation plane which is sub-parallel to planar structural elements of the study area. The maximum axes described as a magnetic lineation which is sub-parallel to the regional strike of the area (Fig. 7-5A). The principal strain Z axes and pole of the AMS (K_3 axes) are absolutely the same, except for limestone (Fig. 7-36).

This correlation shows that the deformation stages in the L-F diagram of the AMS and the Flinn-diagram of strain analysis are coincident with each others.

4.4 STRAIN-VORTICITY ANALYSIS

In the study area, the strain ellipsoids, represented by the *Kalkknotenschiefer* are the result from boudinage processes which may be of chocolate-bar type (Plate 13). Generally, the boudins (*Kalkknoten*) are more competent than the matrix (shale = *Schiefer*). Subsequently, boudins were initially rotated as rigid inclusions. During the rotation, the boudins were arranged in an *en-echelon* array if the individual boudins rotate at different speeds according to the rate of rotation (Wk), (Fig. 4-11A). This rotation line is the same as that of a similarly oriented passive line marker (BORRADAILE 1993). The rotation may take place in both, coaxial and non-coaxial bulk deformations.

The rotation of boudins is always smaller than the rotation of the bed as a whole during pure shear (e.g. Plate 12), (GHOSH 1993). In simple shear, there are two cases, a rotating boudin may lie behind or move ahead of the bed (Plate 12B). In both cases of simple shear, an *en-echelon* arrangement of the boudins will result, constituting an opposite sense of offset.

For the shear strain, the boudins show the shape of barrel (bedding parallel) faces along with asymmetries and outward wedging (progressive shearing: dextral, Plate 12). The original shape of extension fracture boudins may change due to post-fracture plastic deformation (Plate 12B). In all such cases, there must be a shearing parallel to the layering (Plate 12A).

The shearing may be the cause for the boudins. In the initial stages with small offsets of the bedding, the array of displaced rhombohedral fragments has the general appearance of a pinch-and-swell structure. When the fragments are completely separated, they look like ordinary boudins (Plate 12B & 13). The shear-initiated structure is associated with a body rotation of the boudins. Slip along the s_1 -cleavage and rotation of the fracture surfaces take place simultaneously so that the boudins are arranged in an *en-echelon* pattern (Plate 12B).

The aforementioned strain ellipsoids (boudins) rotation could be ductile shear deformation (plastic deformation). That the strain has accumulated by progressive simple shear or other types of steady-state progressive deformation is also possible. The rate of rotation or degree of non-coaxiality is

expressed in the kinematic vorticity number (Wk : TRUESDELL 1953) and may give insight how the finite strain accumulates under various combinations of stretching and vorticity in a 2-D investigation (Fig. 4-11). The Wk can be defined as pure shear: $Wk = 0$, simple shear: $Wk = 1$ and general non-coaxial shear ($Wk = \infty$). For the rigid rotation, PASSCHIER (1997) uses Wn as the kinematic vorticity number e.g. $Wn = 0 \rightarrow Wn = 1 \rightarrow Wn = \infty$ (Wn : related to Wk introduced by PASSCHIER 1997). TIKOFF & FOSSEN (1995) use Wk as the kinematic vorticity number with $Wk = 0 \rightarrow Wk = 1 \rightarrow Wk = 0$ for the steady-state flow (Fig. 4-11).

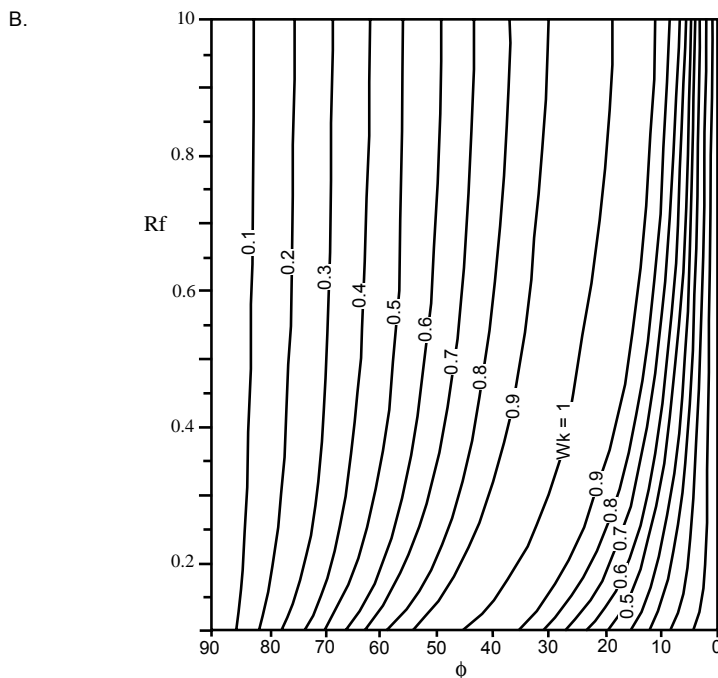
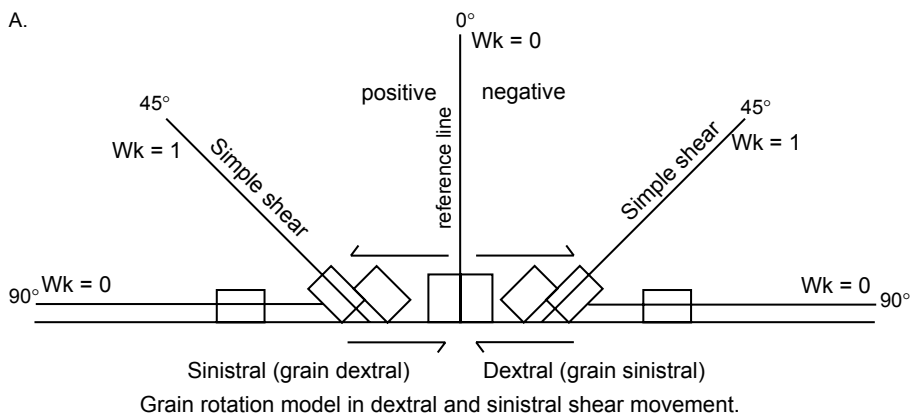


Fig. 4-11. Strain ellipse rotation with corresponding kinematic vorticity number (Wk), (A), Wk development in steady-state flow deformation (B), (TIKOFF & FOSSEN 1995).

The vorticity number determined for the study area seems to be the result of the steady-state progressive deformation developing an *en-echelon* strain pattern, and suggests progressive simple shear (Plate 12B). Thus, the W_k was initially $W_k = 0$, and then approached $W_k = 1$. In the study area, the progressive simple shear reached $W_k = 1$, and the progressive deformation W_k resulted as follows $0 < W_k < 1$ (Fig. 4-11).

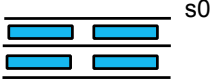
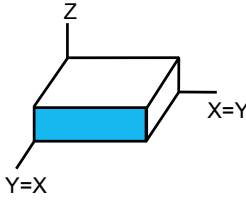
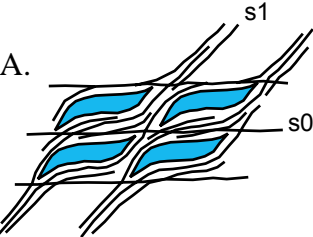
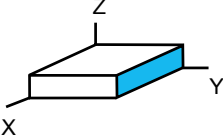
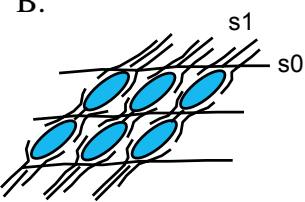
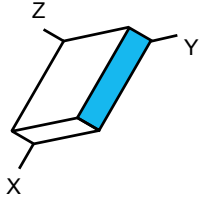
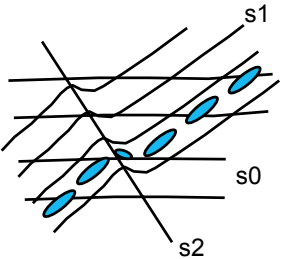
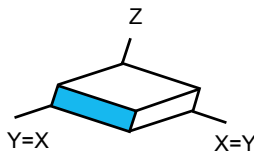
Stage	Sketch	Type	Strain	Finite strain axes
D1		Compaction	Coaxial	
D2	A. 	Cleavage formation (pure shear) e.g. Guntersau syncline	Coaxial	
	B. 	Cleavage development (simple shear) e.g. Ahausen syncline	Non coaxial (shear strain)	
D3		Kink folding (further increment of deformation) e.g. Ahausen syncline	Non coaxial (shear strain)	
D4	Fracturing and faulting (ESE-WNW and NNW-SSE direction)			

Fig. 4-12. Deformation phases in the Weilburg area according to the strain determination on XZ plane. D2-phase gives two types of strain ellipse.

4.5 DISCUSSION

The profiles in the Weilburg area, in the middle Lahn syncline investigated for the strain analysis are characterized by NW vergent structures and a flat lying overthrust (WEBER 1984). Generally, NW vergent cleavage is observed, whereas the style of folding, e.g. differs in the Ahausen syncline: NW vergence asymmetrical fold; Kirschhofen syncline: disharmonic fold (flexural-slip folding), (Fig. 4-3), and the strain deformation, e.g. the Kanapee anticline: no strain deformation is different in local structural units.

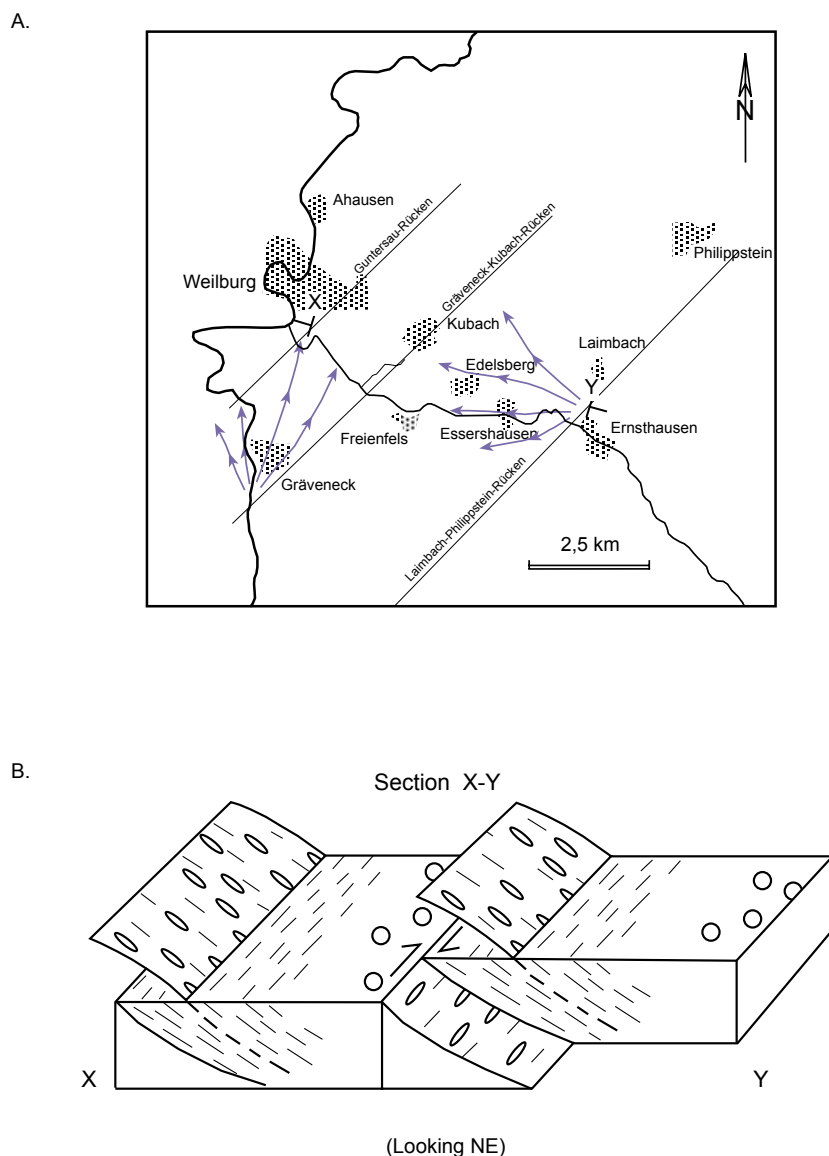


Fig. 4-13. Strain development in half-graben basins in the Weilburg area, the Lahn syncline. A: Location map of half-graben and section X-Y, B: Strain position in antithetic half-graben. Strain in lapilli and pillow lavas indicates s_1 -cleavage plane, thrust plane and strike-slip plane near the boundary between two antithetic half-graben basins

Strain ellipses rotated into the s1-cleavage by progressive simple shear movement (Plate 12). In the Ahausen syncline, a late phase of deformation distinguishes as s1-cleavage kinking (s2-cleavage) on the long limb by stretching along the s2-cleavage, and the s1-cleavage wavy folding on the short limb by compression of the s1-cleavage.

The Kirschhofen syncline developed disharmonic folding (flexural-slip folding) as a transition from vertical tight folds in the SE to overturned folds in the NW (Fig. 3-1 & Plate 2), however long axes of the strain ellipses are lying in the bedding instead of the cleavage.

The Kanapee syncline developing asymmetrical folding exhibits the strain ellipsoid lying in the bedding, parallel to the regional strike (Fig. 4-7).

Thus, strain partitioning is observed in the study area, depending on the angle between the σ_1 direction and the limb and type of fold (Fig. 4-12).

With respect to the vertical tight folds strain deformation has only minor effects (cf. Plate 10: vertical tight fold associated with initial strain, and Plate 12: high strain on the long limb of asymmetrical fold). According to RAMSAY & HUBER (1983A), flexural-slip folding (e.g. Kirschhofen syncline: disharmonic fold) does not imply high strain on limbs (cf. Plate 10), however the internal strain is high, due to the superposed flattening deformation.

Thus, the strain deformation depends on the type of folding, whereby folding is influenced by the syn-rift basin position, e.g. the Kanapee anticline is developed in a former synthetic half-graben basin and its neighbouring Kirschhofen syncline in a full-graben (see Chapter 6).

The s2-cleavage is deformed by the D3-deformation folding (Fig. 4-12), e.g. *Kalkknotenschiefer* and *lapillituff* show further incremental shearing along the s1-cleavage (see above and Plate 13).

According to the strain analysis, the style of tectonic movement can be deduced by locating the shape and position of strain ellipsoids in the study area, e.g. the Freienfels-Ernsthausen and Freienfels-Guntersau sub-areas position as antithetic half-graben basins (filled in the style of an accretionary prism) resulted in strain ellipsoids which are parallel to the s1-cleavage. However, at the rear side of the prism no strain deformation is present in the associated pillow lava and lapilli. In addition, prolate strain ellipsoid which are oriented parallel to the regional trend suggest dextral strike-slip movement at the boundary between two structural units (Fig. 4-13). This is probably due to the superpositioning of orthogonal relative movements on the southern rim of the fold-and-thrust belt by a dextral strike-slip component (indicated by Southern Hunsrück Boundary Fault) during final deformation. Thus, late dextral transpression succeeded by the dextral transtension can be suggested on the basis of the observation of the coaxial compaction strain in layer-parallel shortening to fold development, and non-coaxial strain in layer-parallel shearing through folding and post-folding dextral shear in the regional progressive simple shear development.

CHAPTER 5

RE-ANALYSIS OF PREVIOUS INVESTIGATIONS

CHAPTER 5

RE-ANALYSIS OF PREVIOUS INVESTIGATIONS

This section considers previous investigations on the Rhenohercynian zone and the present study area to discuss tectonic models. An extensional tectonic development in the Rhenohercynian zone has been investigated in many studies, though this is not considered in detail by type and model of current classification, as a continental extension zone similar to recent continental extensional areas, e.g. the Red Sea rifting. Also the present study area has been investigated using other approaches, but mostly, these have been used to figure out the extension style of the Rhenohercynian and the study area before orogenic compression. Besides, some previous studies are selected to apply for the interpretation of flow directions from eruption centre and deformation models: Joint model and drag fold model.

5.1 RHENOHERCYNIAN BASIN

(Continental Extensional Basin)

The Rhenohercynian basin is characterized by an extensional environment (SMITH 1996, PICKERING & SMITH 1995, OCZLON 1992, FLICK et al. 1990, FRANKE 1989B) developed at the southern margin of Avalonia, belonging to the Laurussian pericontinental area (a large-scale shelf) during late Silurian to Lower Carboniferous time.

There are **three** models for continental extension, pure shear, and simple shear models: Wernicke and delamination models, respectively (LISTER et al. 1986), whereby the detachment faults play the major role in the continental extension processes. In addition, continental extension is recognized by important elements of Basin and Range-style tectonics that have not been recognized on passive margins. Pure shear models assume that the detachment fault represents the brittle-ductile transition (DIXON et al. 1989, LISTER & DAVIS 1989, LISTER et al. 1986). A Wernicke model (WERNICKE 1981) suggests that the detachment fault represents a low-angle normal fault that cuts through the entire lithosphere. A delamination model exhibits an alternative geometry in the lithosphere, involving the detachment zone running horizontally below the brittle-ductile transition, steepening and then again running horizontally at the crust-mantle boundary (LISTER & DAVIS 1989, DAVIS 1988, LISTER et al. 1986, cf. DAVIS et al. 1986).

According to the classification of continental extensional rifts by DIXON et al. (1989) and the models of LISTER et al. (1986), Variscan extension could be a simple shear Wernicke model, similar to the Red Sea extensional rift (cf. WERNICKE 1981 and 1985), (Fig. 5-1) which has recently compared with the Rhenohercynian basin by OCZLON (1992). In the Red Sea extensional rift a detachment fault continues almost throughout the entire crust and terminates in a region of concentrated extension in the lower crust. An abundance of basalt flows, sills and dykes is present, the latter being concentrated in the region of greater extension sea-ward of the hinge zone (BELL et al. 1988).

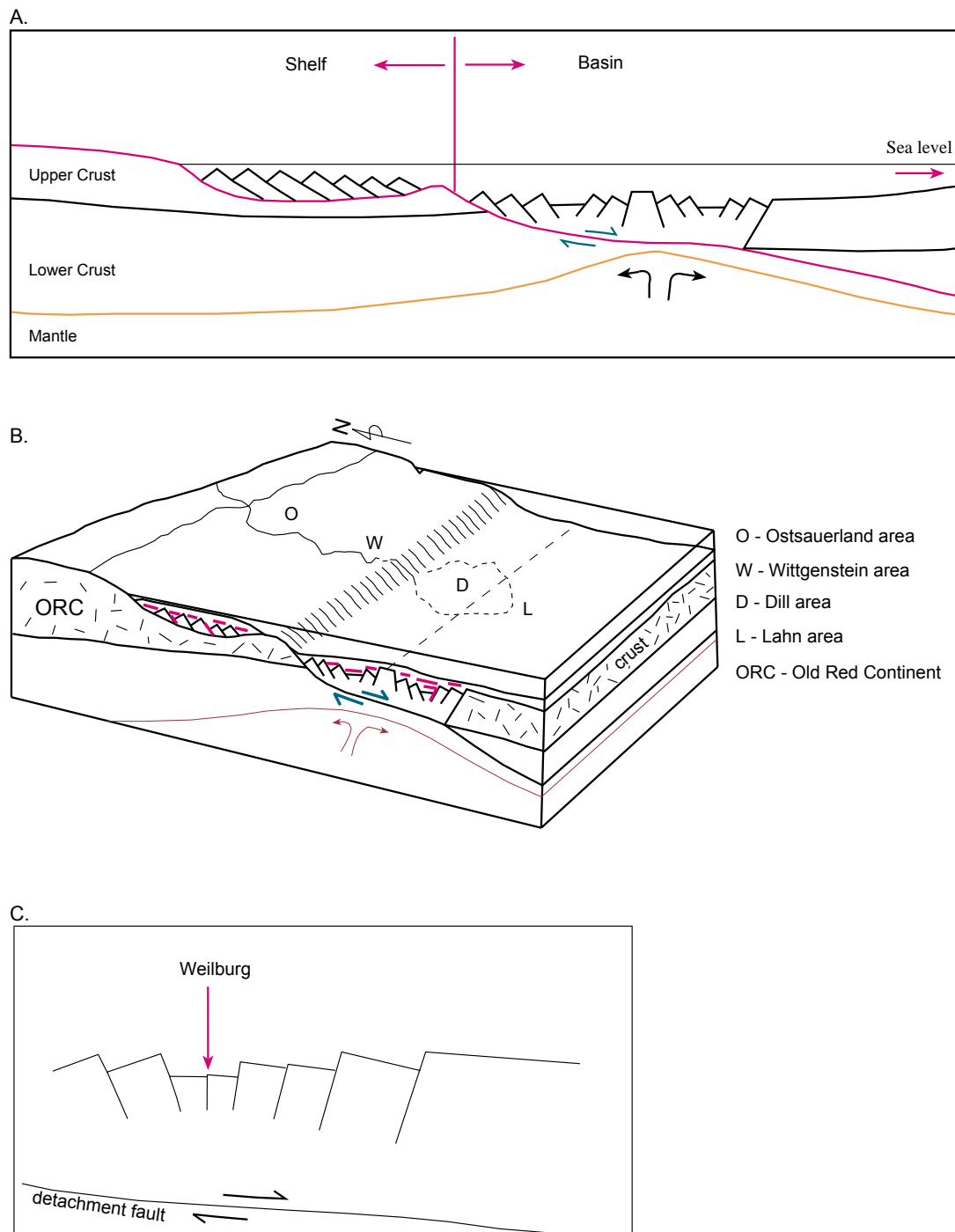


Fig. 5-1. Model for the Rhenohercynian basin during Silurian to Middle Devonian time.

A: Rift development in a simple shear Wernicke model (after WERNICKE 1981 and LISTER et al. 1986)

B: Block diagram of the Rhenohercynian basin through Lahn, Dill, Wittgenstein and Ostsauerland areas.

C: Synthetic and antithetic half-graben and full-graben depositional basins at the Weilburg area.

In the Rhenohercynian zone a mid-crustal décollement, which can be clearly seen in the DECORP 2-N seismic section (FRANKE et al. 1990, DROZDZEWSKI et al. 1985), continued within the upper crust exhibiting the basalt lava, lapillituff and dykes (Lahn-Dill area: FLICK & NESBOR 1988).

On the other hand, extensional tectonics produces half-grabens (domino type: RAMSAY & HUBER 1983B, WERNICKE & BURCHFIEL 1982), whereby facies mosaics are influenced by tectonically induced slopes resulting from hanging-wall downtilting and foot-wall uplift (RAMSAY & HUBER 1983B). Graben structures are often associated with large-scale regional crustal thinning: a phenomenon which can lead to the elevation of crustal isotherms and the upward migration of magma. That arises around rotating fault block sectors, so the extension might then be accommodated by magma fillings at depth and outpouring of lava and pyroclastic material at the surface (e.g. RAMSAY & HUBER 1983B).

5.1.1 Extensional basins in the *Rheinische Schiefergebirge*

During the sedimentation period from Silurian to Carboniferous, the depositional basin called the Rhenohercynian zone belonged to a large-scale shelf area exhibiting a pronounced palaeomorphology (FRANKE et al. 1978).

According to ENGEL et al. (1983) the depositional basin on the shelf developed as tilted fault-bounded blocks (cf. KREBS 1971), which is valid especially for the Lahn-Dill area. The elongated Devonian sedimentary basins and depocentres trend more or less parallel to tectonic structures, and both point toward fault-bounded sinks. LANGENSTRASSEN (1983) also discussed the instability of the shelf with syndepositional fault movement (rifting) which apparently developed a graben-like structure, e.g. in the Siegen trough.

However, small depocentres formed as half-graben structures which are trending along the depositional strike according to the investigations of BÖGER (1981) in the Sauerland anticline, RÖDER (1960) in the Siegen anticline, SOLLE (1960) concerning syndepositional faulting tectonics in the SW part of the Rheinische geosyncline, and BOTTKÉ (1978) in the Brilon Block in the Sauerland anticline. From these investigations it can be concluded that extensional tectonics occurred together with subaqueous rises or swells at different locations, at the same time during Givetian and Adorfian.

For the Lahn-Dill area BEHNISCH et al. (1991) described basins and rises associated with bimodal volcanism related to extension tectonics on the southern shelf of the Old Red Continent. SCHÖNENBERG (1956) and BISCHOFF & SCHÖNENBERG (1956) concluded from the correlation of thicknesses of sedimentation that antithetic faults were formed as step-like ridges and basins similar to half-grabens in the north-eastern part of the Dill syncline near the Hörre zone. Consequently, the syndepositional tectonics of the Rhenohercynian basin suggests that the whole Lahn-Dill area was formed by half-grabens in a rift basin environment (cf. ENGEL et al. 1983).

5.1.2 Rifting in the Lahn-Dill area

In the extensional environments rifting zones develop bimodal volcanism according to TWISS & MOORES (1992), RAMSAY & HUBER (1983B) and ELDHOLM & MONTADERT (1981) which can be

compared to the Lahn-Dill area (BEHNISCH et al. 1991), e.g. the Weilburg area exhibits rhyolites (flows), trachytes (stock), basalts (dykes and sheet flow lava) and bimodal, mainly basaltic volcanoclastics.

The Lahn and Dill areas show generally similar tectonic structures. Near to the dividing Hörre zone, synthetic faults are frequent in the Lahn syncline (present study), antithetic faults in the Dill syncline (SCHÖNENBERG 1956). The main differences appear to be that in the Lahn syncline flat-lying overthrusts are more frequent (WEBER 1981).

5.1.3 Simple shear model

Seismic section in the DECORP 2-N (ONCKEN & WEBER 1995, FRANKE et al. 1990) and bed-length changes in the regional pattern study of DITTMAR et al. (1994) of the Rhenohercynian basin clearly shows two segments: one from Hunsrück to Siegen and one from Siegen to Venn (cf. Fig. 5-1A). In addition, at the Siegen thrust in the east Eifel area, high grade deformation and crustal xenoliths are exposed (Fig. 2-2), (ONCKEN et al. 1999). Thus, the simple shear Wernicke continental extension model fits in nicely with the Rhenohercynian basin development, east of the Rhine river, namely the Ostsauerland, Wittgenstein, Dill and Lahn areas (Fig. 5-1). These can be laterally correlated to the SW in the Rhenish Massif with the East Eifel, Siegen, Mosel and Hunsrück areas (ONCKEN et al. 1999).

5.2 CENTRAL LAHN BASIN

5.2.1 Basin structure

Due to the continental extensional tectonics in the Lahn area, submarine ridges and volcanic islands (Basin and Range-style) were recognized, e.g. obvious in the SW of the Lahn syncline (BREITKREUZ & FLICK 1996, FLICK et al. 1988). In the Weilburg area, middle Lahn syncline, one of the submarine ridges stated by RIETSCHER (1966) coincides with the alignment from Gräveneck-Kubach ridge (Fig. 5-2) which is manifested by reef limestones (Kubach reef limestones: KREBS 1971, RIETSCHER 1966) trending NE-SW in the present position. In general, the central Lahn area has been developed in a rift basin environment by the observation of reef limestones, stratabound iron ore, volcanic eruption centres, and the turbiditic characters of volcanoclastics as exemplified in the Weilburg area.

From the volcanoclastic facies study of FLICK et al. (1990), the central facies is defined by a concentration of submarine lava flows, often with pillows, sub-effusive sills and dykes. Volcanoclastic rocks define the outer two facies: a proximal facies with an intercalation of a considerable number of lava flows, sills and dykes, succeeded by a distal facies in which these are lacking. The facies changes are reflected by the development of the structure of the volcanoclastic particles as well.

According to the facies study in the volcanic sequences of the Givetian/Adorfian period volcanic centres (central facies) are recognized at Gräveneck, Laimbach and Philippstein (Fig. 5-2), (BEHNISCH 1993, NESBOR et al. 1993). The volcanic centres along with the development of reef limestones allow to divide the study area into three sub-basins. Two ridges could be approximately discerned along the

alignment of the Gräveneck eruption centre to Kubach limestone as one ridge and the alignment of the Laimbach-Philippstein eruption centres as another ridge (Fig. 5-1). This seems obvious since eruption centres develop on weak crustal zones and reef limestones develop frequently on the submarine high-level in the photic zone (cf. FRANKE & WALLISER 1983, FRANKE et al. 1978).

Facies distribution implying volcanoclastic sedimentation characterized by turbidites (BEHNISCH 1993) that were produced at canyons or along fault scarps (cf. LEEDER & GAWTHORPE 1987 and ERIKSSON 1980) as well as reef limestones (BUGGISCH & FLÜGEL 1992, KREBS 1971) and iron formations (FLICK et al. 1990, QUADE 1976) developed along submarine high-level ridges (cf. ERIKSSON 1980, FRANKE et al. 1978) indicating a considerable relief. Clearly, these could be produced along grabens and half-grabens by tectonic movements in the extensional environment.

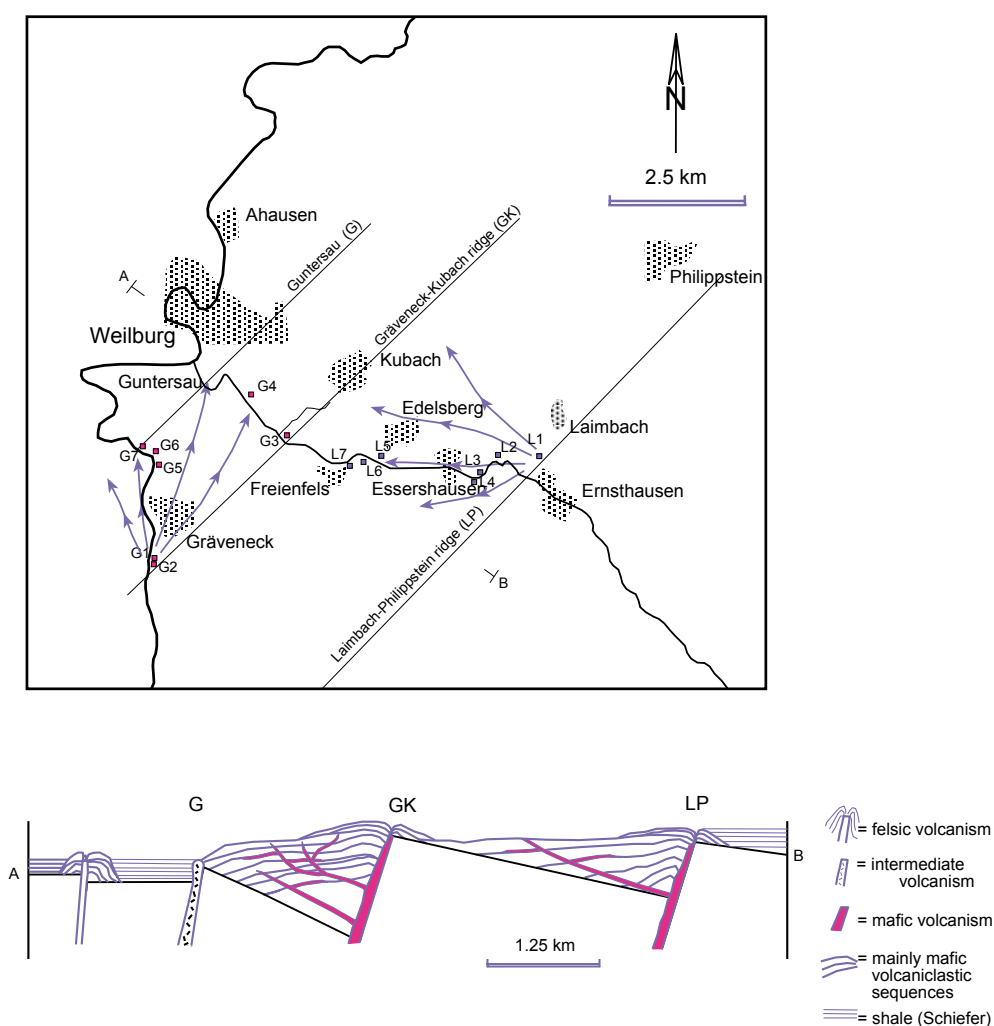


Fig. 5-2. Map: position of rift development in the Weilburg area, cross section (vertically exaggerated): half-graben basin position and volcanic filling during Middle Devonian. This section is restored to a pre-strained length (calculated shortening of the Weilburg area 52 % by the present study).

5.2.2 Volcaniturbiditic facies study

Volcaniturbidites were directly derived from volcanic eruptions (BEHNISCH 1993) following WALKER's (1992) depositional model for turbidites. A volcaniturbiditic facies is generally characterized by hydroclastic fragments (BEHNISCH 1993) exposed along the profiles of Guntersau-Freienfels and Freienfels-Ernsthausen sub-areas showing a sedimentation direction from the volcanic eruption centre to the depositional area in the basin. On this basis, possible depositional flow routes from the Laimbach eruption-centre to the Gräveneck-Kubach ridge and from the Gräveneck eruption-centre to Guntersau ridge can be deduced (Fig. 5-2), using the sedimentary facies study of BEHNISCH (1993). Central, proximal and distal facies (Fig. 5-3) are successively developed within the Guntersau-Freienfels and Freienfels-Ernsthausen basins. To account for the central facies at the Gräveneck and the proximal facies at the profile of Guntersau-Freienfels, the depositional slope must have fallen from south to north (Fig. 5-2).

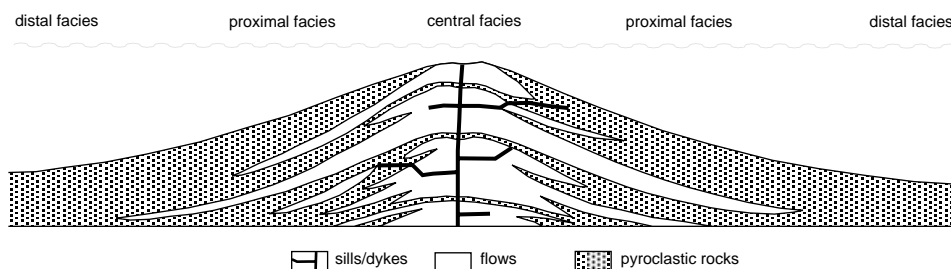


Fig. 5-3. Facies model of a submarine volcano of the Givetian/Adorfian volcanic episode in the Lahn-Dill area. (after FLICK et al. 1990)

5.2.2.1 Freienfels-Ernsthausen sub-area

In the Freienfels-Ernsthausen sub-area a volcanic eruption centre lies near Laimbach which is exposed at Laimbach quarry (at present). From there, volcanic materials (sheet flow lava, pillow lava, lapillituff and ashtuff) flowed out toward the Gräveneck-Kubach ridge. These volcanoclastics have been sedimented as turbidites (BEHNISCH 1993). The turbiditic characters differentiates the depositional environments for the centre, proximal and the distal facies (see volcanic model Fig. 5-3). Outcrops in the Freienfels-Ernsthausen sub-area exemplifying the volcanic facies are as follows (see Fig. 5-2):

L1 (Laimbach): Laimbach quarry is abundant in sheet flow lava, pillow lava, and minor pyroclastic lapillituff. The clastics are vesicular, of soft and foamy appearance, the vesicles being filled with chlorite and calcite. The lapilli are cemented by carbonate. Typical columnar jointing (indicating a volcanic pipe) is visible, definitely pointing to an eruptive centre.

L2 (Mühlfeld): Ashtuff can be seen in a road-cut which is characterized by lamination (15 cm thick),

cross lamination (1 cm thick) and current ripples, determining the current flow. Coarse sand and silt size alternations (20 cm thick) exhibit rhythmic sedimentation. Also flame structures from dewatering processes in the volcanoclastic sediment are present. These features are typical for proximal facies (JÄGER 1996).

L3 (Essershausen): A small outcrop above the road contains very large reef blocks which are allochthonous (BUGGISCH & FLÜGEL 1992) and volcanoclastics as the finer fraction. Transport distance was relatively short, which indicates proximal facies.

L4 (Essershausen): At the railroad-cut ashtuff consisting of fine sand to silt size (11 cm thick) indicates a Ta-e sequence of BOUMA (BEHNISCH 1993). Clay-size layers in the massive sandy horizons developing LOWE-sequences show load-casts at their base. Between these two sequences a sedimentation break can be observed. These are indicators of a distal facies.

L5 (Edelsberg): In the road-cut epiclastics crop out showing rounded grains, especially of metabasaltic fragments from the littoral zone, together with ashtuff epiclastics with metabasalt and reef fragments, and lapillituff layers which differ in thickness (9 cm, 2 cm, 20 cm, 2 cm). These together point to distal facies.

L6 (Heckerberg): In a road-cut on a minor road, there occur laminated volcanoclastics fine-grained lapilli to ash size fraction (1.5 m thick). Gravel beds are normal graded with maximum grain size in 1 cm, but inverse graded beds also occurred, whereby the different layers are not in sharp contact. This succession is interpreted as debris flows of a distal facies (BEHNISCH 1993).

L7 (Freienfels): The road-cut consists of volcanoclastics, in which metabasaltic fragments are weakly graded. Fine-grained particles are prominent but the primary structures are obscured by chloritization. These features also indicate a distal facies.

5.2.2.2 Guntersau-Freienfels Sub-area

The profile of the Guntersau-Freienfels sub-area can be attributed to the source of the Gräveneck eruption centre near the Gräveneck village by its trace element study and petrographic analysis (NESBOR et al. 1993), and by the situation within the Guntersau-Freienfels basin. Outcrop examples in the Guntersau-Freienfels sub-area display the following volcanic facies (see Fig. 5-2):

G1 (Gräveneck): Gräveneck is a distinct eruption centre with a 70 m thick metabasalt unit as a feeder dyke containing characteristic clinopyroxene phenocrysts. Volcanoclastic storm deposits are exposed for about 30 m thickness distinguished by graded bedding, cross bedding, and polymict composition. Polymict lapillituff are mostly hematitic and of foamy appearance, and include trachytic fragments. Ash to bomb grained size is dominant in the matrix being fully hematized.

G2 (Gräveneck/Fürfurt): In a railroad-cut an ash fall deposit distinctly crops out including very poor sorting (ash fraction to volcanoclastics of 2 cm diameter) with angular fragments and foamy pyroclasts. The thickness of beds varies from mm to 10 cm. Regular current bedding and localized erosional contacts are to be distinguished at the base. Asymmetrical impact structures of bombs which fell into the ashtuff are observed. Lithoclastics about 50 cm in diameter are embedded in a groundmass of ash and/or fine-grained lapilli characterizing a crater rim facies. These features indicate an eruption centre.

G3 (Guntersau/Freienfels): In the road-cut fall deposits show inverse and normal graded bedding, cross bedding and strong variations in the thickness of bedding (cm to 1 m thick). Load casts mark the contact of bedding. Sedimentary turbulent flows are represented by high-density turbidites as well as by mass debris flows. These features point to a distal facies.

G4 (Lower Weiltal): In the road-cut a typical proximal facies is exposed over about 330 m thickness. Dykes and sills are dominant, displaying porphyritic texture of pyroxene and plagioclase phenocrysts. A thickness of about 180 m is occupied by lava (sheet flows) and volcanoclastics (pyroclastic lapillituff) containing pyroxene phenocrysts to be correlated with the G1 exposure.

G5 (SW Schmidskopf): Volcanoclastic sediments exhibit normal graded high-density turbidites which include pebble- to sand-grained size, pointing to distal facies.

G6 (Wilmersau): In a section along a forestry road high-density to low-density turbidites (base to top) are cropped out which indicate distal facies.

G7 (NW Gräveneck): In a section along a forestry road, a high-density turbidite unit (about 3 m thick), as an indicative of distal facies, can be observed.

5.2.3 Extension Model Correlation

5.2.3.1 Red Sea Type continental extension basin

Comparison between the data of chemical analysis of volcanic rocks from both areas the Red Sea area and the Rhenohercynian area indicates a similar type of continental extension.

In the Red Sea area (the East African Rift – Red Sea System) the Main Ethiopian Rift represents an early stage of continental rifting – the Afar region represents a more advanced continental rift and the Red Sea axial deeps represent true oceanic crust. The Ti-Zr-Y plot distinctly shows the variations of Intraplate to MORB type (Red Sea axial deep), (see COISH et al. 1991).

In the Rhenohercynian zone, the Ostsauerland anticline represents an earlier stage of rifting (i.e. relatively earlier during the continental extension) then, successively, the Wittgenstein syncline and then Dill-Lahn synclines, – whereas the Giessen Ocean represents ocean crust. The Ti-Zr-Y plot

shows the analogue variations of Intraplate to MORB type (see NESBOR 1987 and GRÖSSER & DÖRR 1986), similar to the Red Sea area (cf. COISH et al. 1991). In addition, TiO_2 weight percentages in the Ostsauerland anticline are higher than that in the Lahn-Dill synclines, gradually decreasing to the Giessen MOR-basalt (NESBOR 1987, MEYER 1981), which indicates a thinning basement continental crust to the south coinciding with the marine shelf environment of the Rhenohercynian zone by FRANKE et al. (1978)

5.2.3.1 Japan Sea Type back-arc continental extension basin

The Japan Sea located between mainland Asia and Japanese Islands is described as a large-scale continental extensional margin basin (back-arc basin) by MOORES & TWISS (1995), TWISS & MOORES (1992) and PISCIOTTO et al. (1990), (Fig. 5-4B), where rifting resulted in creation of oceanic crust (cf. PISCIOTTO et al. 1990). The formation of volcanigenic massive sulfide deposits on the continental crust fits in with the back-arc continental extension environment.

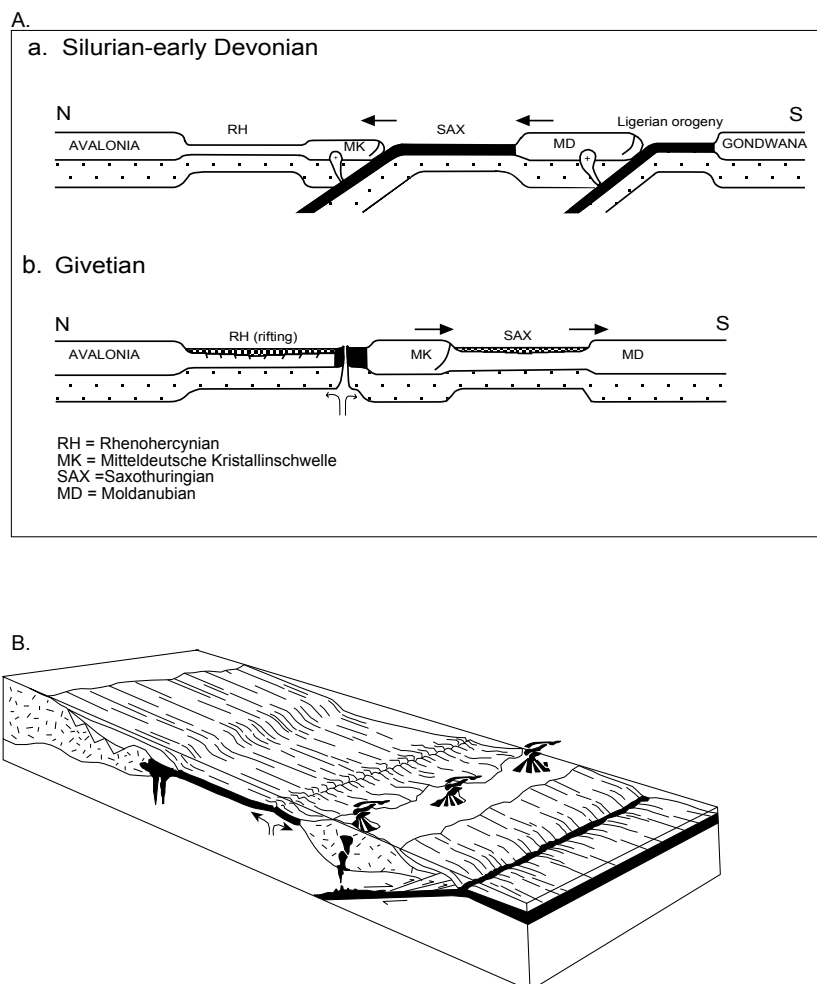


Fig. 5-4. Sketch comparing the Rhenohercynian back-arc basin development (present author, compare with Fig. 2-1), (A) and the block diagram of Japan Sea type back-arc margin (after TWISS & MOORES 1992), (B).

This can be compared with late Silurian to Middle Devonian development in the Rhenohercynian basin comprising the *Mitteldeutsche Kristallinschwelle* (ridge) with the southern extension of the Old Red Continent (Fig. 5-4A). In this model the Giessen Ocean (Giessen MOR-basalt) was developed as back-arc spreading between the margin of the Rhenohercynian and the *Mitteldeutsche Kristallinschwelle*, which was juxtaposed with the Saxothuringian zone later. The massive sulfide deposits of the Moravia-Silesia area, Rammelsberg, Meggen and the other deposits appear to have formed in the extensional tectonic environment: one dominated by crustal extension (SAWKINS & BURKE 1980). Thus, the Japan Sea type back-arc margin model can be used as an analogue model for a Rhenohercynian back-arc continental extension.

5.3 STRUCTURAL FEATURES

5.3.1 Joint development model

Since the study area was affected by compression (normal to the regional strike NE-SW), fractures indicating joints or faults should normally develop as longitudinal- (bc), diagonal- (hko) and cross-joints (ac). For the description of the terms (co-ordinates: a, b, c) used see HANCOCK et al. (1983), ADLER et al. (1961) or HILLS (1972), (Fig. 5-5A). NW-SE joints (ac) are the most prominent (Fig. 3-4 & 5-5) coinciding with the direction of horizontal compression during the neotectonics as well as Variscan tectonics (cf. Fig. 3-3).

A model is outlined to describe the mechanical conditions of the genesis of the fundamental joint system in the study area. In this model, the direction of the major principal stress σ_1 is normal to the fold axis as well as the principal joint set (**bc**), (cf. HILLS 1972 and PRICE 1981). The NW-SE direction of the joint development perpendicular to the regional structure of the Lahn-Dill area is rather pronounced, possibly because of the reaction of the rigid volcanic masses in response to the compression.

Joints developed especially in compression direction NW-SE coincide with an analogue model of the behaviour of brittle material by WILSON (1982), which states that tension fractures, resulting from simple compression may appear in the field as cross-joints at right angles to the axes of folds. Comparison of the laboratory experiment shows that the tension fractures are developed at the angles of less than 45° to that direction on the plane of shear (WILSON 1982).

Other joint directions are NNE-SSW and WNW-ESE trends which are suggested as X-shear and Y-shear (minor Riedel shears) formed in response to local rotation within the array of R shears (Riedel shears). The X and Y shear development became characteristic in the Lahn area during the neotectonics (Alpine orogeny), (MOE 1998).

The border zone between the *Rheinische Schiefergebirge* and the Hessen depression (the northern continuation of the Rhinegraben) was activated during the Rhinegraben sinistral shear movement in the Pliocene. The edges of the Rhinegraben underwent sinistral movement so that the border zones of the *Rheinische Schiefergebirge* were activated by this relative movement, and tension and shear fractures were possibly formed by this shear movement.

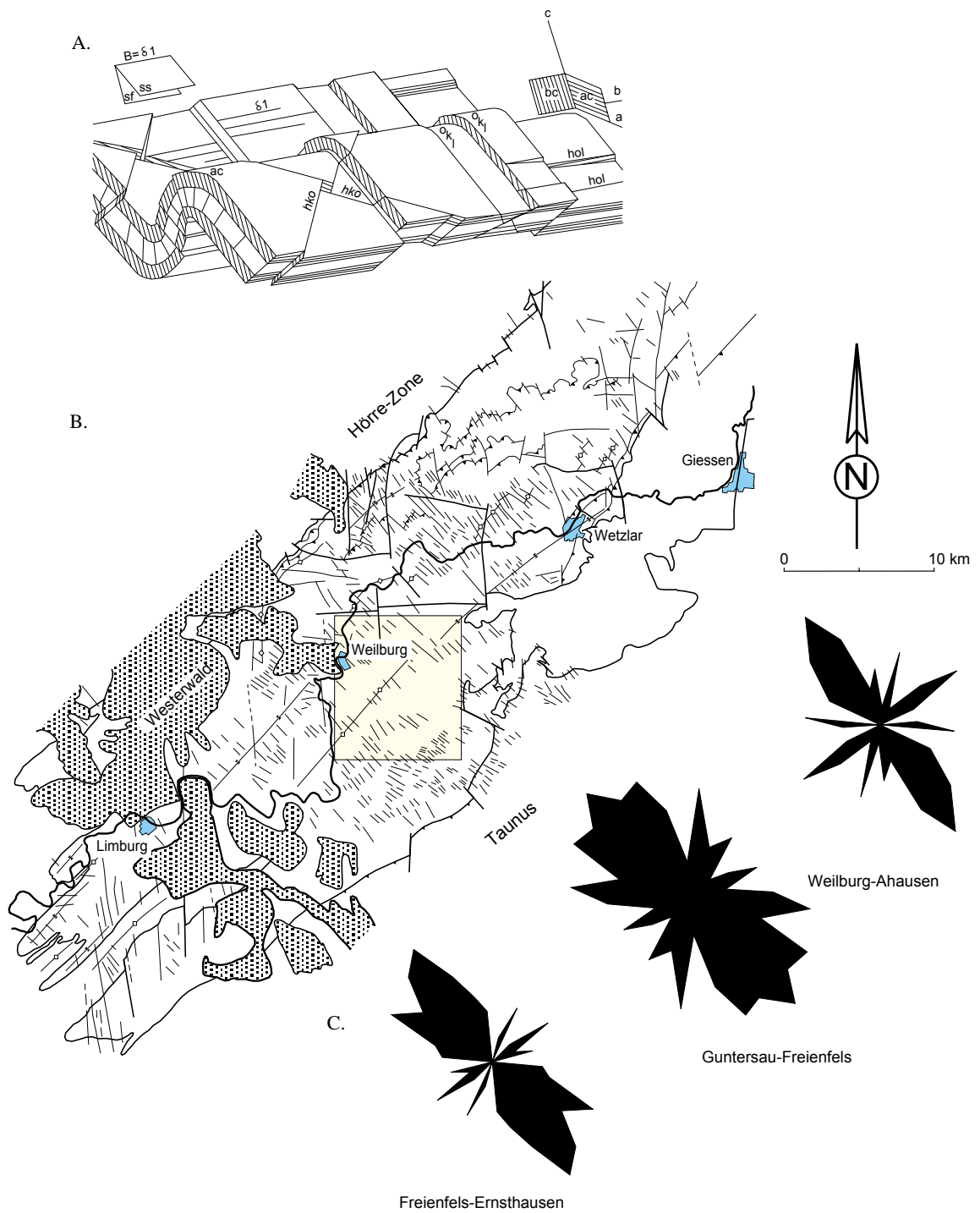


Fig. 5-5. Comparison of nomenclature of joints in a NW vergent fold (after RIETSCHEL & STRIBRNY 1979), (A), the structural development of the Lahn syncline (after KEGEL 1922), (B), and present joint-study of the Weilburg area (C).

5.3.2 Drag fold model

The term drag fold refers to a certain kind of fold with quasi-monoclinic symmetry that may develop in relatively thin competent layers in the flanks of larger folds. The thin layers showing drag folding are generally sandwiched between incompetent beds which, in turn, are interlayered with thicker competent beds (experiment: RAMBERG 1963), (Fig. 5-6). Drag folding is generally assumed to be caused by layer-parallel shearing (BILLINGS 1972, RAMBERG 1963), (Fig. 5-6B). This layer-parallel shear that is characteristic of drag folds makes them to an important tool in tectonic analysis. The vergence of drag folds indicates the position of anticlinal crests and synclinal troughs of the major folds in regions where the major folds are invisible (RAMBERG 1987).

In the study area, bedding as the pre-deformation structure is most prominent among the volcanics especially in volcanoclastics, which are mainly characterized by turbidites (BEHNISCH 1993), being more or less horizontal position. According to the sedimentary facies study the volcanoclastics were directly redeposited from the volcanic eruptions (BEHNISCH 1993) and, thus, controlled by both, sedimentary and volcanic processes. These volcanoclastics can be considered as sediments by exhibiting not only volcanics (e.g. base surge deposits) but also sedimentary structural characteristics (e.g. turbiditic deposits).

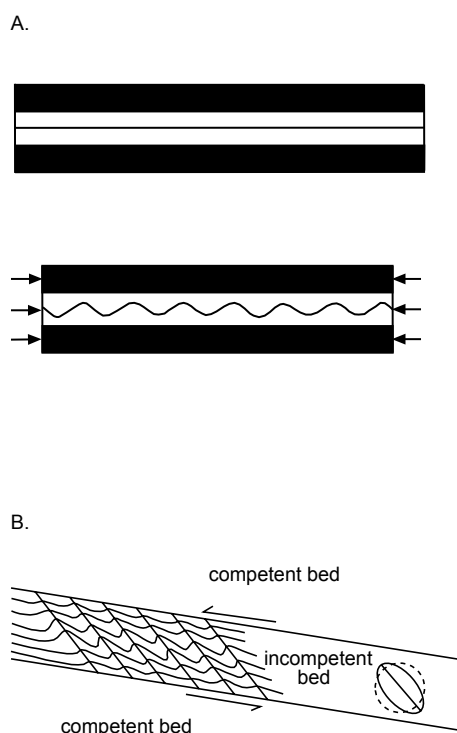


Fig. 5-6. A: A five-layer complex consisting of three relatively competent layers (black) and two relatively incompetent layers (white) sandwiched between two thick slabs of incompetent uniform material which impose a uniform compression upon the multilayer and adjacent material (after RAMBERG 1963); B: Drag folds in a banded incompetent layer sandwiched between competent beds under shear movement (after BILLINGS 1972).

Drag fold structures are only observed in ashtuff layers in the study area. They can be found, e.g. in a railroad-cut between Essershausen and Ernsthausen (see Chapter 3) as thin laminations of ashtuff which differ in grain-size and thickness (JÄGER 1996), (Plate 9). Thus, the mechanism of the drag fold model can be implied on the study area by the ashtuff as incompetent layer and the volcanic mass as competent layer. The ashtuff horizons are folded as incompetent thin layers which are interlayered in volcanic rigid masses, e.g. sheet flow lavas and lapillituff as competent thick layers (cf. RAMBERG 1987). Likewise, the volcanic masses are observed in broken as thrusts, may be due to the movement of a whole rigid mass. And the volcanic masses have not been folded in the Lahn-Dill area (see NESBOR & FLICK 1987B).

Furthermore, the axial cleavage developed in the drag fold is well recognized in the study area (see Plate 9). The axes of a set of drag fold are generally closely parallel to the axis of the major fold with which they are associated (RAMBERG 1987).

CHAPTER 6
OROGENIC COMPRESSION

CHAPTER 6

OROGENIC COMPRESSION

(Inversion tectonics)

Inversion tectonics can be caused by removal of a load (related to isostatic rebound) or by uplifting of rotated fault blocks and rift flank uplift at the margins of large grabens (related to extensional faulting) or due to collisional processes with the rotation of earlier fault blocks (horizontal plate movement).

Inversion tectonics was active in the Weilburg area, the Lahn syncline, part of Rhenohercynian zone. In a zone (fold-and-thrust belt) of the Variscan orogen in Central Europe, inversion tectonics was developed by northward orogenic compression or collision on earlier basinal development. The highest deformation occurs in the south and gradually decreases to the north. The inversion tectonics in the Weilburg area is noticed by the thrust systems and their related fold styles which are different in the local sub-areas (basins).

On top of a siliciclastic basement of Lower Devonian age as pre-rift sediments, depositional basins in the study area are filled with syn-rift sediments of considerable thickness. They are of Middle to Upper Devonian age, accompanied by substantial volcanics, mainly volcanoclastic sequences. This stage reached into lower Lower Carboniferous (cd II), however sediments and volcanics of this age are almost entirely lacking in the area. Consequently, upper Lower Carboniferous (cd III) siliciclastics mark the post-rift sedimentation before inversion by orogenic shortening.

The long profile of the Weilburg area between Ahausen (Lahn valley) and Ernsthausen (Weil valley) provides an insight into the extensional depositional basins which were deformed by later horizontal compression (orogenic compression). A small-scale 2-D model of the inversion tectonics in this long profile can be constructed by the interpretation of the graben type (domino-type), in which synthetic half-graben, antithetic half-graben and full-graben are distinctly delineated by their styles of fold and fault systems.

6.1 INVERSION INVOLVED TECTONIC HISTORY

In Western and Central Europe, the Variscan orogeny evolved during Lower Devonian to Lower Carboniferous time. The Rhenohercynian zone was developed as an ensialic back-arc basin (SMITH 1996, FLOYD 1995, 1982, ZIEGLER 1989, FLICK & NESBOR 1988, ENGEL et al. 1983, PEREKALINA 1981) at the southern margin of Laurussia (more exactly of Avalonia which was accreted during the Caledonian orogeny). Extensional rifting is exemplified throughout the Rhenohercynian zone as a simple shear Wernicke model continental extension (see Chapter 5).

During collision time the upper crust of the Rhenohercynian zone was shortened by 52 % on the average, starting with a shelf greater than 350 km in width (ONCKEN et al. 1999, ONCKEN 1997, DITTMAR et al. 1994). A detachment has been identified from balanced sections and from reflection seismic data to reach a maximum mid-crustal depth of 10 - 12 km below the top of sediments before

deformation. Lower crustal material below the present Rhenish Massif cannot have been deformed significantly during and after collision (ONCKEN 1997). The Cross-sectional area of underthrust lower Rhenohercynian crust thus amounts to a minimum of 2370 km² (ONCKEN 1997) bordered by a detachment fault (e.g. ONCKEN & WEBER 1995) developed from listric normal faults.

This situation is consistent with constraints stated by MORLEY (1988) whereby calculations of the depth of detachment assume listric faulting for basement faults, in which the hanging-wall is pervasively broken up by numerous minor faults, however, the foot-wall is totally undeformed. This concerns a 3 – 12 km thick pile of shallow marine clastics and carbonates of Devonian to Lower Carboniferous age (ONCKEN & WEBER 1995).

A large amount of horizontal compression above the décollement at the back of the wedge, is the main driving force in a fold-and-thrust belt, and the necessary condition for the formation of such belts is a weak basal layer, independent of any surface topographic slope (CHAPPLE 1978). In the southern part of the Rhenohercynian the earlier extensional structures are strongly overprinted by collisional structures (ONCKEN & WEBER 1995). They are better preserved in the middle and northern part, and are represented by growth faults in the early through late Devonian clastic shelf (WERNER 1989, ONCKEN 1989, WEBER 1981). Former listric normal faults were reactivated as reverse faults during collision (FRANKE et al. 1990, ONCKEN 1989).

Thin-skinned tectonics are assumed to the north of the Rhenish Massif in Germany (FRANKE et al. 1991). However, wide and open synclines and narrow upright thrust-related anticlines are only characteristic in the Ruhrcoal-mining area, to the north of the *Rheinische Schiefergebirge* (DROZDZEWSKI et al. 1985). To the west, the structures of the Ardennes developed thin-skinned tectonics in the roof of the London-Brabant Massif (LE GALL 1992, MEISSNER et al. 1981).

6.1.1 Inversion tectonics

2-D profiling is reasonable to adopt for re-evaluation of steep pre-existing faults that were reactivated during inversion. This is evidenced by reactivation of the older normal faults into thrusts and possible creation of new thrusts that might easily amount to several kilometres of thrust overlap. Structures marked by little or no reactivation of earlier normal faults and creation of younger low-angle thrusts will be an additional element of compression.

The strike of the thrust faults in the central Lahn syncline most likely reflects the trend of the margins of the extensional basins. In detail, the geometries of the mid to late Devonian extensional systems control the detachment levels, fault trajectories and apparent fault sequences.

Inversion tectonics is recognized by stratigraphic sequence and development of faults (thrusts) and folds in the Weilburg area.

6.1.2 Basement involved thrust system

During extension the basin of the Lahn-Dill area was formed by different types of sub-basins as half-graben and full-graben in which the half-grabens can be classified according to the later compression direction as synthetic: facing towards the compression direction, and antithetic: facing away from the compression direction.

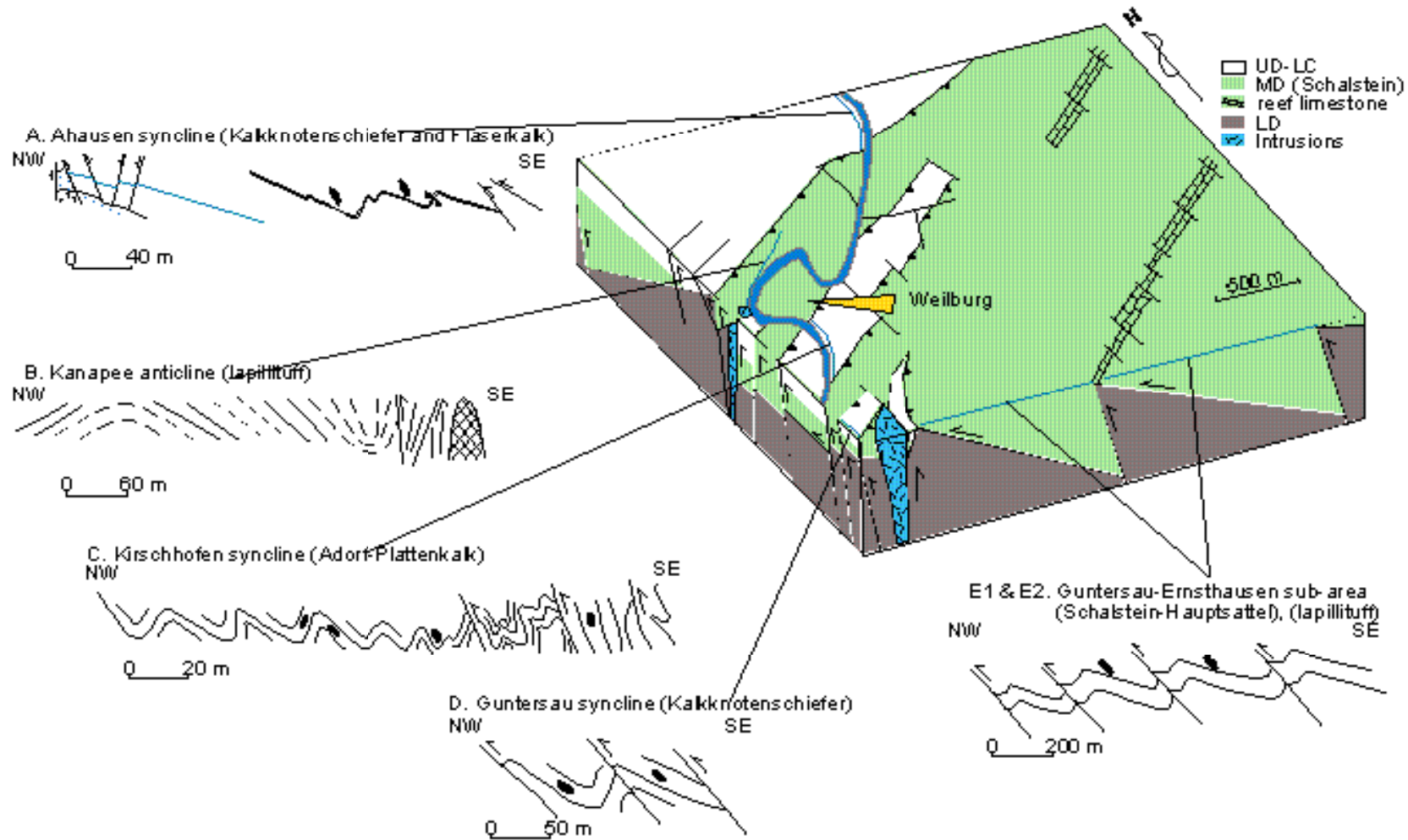


Fig. 6-1. Development of folding with variable strain patterns in different sub-basins with implication to the pre-rift and syn-rift basin position in the Weilburg area. (block diagram based on the geological map in Fig. 1C, modified after RIETSCHEL 1966). (LC = Lower Carboniferous, UD = Upper Devonian, MD = Middle Devonian and LD = Lower Devonian)

During collision the extensional basins were shortened by orogenic compression, whereby the former extensional faults were reactivated. These inversions were controlled by the orientation of the basements and their bordering fault systems.

Basement control played an important role in the inversion tectonics according to the observation of thrust-styles differentiating each part of fault systems, variable folding types in local areas, strain partitioning in different shapes of basins and types of deformation in different basins (Fig. 6-1). In this case, using the field exposures (profiles of road-cut sections) in the syn-rift stratigraphic sequence, the inversion tectonics is defined by the deformation style of basins with the position of sub-basins during extension.

6.1.3 Folding style and basin configuration

Folding in the study area differs in the sub-areas according to the configuration of the basins. These basins were developed as antithetic half-graben basins in the Guntersau-Freienfels sub-area, Freienfels-Ernsthausen sub-area, Guntersau syncline and the Reuschenbach anticline, as a full-graben in the Kirschhofen syncline, and as synthetic half-grabens in the Ahausen syncline, Kanapee anticline, Wehrstein syncline and the Hauslei anticline during the extensional period.

In the Kirschhofen syncline a disharmonic fold style is developed, including a transition from the vertical tight upright fold to overturned fold from south to north, (Plates 1 & 2). The Kirschhofen syncline was formed by the flexural slip on the local detachment fault along the sub-horizontal basin floor.

The antithetic basins were deformed by imbricated thrust and related fold structures slipping on local detachment faults in the style of the accretionary prism type deformation. In the synthetic half-graben, short-cut thrust related asymmetrical plunging folds at the front and extensional faults developed at the rear side of the prism by reactivation of extensional border faults.

These basins contain different rock types, such as volcanics which are encountered as acidic volcanism in the full-graben basin and basic-type volcanism in antithetic and synthetic half-graben.

6.2 INVERSION IN THE WEILBURG AREA

The study area is covered by M.Sc. mapping areas (Heidelberg University) providing profile sections. These were analyzed for a new interpretative approach by use of the structural geological study as guide line. In fact the depositional local basins can be recognized by the reef limestone, iron formations and volcanic eruption centres. Furthermore, fold styles and fault systems marked differences in the neighbouring local basins, defined as synthetic half-grabens, antithetic half-grabens and full-graben.

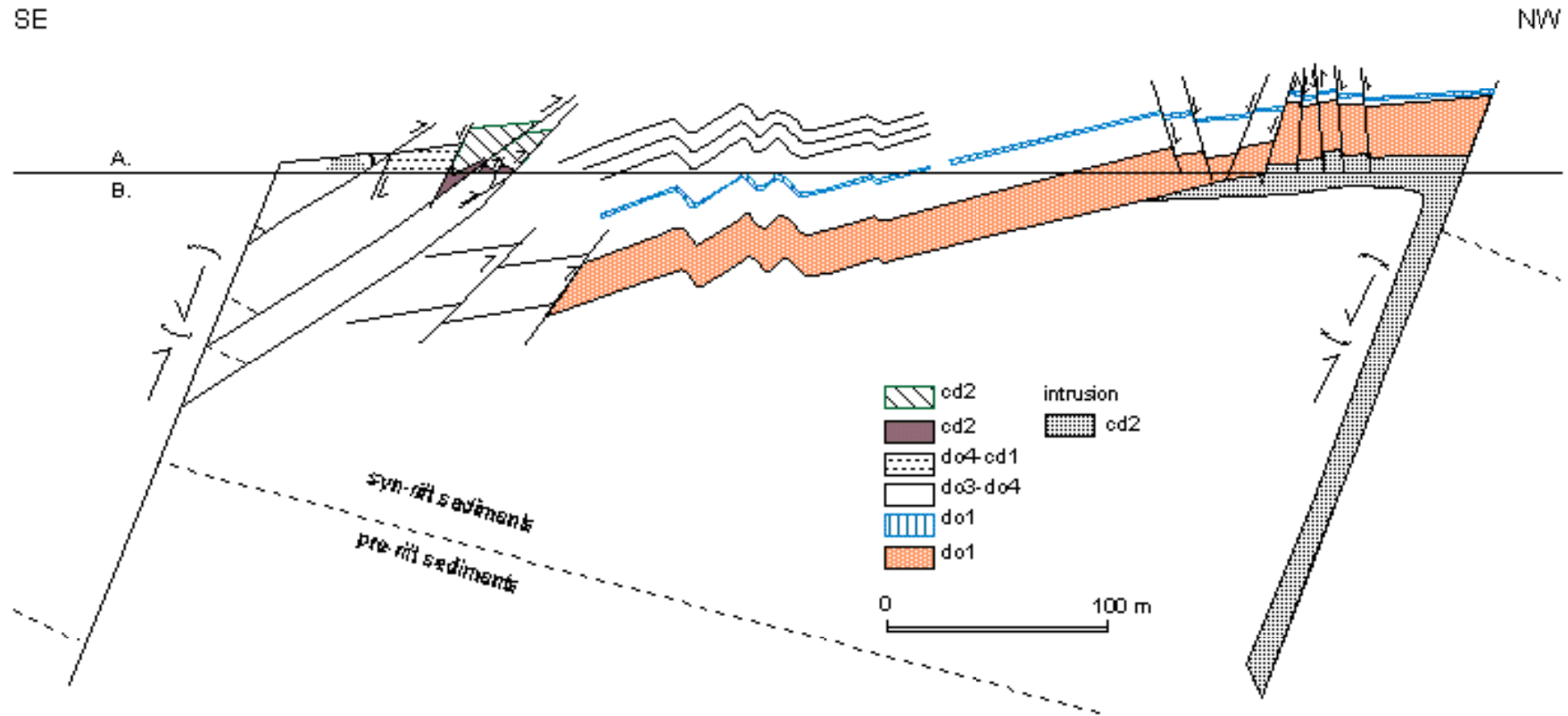


Fig. 6-2. Synthetic half-graben basin deformation at the Ahausen syncline by inversion tectonics during Variscan orogeny moving from SE to NW. A: Road-cut level profile (after SCHLEUNIGER 1989), B: Interpretative sub-profile, arrows in the brackets mark the movement during the extensional period. (signatures in Table 1-1)

6.2.1 Synthetic half-grabens

In the study area, synthetic half-grabens comprise the basis for the Ahausen syncline and the Kanapee anticline. In the **Ahausen syncline** (profile: SCHLEUNIGER 1989, RIETSCHEL 1966) the synthetic half-graben environment is mostly exposed in Upper Devonian to Lower Carboniferous rocks (Fig. 6-2). During the orogenic period, normal faults bordering the half-graben were reactivated as boundary thrusts (extensional boundary thrust). In the Ahausen syncline *alaunschiefer* (black shales), (cd II), (Table 2-1), are indicative of transgressional facies (cf. HERBIG 1998, and WIGNALL 1991) during mainly the late Viséan (cd IIIa) eustatic transgression that continued into Central Europe. This is globally recognized on cratonic shallow shelves by the *alaunschiefer* (black shales) unit (HERBIG 1998).

During inversion, the extensional faults prograded at the rear side of the prism due to the movement of short-cut thrusts to the tectonic direction (Fig. 6-2). Basaltic melt intruded into the Upper Devonian rocks (do 1) during middle Lower Carboniferous (cd II). Contact metamorphism occurred as calc-silicate hornfels as a result of this intrusion (GREIM 1887).

During reactivation and inversion of the extensional border faults of the half-graben, the foot-wall side underwent compression and the hanging-wall side was subjected to extensional forces. Thus, the shallow part of the half-graben basin was affected by foot-wall short-cut thrusts which cut across the uppermost (cd II) and upper (do1 – cd I) syn-rift sediments. At the deeper part of the basin, small extensional faults (normal faults) were developed (Fig. 6-2).

Folding is substantiated by asymmetrical folds (long limb and short limb) with a NW vergence which can be recognized in the layers of the *Rotschiefer* (red shale) and *Kalkknotenschiefer* (lime nodular slate). The type of folding can be classified as close to tight folding (terms of fold: GHOSH 1993, TWISS & MOORES 1992, BILLINGS 1972, FLEUTY 1964), (Fig. 6-2).

The **Kanapee anticline** exposing upper Middle Devonian volcanoclastic sediments, sheet flow lavas and pillow lavas also exhibits the characteristics of the synthetic half-graben type deformation. The type of folding shows a tight folding to an open anticline to the NW (Fig. 6-1). The tight folds were developed near the border fault together with short-cut thrusts at the face of compression bordering the Kirschhofen syncline. Thus, bedding planes show a sub-horizontal position in the outcrops where they are only exposed at the rear side of the prism and show no deformation features in the strain analysis (see Chapter 4).

6.2.2 Antithetic half-grabens

Antithetic half-grabens are developed in the Guntersau-Freienfels (profile: BEHNISCH 1988, and FLICK & NESBOR 1988) and Freienfels-Ernsthausen (profile: after JÄGER 1993) sub-areas. These different small half-graben basins were filled by volcanoclastic sediments, sheet flow lavas and pillow lavas from different sources in terms of volcanic centres of the Weilburg area during the Middle Devonian.

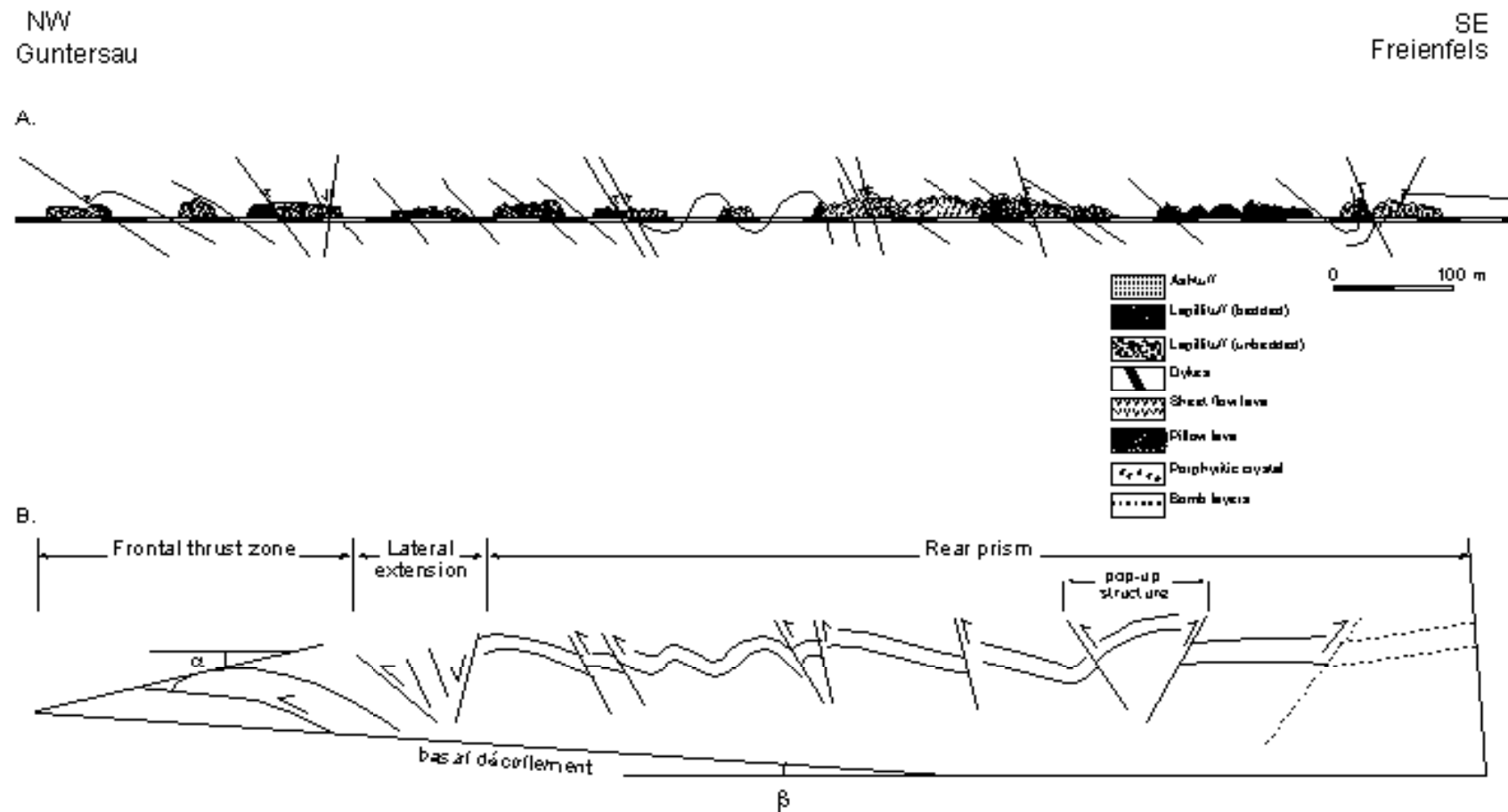


Fig. 6-3. Accretionary prism type deformation in the antithetic type half-graben of the Guntersau-Freienfels sub-area. A: Profile of the Guntersau-Freienfels sub-area (after BEHNISCH 1988), B: Interpretative accretionary prism of the Guntersau-Freienfels sub-area. (Length of section about 2 km, = outline of structures), (α = angle of topographic relief, β = dip angle of rigid base)

During orogenic movement the antithetic half-grabens reacted like an accretionary prism (Fig. 6-3) with its deformation toe at the NW (Plate 8), (cf. GUTSCHER et al. 1996 and MALTMAN et al. 1993). The antithetic half-graben deformation coincides very well with sandbox experiments of GUTSCHER et al. (1996) representing the accretionary prism-type deformation. According to GUTSCHER et al. (1996), MALTMAN et al. (1993) and PLATT (1986), this can be divided into:

1. Frontal thrust zone,
2. Lateral extension (PLATT 1986)
3. Rear prism
 - Upper prism,
 - Lower prism and
4. Basal décollement (MALTMAN et al. 1993).

Frontal thrust zone: Thrusting is accompanied by the steepening of the bedding. In this case, lapillituff layers (Middle Devonian) were overthrust upon the *Adorf-Plattenkalk* (Upper Devonian), (Plate 8). At the contact zone brecciation and scaly texture (small flat lapilli: BEHNISCH 1988) are present along the basal décollement (cf. MALTMAN et al. 1993).

Lateral extension: Extensional faults (normal faults) are developed behind the frontal thrust zone (Fig. 6-3) which will internally push the front forwards and produce compressional structures at the front. A convergent orogenic wedge, may start to extend horizontally under certain conditions (according to PLATT 1986 and ENGLAND 1983), e.g. where α (surface slope) and h (prism thickness) exceed certain values over a major portion of the wedge, so that extension begins at the rear prism (Fig. 6-3).

Rear Prism: *Upper prism*: It is represented by break thrusts (cf. GUTSCHER et al. 1996, and MALTMAN et al. 1993) and variation of bedding dip with depth(?), steepened and inverted bedding (cf. MALTMAN et al. 1993) in the shallow horizon together with some fold and pop-up structures (Fig. 6-3), (cf. LALLEMAND et al. 1994). Extensional faulting is observed behind the frontal thrust zone which is controlled by α and β angles (Fig. 6-3). If the α angle is slightly too small, the frontal zone develops an out of sequence thrust, whereas the rear prism is removed from above by extension.

Lower Prism: It is not exposed in the profile because it lies below the level of the road-cut.

Basal décollement: The basal décollement (indicating local décollement) of the deformation toe is encountered at the frontal thrust zone under the overthrust (Fig. 6-3). Commonly, most fold-and-thrust belts have several features, including a characteristic wedge shape and a basal zone of décollement below which there is no deformation (CHAPPLE 1978).

Buckling folds can be related to the emplacement of the thrust (fault related folding: Plate 9 & Fig. 6-3). Backlimb thrusts (fault geometry: GHOSH 1993, MORLEY 1988, BUTLER 1982) are common in the field (Plate 9).

The pop-up structure in the rear prism consists of a fine-grained ashtuff characterizing a NW verging anticline. This tuff is thrust over a lapillituff to the SE and a sheet flow lava to the NW (Fig. 6-3). The ashtuff is a NW verging anticline due to the drag effect at the north-western thrust (cf. GHOSH 1993).

Anisotropy of Magnetic Susceptibility (AMS) applied to the accretionary prism deformation: In accretionary prisms, the deformation toe is more deformed than the prism body which can be recognized by the AMS study, e.g. T-P^l (T = shape factor, P^l = anisotropy degree) relation (JELINEK 1981) of the lapillituff from the Guntersau-Freienfels sub-area (Fig. 7-10). Samples from the deformation toe show higher anisotropy or more flattening than those from the prism body. As well, the progressive simple shear direction can be interpreted from the data set (cf. BORRADAILE & HENRY 1997). Furthermore, the T-P^l relation of lava together with lapillituff shows a smaller cluster for the lava enclosed by the cluster of the lapillituff. The lava was not deformed, based on an anisotropy degree of P^l = 1.06, which is comparable to undeformed sediments (HROUDA & HRUSKOVA 1990, HROUDA et al. 1978, DVORÁK & HROUDA 1972). Tectonically, the lava acted as a competent layer which was not deformed according to the model of competent volcanic masses movement (see Chapter 5: drag fold model). On the other hand, the lapillituff was deformed as incompetent layer according to the relationship between lava and lapillituff in the T-P^l diagram (Fig. 7-9).

In the Freienfels-Ernsthausen sub-basin the pillow lava reacted totally different on deformation between the deformation toe (Plate 4B) and the rear prism body (Plate 5) as substantiated by the field observation and the AMS study. The AMS (relation in the T-P^l diagram) of these pillow lavas shows a different anisotropy degree or flattening of deformation grade with respect to the deformation grade which is higher in the deformation toe (Fig. 7-14).

6.2.3 Full-graben

The full-graben profile in the Kirschhofen syncline mostly exposes Upper Devonian *Adorf-Plattenkalk* and *Kalkknotenschiefer* which includes Lower Carboniferous basaltic intrusions. This profile is marked by disharmonic folding (Fig. 6-4), exhibiting a transition from sub-vertical tight upright folding to overturned folding (terms of fold: GHOSH 1993, TWISS & MOORES 1992, BILLINGS 1972, FLEUTY 1964) from SE to NW. This type of folding indicates a sub-horizontal floor basin before deformation which was activated as a detachment fault. During compressive deformation this local detachment fault on the basin floor developed flexural-slip folding (cf. Rocky Mountain building: GHOSH 1993, flexural-slip folding on the décollement zone: OGAWA 1982 and a transition from upright to recumbent folding: SANDERSON 1979). The fault system develops a transition from a sub-vertical reverse fault to a NW verging thrust fault from SE to NW. This type of folding and fault system indicates a full-graben basin for the Kirschhofen syncline which was developed on the local detachment zone (it may be a local detachment fault with respect to the basin floor which has existed since basin extension). Transitional changes in the position of the s₁-cleavage are observed from sub-vertical to the SE to inclined (30° SE) to the NW (Fig. 6-4), (Plates 1 & 2).

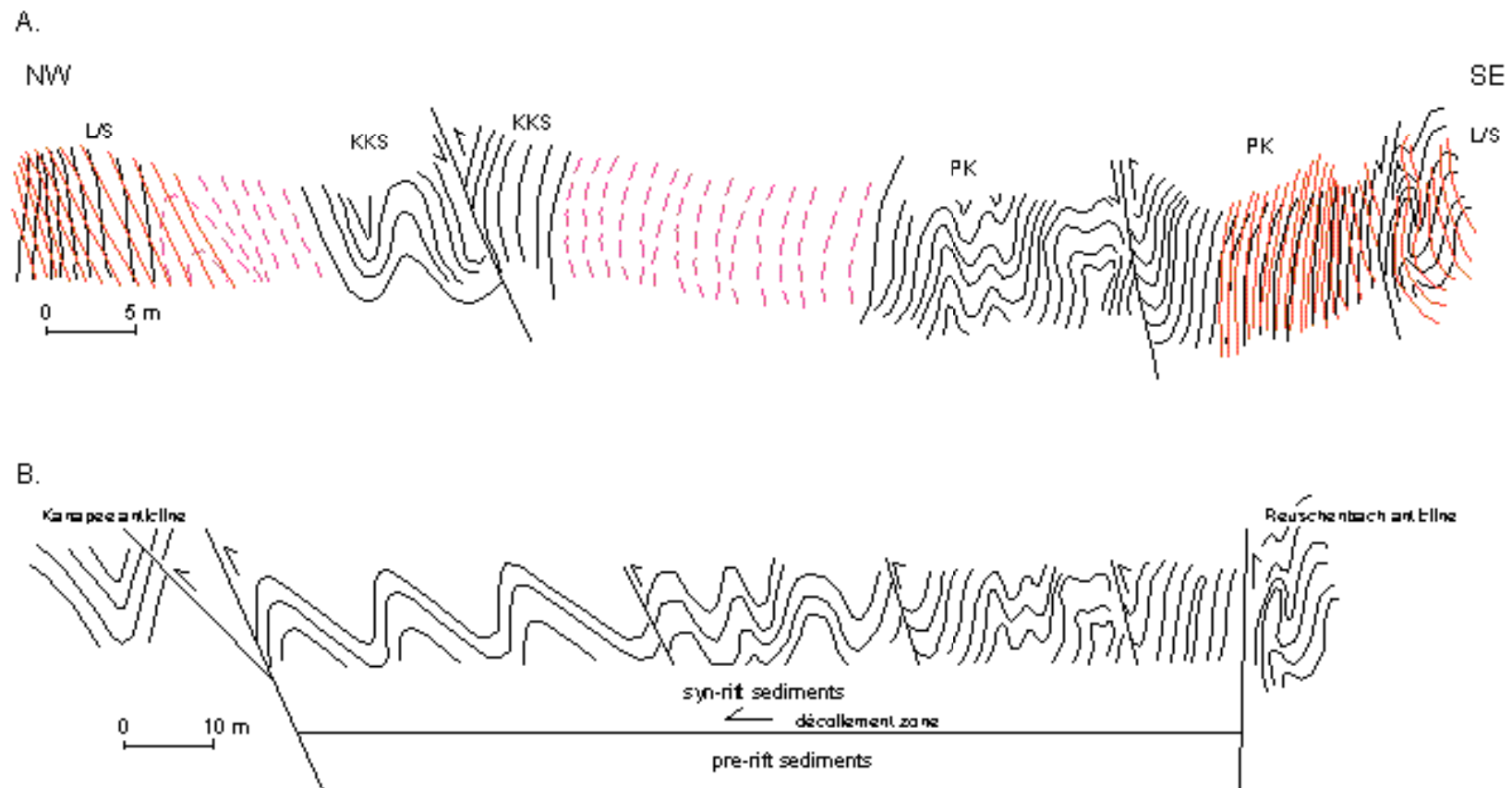


Fig. 6-4. Structural profile of the Zeppelinfels near Weilburg (Kirschhofen syncline) exhibiting the fold development in the Upper Devonian Adorf-Plattenkalk and Kalkknotenschiefer.
 A: Profile of the Kirschhofen syncline, B: Interpretation of the full-graben basin of the Kirschhofen syncline (Depth of border between pre-rift and syn-rift sediments not to scale)

L/S=Lappil tuff and slate interbedded, KKS=Kalkknotenschiefer, PK=Plattenkalk
 Thin line=cleavage, medium line=bedding, thick line=fault.

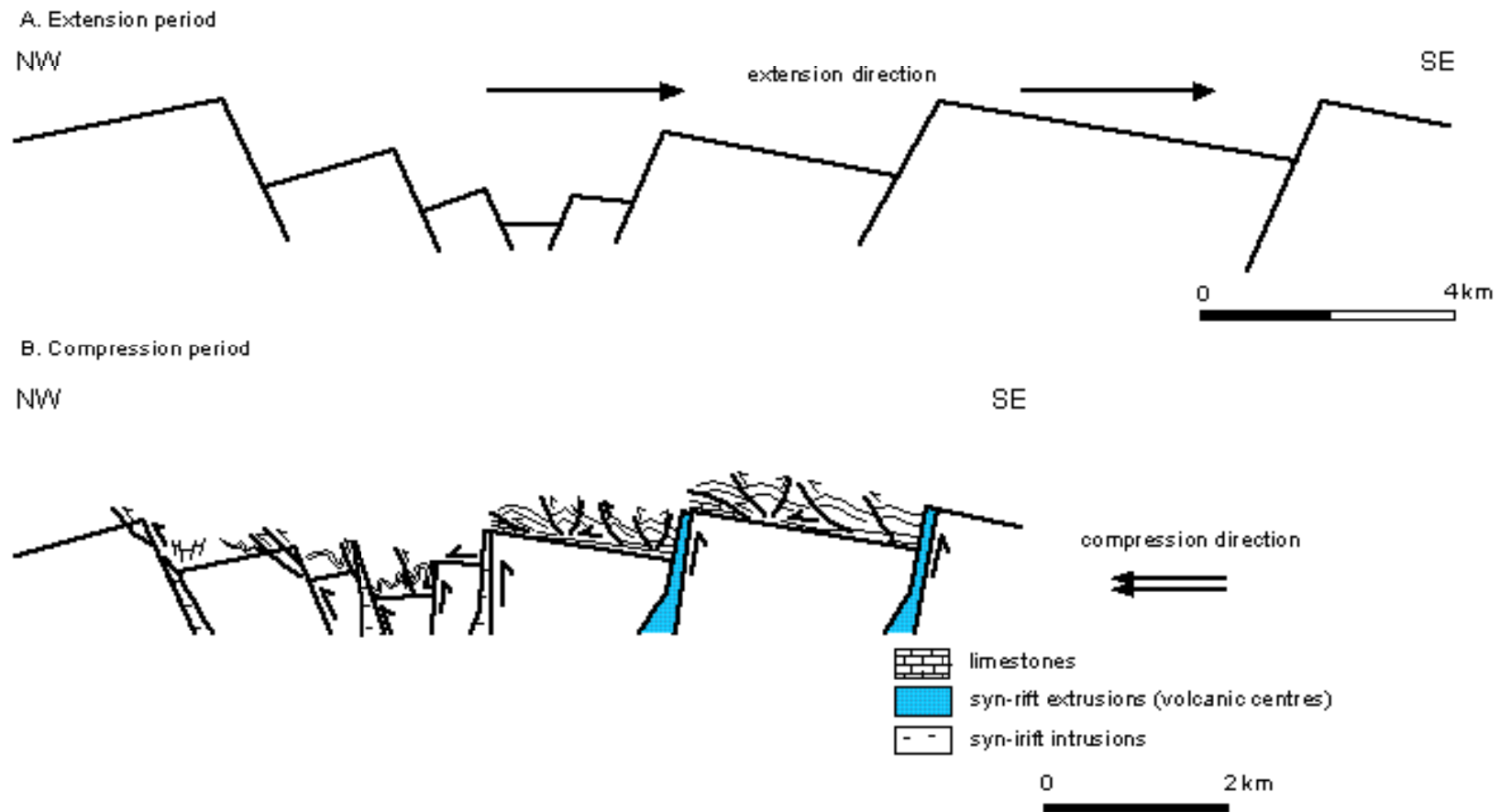


Fig. 6-5. Sketch showing the style of inversion tectonics with the development of fold style and fault system in the Weilburg area, Lahn syndine, Rhenohercynian zone, from extension (A) to compression period (B).

6.3 DISCUSSION

As part of Variscan Europe the Rhenohercynian basin, site of the present study area, developed crustal extension accompanying Lower Devonian to Lower Carboniferous sedimentation prior to horizontal compression during the Variscan orogeny in the Carboniferous time. Under collision NW verging thrust systems developed in the whole area, however, these exhibit a different style and system according to the configuration of inversion (Fig. 6-5). The thrust systems were controlled by the basement in terms of the extensional position in graben basins: bordering antithetic half-grabens, synthetic half-grabens and full-graben (cf. Fig. 6-6).

In fact, each sub-basin has its own local detachment fault, e.g. the Guntersau-Freienfels antithetic half-graben and the Kirschhofen full-graben have been moved on their local detachment faults indicating depositional basin floors. The folds differ as well in type according to their basin configuration, associated with the thrust systems. The local detachment faults are situated between pre-rift sediments of Lower Devonian (at least: Lower Devonian and older) and syn-rift sediments.

Syn-rift sedimentation starting shortly before the onset of the lower Middle Devonian was accompanied periodically by volcanic activities yielding volcanogenic sediments. Syn-rift sediments reacted, on deformation, as accretionary prisms in antithetic half-graben, flexural-slip folding in full-graben on the local detachment faults and short-cut thrust related asymmetrical folding in synthetic half-graben.

Extensional boundary thrusts can be observed between the structural units, being however absent in the antithetic half-graben basins, where local detachment faults were active and developed overthrusts at their deformation toe (Plate 8). The antithetic half-grabens show overthrusts at the deformation toe by the foot-wall uplifting over the younger rocks (Upper Devonian (Adorf): *Plattenkalk*) during the compression period. That means that there was no barrier to overthrust (barrier: steep scarp of extensional border fault) at their deformation toe of the antithetic half-grabens. The antithetic half-grabens were deformed similar to accretionary prism-type deformation according to evidence concerning the characteristics of thrust systems.

However, the full-graben has a barrier of steep scarp of extensional border faults at the front of the graben, indicated by the disharmonic folding (a transition from sub-vertical tight upright folds to overturned folds). Together with this folding a transition of sub-vertical reverse faults to NW facing thrusts is observed.

In the synthetic half-grabens, extensional boundary thrusts movement is distinctly reactivated. Due to this movement short-cut thrusts at the front of compression are well developed (cf. MCCLAY & BUCHANAN 1992). Consequently, extension fault structures (normal faults) at the rear side of the prism are developed to accommodate for the short-cut thrust movements pushing the front forwards of the neighbouring basin at the synthetic half-grabens during the basin inversion (cf. PLATT 1986).

Style of folding can also be differentiated in sub-basins as disharmonic folding (flexural-slip folding) in full-graben, asymmetrical folding in synthetic half-graben, and thrust fault related buckle folding in antithetic half-graben.

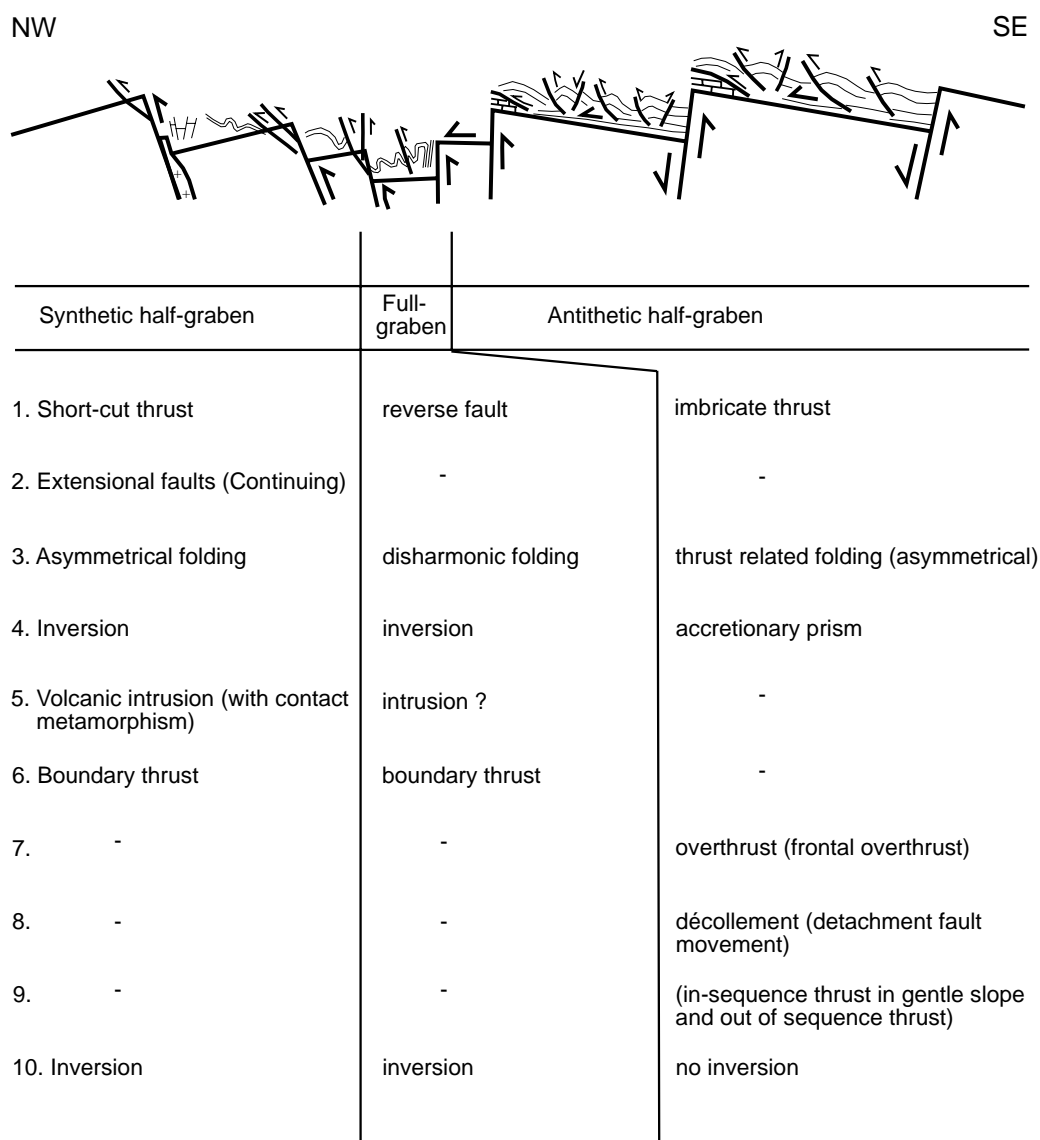


Fig. 6-6. Structural development of inversion tectonics as revealed along the long profile of the Weilburg area: comparison of the structural characters of the different half-grabens.

Generally, in the study area the shortening of about 50 % was initiated in the inversion tectonics by the horizontal tectonic compressive force from SE to NW (cf. the cross section through Fig. 6-5), (Fig. 6-5 and 6-6), (cf. COWARD 1994, McCLAY & BUCHANAN 1992 and COWARD et al. 1991).

The Kirschhofen syncline could be a centre of a small graben system by the extensional faulting due to the higher propagation of graben tectonics (cf. McCLAY & ELLIS 1987). The extensional border faults are quite closely spaced around the Kirschhofen syncline. Thus, the potential for intrusive dykes and volcanic centres was relatively higher than in other local sub-basins. The synthetic and antithetic half-graben are situated on either side of the Kirschhofen syncline.

CHAPTER 7
MAGNETOFABRIC ANALYSIS

CHAPTER 7

MAGNETOFABRIC ANALYSIS

(Anisotropy of Magnetic Susceptibility: AMS)

The Anisotropy of Magnetic Susceptibility (AMS) is a non-destructive approach for studying the average magnetofabrics of a small sample of rock. The AMS technique principally involves the collection of oriented rock samples to determine the three-dimensional magnetic susceptibility ellipsoid, which can then be interpreted in terms of the absolute magnitude of strain. In addition, the magnetofabric analysis is a very sensitive means of geological interpretation, e.g. geological structures. However, it requires knowledge of the physical and geological background. Magnetofabric analysis can now be performed very quickly, and the technique is restorative. Thus, this type of study has gained a considerable acceptance among structural geologists. In the present study, using magnetofabric analysis the interpretations of various structural developments in terms of flow-directions of sheet flow lava, current directions of lapillituff (hydroclastics and epiclastics) in the extensional environment which are later deformed under compressional environment are available to suggest the initial orientation and changes to present-day.

7.1 MAGNETIC SUSCEPTIBILITY

The magnetic susceptibility K , a dimensionless material constant, is proportionally directly related to the strength of induced magnetization (M) under the influence of the strength of the applied field (H). Thus, the magnetization M ,

$$M = KH$$

(where M = magnetic dipole element per unit volume (in A/m), H = magnetic field strength (A/m), and K = magnetic susceptibility in SI unit), (TARLING & HROUDA 1993, CARMICHAEL 1989)

Five different types of magnetisms can be distinguished: dia-, para-, ferro- and ferri-magnetism and anti-ferromagnetism.

Diamagnetism is a common material property in which a magnetization is produced in the opposite direction to that of the applied field. The electron shells are complete and the electron spins precess under a magnetic field. It has a negative susceptibility which is often in the region of 10^{-5} (SI) for common rock-forming minerals, e.g. quartz, feldspar, calcite (Table 7-1).

Paramagnetism is a material property in which a magnetic element has the same direction as the applied field. The electron shells are incomplete and the electron spins precess. Paramagnetism has positive susceptibility which extends over several orders of magnitude mostly 10^{-2} - 10^{-4} (SI) for common rock-forming minerals, e.g. biotite, hornblende (Table 7-1).

Mineral	K 10 ⁻⁶ SI	Kmax (Kx)	Kint (Ky)	Kmin (Kz)	P (Kx/Kz)	Remarks
DIAMAGNETIC						
Plagioclase	2.7					
Orthoclase	12.0	1,041	1,020	0,843	1.23	Crystal anisotrp. Kx II <a> Ky II Kz II <c>
Quartz	13.4				1.00	
Calcite	13.8				1.01	
					1.11	
					1.13	Kx II <c>
PARAMAGNETIC						
Epidote	1009	1.006	0.993	0.991	1.01	Kx II Ky II <c> Kz II <a>
Augite	555				1.08	Ky II
Orthopyrox.	1111				1.40	
Hornblende	207					Crystal anisotrp.
	5046				1.21	
	723				1.08	
Actinolite	1327				1.40	Kx II <c>
	8920	1.347	0.917	0.809	1.65	
	3560	1.076	0.982	0.947	1.13	
Crocidolite	6500	1.083	1.027	0.899	1.20	Crystal anisotrp.
	333	1.052	0.992	0.958	1.09	
Glaucofph.	787	1.094	1.006	0.908	1.20	Kx II (001) Ky II (001) Kz II <c>
Chlorite	358	1.093	1.060	0.864	1.26	
Biotite	70	1.287	1.058	0.743	1.73	Crystal anisotrp.
	1550	1.128	1.023	0.866	1.30	
	370	1.063	1.020	0.921	1.15	
	1230	1.114	1.106	0.812	1.37	
	1180	1.098	1.095	0.832	1.31	
Phlogopite	998	1.107	1.096	0.824	1.34	Crystal anisotrp.
	1290	1.108	1.107	0.814	1.36	
Muscovite	1180	1.098	1.091	0.830	1.31	
	165	1.159	1.052	0.820	1.41	
FERRI-,ANTIFERROMAGNETIC						
Magnetite	5800000	1.063	0.989	0.951	1.11	form anisotrop.- metamorph detrital experiment Middle value from metam. u. magmat. rocks theoretic value of middle like grains with X/Z = 10
	6200000	1.108	0.964	0.936	1.18	
					1.4	
					7	
Ti-Magnetite	10000					Crystal anisotrp. Kx Ky II (0001) Kz II <c>
Pyrrhotite	1500000	10.24	3.68	0.027	to ab. 10000	
Ilmenite	ab. 6000	9.10	3.91	0.028	379.2	metamorph. metamorph. Ilmenite is <u>paramagnetic</u> at room temperature!
					325.0	
Ilmenite-Haem.	26000				1.08	Crystal anisotrp. Kx Ky II (0001) Kz II <c>
					1.4	
Haematite	1321				15	Crystal anisotrp. Kx Ky II (0001) Kz II <c>
					to >100	
Goethite	7000				>100	Crystal anisotrp. Kx Ky II (0001) Kz II <c>
					10000	
Limonite	1357				1.28	
Siderite	11058					
Pyrite	3000					
	5000					
	1000					

Table. 7-1. (Volume-) Susceptibility and anisotropy (crystal or grain shape controlled) of the most common metamorphic minerals (after JUCKENACK 1990).

Ferromagnetism is a basic physical property which has very much stronger positive susceptibilities than paramagnetic minerals and may also carry a strong remanent magnetization, i.e. magnetization remains after the external magnetic field has been removed. It has spontaneous magnetization, superimposed on paramagnetism, e.g. metals as Ni, Fe, Co.

Anti-ferromagnetism is a physical property, in which the two magnetic lattices are equally strongly magnetized (anti-parallel) and show no net magnetization, e.g. FeS₂, Mn₂O₃.

Ferrimagnetism is a physical property, in which one magnetic lattice is more strongly magnetized and exhibits a net magnetic field, e.g. Fe₃O₄.

A magnetic domain is a volume element which has a north and a south poles. Each domain is separated from its neighbour by a narrow Bloch wall. The domain size is >100 μm which depends on the mineral and the Bloch wall is about 50 - 5000 atom-distances wide.

Without the external-aligned forces the domains arrange themselves to minimize the magnetostatic energy associated with their surface poles. For this alignment two mechanisms, namely Bloch wall displacement and rotation process, are distinguished. The displacement of the Bloch wall in the crystal can be reversible or irreversible after the removal of the external field. The irreversible changes lead to a remanent magnetization.

Thermal activity acts against an order of magnetic single elements and leads to the disappearance of the spontaneous magnetization at a specific material temperature (Curie temperature: T °C). In the polymagnetomineralic rock the volume susceptibility results from the sum of its single mineral susceptibilities:

$$K_{\text{rock}} = V_d K_d + V_p K_p + V_f K_f$$

(K_d, K_p, K_f = single mineral susceptibilities of diamagnetic, paramagnetic and ferro(i)magnetic components and V_d, V_p, V_f = their volume susceptibilities)

The susceptibilities of important rock-forming minerals are listed in Table 7-1. Most rock-forming minerals have a poor crystallosymmetry, which can lead to an intrinsic anisotropy of rock physical properties with weak and strong potentials of magnetism. An overview of the anisotropy of magnetic susceptibility is shown in Table 7-1.

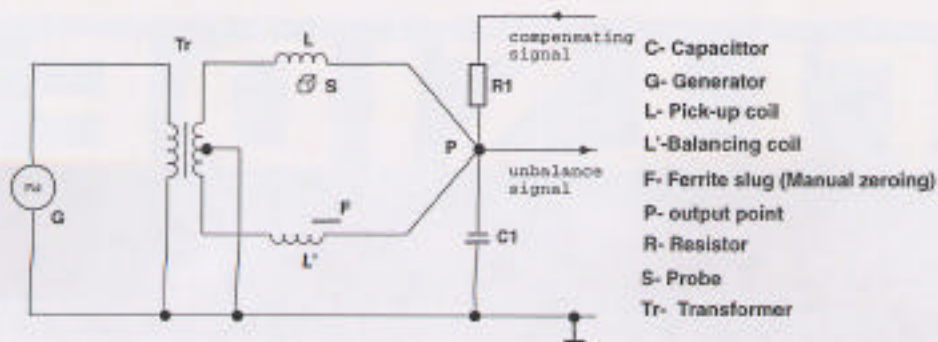
Anisotropy of Magnetic Susceptibility (AMS)

The anisotropy of magnetic susceptibility is observed in most minerals so that the rock susceptibility is direction-independent and depends on the following factors:

1. The crystal anisotropy of the individual mineral
2. The shape anisotropy of the individual mineral
3. Frequency and distribution of dia-, para-, ferro- and ferri-magnetic minerals

The crystal anisotropy minerals (Table 7-1) connect the potential of magnetism with the position of crystallographic axes, they constitute by the diamagnetic and paramagnetic silicates, and weak ferrimagnetic and anti-ferromagnetic ore minerals.

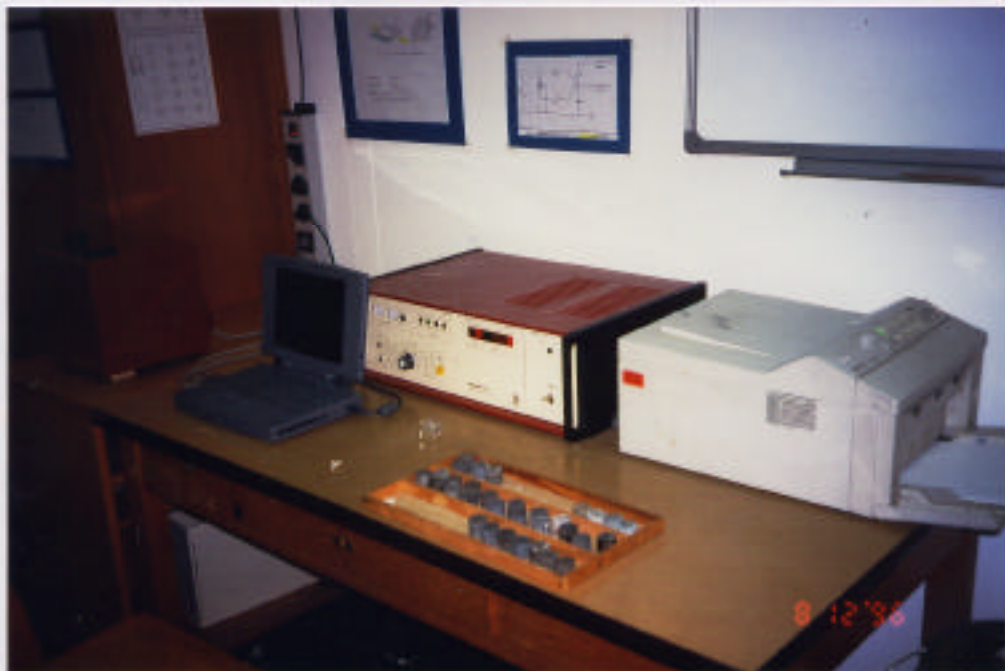
The shape anisotropy is important for magnetic ore minerals with a very large susceptibility, e.g. magnetite.



SPECIFICATIONS OF Kappabridge KLY-2

Magnetic field intensity (r.m.s value)	300 Am^{-1}
Operating frequency	920 Hz
Field homogeneity	0.2 %
Homogeneity area	Cylinder space, $d = 43 \text{ mm}$, $h = 41 \text{ mm}$
Cylinder specimen	$d = 25.4 \text{ mm}$, $h = 22 \text{ mm}$
Cubic specimen	$20 \times 20 \times 20 \text{ mm}$
Measuring vessel for fragment specimen	40 cm^3
Nominal specimen volume	10 cm^3
Digital display	0-1999 units
Measuring ranges	11 ranges ($200\,000 \times 10^{-6} \text{ SI}$)
Sensitivity for specimen (for $V=10 \text{ cm}^3$)	4×10^{-5}
Accuracy within one range	$\pm 0.1 \%$, ± 1 count
Accuracy of the range divider	$\pm 0.3 \%$
Accuracy of absolute calibration	$\pm 3 \%$
Power requirements	220 v, 50 Hz
Large specimen pick-up unit	28 kg

Fig. 7-1. Circuit diagram of Kappabridge KLY-2 (after GEOFYZIKA Brno, CZ)



The AMS can be described as a symmetrical tensor in two orders. There is an intrinsic value of matrix tensors with the principal susceptibility sets in K_{11} , K_{22} and K_{33} which correspond to the orthogonal principal axes of the AMS ellipsoid $K_1 > K_2 > K_3$. The K_1 and K_2 axes define the foliation. The direction of K_1 long axes corresponds to the magnetic lineation and K_3 axes represent the pole of the magnetic foliation.

7.2 ANALYSIS OF DATA

Measurement: The AMS measurement was carried out with a Kappabridge KLY-2 at room temperature (Geofyzika Brno, CZ, JELINEK 1980), (Fig. 7-1), using the ANISO 10-14 programs (JELINEK 1977) for calculations. Samples for the AMS measurement are standardized to a constant size in cylinder shape: 2.5 cm diameter x 2.2 cm length, the proportions ensuring the best approach of spherical sample geometry (Fig. 7-2). The cylinder is marked with the field orientation on the top surface and on the cylinder. This marking is used for sample orientation in the AMS measurement correlated to the stereoplots in the lower hemisphere of the AMS ellipse. The AMS is measured in 15 different positions (Fig. 7-2). The KLY-2 Kappabridge has a sensitivity of 5×10^{-6} SI in detected anisotropy as low as 0.1 %.

The description of the AMS was suggested by HROUDA (1982) in different parameters which are derived from using principal axes ratio and different susceptibility. The principal susceptibility ellipsoid axes are referred as the maximum, intermediate and minimum volume susceptibility axes in SI units of $K_1 \geq K_2 \geq K_3$.

Analysis: The calculations of the program ANISO 10-14 are used following analysis by the Kappabridge KLY-2.

Total anisotropy H depends on:

$$H = K_1 - K_3 / K_m \quad \text{OWENS (1974A)}$$

K_m = mean susceptibility

The parameter of the mean susceptibility K_m :

$$K_m = (K_1 + K_2 + K_3) / 3$$

The intensity of the preferred orientation of magnetic minerals in a rock is indicated by the anisotropy degree factor P:

$$P = K_1 / K_3 \quad \text{HELLER (1973), JANÁK (1972), HROUDA et al. (1971)}$$

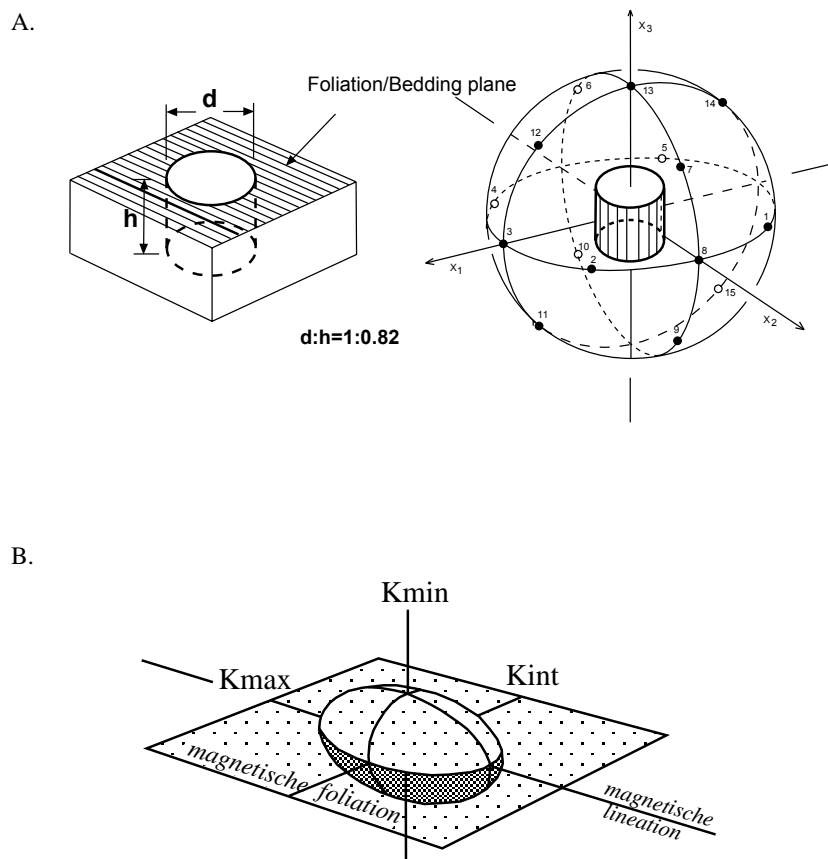


Fig. 7-2. A: Geometry of measurement setting of Anisotropy of Magnetic Susceptibility (AMS), (after JELINEK 1977), B: The AMS ellipsoid (after De WALL 1991)

The corrected anisotropy degree P^I is determined by:

$$P^I = \exp\sqrt{\{2[(\eta_1 - \eta)^2 + (\eta_2 - \eta)^2 + (\eta_3 - \eta)^2]\}} \quad \text{JELINEK (1981)}$$

where $\eta_1 = \ln K_1$, $\eta_2 = \ln K_2$, $\eta_3 = \ln K_3$ and $\eta = (\eta_1 \cdot \eta_2 \cdot \eta_3)^{-3}$

The character of the magnetofabric is indicated by the shape factor T :

$$T = [2 \ln(K_2/K_3) / \ln(K_1/K_3)] - 1 \quad \text{JELINEK (1981)}$$

If $0 \leq T \leq 1$ magnetofabric is planar.

$-1 \leq T \leq 0$ magnetofabric is linear.

The shape of the susceptibility ellipsoid U is determined by:

$$U = 2K_2 - K_1 - K_3 / K_1 - K_3 \quad \text{JELINEK (1981)}$$

The analogy between the shape factor, T and U, is obvious. If the anisotropy degree is low, the values of these factors are practically equal.

The shape of susceptibility ellipsoid D depends on:

$$D = (F-1)/(L-1) \quad \text{KLIGFIELD et al. (1977), HROUDA (1976)}$$

$$D = 0 - 1 \text{ (Flattening)}$$

$$D = 1 - \infty \text{ (Constriction)}$$

The magnetofabric is defined by the geometric elements: the groups of K_1 and K_3 are the magnetic lineation and the pole of magnetic foliation, respectively. Intensities of lineation, L, and foliation, F, are determined by:

$$L = K_1/K_2 \text{ - parallel to maximum susceptibility direction,}$$

$$F = K_2/K_3 \text{ - perpendicular to minimum susceptibility direction}$$

The axial ratio plot of AMS is the ratio of the magnetic foliation to the magnetic lineation. The degree of lineation and foliation E depends on:

$$E = L/F \quad \text{KHAN (1962), FLINN (1962)}$$

The q-factor for unconsolidated sediments is found from:

$$q = 2(K_1 - K_2)/(K_1 + K_2 - 2K_3) \quad \text{HROUDA (1979), GRANAR (1958)}$$

AMS fabrics and its interpretations

There are three types of AMS fabrics in the basic spatial pattern (TARLING & HROUDA 1993, ROCHETTE et al. 1992, ROCHETTE et al. 1991, KNIGHT & WALKER 1988, ELLWOOD 1978, KLIGFIELD et al. 1977) for the AMS study.

Type 1: The K_3 axes of individual specimens are tightly clustered about their site means. The K_1 and K_2 axes are dispersed about a great circle to form a complete or partial girdle (possible shape: Oblate).

Type 2: The K_1 , K_2 and K_3 axes of individual samples are all grouped about their respective site means (possible shape: Triaxial).

Type 3: The K_1 axes are tightly clustered about their site mean and the K_2 and K_3 axes are dispersed about a great circle to form a complete or partial girdle (possible shape: Prolate).

The AMS fabrics were first noticed by GRAHAM (1954) who described the magnetic anisotropy of petrofabric elements as follows:

1. Various flat-lying sediments have a nearly oblate susceptibility ellipsoid, with the minimum normal to the bedding.
2. A folded ferruginous sandstone has maximum susceptibility normal to the bedding, and the minimum is normal to the direction of the fold axis throughout the fold.
3. Two schists have minimum susceptibility normal to the foliation and maximum susceptibility parallel to the lineation.
4. Two diabase dykes with no obvious preferred orientation of feldspar laths have pronounced anisotropy ellipsoids that differ in the two cases in their relationships to the dyke walls.

Later, DVORÁK & HROUDA (1972) described the AMS fabrics in detailed correlations with geological structures as following:

1. The maximum susceptibility directions (magnetic lineation) are well concentrated along their mean direction and are very close to the delta axes (line of intersection of bedding with cleavage) and the minimum susceptibility directions (normal of magnetic foliation) are also well concentrated along their mean direction and are close to the directions of the bedding poles. It can be concluded that the magnetofabric is evidently not of sedimentary origin and must be the product of a deformation.
2. The maximum susceptibility directions are relatively widely dispersed along their mean direction and partly intermixed with the intermediate susceptibility directions so that an ellipsoid is close to rotation. On the other hand, the maximum and intermediate susceptibility directions lie in the close vicinity of the bedding plane and the minimum susceptibility directions are very well concentrated along their mean direction and agree very well with the directions of the bedding poles. In such case, a magnetic anisotropy did not originate by sedimentation, but is again of deformational origin.
3. The low magnetic anisotropy is between 1.05 and 1.1 and the values of magnetic foliation are much higher than those of magnetic lineation and the maximum susceptibility directions are widely dispersed along their mean direction, which is usually parallel to the water current direction.

Recently, ROCHETTE et al. (1992) interpreted the AMS fabrics as petrofabrics as follows:-

1. AMS ellipsoid is coaxial to the petrofabric: the K_3 axis is perpendicular to the foliation, which may be the bedding plane in sedimentary rocks, the flattening plane for solid state deformed rock or magmatic foliation in magmatic rock. The K_1 axis is parallel to the petrofabric lineation which may be a tectonic lineation or a magmatic flow direction or a palaeocurrent direction for sediments.
2. The shape of AMS ellipsoid is directly related to rock fabric. There is a simple quantitative relationship between L or F (or other parameters linked to the relative length of the susceptibility axes) and the intensities of linear or planar preferred orientations, respectively. In the case of solid-state deformation this implies a direct relationship between AMS and strain. In many cases only a semi-quantitative interpretation is possible; i.e. a more anisotropic rock is more strained.
3. AMS measurement is not affected by natural or artificial remanent magnetizations.

7.3 STUDY OF AMS

In the investigated area, the profiles at the road-cut are well exposed at the Weil stream valley which is approximately perpendicular to the strike of regional structures. For the AMS study more than 100 samples were taken in different types of lithology and structural positions from the profiles. At least 5 cylinders were obtained from each sample, thus a total of about 600 cylinders were measured. In accordance with the three sub-areas, Weilburg-Ahausen, Guntersau-Freienfels and Freienfels-Ernsthausen, the AMS data are grouped for analysis and interpretations (AMS data in Appendix A and B).

Data are plotted on the different diagrams such are stereoplots (in the lower hemisphere), L-F (Flinn-diagram), T-P^l (Jelinek-diagram) and P^l-Samples diagrams. Stereoplots for sheet flow lavas, lapillituff and dykes of the study area are very useful to interpret the flow-, current-, and intrusive-direction. In addition, in the study area different local basins were observed to be antithetic, synthetic half-graben and full-graben basins. Almost all of the basins are deformed by orogenic compression which is partly confirmed by the AMS using T-P^l and P^l-Samples diagrams.

7.3.1 AMS applied to regional structures

The K₁ and K₂ axes are dispersed in a great circle of the magnetic foliation which corresponds with the regional orientation of the s1-cleavage (Fig. 7-3B), NE-SW trending with SE dipping 30 - 40°. In the Guntersau-Freienfels sub-area, magnetic foliation is exactly related to the s1-cleavage except for some samples which are dykes. In the Freienfels-Ernsthausen sub-area, the magnetic foliation is observed constituting two trends: one can be correlated to the s1-cleavage; the other one dips 70° towards NE (Fig. 7-3A & B) and may be younger than the s1-cleavage.

The magnetic lineation K₁ axes are oriented prominently in a NE-SW direction which coincides with the regional Variscan structural trend in the *Rheinische Schiefergebirge*. The Guntersau-Freienfels sub-area reveals exactly the same trend except for dykes. In the Freienfels-Ernsthausen sub-area the two regional magnetic trends are also prominent in NW-SE and NE-SW orientations (Fig. 7-3A).

The magnetic K₃ axes are generally normal to the magnetic foliation. The pole diagrams of the s1-cleavage and the K₃ axes stereoplots are identical. The stereoplots of the AMS in the sub-areas generally show oblate magnetofabrics (Fig. 7-4).

7.3.2 AMS applied to sheet flow lava

The flow direction of the sheet flow lava can be inferred from the source area (central facies) within the sedimentary basin with respect to the half-graben basins. The AMS fabrics of the sheet flow lava clearly resembles the regional structure, especially as s1-cleavage or folding. The anisotropy degree (P^l) has a maximum about 1.06.

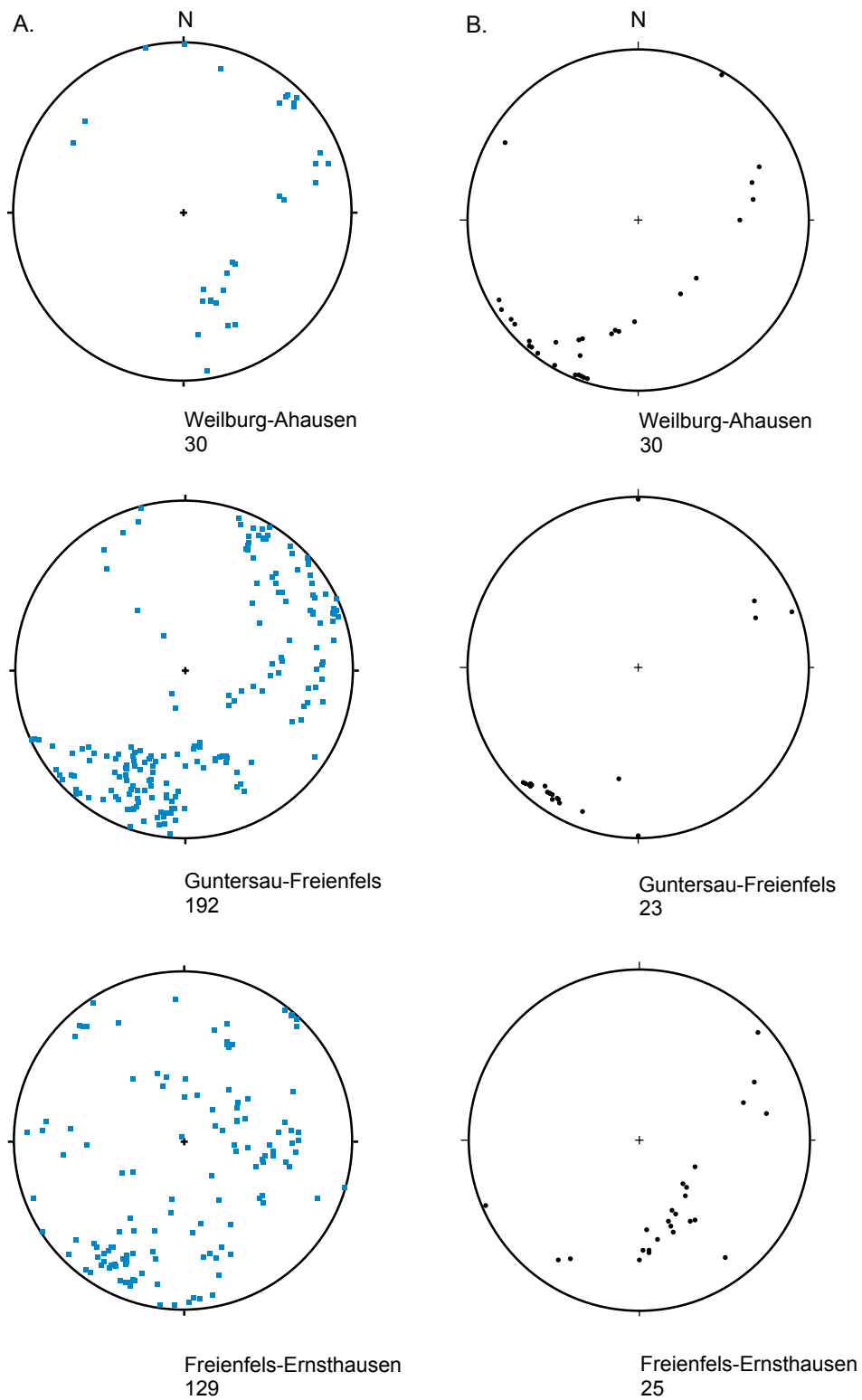


Fig. 7-3A. Comparison of magnetic lineation (K_1) of AMS (A) and intersection lineation (B) of each sub-area in the Weilburg area.

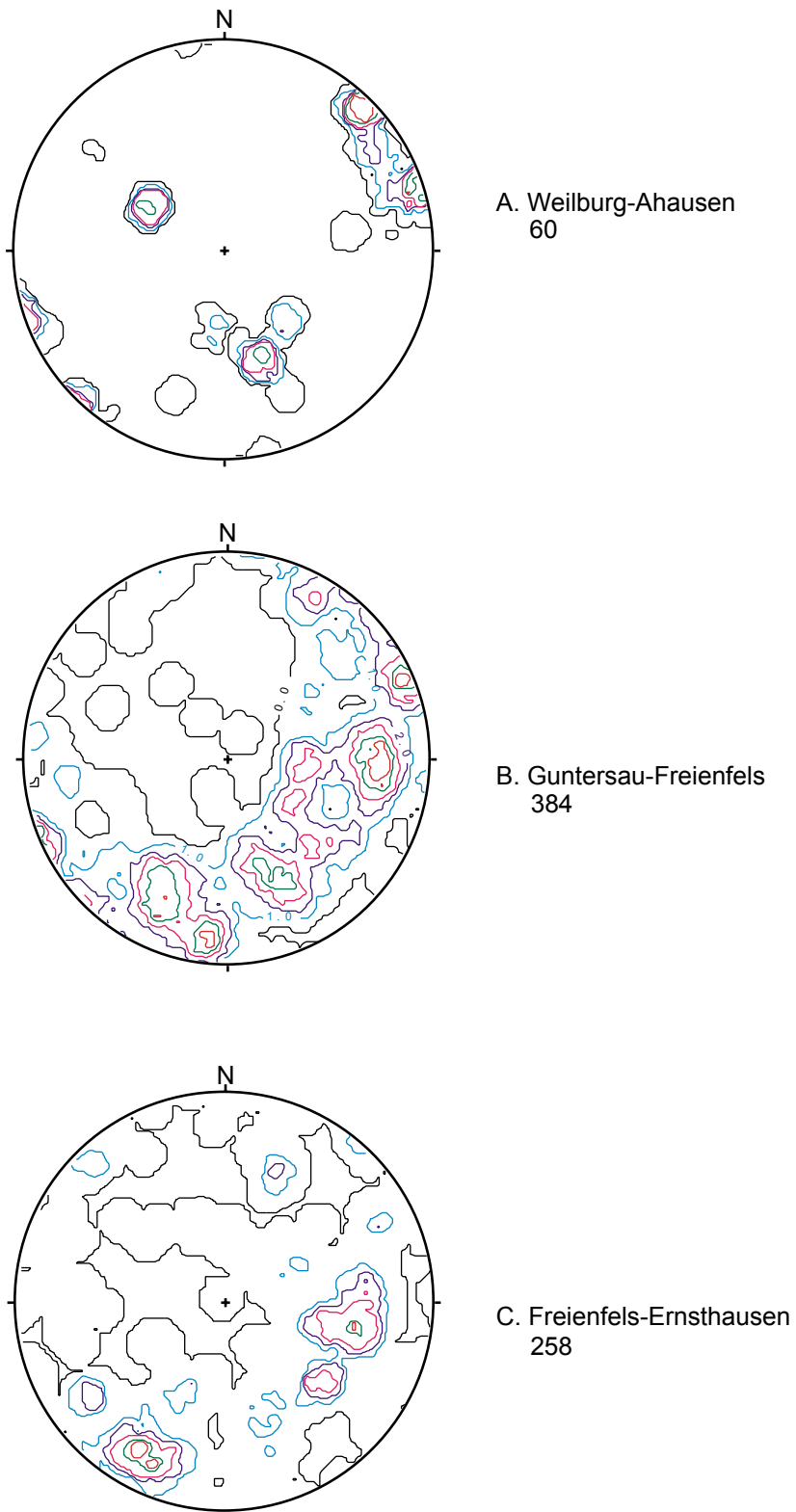


Fig. 7-3B. Contour in stereoplots of the magnetic foliation of the Weilburg area

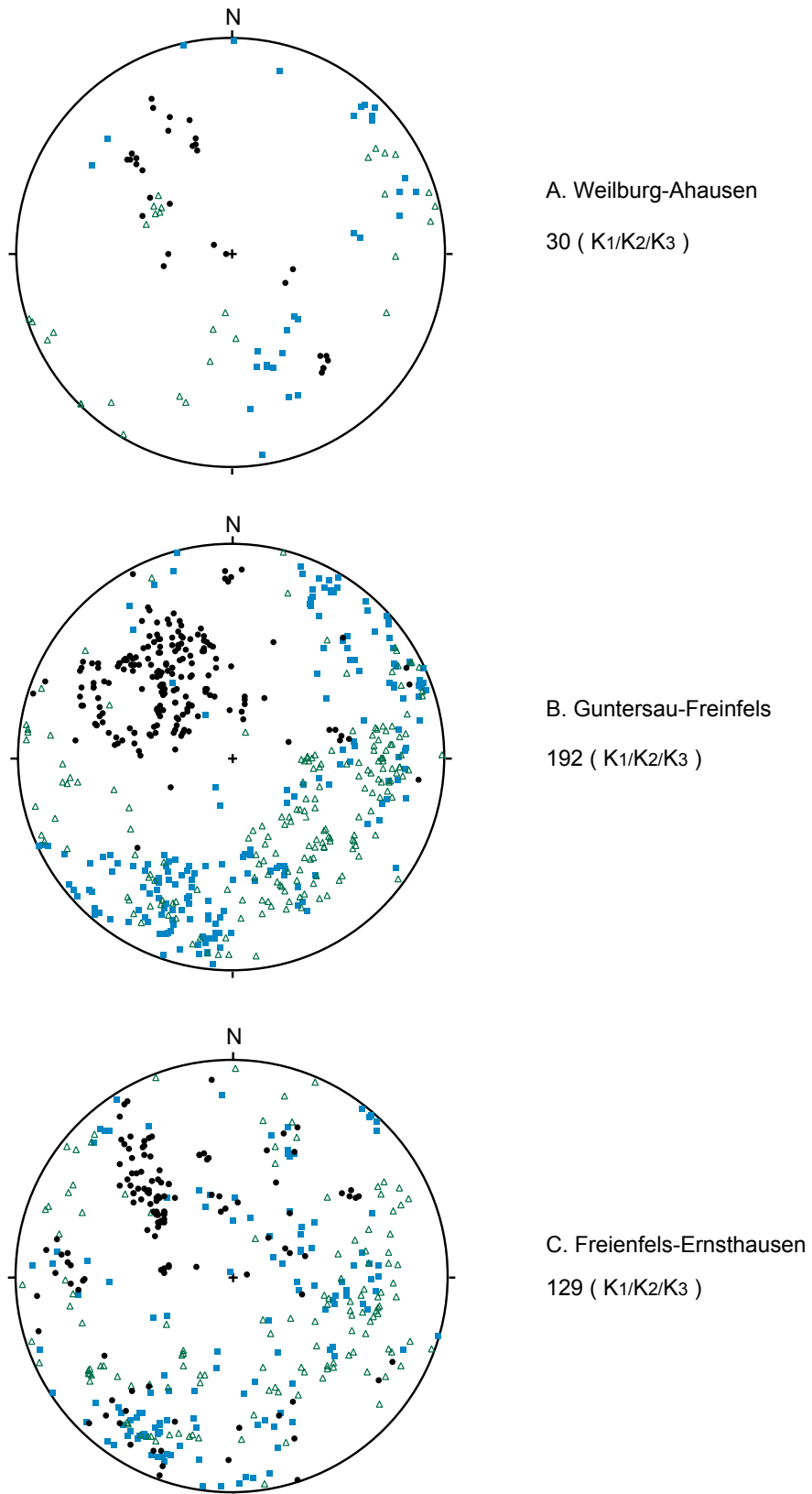


Fig. 7-4. Magnetofabrics (AMS values of K1, K2, K3 stereoplot) of the Weilburg area.
K1, K2, K3 = maximum, intermediate, minimum axes of AMS.

■ K1 △ K2 ● K3

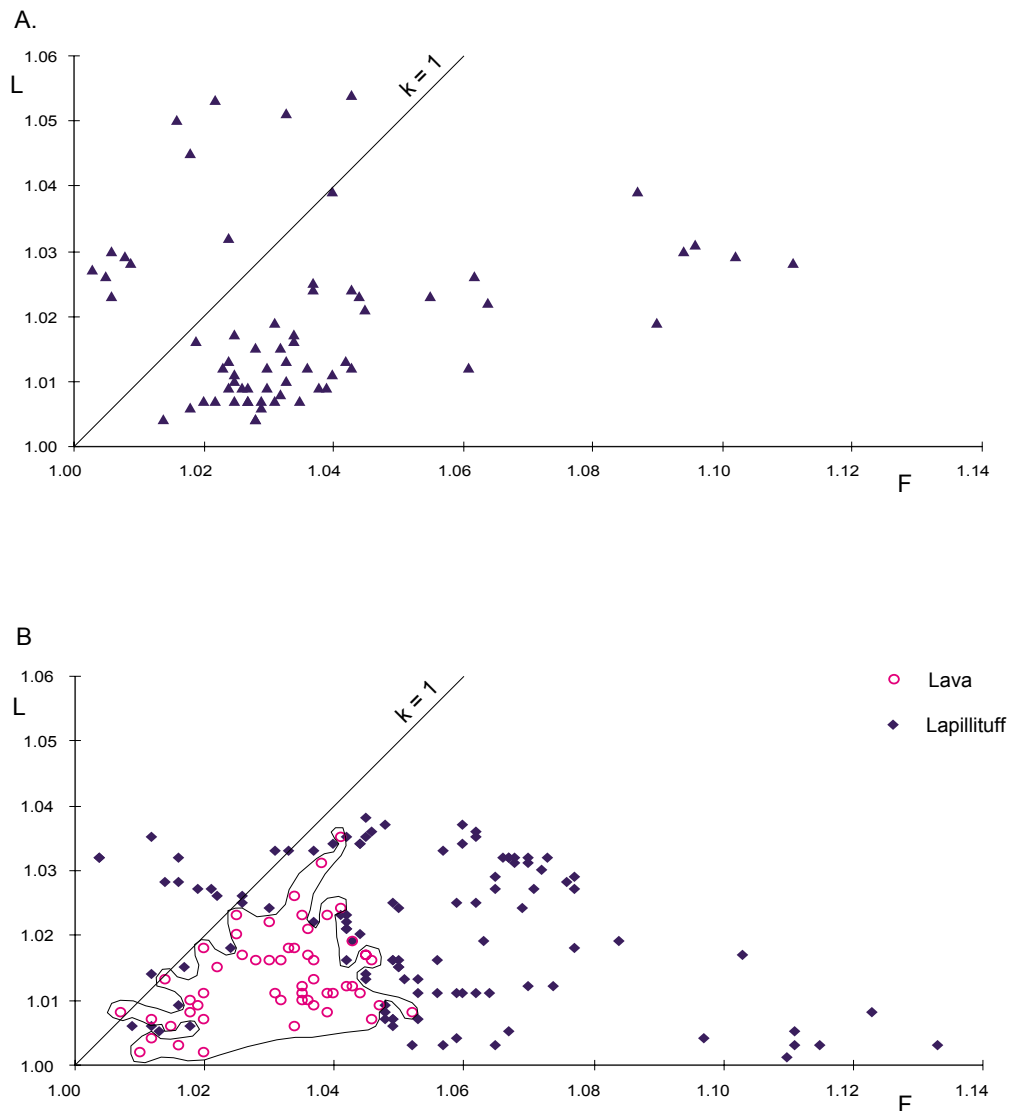


Fig. 7-5. L-F diagrams of dyke, sheet flow lava and lapillituff of the Guntersau-Freienfels basin in the Weilburg area, A: dyke, B: sheet flow lava and lapillituff (Flinn-diagram, after FLINN 1962 and KHAN 1962).

L-F diagrams also show only the oblate field near the undeformed position, the F-value being less than 1.05. In the L-F diagrams, some data are on the plain strain line ($k = 1$), which perhaps is typical for undeformed rocks, e.g. lava or newly formed minerals, i.e.- quartz, calcite and chlorite with their associated magnetic minerals or tectonic plain strain.

The L-F and T- P^I diagrams (Fig. 7-5 & 7-6) show that the sheet flow lava data-points are well clustered in the distribution of the lapillituff data-points. It means that the lava should be less deformed than lapillituff during the deformation. This could be despite the fact that they are deformed together under the same conditions, the sheet flow lava performed according to the mass-movement model as the competent layer (e.g. RAMBERG 1987). Thus, the lava was not as deformed as the lapillituff.

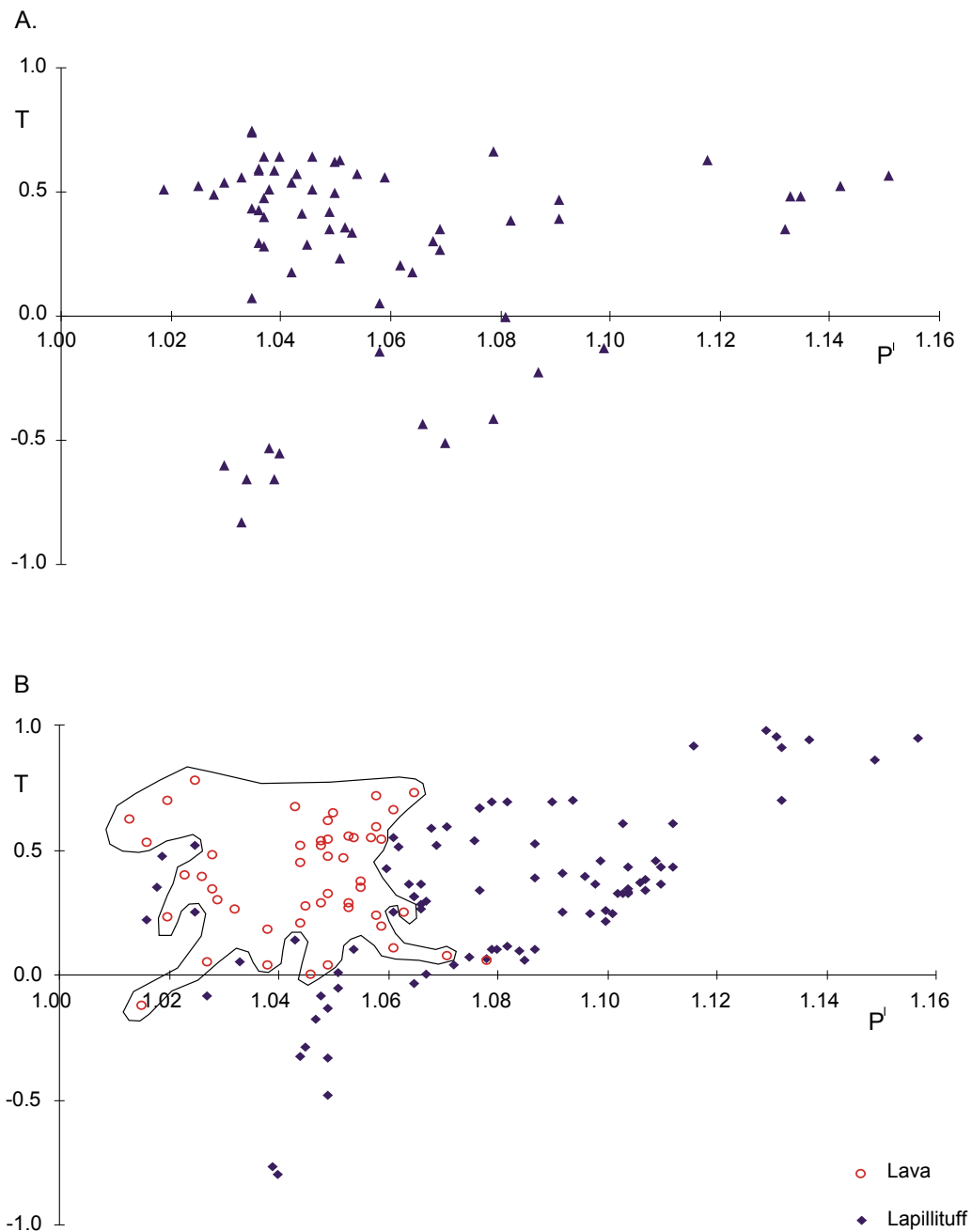


Fig. 7-6. T-P^I diagrams of dyke, sheet flow lava and lapillituff of the Guntersau-Freienfels sub-area in the Weilburg area, A: dyke B: sheet flow lava and lapillituff (Jelinek-diagram, after JELINEK 1981).

The flow directions in sheet flow lavas, were obtained by KHAN (1962) who suggested that the mean intermediate susceptibility (K_2) was roughly parallel to the flow direction of sheet flow lavas although the scatter of the main susceptibility was high. KOLOFIKOVA (1976, reported by HROUDA 1982) found a good link between the direction of the maximum axis of susceptibility and the flow direction, but only in the intermediate and not in the frontal parts of the flow. MACDONALD et al. (1992) also showed a

parallelism between the principal maximum susceptibility and lineations assumed to be produced by laminar flow of lava sheets. CANON-TAPIA et al. (1995) found that either the mean maximum or the mean intermediate susceptibility axes point in the same direction as the geologically inferred flow direction.

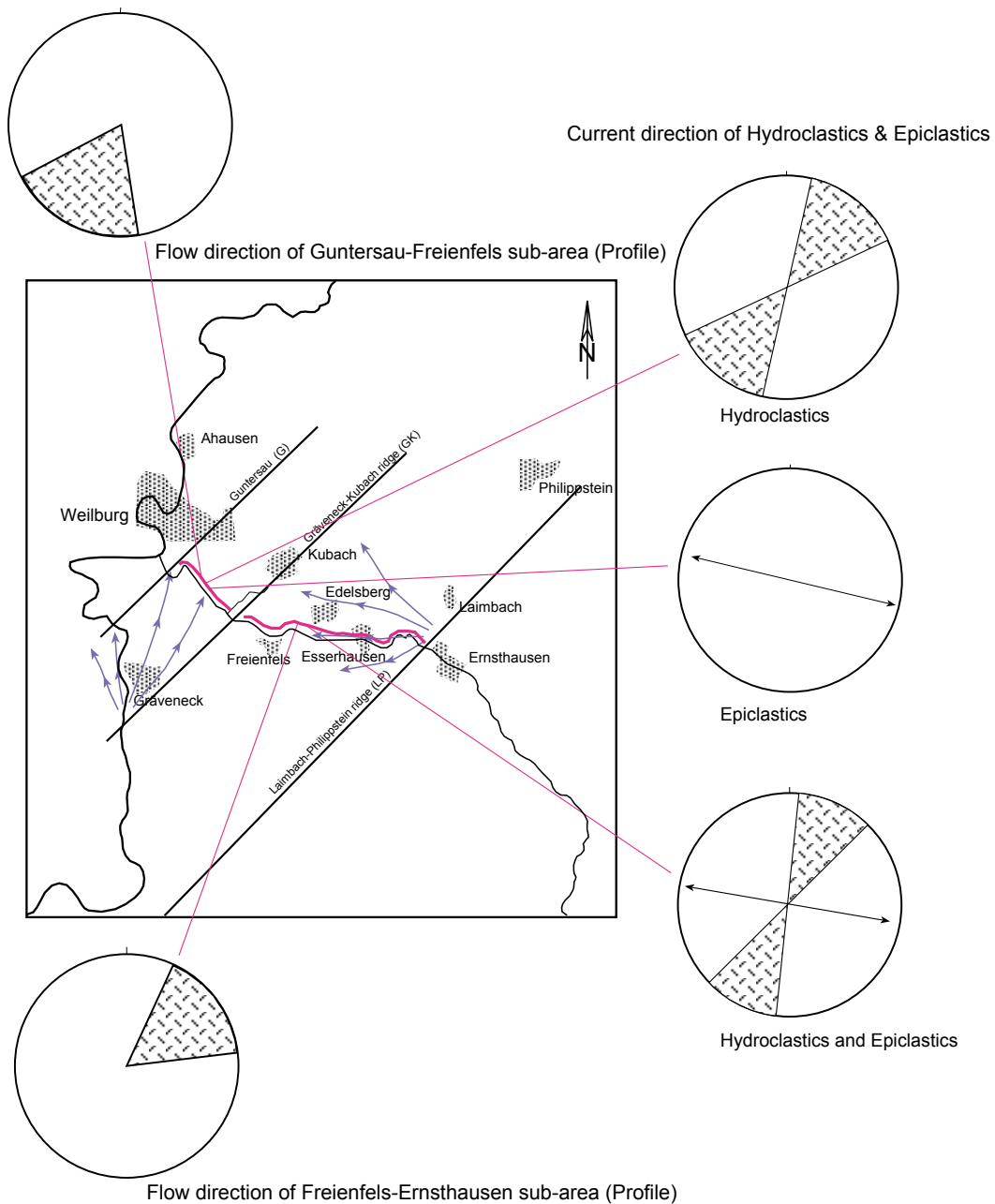


Fig. 7-7. Sketch showing the interpretation of flow direction in sheet flow lava, and current direction in hydroclastics and epiclastics in the Weilburg area.

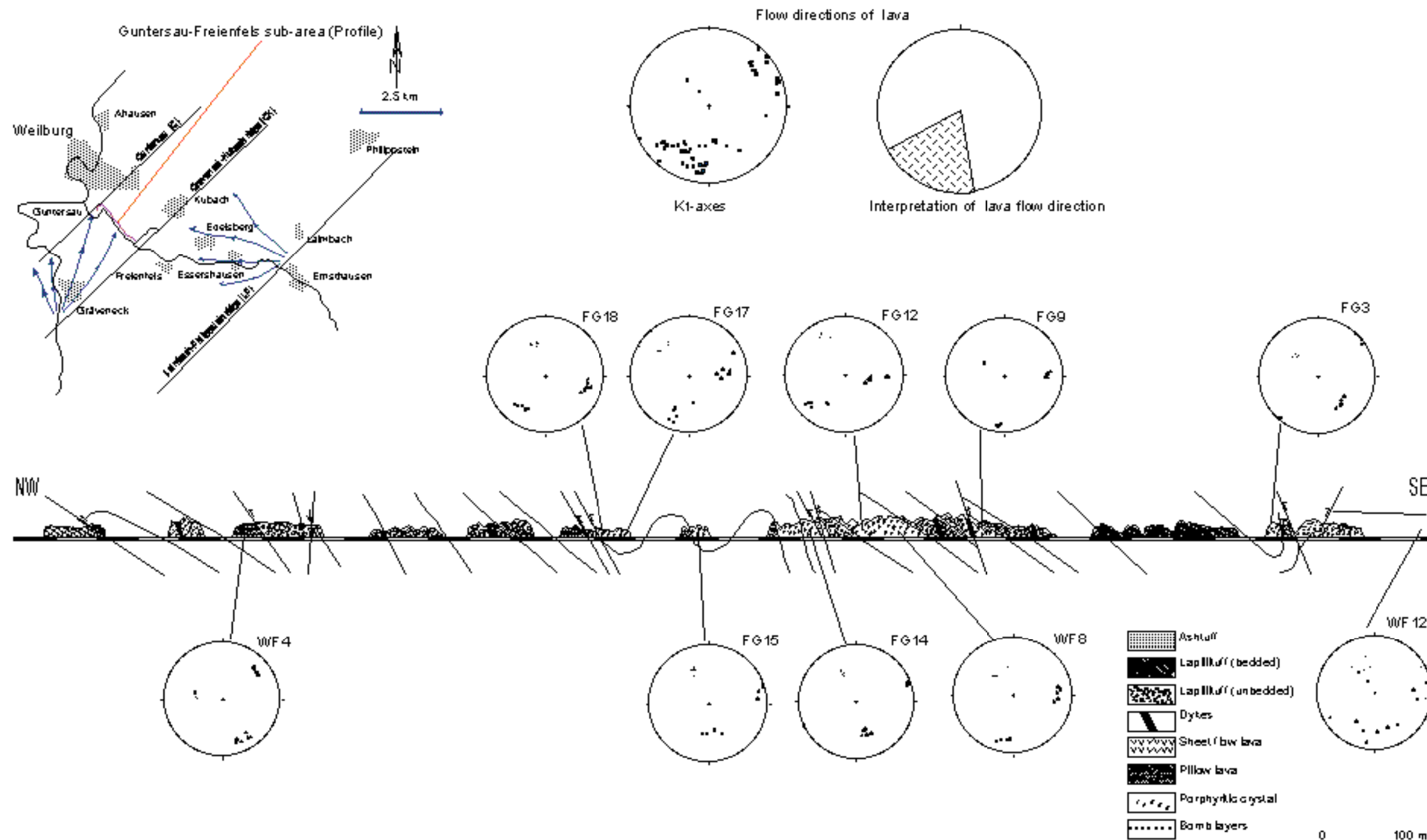


Fig. 7-8. AMS fabrics distribution of sheet flow lava at the Guntersau-Freienfels sub-area in the Weilburg area. (Profile along the Weiltal-road by BEHNISCH 1988)

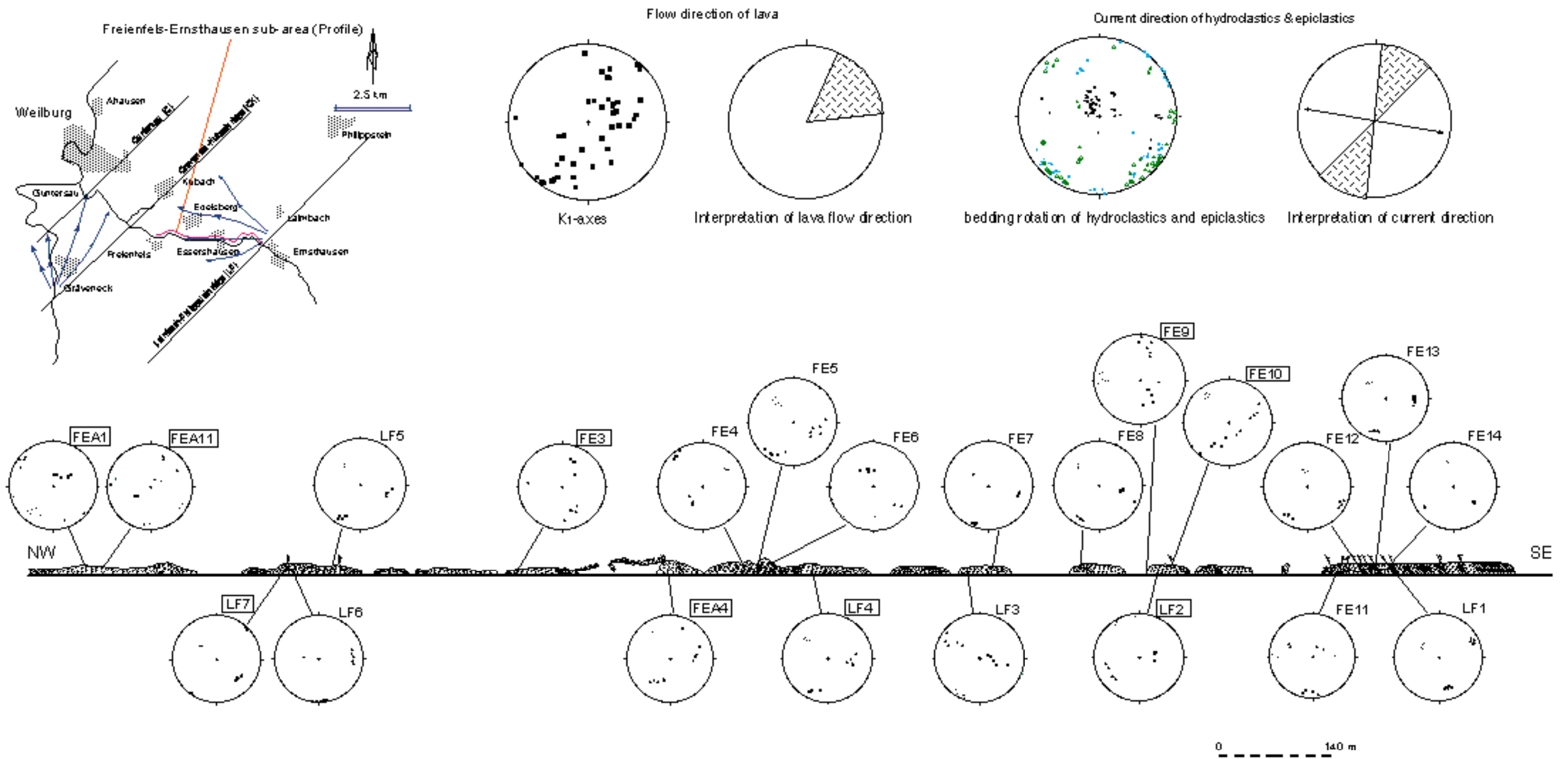


Fig. 7-9. AMS fabrics distribution of sheet flow lava and lapillituff at the Freienfels-Ernsthausen sub-area in the Weilburg area.

FEA = Lava, LF = Lapillituff (Profile along the Weital-road by JÄGER 1993), (Symbols explanation in Fig.7-8)

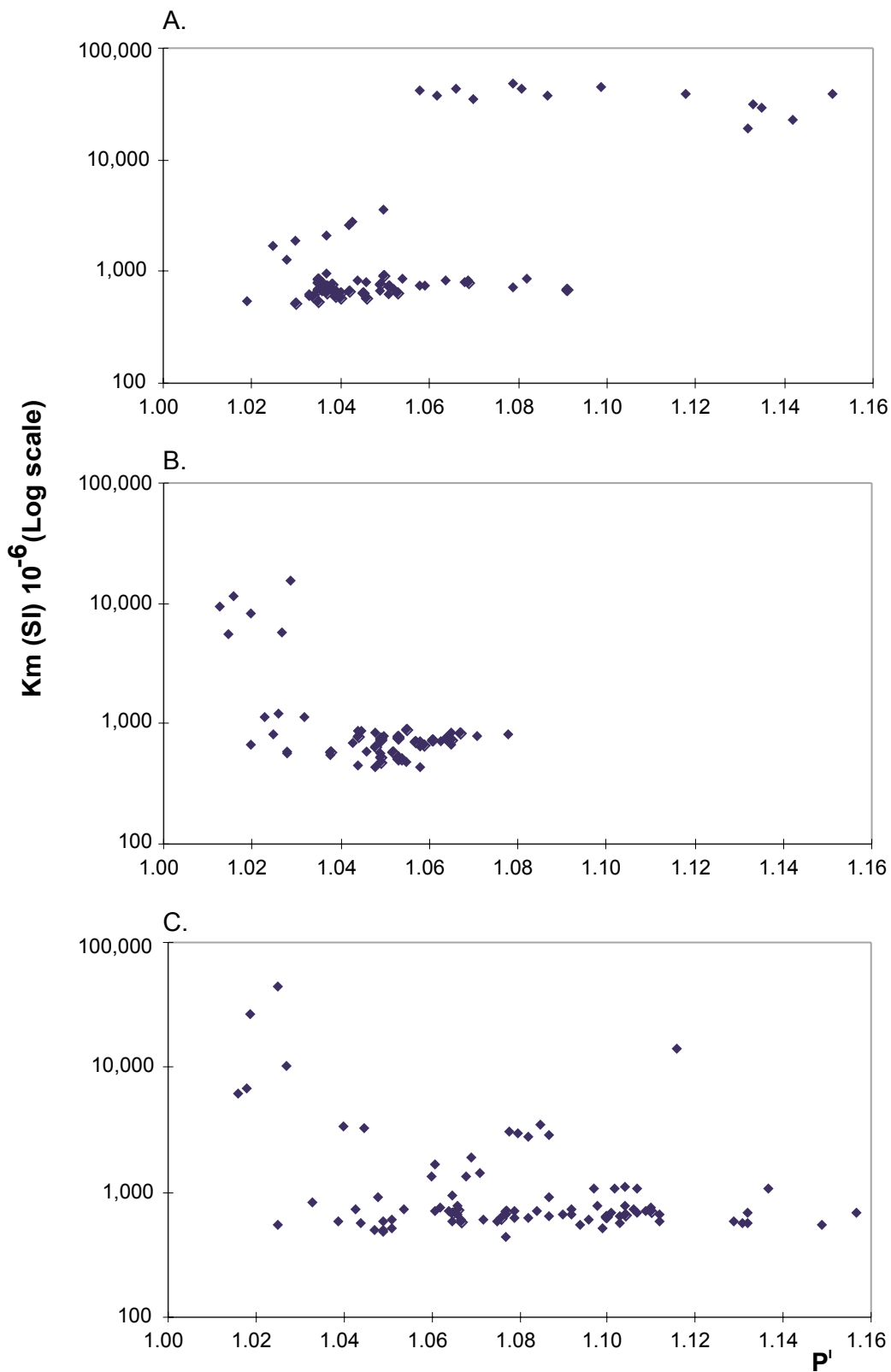


Fig. 7-10. K_m mean AMS vs P^I diagrams of dyke (A), sheet flow lava (B) and lapillituff (C) of the Weilburg area.

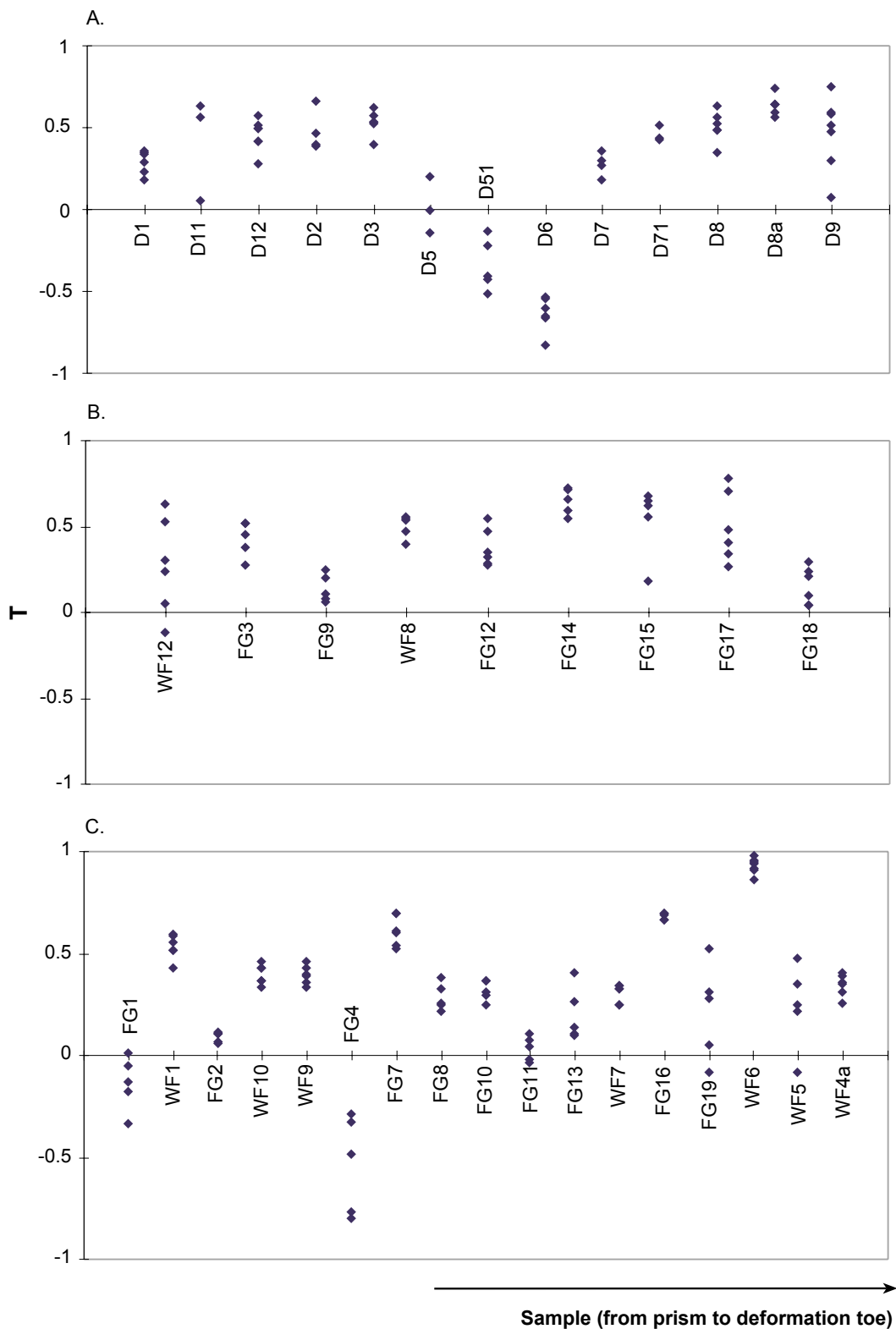


Fig. 7-11. T vs Samples diagrams of dyke (A), sheet flow lava (B), and lapillituff (C) of the Guntersau-Freienfels sub-area in the Weilburg area.

At the Guntersau-Freienfels sub-area the AMS data show the same orientation as the regional structure except for the FG3 and FG14, which are specific in the analysis only in category of the AMS. The AMS axes are well clustered, e.g. the K_1 and K_2 axes are on the foliation plane and the K_3 axes are very near to its pole. At the Freienfels-Ernsthausen sub-area, the AMS data are generally consistent.

For determining flow directions of the sheet flow lava the mean maximum axes (K_1) can be used according to KHAN (1962), MACDONALD et al. (1992) and CANON-TAPIA et al. (1995). Sometimes the intermediate axes (K_2) are used instead if in case the K_1 axes are dispersed.

At the Guntersau-Freienfels sub-area, the inferred flow direction referring to the source of the magma (e.g. Grävneck central facies: NESBOR et al. 1993) from the SW (Fig. 7-7), is generally coincident with the flow direction determined by AMS interpretation. Thus, the average flow direction of the inferred flow directions and the K_1 axes direction are about 160 - 230° N azimuth and 20 - 50° plunge (Fig. 7-7 & 7-8).

In the Freienfels-Ernsthausen sub-area, with regard to the source area at Laimbach (central facies) the inferred flow direction is very consistent with the K_1 axes direction from the NE (Fig. 7-7). The average flow direction of the inferred flow directions and the K_1 axes direction are about 030 - 080° N azimuth and 20 - 50° plunge (Fig. 7-7 & 7-9).

Furthermore, the K_m - P^l and T-Samples diagrams of the sheet flow lava (Fig. 7-10, 7-11) are not distinguishable, because its P^l value shows stability at the maximum 1.06 in the oblate shape, which can be compared with undeformed sedimentary origin of the P^l value, 1.05 (HROUDA & HRUSKOVA 1990, HROUDA et al. 1978, DVORÁK & HROUDA 1972)

7.3.3 AMS applied to lapillituff

Lapillituff are the dominant rock type in the study area namely in the profiles of the Guntersau-Freienfels and Freienfels-Ernsthausen sub-areas. There are **three** types of lapillituff: pyroclastics, hydroclastics and epiclastics. Lapillituff containing detrital fragments of the sheet flow lava, pillow lava, lapillituff and limestone, are referred to as epiclastics. Hydroclastic lapillituff are found in particular in turbiditic sedimentary environment. The hydroclastics dominate, but pyroclastics are very rare, e.g. Gänsberg, and the epiclastics intermix with the hydroclastics.

The lapillituff were under compressive stress (load pressure) after the sedimentation, therefore, the K_3 axes are generally developed parallel to the direction of maximum compressive stress (BORDÁS 1992, LOWRIE 1989, ELLWOOD 1982). Accordingly, the lapillituff can be expected that the compaction of tuff, after sedimentation should be nearly horizontal (< 20° angle with horizontal plane) by the unfolding of the magnetic foliation (Fig. 7-12).

Following GRAHAM (1949), sedimentary rocks retained a direction of magnetization through a long period of geologic time. As in a epiclastics, e.g. all the clasts have the same directions of magnetization then these polarizations must be regarded as ones that were acquired after the clasts became embedded. The epiclastic lapillituff generally shows higher K_m value (above normal K_m values) because pillow lava fragments are included.

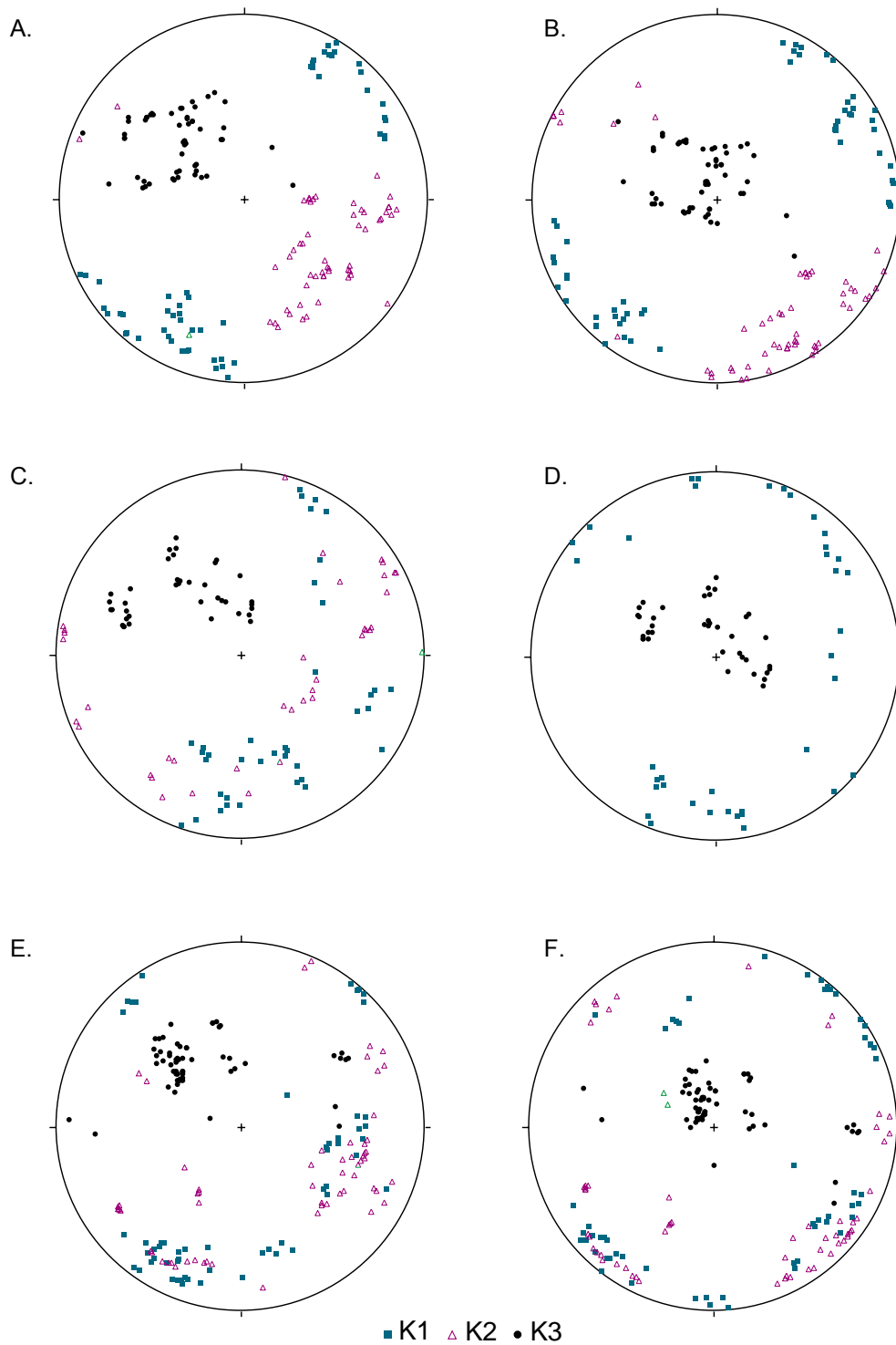


Fig. 7-12. AMS stereoplots (lower hemisphere) of lapillituff (hydroclastics and epiclastics) of the Weilburg area.
 A: Hydroclastic lapillituff of the Guntersau-Freienfels sub-area, B: bedding rotation of A, C: Epiclastic lapillituff of the Guntersau-Freienfels sub-area, D: bedding rotation of C, E: Hydroclastics and epiclastics of the Freienfels-Ernsthausen sub-area and F: bedding rotation of E.

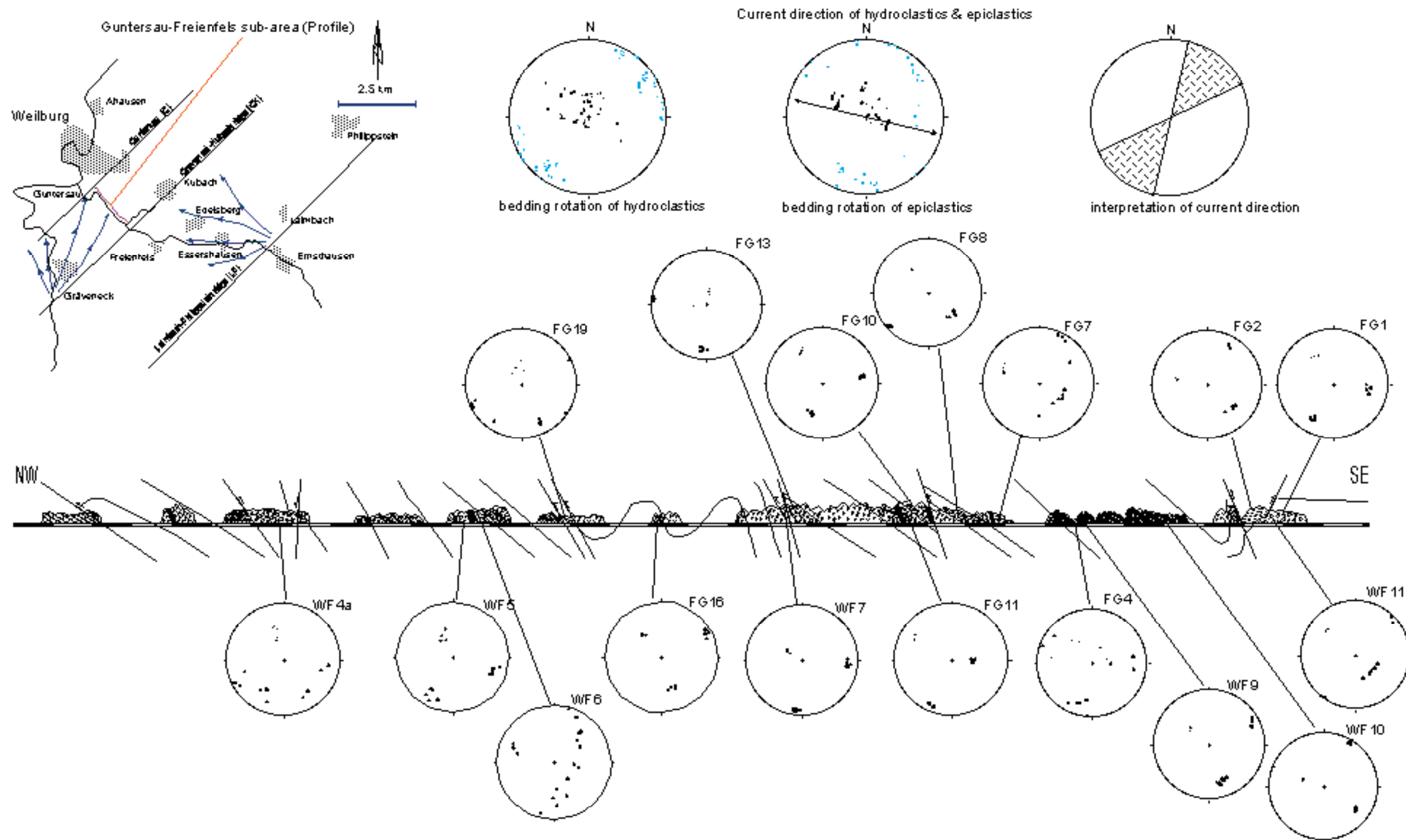


Fig. 7-13. AMS fabrics distribution of lapillituff (hydroclastics and epiclastics) of the Guntersau-Freienfels sub-area in the Weilburg area. (Profile along the Weiltal-road by BEHNISCH 1988), (Symbols explanation in Fig. 7-8)

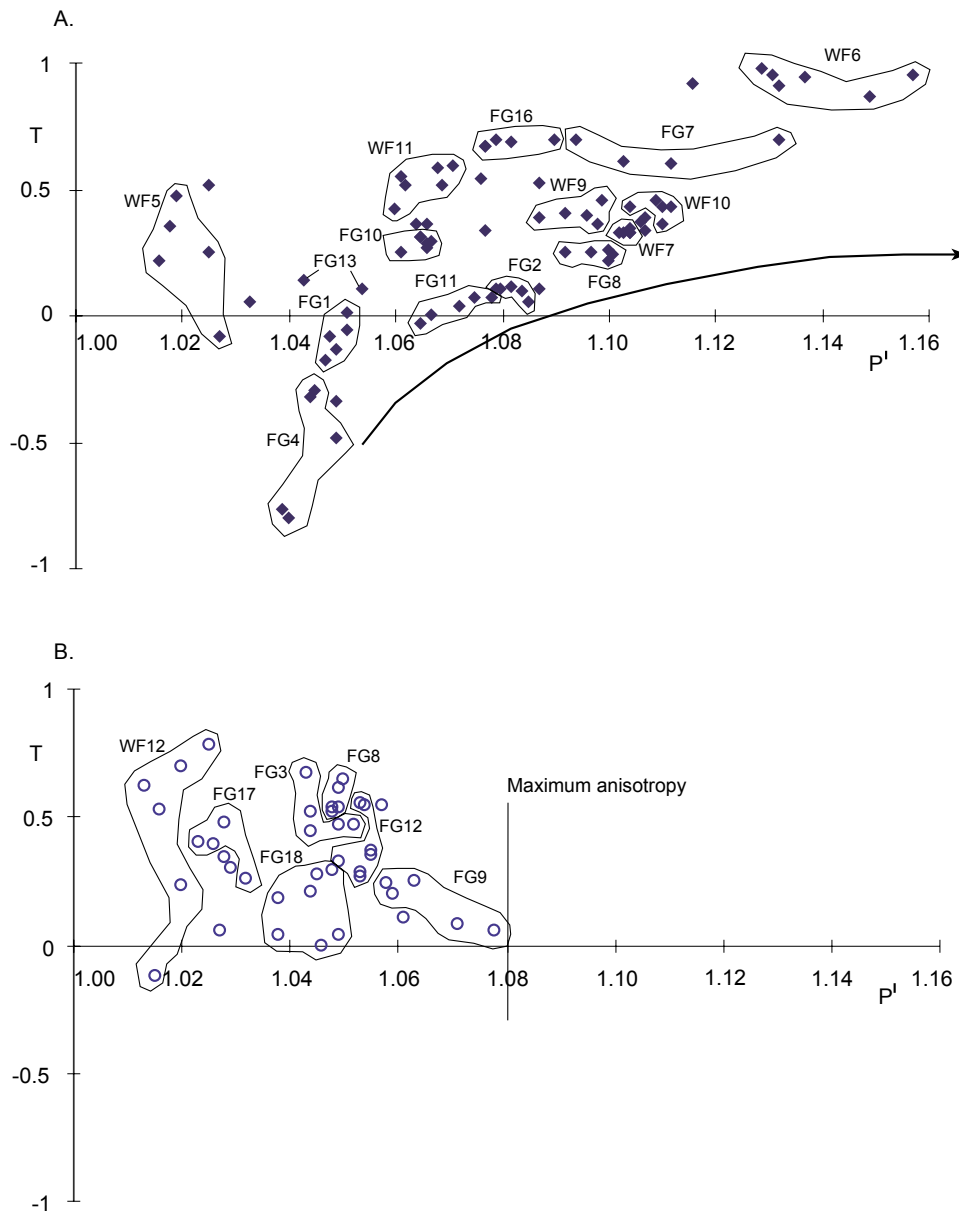


Fig. 7-14. Showing high anisotropy degree related to the accretionary prism-type deformation in the local half-graben basin as exemplified in T-P' diagrams of lapillituff (A) and sheet flow lava (B) from the Guntersau-Freienfels sub-area, (Jelinek-diagram: after JELINEK 1981). Arrow indicates progressive deformation. Sample locations in Fig. 7-8 & 7-13)

However, if the polarization in these pebbles are dispersed, stability of magnetization of each pebble is indicated. When the magnetofabric in a fold is unfolded by rotation around the fold axis (Fig. 7-12) most of K_1 and K_3 axes become horizontal. Thus, it can be concluded that the magnetofabric originated earlier than the folding (cf. HROUDA 1978). As a whole, the magnetofabrics rotated during the folding, demonstrating the buckle type of folding (cf. HROUDA 1978) with the thrust formation (see Fig. 7-13) regardless of the s_1 -cleavage and bedding relation.

On the other hand, the magnetofabric was probably controlled by the s1-cleavage generation rather than by folding. The s1-cleavage formation is later than the folding in the *Rheinische Schiefergebirge* (RUTTEN 1955). However, the s1-cleavage developed perpendicular to the maximum shortening direction (cf. HROUDA 1976 and DIETERICH 1969), probably during the folding.

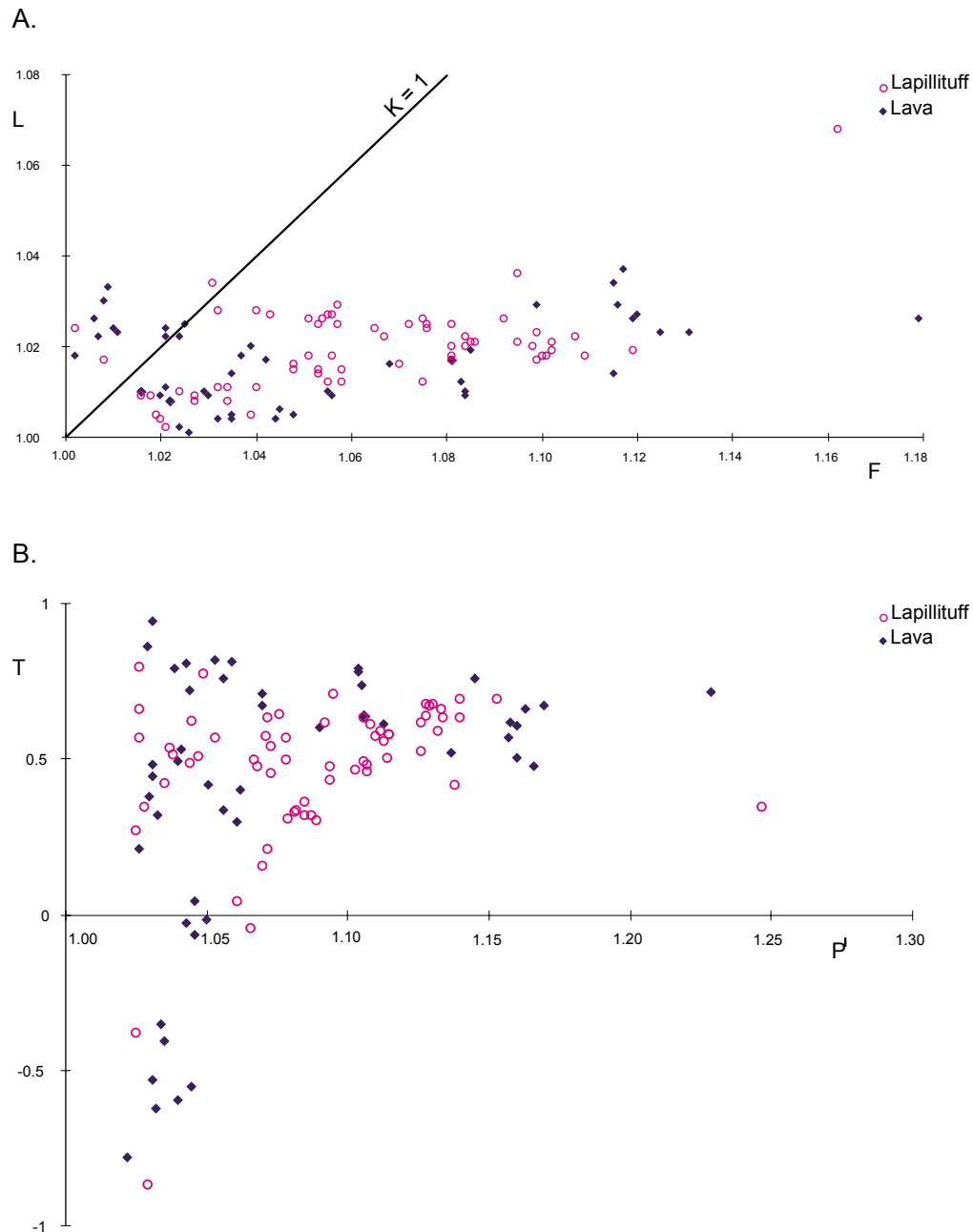


Fig. 7-15. Different AMS distribution between lapillituff and sheet flow lava exemplified in L-F and T-P^I diagrams of the Freienfels-Ernsthausen sub-area (Flinn-diagram: after FLINN 1962 and KHAN 1962, Jelinek-diagram: after JELINEK 1981).

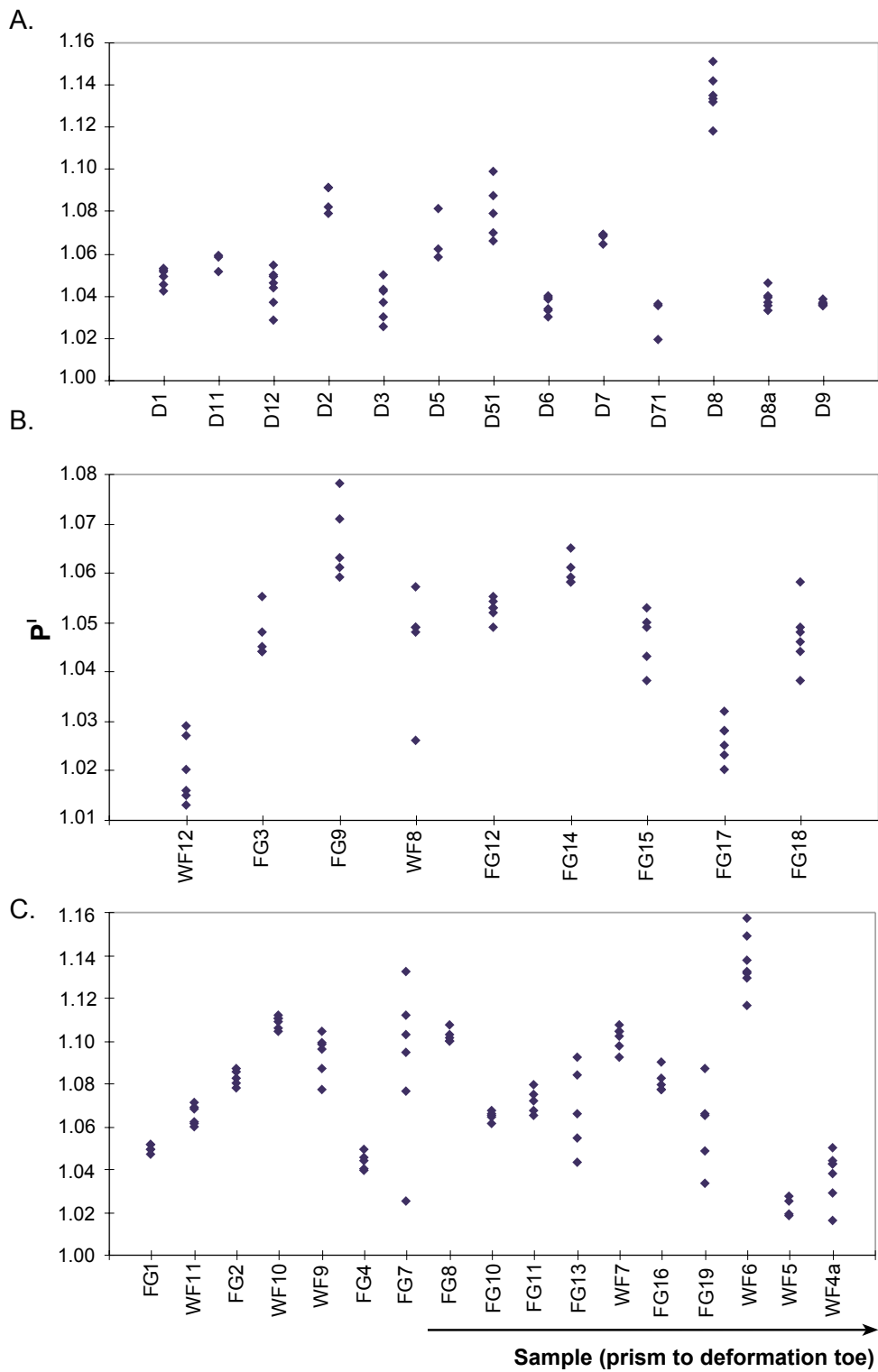


Fig. 7-16. P^I vs Samples diagram of dyke (A), sheet flow lava (B) and lapillituff (C) of the Guntersau-Freienfels sub-area in the Weilburg area.

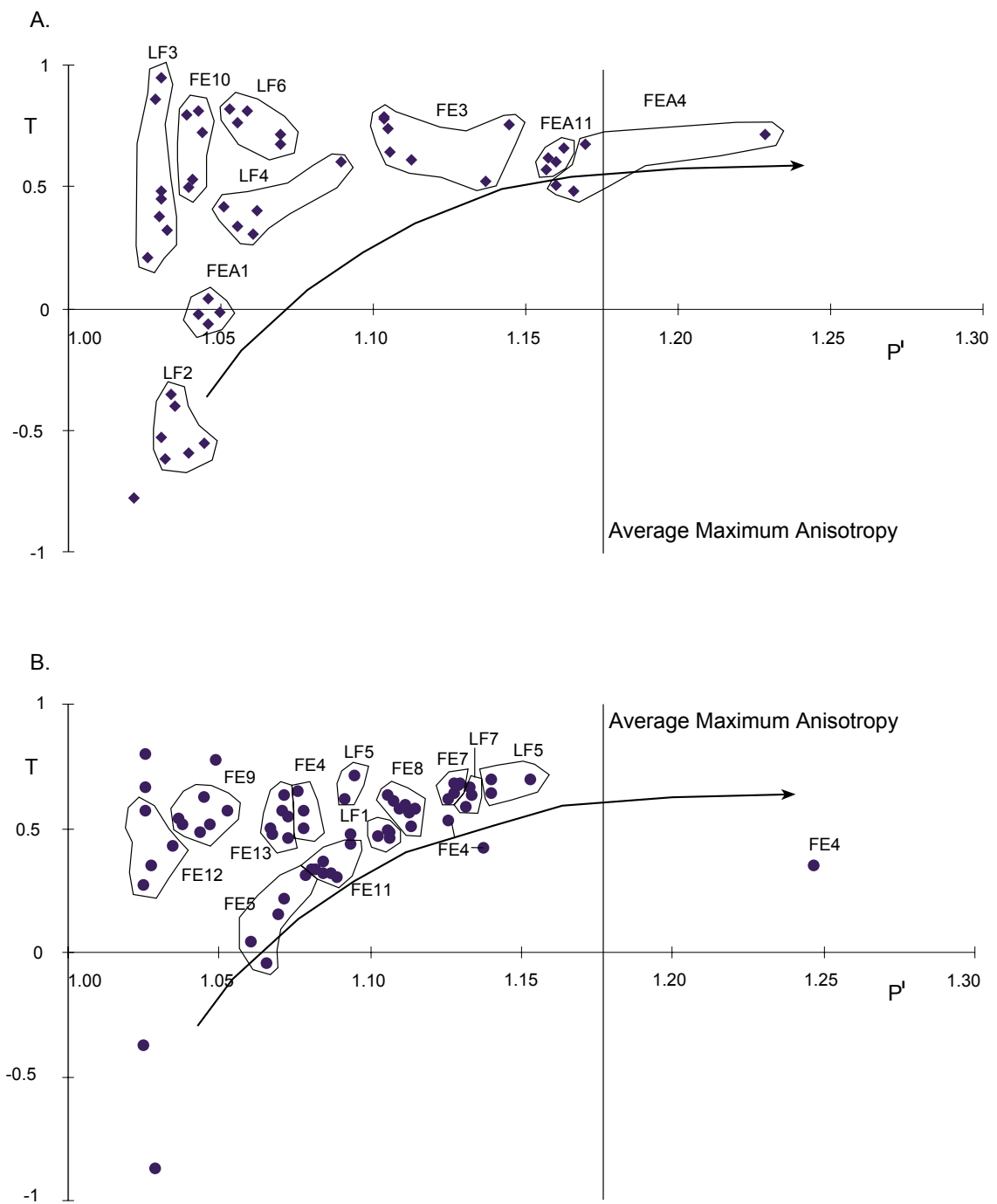


Fig. 7-17. Showing high anisotropy degree related to the accretionary prism-type deformation in the local half-graben basin as exemplified in T-P' diagrams of lapillituff (A) and sheet flow lava (B) from the Freienfels-Ernsthäusen sub-area, (Jelinek-diagram: after JELINEK 1981) and the same average maximum anisotropy degree in sheet flow lava and lapillituff. Arrow indicates progressive deformation.

The anisotropy degree (P^I) in the Guntersau-Freienfels sub-area surpasses that of the sedimentary origin, showing 1.06 - 1.16 (Fig. 7-5), (cf. sedimentary origin $P^I = 1.05$: DVORÁK & HROUDA 1972, HROUDA et al. 1978, HROUDA & HRUSKOVA 1990), which gives evidence that the magnetization was affected by deformation or s1-cleavage formation. DVORÁK & HROUDA (1972) discussed a similar situation where the magnetic foliation reacted on deformation staying parallel to the bedding (Fig. 7-12). This may be evidence for some kinematically active plane parallel to the bedding.

In the stereoplot of the lapillituff, especially for epiclastic lapillituff, the K_1 and K_3 axes give separate orientation after the bedding correction (Fig. 7-12), which indicates the current direction for the debris flow (cf. TARLING & HROUDA 1993 and ELLWOOD & LEDBETTER 1977) across the rift-basin (e.g. profile of BEHNISCH 1993). For hydroclastic lapillituff the current direction parallels the rift-basin (cf. RAVNAS & STEEL 1997), (Fig. 7-7).

L-F and T- P^I diagrams of the lapillituff show flattening and progressive deformation due to plastic deformation (Fig. 7-5, 7-6, 7-14 & 7-15), (cf. BORRADAILE & HENRY 1997). The K_m - P^I diagram of lapillituff is not distinguishable but it shows low-grade metamorphism (cf. BORRADAILE & HENRY 1997). The P^I -Samples and T-Samples diagrams show the thrust development by its progressively higher anisotropy degree closer to the thrust front (Fig. 7-10, 7-16 & 7-11). On the other hand, the thrust front (detachment fault) or deformation toe of the accretionary prism deformation, shows the higher anisotropy degree due to greater deformation (Fig. 7-17).

7.3.4 AMS applied to mafic dyke

Mafic dykes are only developed in the Guntersau-Freienfels sub-area, about ten dykes altogether ranging from 30 cm to 1.5 m in width. Discordant to the neighbouring rocks (Plate 15 & 16) they dip 60 - 90° toward SE. They partly parallel and partly cut the s1-cleavage.

The AMS study of dykes: By comparing, AMS technique and microscopic analysis, KHAN (1962) has shown that the physical orientations of long, intermediate and short axes in the morphology of magnetite grains correspond very closely to the principal AMS ellipsoid axes. JEFFREY (1922) has shown that the K_1 axes will align normal to both the flow direction and the direction of maximum velocity gradient during laminar flow. REES (1968, 1979) suggested that the elongated grains may align parallel to the flow direction and presented two types of mechanism whereby initially a random dispersion of elliptical grains might achieve a statistically preferred orientation as a result of simple shear. OWENS (1974A) indicated that a mixture of prolate and oblate grains will develop a preferred orientation of the long axes (K_1) in the flow direction and the short axes (K_3) normal to the flow direction in the plane of shear. KNIGHT & WALKER (1988) pointed out that the principal AMS axes for samples from a dyke are tightly grouped on equal-area plots and for most of the dykes the maximum number of AMS axes plot near the pole of the dyke.

Stereoplots of the AMS fabrics can be classified into three categories (compare with AMS fabric types) of dykes in the Weilburg area:

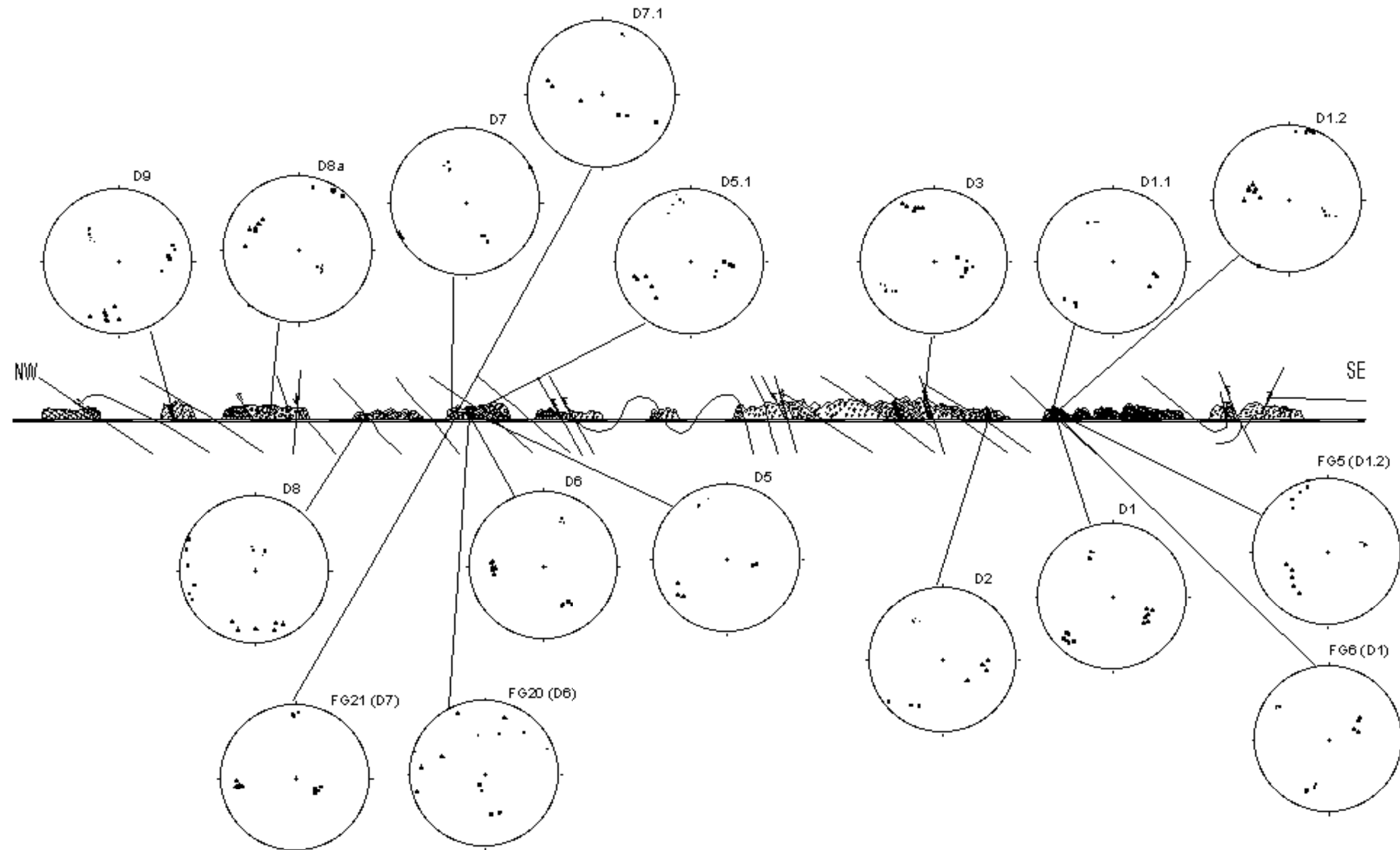


Fig. 7-18. AMS fabrics distribution of dykes (metabasaltic composition) of the Guntersau-Freienfels sub-area in the Weilburg area. (Profile along the Weiltal-road by BEHNISCH 1988), (Symbols explanations in Fig. 7-8)

Category I:- Cluster of the K_1 axes along with girdles of the K_2 and K_3 axes may imply that individual magnetic grains resemble prolate ellipsoids. According to KNIGHT & WALKER (1988) those ellipsoids were aligned together with the K_2 and K_3 axes of nearly equal dimension during the primary magma flow.

Category II:- The K_1 and K_2 axes cluster on the foliation great circle and K_3 axes, perpendicular to the foliation trend, imply oblate ellipsoids. The foliation plane parallel to the dyke representing the emplacement direction is most likely a primary feature, related to magma flow during the dyke injection (KNIGHT & WALKER 1988).

Category III:- Well grouped K_3 axes near the pole of the dyke, symmetrically disposed on either side of the dyke indicate the flow azimuth, i.e. the magma flow direction (KNIGHT & WALKER 1988, ELLWOOD 1978).

D6 and FG20 plots (Fig. 7-18) of dykes (Category I) show the well grouped K_1 axes and the K_2 and K_3 axes are dispersed along the plane. The ellipsoids are prolate. The D6 dyke shows SW dipping magnetic foliation and the magnetic lineation (K_1 axes) is oriented at 145 - 155° N azimuth and plunge 35 - 40°.

FG6, D1, D1.1 and D2 plots (Fig. 7-18) of dykes (Category II) show clustering of the magnetic lineation K_1 axes with average azimuth and average plunge to either side of dyke trend. The K_3 axes are clustered and 30 - 40° plunge. This type shows SE dipping magnetic foliation, and K_1 axes are oriented at 220 - 230° N azimuth and 15 - 20° plunge. Dykes are average about 1.5 m wide. It can be deduced that the dykes were emplaced along NE direction parallel with the basin margin, e.g. the D1 dyke cuts across the bedding and an intrusion contact effect was observed due to the truncation of the bedding (laminated lapillituff) along the dyke wall.

D1.2 and FG5 plots (Fig. 7-18) of host rocks at the contact zone (Category II) show well grouped AMS axes but the K_1 and K_2 axes are dispersed in their group on the foliation great circle. The foliation direction is generally west dipping. This type shows the K_1 axes at 006 - 020° N azimuth and 1 - 5° plunge. In the T-P^l diagram of a dyke (Fig. 7-19) the host rock shows a transition from undeformed to deformed stage of dykes in terms of in the anisotropy degree, however both, dyke and host rock fall into the oblate field. In addition, the chilled zones are observed to be relatively more deformed than dyke and host rock (Fig. 7-19).

D3 plot (Fig. 7-18) of dykes (Category II) shows well grouped AMS axes but the K_1 axes are dispersed and show a somewhat anomalous trend of 080 - 020° N azimuth and 45 - 65° plunge. This type shows NE dipping magnetic foliation. The D3 dyke is parallel to the s1-cleavage, nevertheless the wall rocks reveal the intrusive relationship. Thus, the K_1 axes resemble the magma emplacement direction (cf. KNIGHT & WALKER 1988 and ELLWOOD 1978).

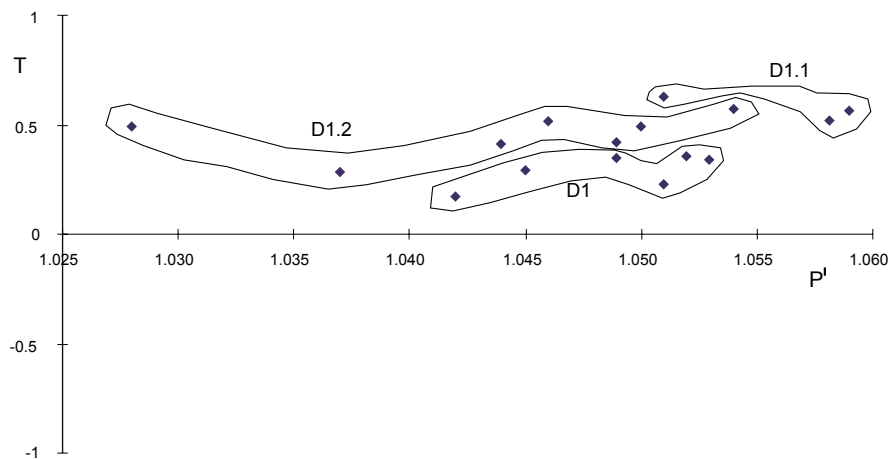


Fig. 7-19. T-P^l diagram of dyke (D1), chilled zone (D1.1) and host rock (D1.2) of the Guntersau-Freienfels sub-area in the Weilburg area, (Jelinek-diagram: after JELINEK 1981)

D5, D5.1, D7 and D9 plots (Fig. 7-18) of dykes (Category II) show well grouped AMS K_1 and K_2 axes on the foliation plane and the K_3 axes at the pole of its foliation. The K_1 and K_2 axes are similarly clustered, however, the K_2 axes are statistically not significant. Therefore, the emplacement direction must be derived from the SE according the K_1 axes direction. This type shows SSE dipping magnetic foliation and the K_1 axes oriented at 080 - 110° N azimuth and 57 - 65° plunge for D5, 30 - 40° plunge for D9. The D5 dyke is discordant with the s1-cleavage. The clusters of AMS ellipsoid axes indicate the narrow width. Thus, magma emplacement came from the east, following the orientation of the K_1 axes. The D7 dyke is concordant with the s1-cleavage, and its K_1 axes are oriented at the foliation direction, thus, the D7 could be emplaced from the south (Fig. 7-18).

The D8A plot (Fig. 7-18) of a dyke (Category II) shows the clearly clustered K_3 axes as the pole of the foliation which is dipping in the opposite direction of the dyke plane. This dyke is about 30 cm wide and horizontally displaced. These displacements are postulated to belong to the neighbouring thrust-fault system (see Plate 17A).

The D8 plot (Fig. 7-18) of a dyke (Category III) shows the well clustered K_3 axes, however, the K_1 and K_2 axes are dispersed on the foliation plane at the sub-horizontal position. The feature may be a low-angle intrusive sheet with a less variable dip (cf. KNIGHT & WALKER 1988). In comparison with the host rock, the dyke is more competent because of the observation of cleavage refraction. The K_1 and K_2 axes are dispersed on the foliation plane, however, the average of the K_1 axes is used for determining the flow direction. This type shows SSW dipping magnetic foliation and the K_1 axes are oriented at 250 - 290° N azimuth and 2 - 15° plunge. In addition, the anisotropy degree P^l is above the average, about 1.16, thus, the dyke should be deformed by horizontal compression during Variscan deformation, thus demonstrating to be originated as a sill.

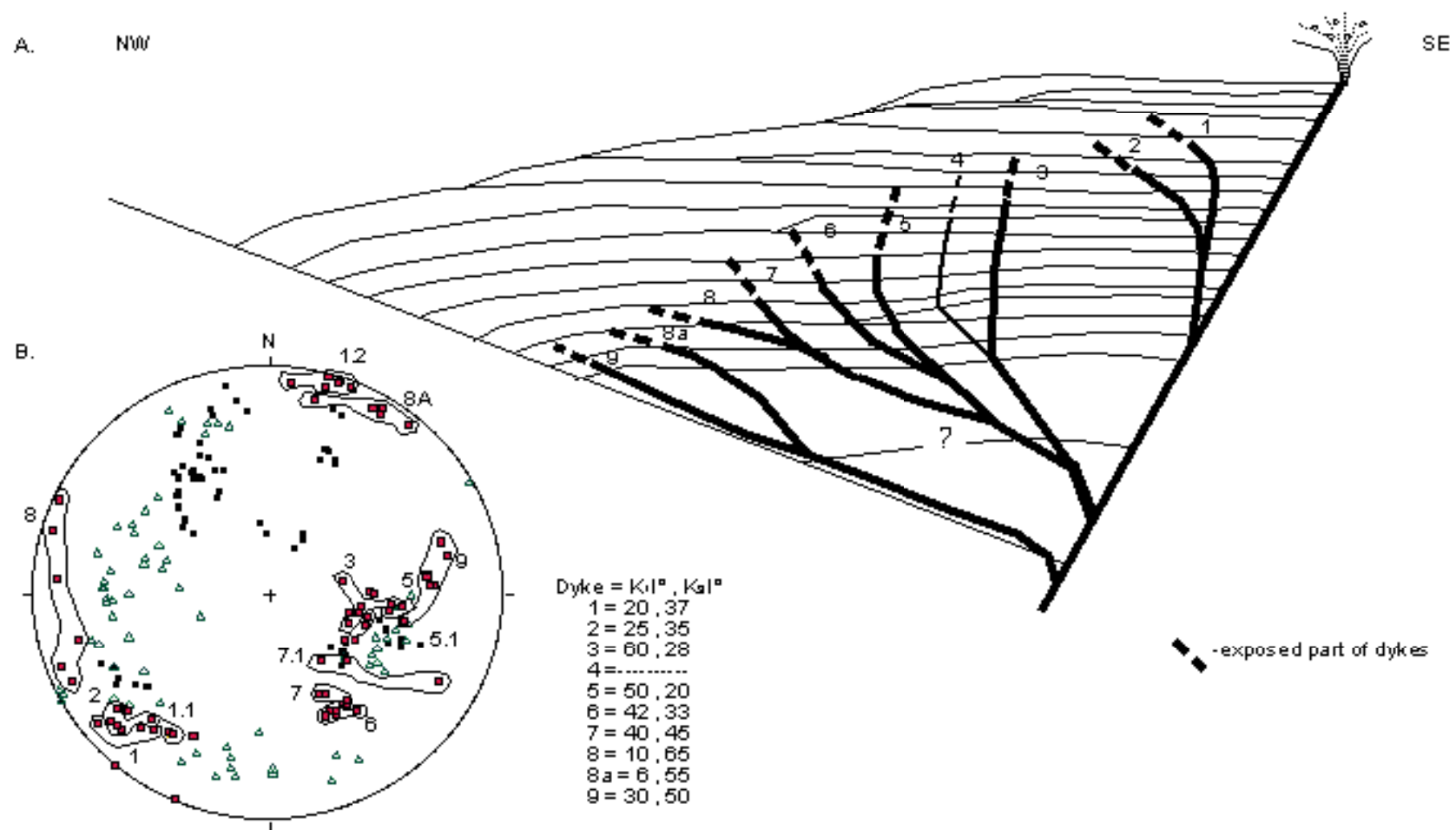


Fig. 7-20. A: Reconstruction of the pattern of dykes in the half-graben volcanism at the Guntersau-Freientfels sub-area, based on the inclinations (I) of K_1 and K_2 in stereonet (B) and field observations, B: Stereonet of all dykes from the Guntersau-Freientfels sub-area in the Weilburg area. (Numbers indicate samples)

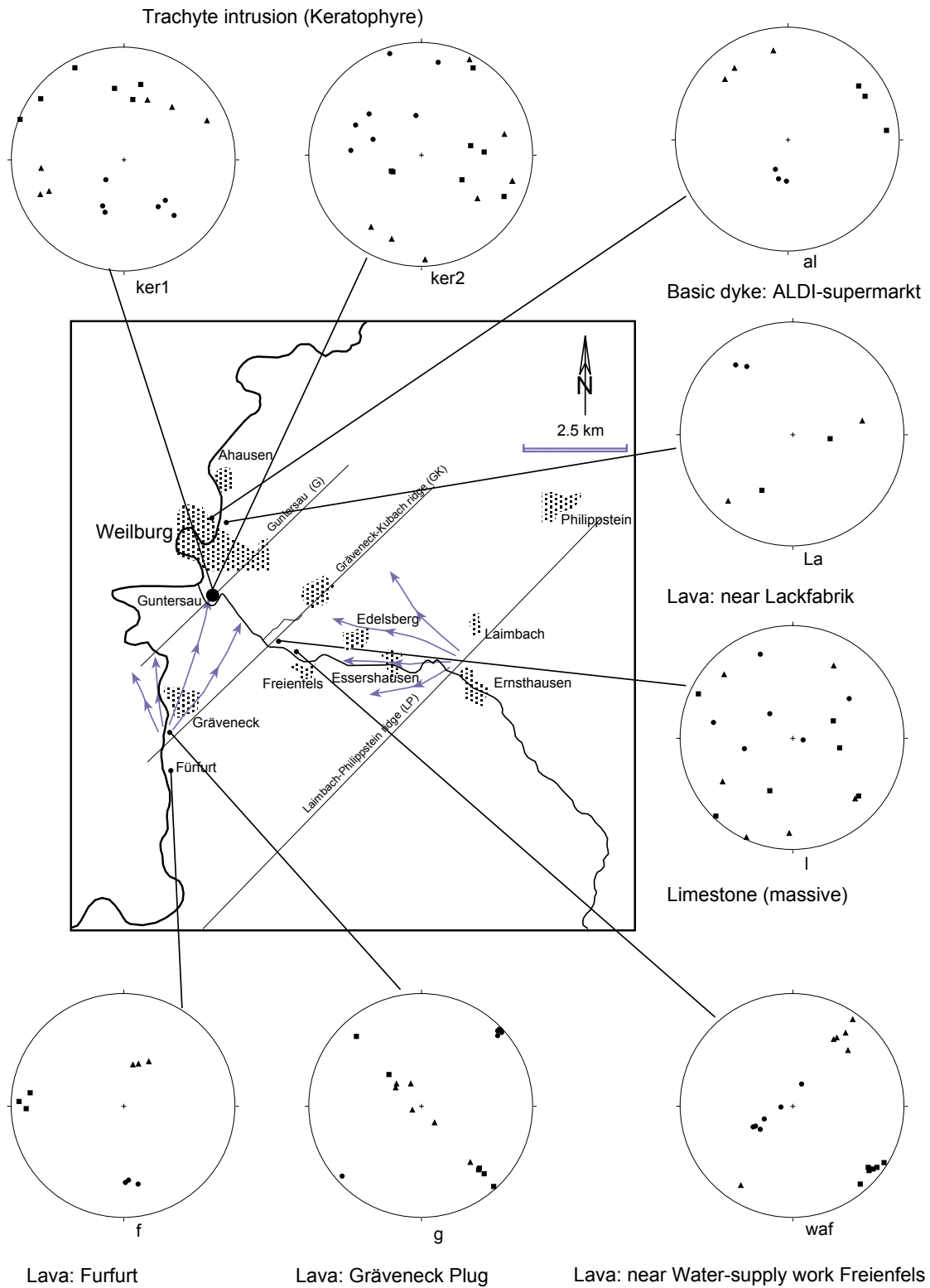


Fig. 7-21. AMS fabrics distribution in miscellaneous rocks of the Weilburg area.

The AMS data for the dykes show the flow direction according to the K_1 axes orientation and its plunge. Sometimes instead of the K_1 axes, the K_2 axes orientation and plunge are used in this reconstruction of dykes at the profile of the Guntersau-Freienfels sub-area as a half-graben basin (Fig. 7-18). The D3 dyke can be used as the reference dyke indicating the inclination of the K_1 axes which have the highest angle of about 60° . Thus, the others are emplaced away from either side of it (see Fig. 7-18). The D1.2 and FG5 host rocks are easily recognized by their direction on AMS stereoplots. The AMS data for the dykes of the Guntersau-Freienfels basin using the mean K_1 axes direction, (Fig. 7-20) indicate the source area of the dykes mean the extensional border fault to the south (Fig. 7-20) because of an antithetic half-graben development (northward shallowing) of the Guntersau-Freienfels basin. According to this source area and the K_1 axes direction, the D3 dyke at the centre, the other D1 and D2 dykes in the SE and D4, D5, D6, D7, D8, D8A and D9 dykes in the NW can be located in the present position of the Guntersau-Freienfels basin-profile (along NW-SE). The inclination angle of the K_1 axes indicates the emplacement source (GLEN et al. 1997, STAUDIGEL et al. 1992, PALMER et al. 1991, KNIGHT & WALKER 1988), so that the D1 and D2 dykes are between 15° - 30° , the D3 dyke is about 60° and the D5 to D7 dykes change as a transition from 60° to 40° . And the D8 and D8a dykes are characterized as sill, whereas the D9 dyke becomes steeper again (Fig. 7-20). Dykes D9, D8a and D8 originated at relatively deep seated conditions according to the inclination angle of K_3 axes (cf. HOUSEN et al. 1996), (see details in Fig. 7-20).

Dyke in Weilburg (near ALDI supermarket): This dyke is exposed in the compound of the ALDI supermarket in Weilburg. The AMS plot (Fig. 7-21) shows a nearly horizontal position. The K_1 and K_2 axes are slightly dispersed along the foliation, whereas the K_3 axes are well clustered. The orientation is NE about 060° - 080° N azimuth and about 20° plunge.

7.3.5 AMS applied to pillow lava

Pillow lavas have very considerable potential as strain indicators (BORRADAILE et al. 1989). In this case, a detailed understanding of their tectonic deformation is required to deduce their original orientation (BORRADAILE & POULSEN 1981). At the Freienfels-Ernsthausen sub-area, pillow lavas exhibit strain ellipsoids with long axes parallel to the s_1 -cleavage (Plate 4B). However, some (near the junction of Laimbach and Weiltal road) are still undeformed, showing simple cusped shape and original bilateral symmetry (Plate 5). The AMS study of pillow lavas can detect the grade of deformation in terms of low-grade facies (Fig. 7-22). The pillow lava reveals comparatively high AMS-values but the average anisotropy degree (P^1) value 1.06 - 1.08 is the same as the maximum average anisotropy value of lavas (sheet flow lava and pillow lava together) of the Weilburg area.

The study area is generally penetratively deformed by the s_1 -cleavage development as a regional structure, and so far the magnetic foliations show SE dipping as the s_1 -cleavage (Fig. 3-9). The stereoplots of the pillow lava show different positions for the axes of K_1 , K_2 and K_3 (Fig. 7-23). The flow direction of pillow lavas is normally not detectable with AMS because of deformation. However, without AMS the inferred flow directions can be noticed by referring to the source areas and their basin position in terms of the half-graben basin.

Within the half-graben basin of Freienfels-Ernsthausen sub-area the AMS fabrics has been used as a strain indicator (cf. KLIGFIELD et al. 1977). Highly deformed pillow lava shows its long axes parallel to the s_1 -cleavage (Plate 8B) and the high anisotropy in the T-P^I diagram (Fig. 7-24). The strong flattening shows in the L-F diagram (Fig. 7-25) which can be used as a deformation path. Pillow lavas can be used as a strain indicator (KLIGFIELD et al. 1977) in terms of progressive strain deformation (Fig. 7-24 & 7-25).

The pillow lavas of the Freienfels-Ernsthausen sub-area from different localities are deformed in different intensities. Undeformed pillow lavas occurs mostly near their source area where the extensional border fault was developed at the half-graben basin. The highly deformed pillow lavas are to be found away from the source, where the half-graben was shallowing or the deformation toe of an accretionary prism was located during orogenic shortening. During the compression according to the observation of the pillow lava deformation and thrust front (Plate 8B), the deformation toe is more deformed than the rear side of the prism body (Fig. 7-24 & 7-25).

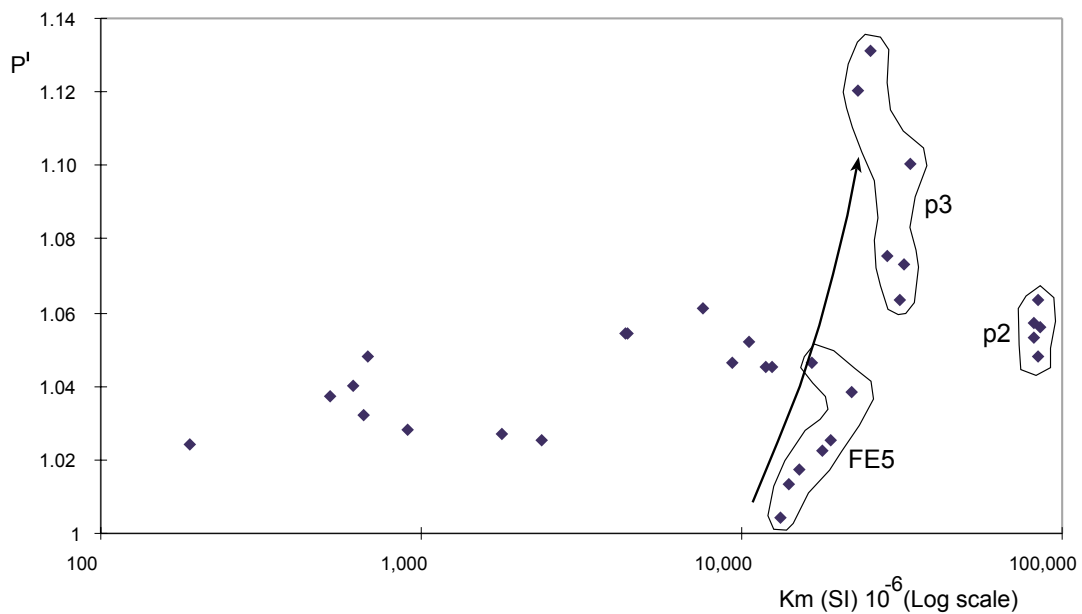


Fig. 7-22. P^I vs K_m mean AMS diagram of pillow lava of the Weilburg area (diagram: after FULLER 1963 and BORRADAILE & SARVAS 1990). Arrow indicates the form of low-grade facies (after BORRADAILE & HENRY 1997) in the Freienfels-Ernsthausen sub-area.

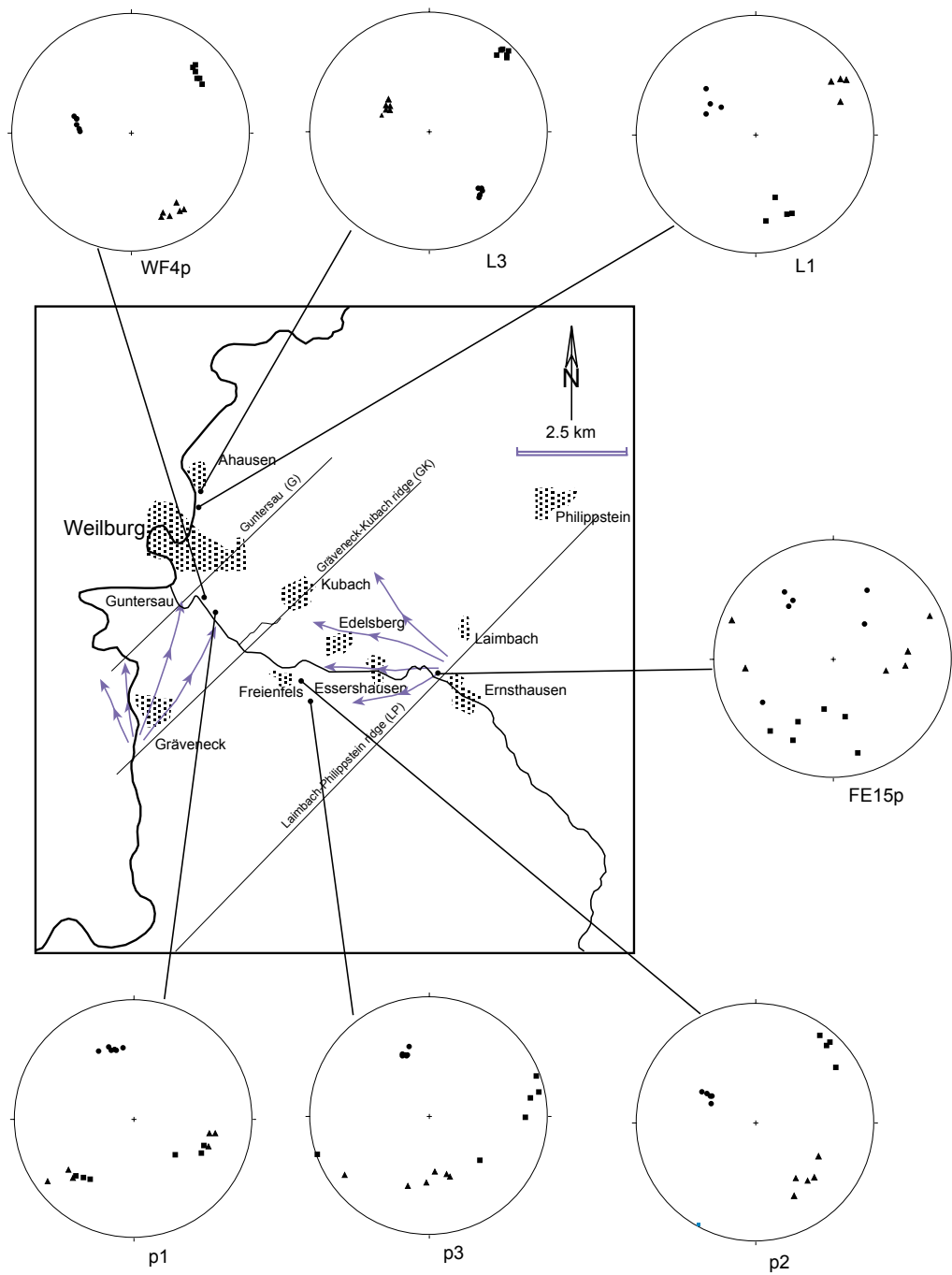


Fig. 7-23. Spatial distribution of pillow lavas with corresponding AMS fabrics in the Weilburg area.

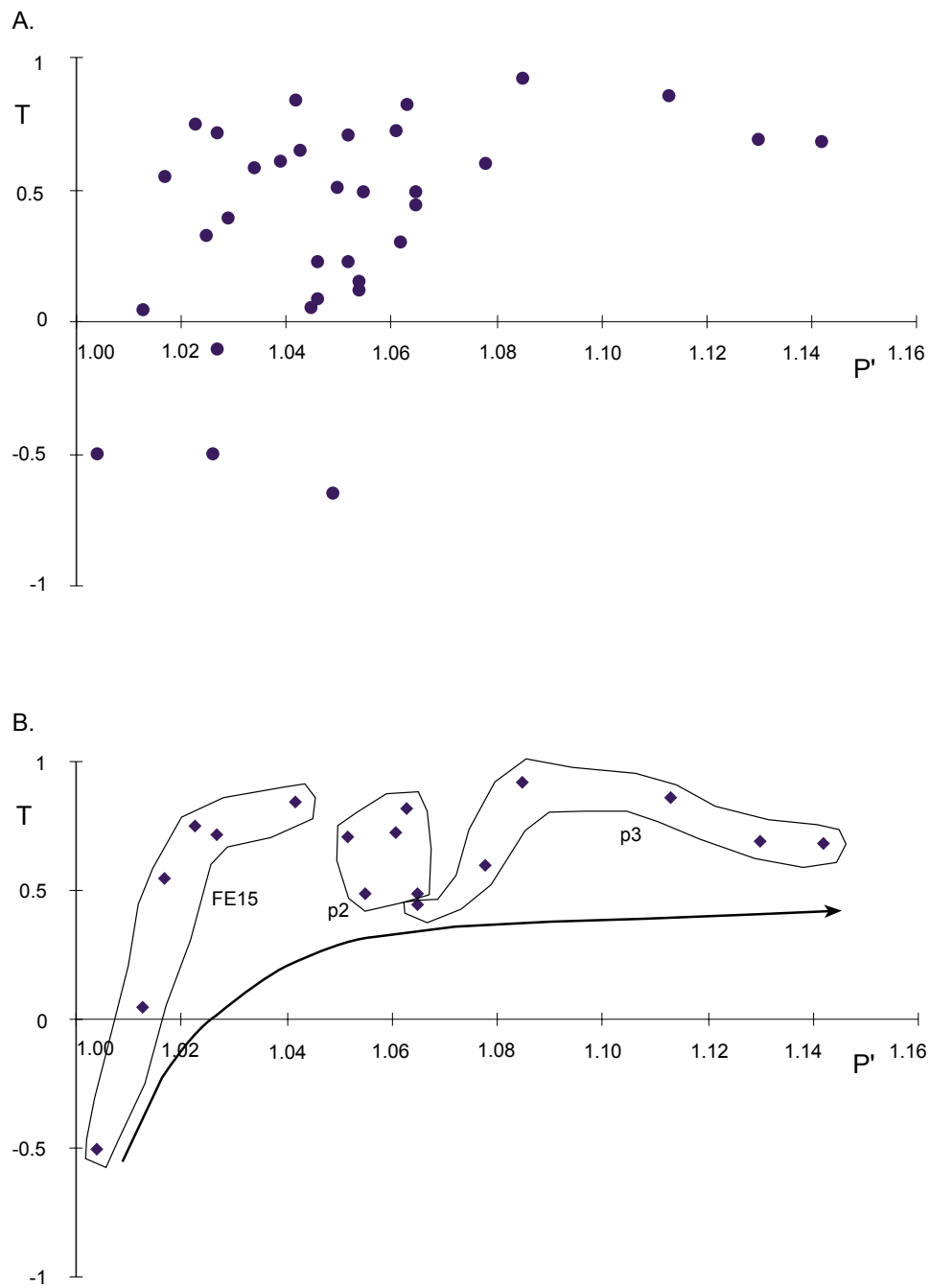


Fig. 7-24. T- P' diagrams of pillow lava of the Weilburg area (A) and exclusively the Freienfels-Ernsthäusen sub-area with arrow to high anisotropy (B). (Jelinek-diagram: after JELINEK 1981). Arrow indicates progressive deformation.

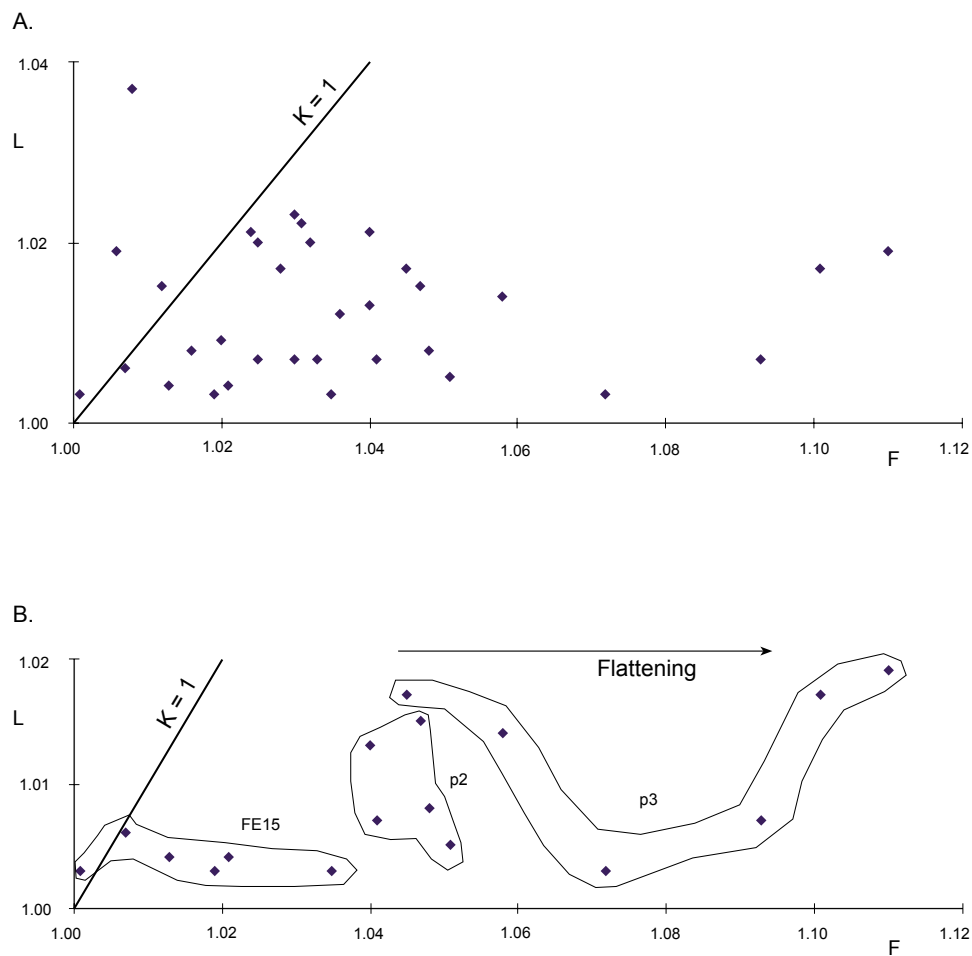


Fig. 7-25. L-F diagrams of pillow lava of the Weilburg area (A) and specifically the Freienfels-Ernsthausen sub-area showing the high anisotropy direction (B) (Flinn-diagram, after FLINN 1962 and KHAN 1962).

7.3.6 AMS applied to limestone

Limestones in the study area from which the AMS is measured fall into two types: massive limestone and epiclastic fragments in the lapillituff. Epiclastic fragments have their long axes parallel to the intersection lineation about $055^{\circ}/55^{\circ}$. Of course, this limestone fragments embedded in the fine lapillituff-matrix could be a result of plastic deformation by the stretching along the regional trend, which is deformed under very low-grade to low-grade regional metamorphism (cf. Fig. 7-26). The AMS stereoplot shows that the maximum susceptibility K_1 axes are relatively widely dispersed and partly totally intermixed with the intermediate susceptibility K_2 axes (Fig. 7-27). Thus, thinking in terms of a magnetic ellipsoid, it is close to rotational (DVORÁK & HROUDA 1972). The K_3 axes agree very well with the direction of the bedding poles (Fig. 7-27). However, the K_1 and K_3 axes inversely changed their position (BORRADAILE & HENRY 1997, see details in text of ROCHETTE et al. 1992, ROCHETTE 1988) when compared with the principal finite strain axes.

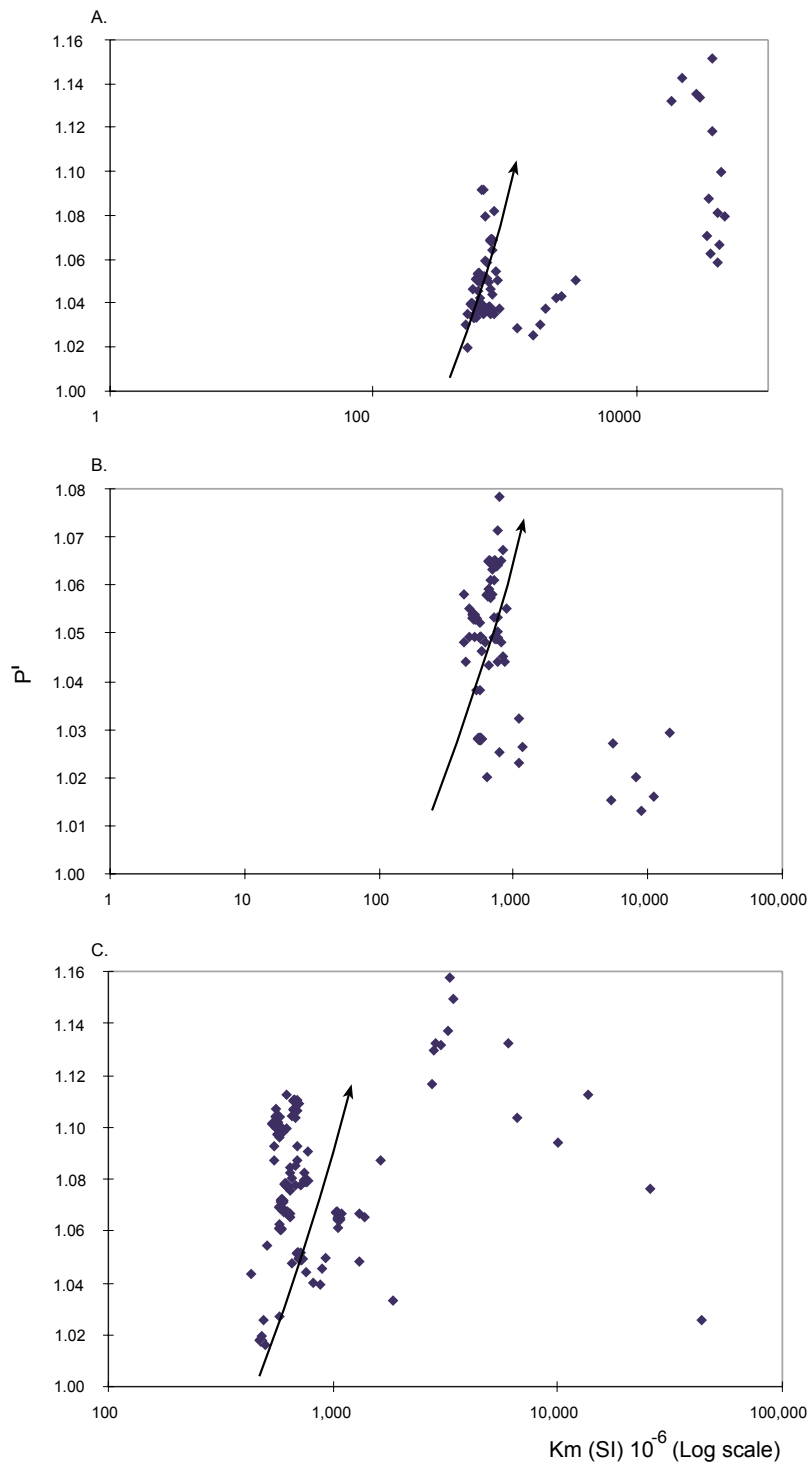


Fig. 7-26. P^l vs K_m mean AMS diagrams of dyke (A), sheet flow lava (B) and lapillituff (C) in the Guntersau-Freienfels sub-area, in the Weilburg area (diagram: after FULLER 1963 and BORRADAILE & SARVAS 1990).

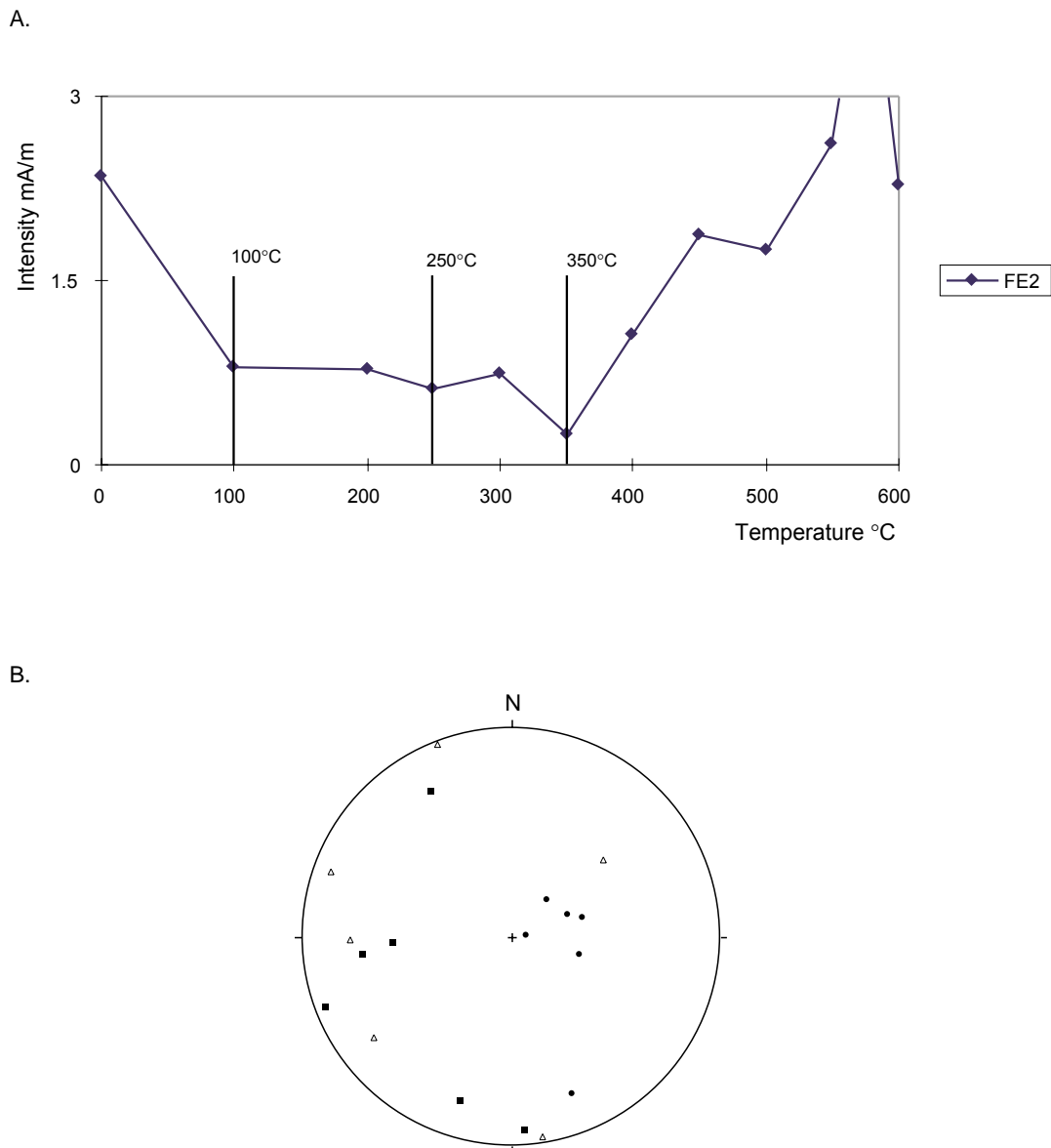


Fig. 7-27. A: Magnetic intensity vs Temperature diagram for the magnetic minerals to determine in the Curie temperature in °C by the demagnetization in TRM (Thermal Remanent Magnetization) method. Data from limestone epiclastics near Freienfels in the Weilburg area. B: The AMS fabrics of limestone fragments.

According to MCCABE et al. (1985) most carbonate sediments show clearly defined sub-horizontal magnetic foliations and occasional well-developed magnetic lineations. GRAHAM (1949) stated that the direction of magnetization can be retained in the sedimentary rock without changes through the long period of geologic time. In the inverse magnetofabrics situation the K_1 and K_3 axes exchange their role. Inverse magnetofabrics are very common in limestone (BORRADAILE & HENRY 1997) and carbonate-bearing rocks (ROCHETTE 1988). In this case, the K_3 axes direction are well clustered around the horizontal pole axis while the K_1 axes direction shows a mean horizontal orientation. The

massive reef limestone has the attitude about $062^{\circ}/15^{\circ}$ in bedding planes. These are totally different from regional structure. However, in the AMS stereoplots of the massive limestone two orientations can be traced: one is parallel to regional trend or the intersection lineation ($055^{\circ}/55^{\circ}$) and one corresponds to the direction of s1-cleavage. Anyway, the massive limestone has actually no prominent direction such as foliation or lineation.

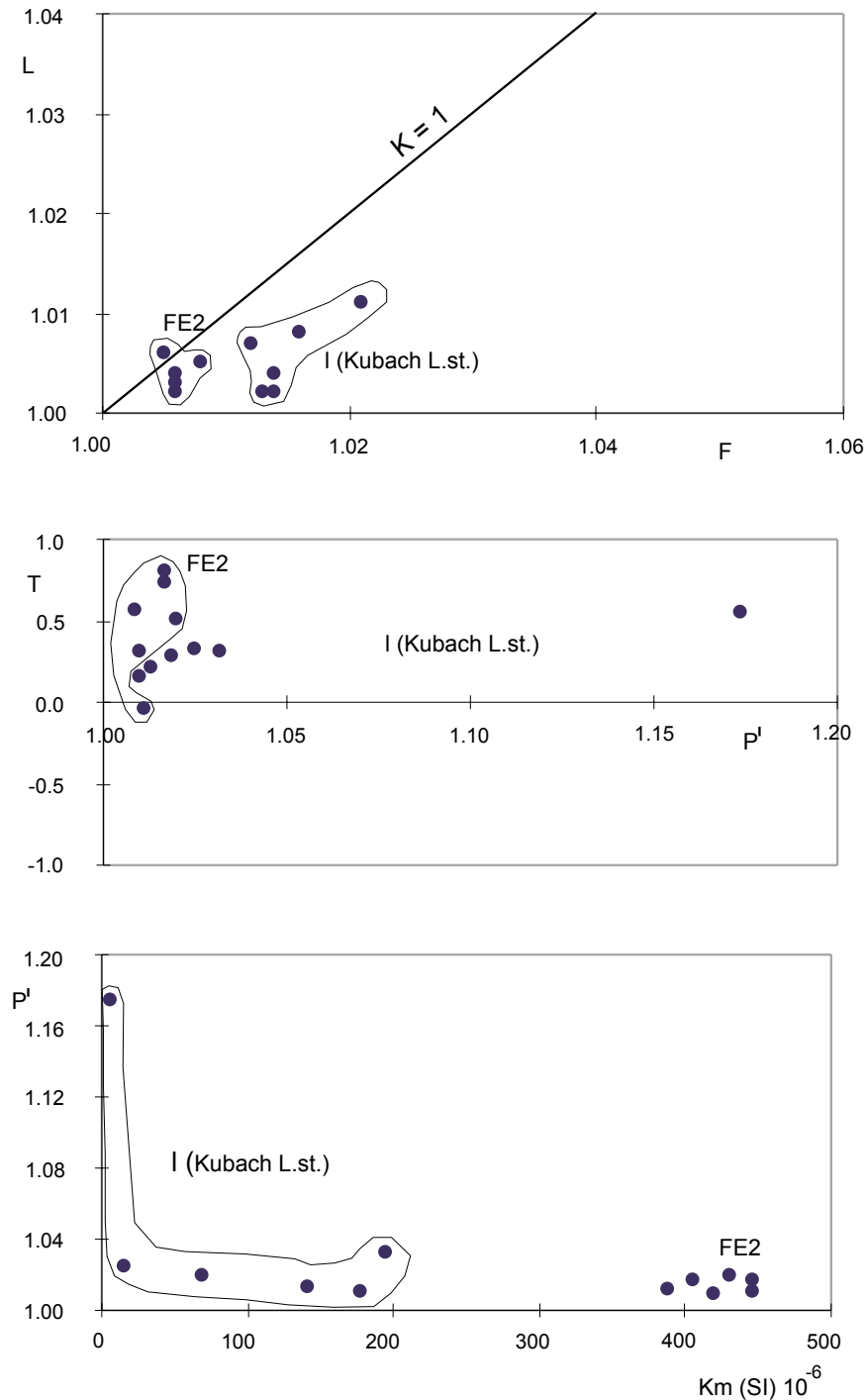


Fig. 7-28. AMS characteristics in L-F, T-P^l and P^l-K_m diagrams of limestone (massive and epiclastic) in the Weilburg area. (Flinn-diagram, after FLINN 1962 and KHAN 1962; Jelinek-diagram: after JELINEK 1981)

K_1 and K_3 axes in the inverse and normal magnetofabrics of limestone:

Normal case:

K_1 = lineation

K_3 = pole of schistosity

Inverse case:

K_3 = parallel to the linear preferred orientation

K_1 = perpendicular to it

Magnetic minerals in limestone are goethite and pyrrhotite in Figure (7-27) shown by the Curie temperature. Pyrrhotite is of two types: mixed and monoclinic determined by the measurement of TRM (Thermal Remanent Magnetization) method.

The AMS data of limestone are analyzed by L-F, T-P^l and P^l-K_m in which core sample data show different mean susceptibilities, but the anisotropy degree of these are nearly the same (Fig. 7-28).

7.3.7 AMS applied to strain

The shape of the AMS ellipsoid axes ($K_1 > K_2 > K_3$) are ideally correlated to the principal axes of the strain ellipsoid ($X > Y > Z$) in the deformation stage,

e.g. $X//K_1$, $Y//K_2$, $Z//K_3$.

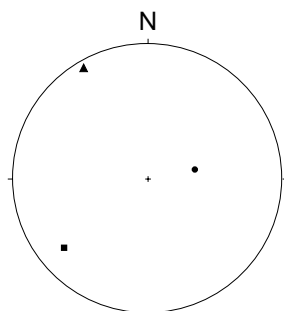
A body is changed in size and shape during the deformation. The co-ordination system of the strain in a fold (Fig. 4-1) is used, i.e. XY plane parallel to the layering the Y axis parallel to the fold axis. The 3-D strain is calculated on all the planes as XZ, XY and YZ.

The magnetofabric data and the strain fabrics show (Fig. 7-29 A & B) that the K_1 axes are generally parallel with the bedding-cleavage intersection.

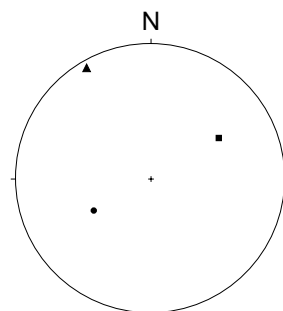
In the quantitative comparison of the AMS and the principal strain axes, the K_3 axes in most of the samples are parallel to the Z direction. This implies a correlation between K_1 axis and X axis, and K_2 axis and Y axis.

The present study tried to consider the correlation in different kinds of rocks, such as epiclastic limestone fragments, epiclastic pillow fragments, lapillituff, *Mandelstein* (amygdaloidal basalt), and pillow lava. The limestone shows inverse fabrics as the exchange of K_1 and K_3 axes (Fig. 7-29A). Pillow fragments are prolate in shape but inverse in the K_1 and K_3 axes, lapillituff (Guntersau-Freienfels sub-area) shows an inverse position of the K_1 and K_2 axes (Fig. 7-29B), *Mandelstein* has different positions of the K_1 and K_2 axes, pillow lava shows in different regarding the K_1 and K_2 axes. Therefore, the correlation between strain and magnetofabric analysis is not consistent. The Flinn-diagrams of the AMS and the strain are generally equivalent in oblate and prolate shape, but exception for limestone. In the limestone epiclastics the X axis is parallel to the intersection lineation with a prolate ellipsoid (Fig. 7-30). In the L-F diagram, the K_1 and K_3 axes should be inverted in the prolate field. In the correlation of the AMS and the principal strain axes, the K_1 and K_2 axes when compared to the X and Y axes are mostly in an inverse position in their orientation, e.g. K_1 and Y, K_2 and X. In this study, while the strain ellipsoids are parallel to the s₁-cleavage, the K_1 axes are defined

Limestone (fragment)
sample No. FE2

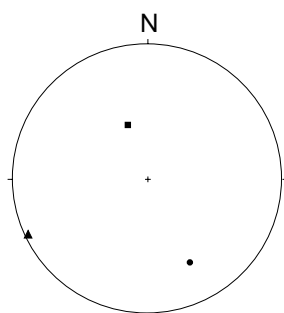


AMS
K1 = 230/20
K2 = 330/5
K3 = 080/60

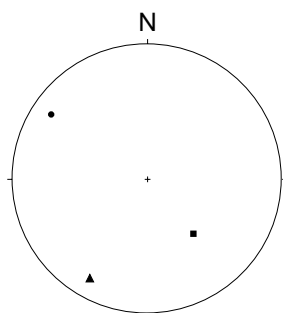


Strain
x = 060/40
y = 330/5
z = 240/50

Pillow fragments (Edelsberg)
sample No. FE6

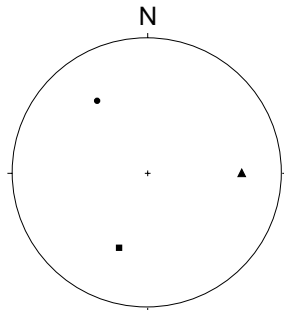


AMS
K1 = 340/55
K2 = 245/2
K3 = 153/30



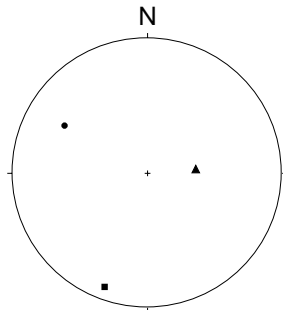
Strain
x = 145/45
y = 210/15
z = 304/15

Lapillituff (Guntersau)
sample No. FG10

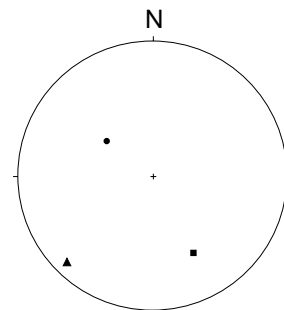


AMS
K1 = 200/40
K2 = 090/30
K3 = 325/35

sample No. FG11



AMS
K1 = 200/10
K2 = 085/60
K3 = 300/30

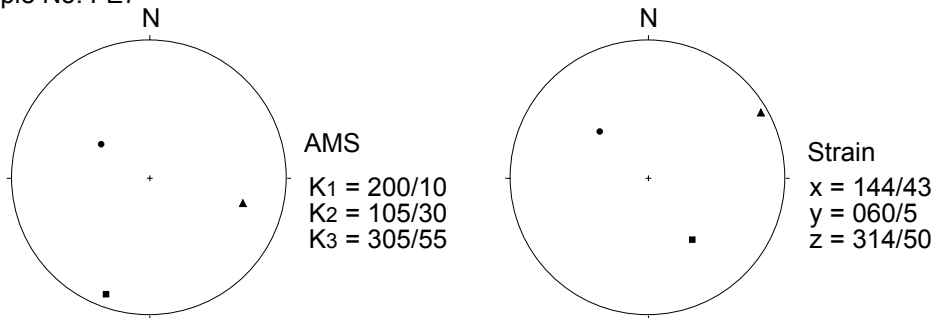


Strain
x = 152/35
y = 225/10
z = 306/60

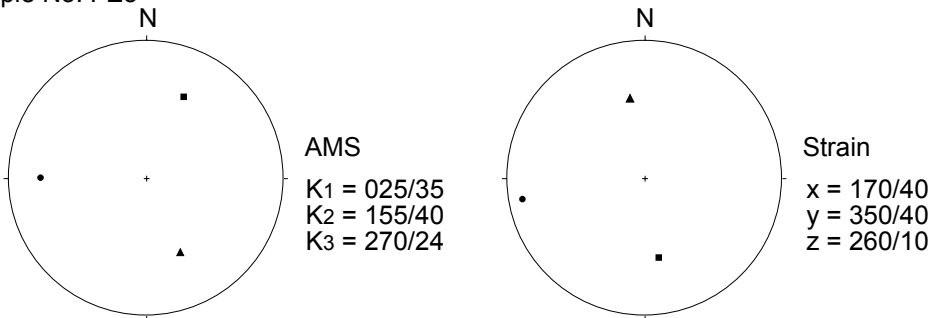
Fig. 7-29A. Correlation between AMS and strain in the Weilburg area.

■ = K1 or X , ▲ = K2 or Y , ● = K3 or Z.

Lapillituff (Essershausen)
sample No. FE7



Mandalstein (Freienfels)
sample No. FE3



Pillow lava (Weinbach)
sample No. p3

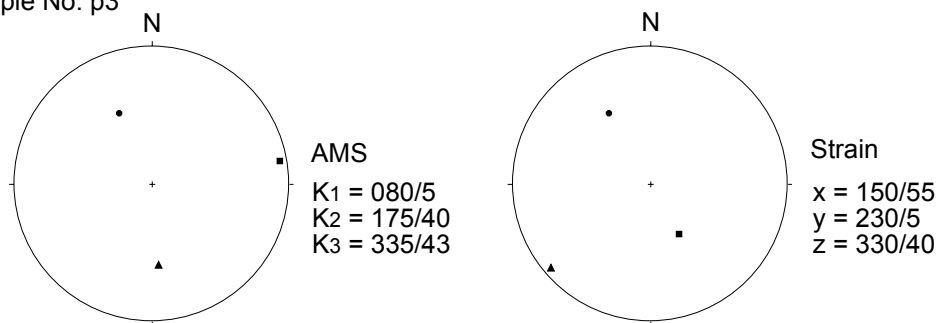


Fig. 7-29B. Correlation between AMS and strain in the Weilburg area.

■ = K1 or X , ▲ = K2 or Y , • = K3 or Z.

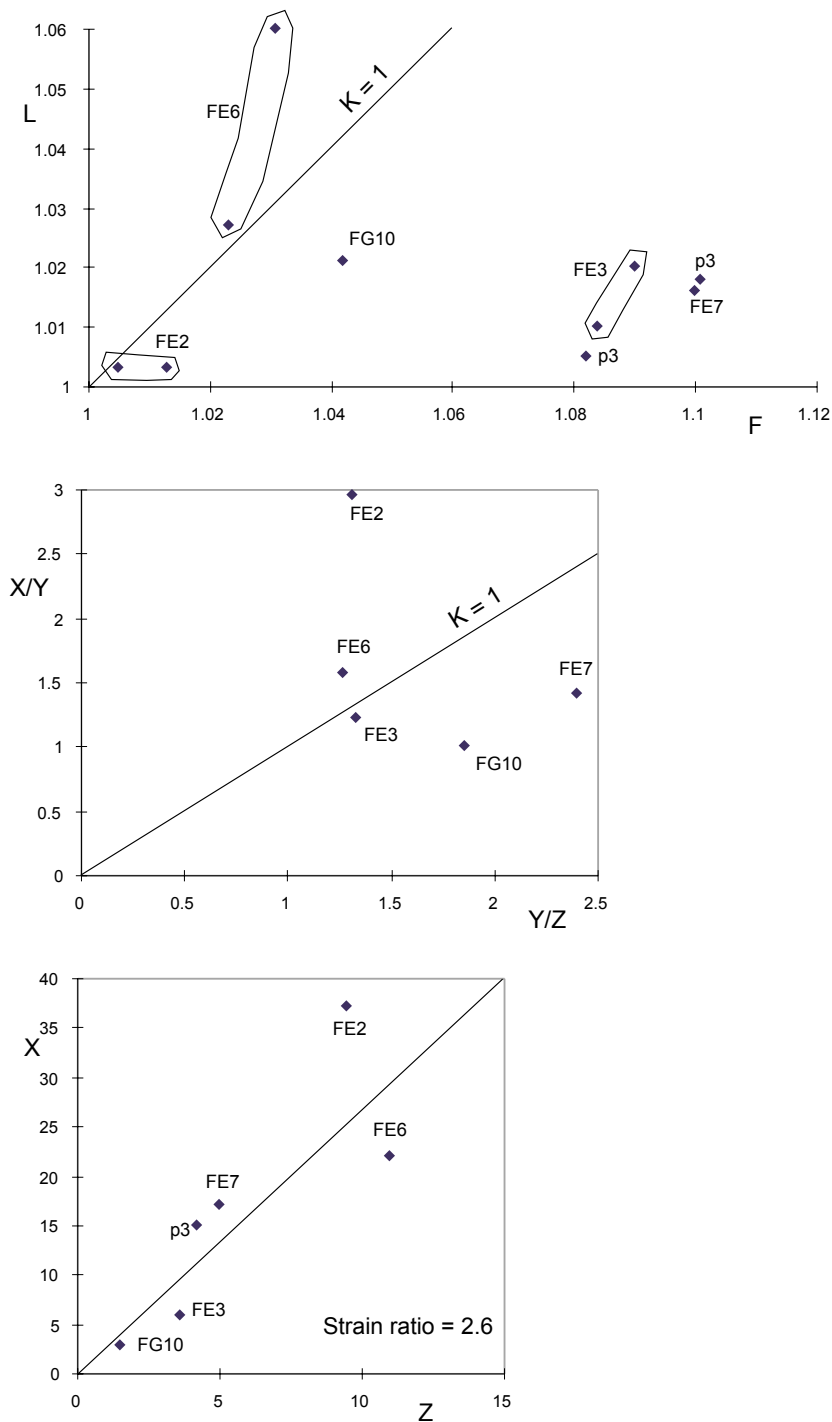


Fig. 7-30. Diagrams for correlation between AMS and strain by L-F and X/Y vs Y/Z (Flinn diagram), and X-Z (strain ratio) diagrams of the Weilburg area. (Flinn-diagram, after FLINN 1962 and KHAN 1962)

Table 7-2. Finite strain and magnetic susceptibility principal values used in the correlation diagram in Fig. 7-38.

Rock type	Sample No.	ϵ_1	M1	ϵ_2	M2	ϵ_3	M3	Localities
Limestone fragments	FE2	1.3	0.0059	0.18	0.0037	0	-0.0094	Freienfels-Ernsthausen
Pillow lava fragments	FE6	0.78	0.052	0.33	-0.004	0.095	-0.048	Freienfels-Ernsthausen
Lapillituff	FG-10	-0.22	0.026	-0.69	0.0072	-0.9	-0.034	Guntersau-Freienfels
Lapillituff	FE7	-0.1	0.043	-0.69	0.025	-1.38	-0.068	Freienfels-Ernsthausen
Mandelstein	FE3	-0.51	0.034	-0.91	0.022	.9	-0.056	Freienfels-Ernsthausen
Pillow lava	p3	0.4	0.033	-0.69	0.026	-0.9	-0.06	Freienfels-Ernsthausen

as the magnetic lineation which is parallel to the fold axis. This is commonly observed, but K_1 axis does not represent the X strain axis (cf. BORRADAILE & HENRY 1997). Instead, the maximum K_1 axis is parallel to the intermediate stretch, Y axis.

Thus, $X//K_2$, $Y//K_1$, $Z//K_3$.

In comparison with the final stage of the strain path, the Z axis is perpendicular to the XY-plane so that the intermediate strain axis becomes parallel to Y axis. This can be achieved by steady grain rotation. Thus, axis-swapping can occur where the initial magnetofabric investigation reveals K_3 axes close to X axes (cf. Fig. 4-6B), then K_3 axes transformed to become K_2 axes and then finally K_1 axes. Present stage is $K_1 // Y$, parallel to fold axes because the bedding fabric is incompletely overprinted (cf. BORRADAILE & TARLING 1984)

Quantitative relationships: The principal normalized susceptibilities have been plotted against the principal (equal volume normalized) finite strains (Fig. 7-31). The data are scattered and no linear relationship between strain and magnetic anisotropy is observed over the range of strain indicated.

The principal logarithmic strain $\epsilon_i = \ln(1-e_i)$ can be determined directly from the normalized principal susceptibility differences {defined such that $M_i = (k_1 - k')/k'$ where $k' = (k_1 + k_2 + k_3)/3$ using the relationship $\epsilon_i = \alpha M_i$ where $\alpha = 11.1$ (maximum), 0 (intermediate) and 20 (minimum), (Fig. 7-31)}. As a result, the regression line does not pass through the origin of the plot, in fact, the X long axes are parallel to the s_1 -cleavage, whereas the K_1 axes are consistent with the intersection of bedding and cleavage. Thus, the strain deformation has not affected the magnetization.

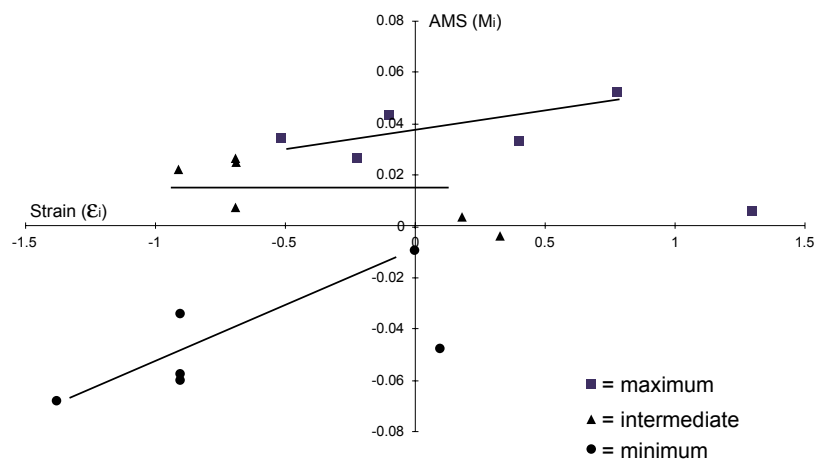


Fig. 7-31. Correlation of normalized principal magnetic susceptibilities M_i and logarithmic strain ϵ in volcanic rocks from the Weilburg area (diagram: after KLIGFIELD et al. 1981).

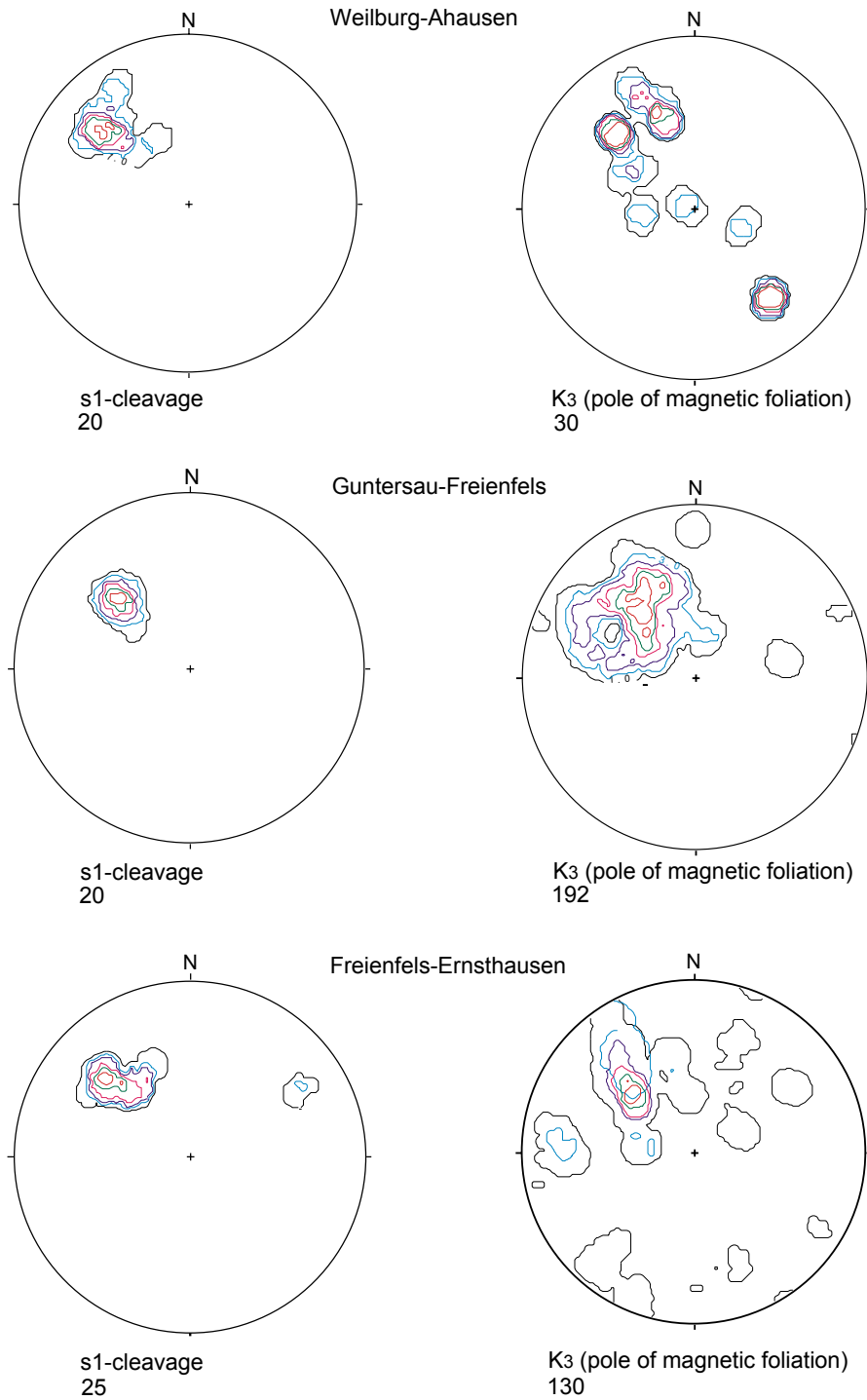


Fig. 7-32. Comparison of the fabric diagrams between pole of s1-cleavage and pole of magnetic foliation (K_3) in each sub-area in the Weilburg area.

Generally, in this study, the AMS ellipsoids especially the K_1 and K_2 axes, are developed in the cleavage planes, i.e. magnetic foliation is parallel to s_1 -cleavage, but the relation between the principal strain axes and the AMS ellipsoid axes: X and K_1 and Y and K_2 axes are not regular, nevertheless K_3 and Z axes are generally regularly parallel except in limestone. The K_2 axes are usually parallel to the regional strike (KLIGFIELD et al. 1982), but in this study the K_1 axes are parallel to the regional strike. Principal strain Z axes and pole of the AMS (K_3 axes) are absolutely the same except for limestone (Fig. 7-32). KLIGFIELD et al. (1981) and COGNÉ (1988) show the strain influence on the AMS ellipsoid axes in the pencil structure development, but HIRT et al. (1988) show no universal correlation. The correlation of magnetofabric and strain data is not universal or not a routine substitute for strain deformation (LOWRIE 1989, BORRADAILE 1988, KLIGFIELD et al. 1981, RATHORE 1980).

7.4 NATURAL REMANENT MAGNETIZATION (NRM)

Magnetic mineralogy study in sheet flow lava (basaltic rocks), dyke lava, lapillituff (pyroclastics, hydroclastics and epiclastics) was carried out by TRM-demagnetization (Thermo Remanent Magnetization) using a MINISPIN MAGNETOMETER (Fig. 7-33) to get the magnetic minerals: pyrrhotite, maghaemite, magnetite and hematite(?) by the Curie/Neel temperature °C (Fig. 7-34A & B, 7-35A & B), (TARLING & HROUDA 1993), (TRM data in Appendix-C).

Magnetic minerals:

Pyrrhotite: The Curie temperature of pyrrhotite, 320 °C, is almost the same as the temperature at which it decomposes to magnetite (or hematite if sufficient oxygen is available). Pyrrhotite is common in basic volcanic rocks (TARLING & HROUDA 1993, WHITNEY & STORMER 1983) and occurs in low-grade metamorphic zones (cf. Fig. 7-26), (ROCHETTE 1987).

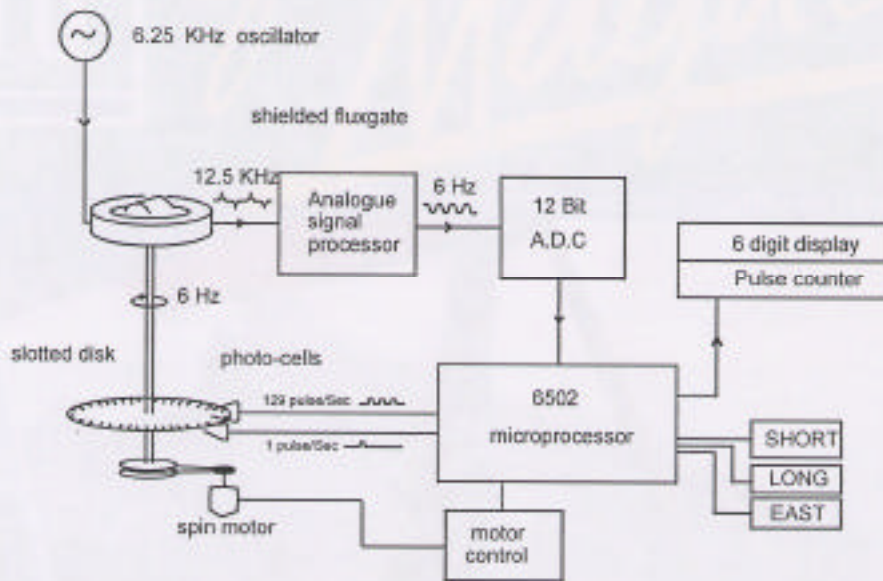
Maghaemite: The composition of maghaemite is essentially that of haematite. This mineral is a common constituent of lodestones (NAGATA 1961) and natural maghaemite converts to hematite at temperatures in the range 300 °C - 350 °C.

Magnetite: The Curie temperature is 578 °C.

Curves (data in appendix-C, Fig. 7-34A & B and 7-35A & B) show the temperature about 200 °C for which was mentioned by De WALL (1991) that the pyrrhotite occurs in two types: the first with a Curie temperature of 300 °C is monoclinic pyrrhotite; the second with a Curie temperature 200 °C is a mixed type (monoclinic and hexagonal systems) pyrrhotite.

Because of the temperature of 450 °C there could often be maghaemite which changes into haematite between 350 °C - 450 °C by increasing temperature in laboratory (TARLING & HROUDA 1993, TARLING 1983).

Following the measurement of the TRM, magnetite and pyrrhotite minerals are included as a main constituent in all of the volcanics (Fig. 7-34A & B and 7-35A & B). On the other hand, the main constituent minerals are pyroxenes: e.g. augite which is also a high iron-content mineral, however, most were changed into chlorite minerals.



SPECIFICATIONS

Sample size	2.54 cm diameter 2.2 cm high
Spin number	24 (short) or 120 (long) ; 6 seconds or 22 seconds
Data indication	5 digit LCD display and +/- indicator
Range	0.1 to 2500 mA/m in 4 decade steps.
Noise	Less than 0.025 mA/m for any axis for long (4spin) mode.
Power supply	120 or 240 volt AC, 50/60 Hz or Internal Battery. Battery charge lasts about 8 hours. The battery charger works from 120 or 240 volts or a car battery. Power consumption: 6 watts
Dimensions	42 cm high, 32 cm wide, 18 cm thick
Weight	less than 10 kg.

Fig. 7-33. Instrumentation diagram of Minispin Magnetometer (after MOLSPIN Newcastle, NE).



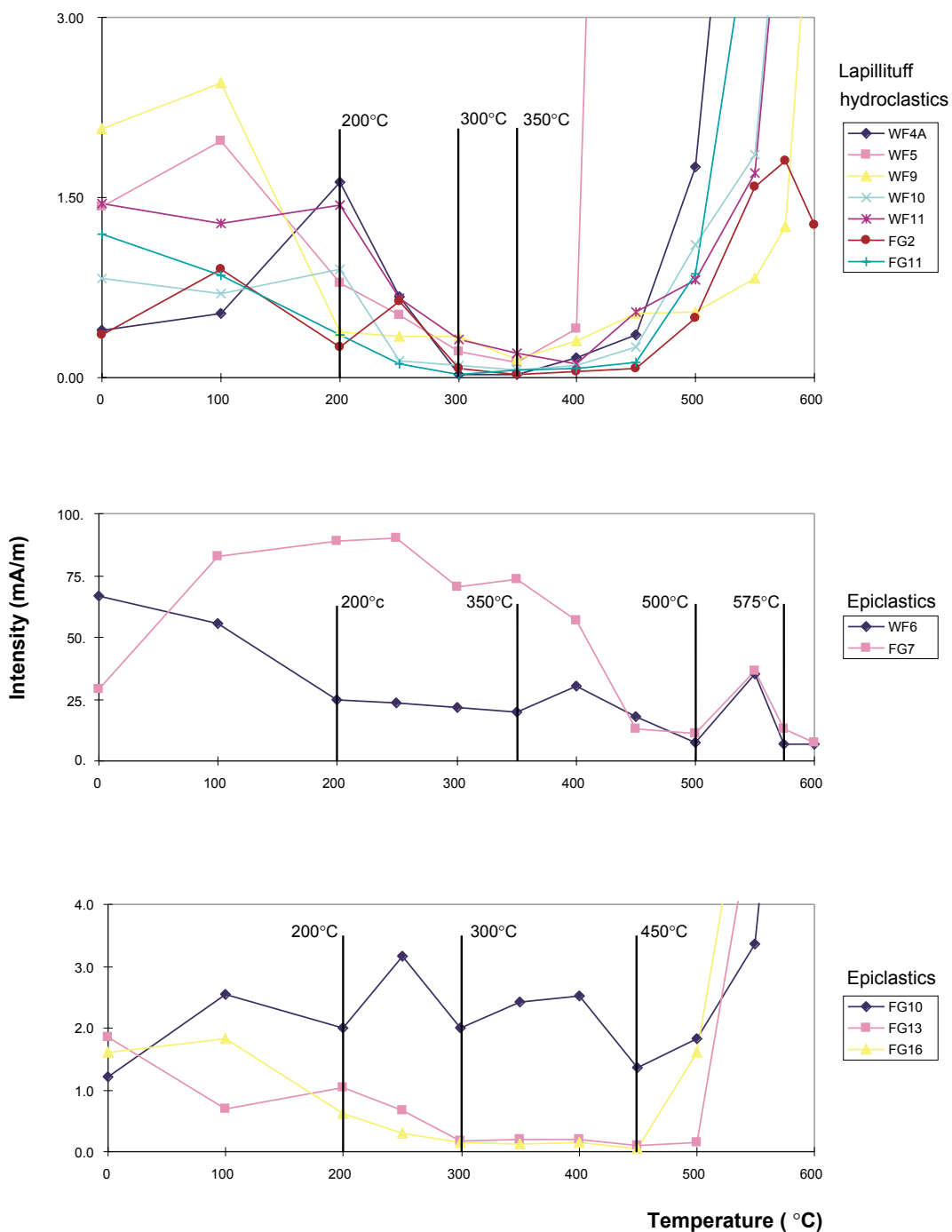


Fig. 7-34A. Magnetic intensity vs temperature diagrams for the magnetic minerals to determine in the Curie temperature in (°C) by the demagnetization in TRM (Thermal Remanent Magnetization) method. Data from lapillituff of the Guntersau-Freienfels sub-area in the Weilburg area.

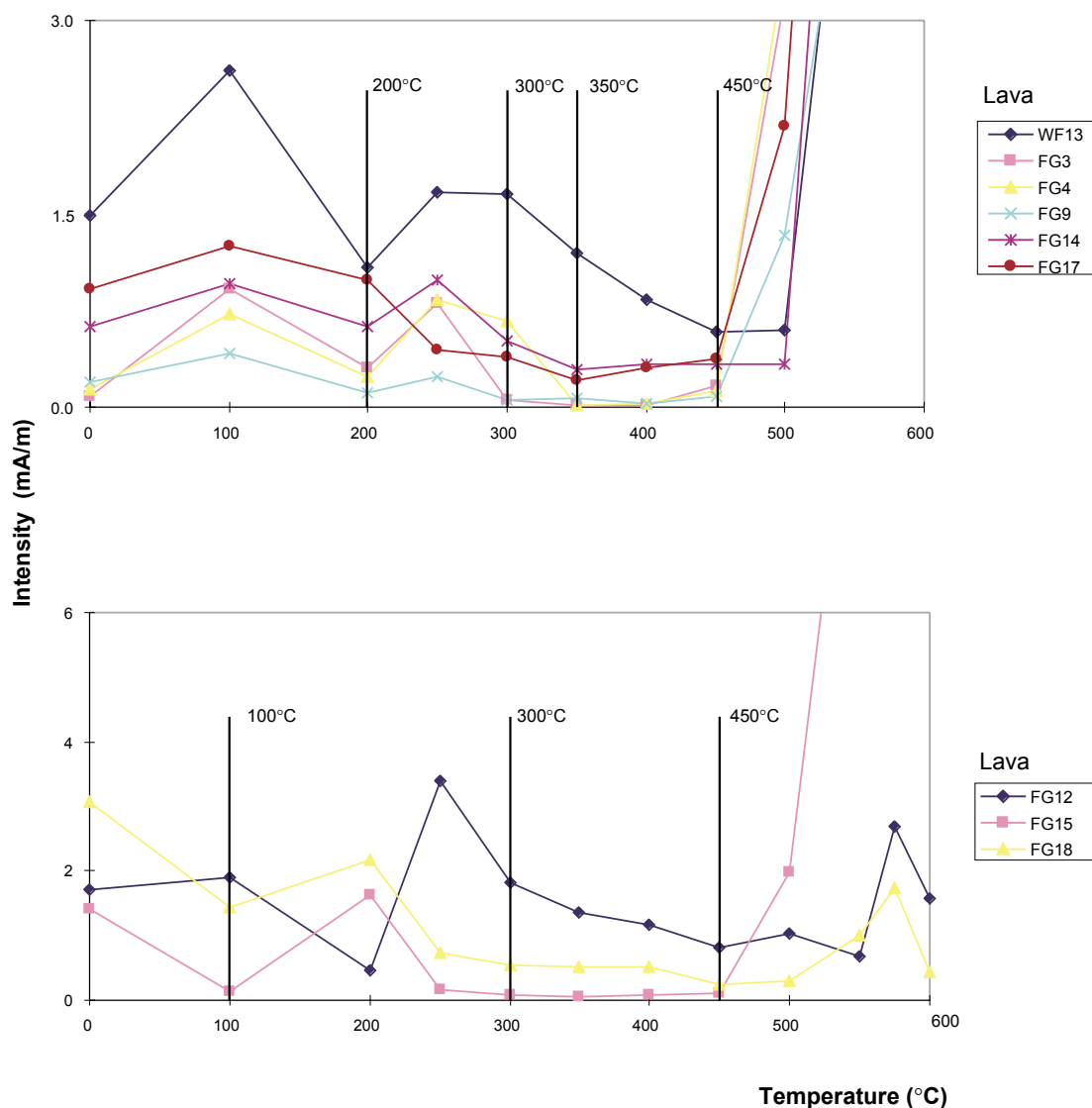


Fig. 7-34B. Magnetic intensity vs temperature diagrams for the magnetic minerals to determine in the Curie temperature in °C by the demagnetization in TRM (Thermal Remanent Magnetization) method. Data from sheet flow lava of the Guntersau-Freienfels sub-area in the Weilburg area.

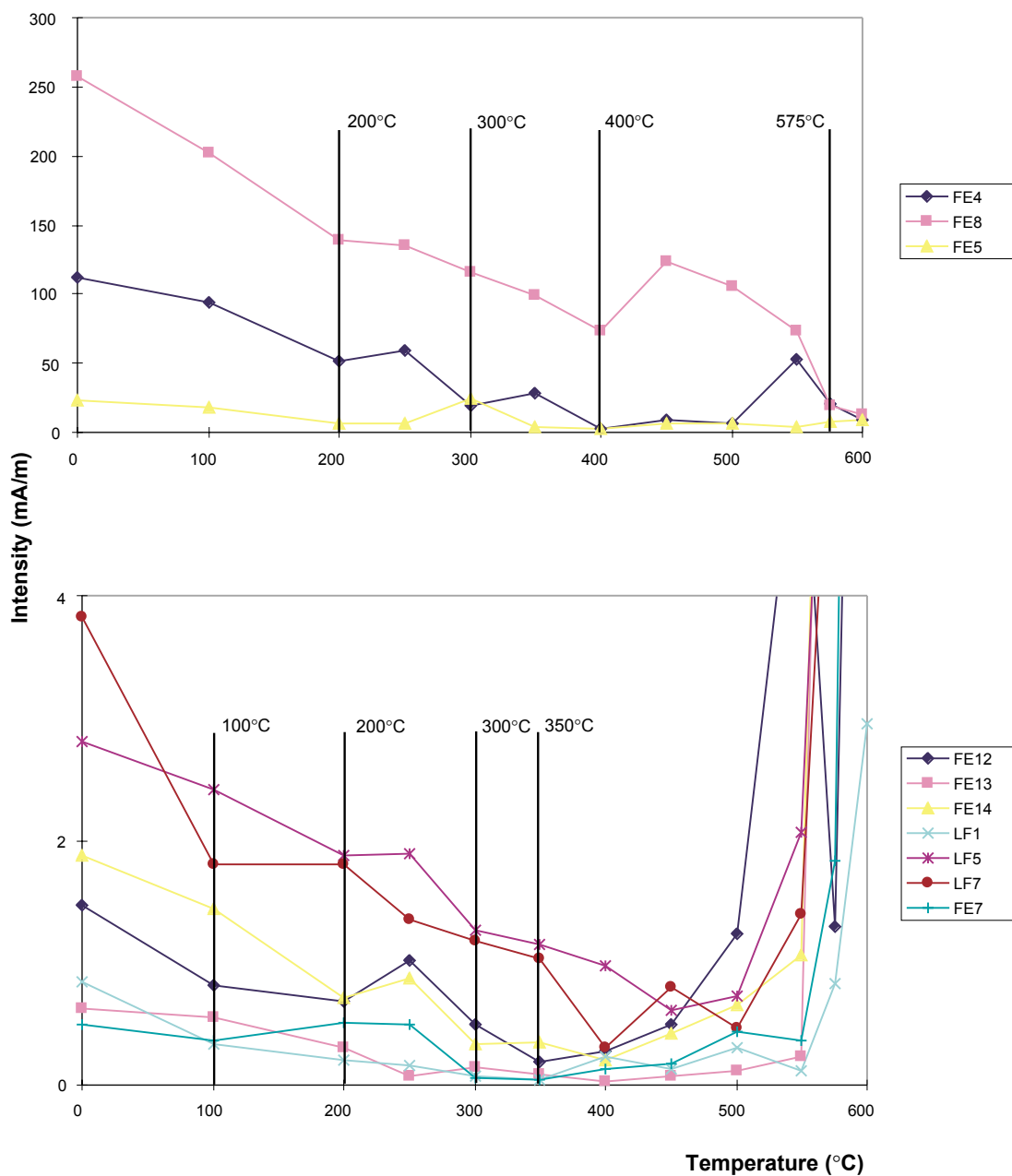


Fig. 7-35A. Magnetic intensity vs temperature diagrams for the magnetic minerals to determine in the Curie temperature in °C by the demagnetization in TRM (Thermal Remanent Magnetization) method. Data from lapillituff of the Freienfels-Ernsthausen sub-area in the Weilburg area.

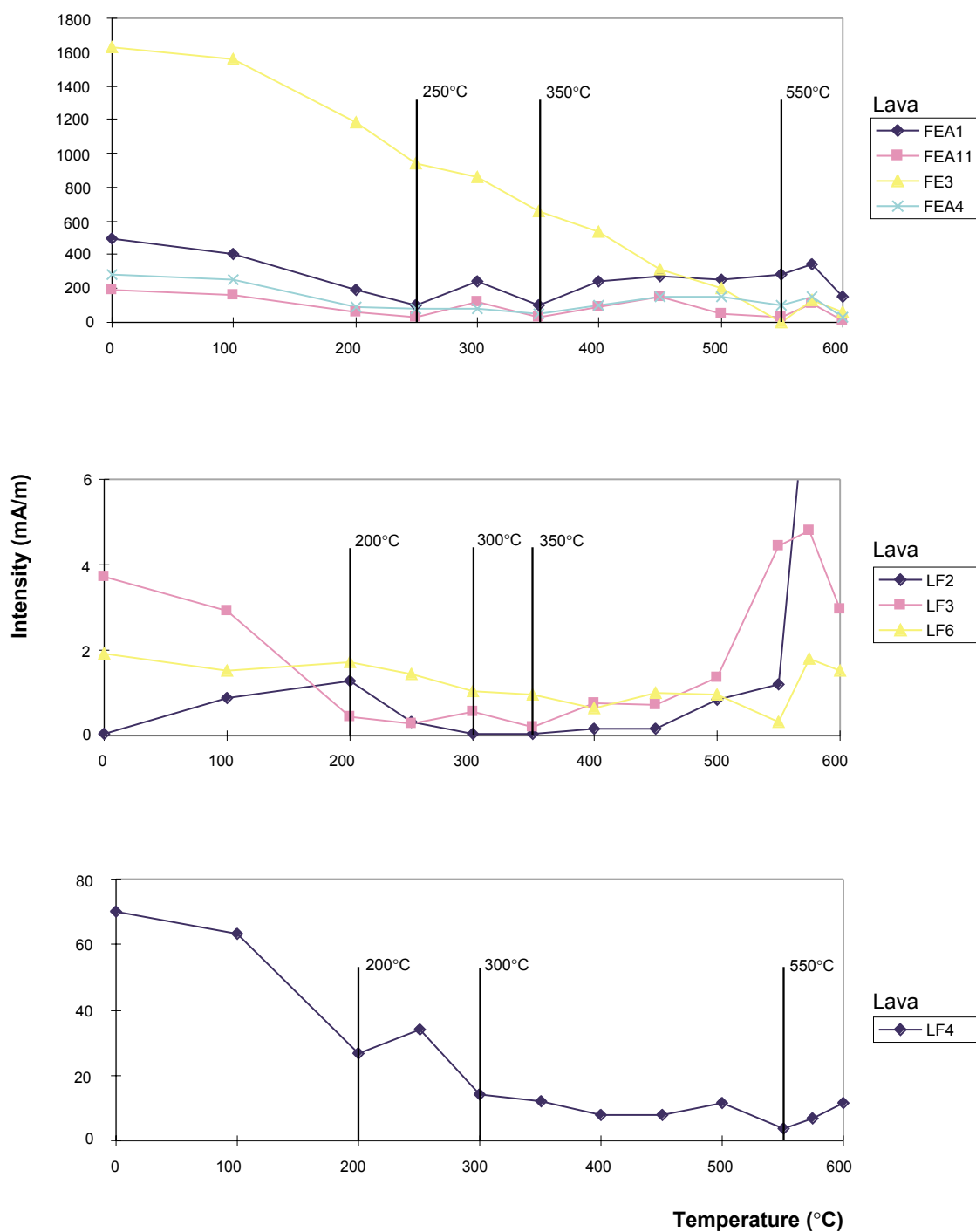


Fig. 7-35B. Magnetic intensity vs temperature diagrams for the magnetic minerals to determine in the Curie temperature in °C by the demagnetization in TRM (Thermal Remanent Magnetization) method. Data from sheet flow lava of the Freienfels-Ernsthäusen sub-area in the Weilburg area.

According to diagrams of AMS vs Samples and NRM vs Samples (Fig. 7-36), the sub-areas such as Weilburg-Ahausen, Guntersau-Freienfels and Freienfels-Ernsthausen generally exhibit different susceptibilities (AMS) and magnetizations (NRM) which indicate different sources. Even neighbouring sub-areas, e.g. Guntersau-Freienfels and Freienfels-Ernsthausen show different values.

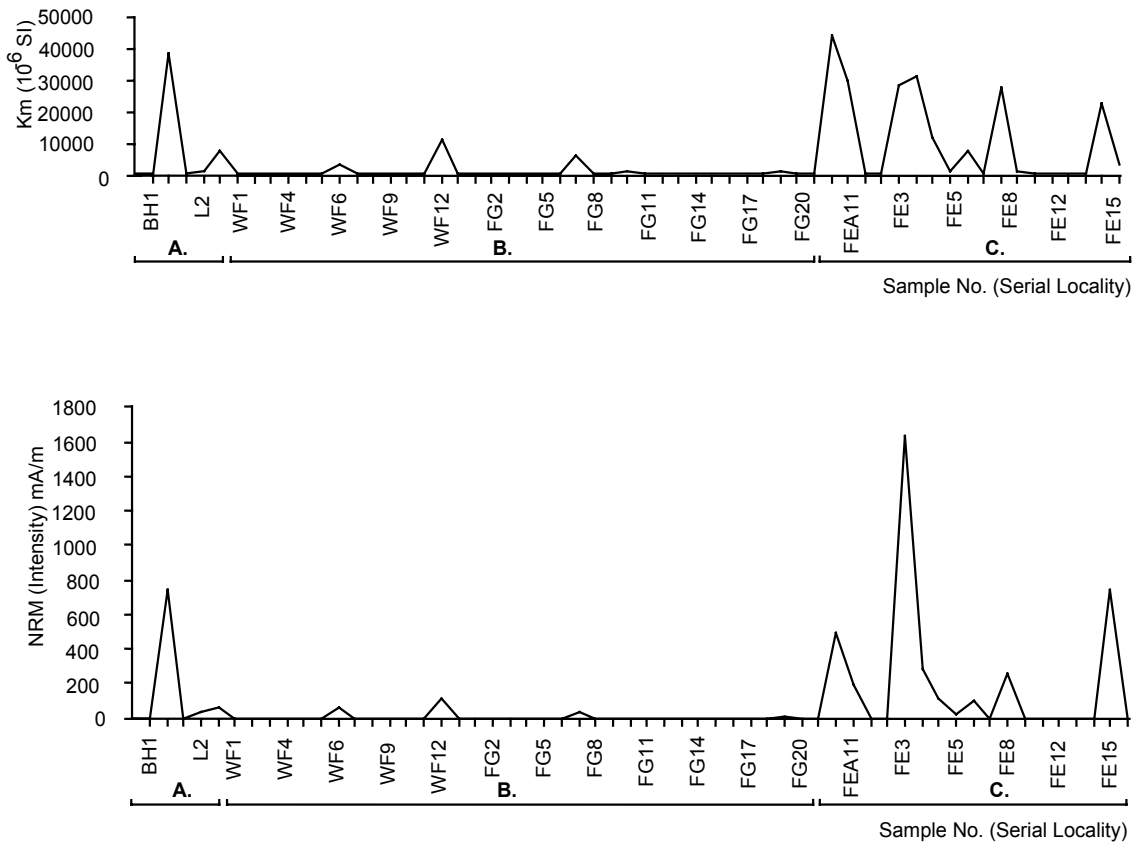


Fig. 7-36. Mean Magnetic Susceptibility (K_m) and Natural Remanent Magnetization (NRM) vs Sample number (locality) in different sub-areas of the Weilburg area.

- A. = Weilburg-Ahausen sub-area
- B. = Guntersau-Freienfels sub-area
- C. = Freienfels-Ernsthausen sub-area

CHAPTER 8
DISCUSSION AND CONCLUSIONS

CHAPTER 8

DISCUSSION AND CONCLUSIONS

The structural development of the Weilburg area is revealed by the present study using field (including previous investigations) and laboratory (strain and magnetofabric analyses) techniques. The Weilburg area is situated on the Lahn river in the *Rheinische Schiefergebirge*, part of the Rhenohercynian zone in the Variscan orogen. The Rhenohercynian zone is interpreted as a back-arc continental extensional basin, but so far, as this study is concerned, the area involved was characterized by a rifting basin environment during the depositional period, whereas it later participated in the Variscan orogeny.

During the Variscan orogeny (under orogenic compression), inversion tectonics noticed by the reactivation of pre-existing extensional border faults indicated by the boundary thrusts. Small rift basins (half-grabens) filled with syn-rift sediments started development shortly before the end of the Lower Devonian. Syn-rift sediments (Middle Devonian to Lower Carboniferous) are accompanied by small scale (cm-scale) syndepositional structures (fold and fault) caused by slumping. The post-rift episode started with the beginning of the Variscan orogeny: upper Lower Carboniferous (cd III). The syn-rift basins are partly determined by previous investigations with respect to facies distribution of volcanoclastics (mainly volcaniturbidites), localities of reef development, iron-ore formation and volcanic centres. The rift basins are distinguished here as antithetic half-graben, synthetic half-graben and full-graben with regard to the orogenic compression direction.

These basins are deduced by different deformations of fold styles and fault systems according to their configuration, e.g. accretionary prism-type deformation by imbricate fault system in the antithetic half-graben basins, short-cut thrust fault system and corresponding asymmetrical-type folding in the synthetic half-graben basins and a transition of sub-vertical to NW vergent fault system and associated disharmonic-type folding (flexural-slip folding) in the full-graben basin.

Accretionary prism-type deformation in the antithetic half-graben can be proposed by their fold types and fault systems, and the magnetofabric analysis. However, synthetic half-grabens and full-graben are only confirmed by their fold types and fault systems. Imbricated thrust development within the accretionary prism can be determined by the anisotropy degree (P^1). The rock sequence of antithetic half-graben basin either normal or reverse in terms of its younging upward position is related to the inclination angle of the AMS principal K_3 axes. Consequently, inferred flow directions of sheet flow lava and inferred current directions of hydroclastics and epiclastics in these basins recognized are verified by the magnetofabric analysis.

Based on the field investigations, bedding, cleavage, lineations, folds, faults and joints developments are coincident with their deformed basin positions and demonstrate two phases of tectonic movement. The intersection lineation (s_0/s_1) on stereoplot shows superposed folding. In addition, cleavages show locally two phases of deformation, in which s_1 -cleavage formation was clearly as early Variscan and s_2 -cleavage as late Variscan. Thus, basin and dome structure is revealed in the Weilburg area.

Dyke emplacement dominated only in the Guntersau-Freienfels sub-area which can be reconstructed for the pre-deformation position in the antithetic half-graben using the declination and inclination values of the AMS principal axes of the K_1 and K_3 axes. The current direction of epiclastic lapillituff, being across the half-grabens, is substantiated by the magnetofabric analysis as debris flows. Generally, the magnetofabrics are inter-related to the constituents of magnetic minerals, e.g. magnetite, haematite, pyrrhotite, which are determined by the Thermal Remanent Magnetization (TRM) measurement.

The deformation is exemplified by 2-D and 3-D strain analyses using strain ellipses and ellipsoids which are different depending on types of folding in local basins. R_f/ϕ fabrics show ellipses in the initial axes ratio (R_i , θ), whereas superposed deformation with its strain path can be revealed. The strain path concerning 3-D strain shows deformation phases which are consistent with field investigations in terms of deformation phases as D1 - D4 as well. The long X-axis direction of the strain ellipsoid is commonly parallel to the s1-cleavage, however, generally related to the type of folding, e.g. parallel to bedding in flexural-slip folding in the Kirschhofen syncline.

Thus, the basin configuration controls not only sedimentation processes but also synkinematic movements, related deformations. The recognition of basins can be evaluated where the structures with respect to the development of folds and faults, and strain deformation in their basins.

Transpressional to Transtensional tectonics: According to the 2-D strain analysis using the XZ plane, strain ellipses are rotated from their position lying in the bedding to lying in the s1-cleavage. The s1-cleavage represents an axial cleavage. The strain ellipses demonstrate the preferred orientation along the s1-cleavage (Plate 12B). This point suggests that transtensional strain was progressively developed after the transpressional strain by the regional tectonic movement during the late Variscan. The tectonic movement (Fig. 8-1) is postulated as, (1) northward, (2) during the continuous of northwards collision, the buttress of London-Brabant Massif was directly against this tectonic movement, and (3) the northward movement was changed into NW direction in the Rhenohercynian zone by the oroclinal bending around the SE front of the London-Brabant Massif. With the onset of collision with the London-Brabant Massif, the area (*Rheinische Schiefergebirge*) experienced dextral shearing stress, as documented by the dextral movement of the Southern Hunsrück Boundary Fault. Consequently, the transtensional deformation in the area is substantiated by the preferred orientation of the finite strain ellipses during the continuous dextral movement of the Variscan orogeny.

Summary of tectonic movement: By use of field data and strain analysis the history of the tectonic movement the Rhenohercynian zone can be constructed (see above). The tectonic history is complex, even on a local scale. The area under investigation includes several sub-areas, each of which exhibits somewhat different types of deformation.

1. Several mutual aspects are evident in Lower Devonian rocks in the north of the zone which show only very slight deformation (ONCKEN 1988), a pre-folding state is preserved with a preferentially N-S trending extension attributed to the stage of basin development.

2. The stage of folding itself, during Carboniferous, shows strong regional and temporal heterogeneity under frequently altering states, after an initial stage of a semi-homogeneous stress field (ONCKEN 1988). This development means, simultaneously, an uncoupling at larger thrust zones with diverging deformation history of hanging-walls and foot-walls.
3. Movement patterns in the north (the *Rheinische Schiefergebirge*, Rhenohercynian zone) give evidence for subsequent clockwise rotation of the stress field which is only weakly represented in the south. On the other hand, there is clear evidence of a still younger counterclockwise rotation of the stress field which only affects the southern massif (ONCKEN 1988).

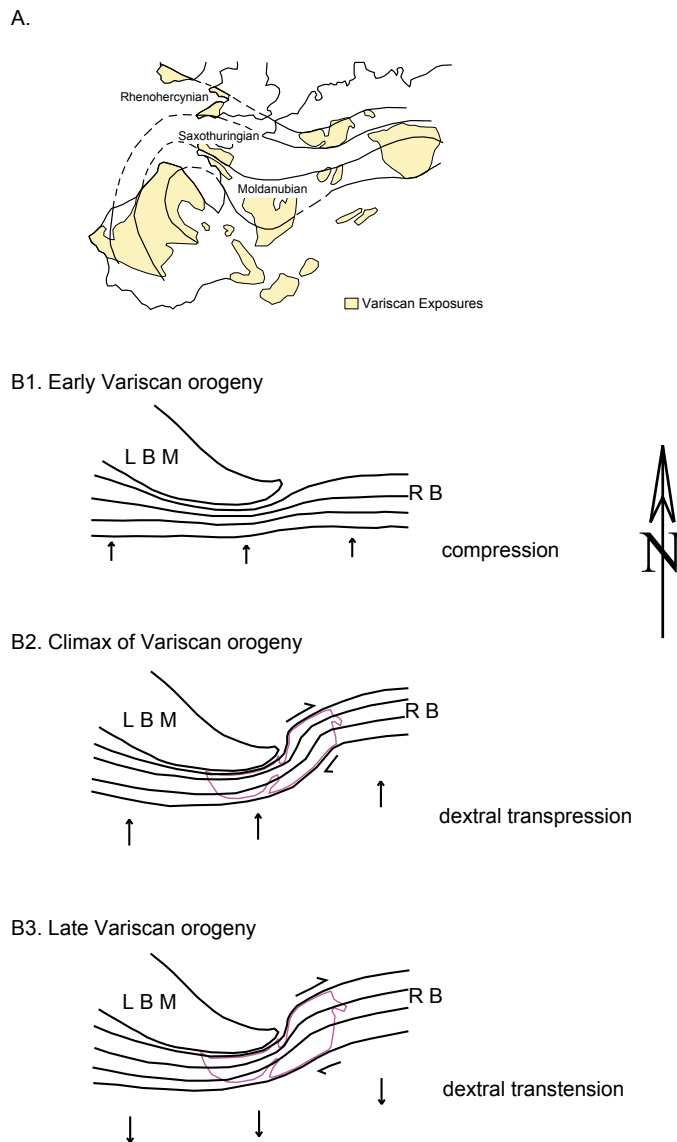


Fig. 8-1. Sketch showing the mechanism of folding in the Rheinische Schiefergebirge during the Variscan Tectonic movement.

A. Present Variscan orogen in Europe (KOSSMAT 1927)

B. Tectonic movement and the buttress of the London Brabant Massif.

L B M = London Brabant Massif

R B = Rhenohercynian Basin

↑ = Direction of tectonic movement

4. This is probably due to the superposing of orthogonal relative movements on the southern rim of the fold belt by a dextral strike-slip component during final deformation, thus indicating late dextral transpression succeeded by dextral transtension (Fig. 8-1).

The final extensional stage is related to late Palaeozoic uplift and crustal stretching perpendicular to the strike of the fold belt. Followed by a change of direction of extension, this state of stress obviously extends into the present.

Neotectonics: The tectonic framework of Europe is the position of an unstable block in the foreland of the Alpine collisional belt, in which intra-plate tectonic movement has been active in different intensities from late Triassic until present-day. Maximum horizontal stress (S_{Hmax}), north of the Rhinegraben is oriented NW-SE (N135°E). Based on the fault development and the joint study of the Weilburg area, in the Lahn syncline, NW-SE, WNW-ESE and NNW-SSE oriented faults and joints are pronounced. Following MEYER et al. (1983), NNW-SSE and WNW-ESE orientations were active from Upper Miocene to Pleistocene times, which show as X and Y minor Riedel shear under the maximum horizontal stress (S_{Hmax}) in the *Rheinische Schiefergebirge*. Consequently, Variscan-age NW-SE faults and joints could have been reactivated by neotectonics.

REFERENCES

REFERENCES

- ADLER, R., FENCHEL, W. & PILGER, A. (1974): Statische Methoden in der Tektonik II: Das Schmidt'sche Netz und seine Anwendung im Bereich des Makroskopischen Gefüge. *Clausth. Tekt. H.*, **4**, 1-111.
- AHLBURG, J. (1918A): Geologische Karte von Preußen, 1:25000 Bl.5516 Weilmünster mit Erläuterungen. *Preuß. Geol. L.-Amt*, Berlin.
- AHLBURG, J. (1918B): Bl. Merenberg (5415). *Erl. Geol. Kt. Preußen und benachb. B.-St., Lfg.*, **208**, 1-128.
- AHLBURG, J. (1918C): Bl. Braunfels (5416). *Erl. Geol. Kt. Preußen und benachb. B.-St., Lfg.*, **208**, 1-120.
- AHORNER, L. (1975): Present-day stress field and seismotectonic block movements along major fault zones in Central Europe. In: N. PAVONI & R. GREEN (ed.), Recent crustal movements. *Tectonophysics*, **29**, 233-249.
- AHORNER, L., MURAWSKI, H., & SCHNEIDER, G. (1972): Seismotektonische Traverse von der Nordsee bis zum Apennin. *Geol. Rundsch.*, **61**, 915-942.
- AHRENDT, H., CLAUER, N., HUNZIKER, J. C. & WEBER, K. (1983): Migration of folding and Metamorphism in the Rheinisches Schiefergebirge Deduced from K-Ar and Rb-Sr Age Determination. In: H. MARTIN & F. W. EDER (ed.), Intracontinental Fold Belts. Springer, Heidelberg, 323-338.
- AVERBUCH, O., De LAMOTTE, D. F. & KISSEL, C. (1992): Magnetic fabric as a structural indicator of the deformation path within a fold-thrust structure: A test case from the Corbieres (NE Pyrenees, France). *J. Struct. Geol.*, **14**, 461-479.
- BADHAM, J. P. N. & HALLS, C. (1975): Microplate tectonics, oblique collisions, and evolution of the Hercynian orogenic systems. *Geology*, **3**, 173-376.
- BAILEY, E. B. (1935): Tectonic Essays, mainly Alpine. 200 p., Clarendon, Oxford.
- BALLY, A. W., BERNOUILLI, D., DAVIS, G. A. & MONTADERT, L. (1980): Listric normal faults. In: C3,6, Geology of Continental Margins. *26C, Congr. Geol. Intern. Paris 1980* Colloque, 87-101.
- BANKWITZ, P. (1966): Über Klüfte II. *Geologie*, **15**, 8, 896-941.
- BEACH, A. (1975): The geometry of en-echelon vein arrays. *Tectonophysics*, **28**, 245-62.
- BECHER, J. P. (1789): Mineralogische Beschreibung der Oranien-Nassauischen Lande, nebst einer Geschichte des Hütten und Hammerwesens. 624 p., Neue Akademische Buchhandlung, Marburg.
- BEHNISCH, R. (1988): Geologische Kartierung des unteren Weiltales zwischen Guntersau and Freienfels in der mittleren Lahnmulde (Südliches Rheinisches Schiefergebirge). *Diplomkartier., Geol.-Paläont. Inst., Univ. Heidelberg*, 58 p.
- BEHNISCH, R. (1990): Der fazielle Aufbau eines Vulkangebäudes der Givet/Adorf-Phase im Schalstein-Hauptsattel, mittlere Lahnmulde Rekonstruktion im Ausschnitt des nördlichen Weiltales. *Diplomarbeit, Geol.-Paläont. Inst., Univ. Heidelberg*, 101 p.
- BEHNISCH, R. (1993): Faziesabhängige Ablagerungsprozesse devonischer Vulkaniklastite im Schalstein-Hauptsattel (Mittlere Lahn-Mulde). *Geol. Abh. Hessen*, **98**, 89-149.
- BEHNISCH, R., FLICK, H., HORN, M. & NESBOR, H. D. (1991): Paläogeographische Rekonstruktion submariner Vulkankomplex im Devon des Lahn-Dill-Gebiets (südliches Rheinisches Schiefergebirge). *Nachr. Deutsch. Geol. Ges.*, **46**, 13.
- BEHRMANN, J., DROZDZEWSKI, G., HEINRICHS, T., HUCH, M., MEYER, W. & ONCKEN, O. (1991): Crustal scale balanced cross sections through the Variscan fold belt, Germany, the central EGT-segment. *Tectonophysics*, **196**, 1-21.

- BELL, R. E., KARNER, G. D. & STECKLER, M. S. (1988): Early Mesozoic rift Basin of Eastern north America and their gravity anomalies: The role of detachments during extension. *Tectonics*, **7**, 447-467.
- BENDER, P. (1965): Der Nordostteil der Lahnmulde zwischen Salzböde-, Aar-, und Biebertal. *Diss., Geol.-Paläont. Inst., Univ. Marburg.*, 140 p.
- BERTHELSEN, A. (1992): Mobile Europe. In: D. BLUNDELL, R. FREEMAN & S. MUELLER (ed.), A continent revealed-the European Geotraverse. Cambridge University, Cambridge, 11-32.
- BILLINGS, M. P. (1972): Structural Geology. 3rd ed., 606 p. Prentice-Hall, New Jersey.
- BISCHOFF, G. & SCHÖNBERG, R. (1956): Über das Einwandern des basischen Magmas in ortho- und parageosynklinale Räume (Paraná-Becken und Dilltrog). *N. Jb. Geol. Paläont. Monatshefte*, **1956**, 497-505
- BÖGER, H. (1981): Stratigraphische, fazielle und tektonische Zusammenhänge im Unter-Devon des Sauerlandes (Rheinisches Schiefergebirge) und der Kaledonisch-variszische Umschwung. *Mitt. Geol. -Paläont. Inst. Univ. Hamburg*, **50**, 45-58.
- BONJER, K. P. (1981): The seismicity of the Upper Rhinegraben - a continental rift system. In: J. PETROVSKI & C. R. ALLEN (ed.), Proc Int. Res. Conf. Intra-cont. Earthqu., Ohrid, Yugoslavia, 17-21 Sept. **1979**, 107-115.
- BORDÁS, R. (1992): Magnetic fabric and strain in Miocene volcanics in the southern margin of the Bükk mountains, Hungary. *Phys. Earth Planet. Inter.*, **70**, 205-213.
- BORRADAILE, G. J. (1988): Magnetic susceptibility, petrofabrics and strain. *Tectonophysics*, **156**, 1-20.
- BORRADAILE, G. J. (1993): Strain and magnetic remanence. *J. Struct. Geol.*, **15**, 383-390.
- BORRADAILE, G. J. & POULSEN, K. H. (1981): Tectonic deformation of pillow lava. *Tectonophysics*, **79**, T17-T26.
- BORRADAILE, G. J. & TARLING, D. H. (1984): Strain partitioning and magnetic fabrics in particulate flow. *Can. J. Earth Sci.*, **21**, 694-697.
- BORRADAILE, G. J. & SARVAS, P. (1990): Magnetic susceptibility fabrics in slates: structural, mineralogical and lithological influences. *Tectonophysics*, **172**, 215-222.
- BORRADAILE, G. J. & HENRY, B. (1997): Tectonic applications of magnetic susceptibility and its anisotropy. *Earth Science Reviews*, **42**, 49-93.
- BORRADAILE, G. J., TELLA, S. & MCARTHUR, J. (1989): Magnetic fabric as a kinematic indicator of faults: A test case. *Ann. Tectonica*, **3**, 3-11.
- BOTTKE, H. (1978): Zur faziesgebundenen Tektonik der Briloner Scholle (Ostsauerland, Rheinisches Schiefergebirge). *Z. dt. geol. Ges.*, **129**, 141-151.
- BOUCHEZ, J.-L. (1977): Plastic deformation of quartzites at low temperature in an area of natural strain gradient. *Tectonophysics*, **19**, 25-50.
- BRECHT, G. (1995): Räumliche Verteilung von Porphyroblasten und ihre Form: Beispiele aus den N-Norwegischen Kaledoniden. *Diplomarbeit, Geol.-Paläont. Inst., Univ. Heidelberg*, 107 p.
- BREITKREUZ, C & FLICK, H. (1996): Sedimentation am trachytisch/alkalirhyolithischen Inselvulkan von Katzenelnbogen-Steinkopf (Devon/Rheinisches Schiefergebirge). *Geol. Jb. Hessen*, **125**, 5-16.
- BUCH, LEOPOLD VON (1849): Betrachtungen über die Verbreitung und die Grenzen der Kreide-Bildungen. *Naturh. Ver. Preus. Rheinl., Verh.*, 210-242.
- BUCK, W. R., MARTINEZ, F., STECKLER, M. S. & COCHRAN, J. R. (1988): Thermal consequences of lithospheric extension: pure and simple. *Tectonics*, **7**, 213-234.
- BUGGISCH, N. & FLÜGEL, E. (1992): Mittel- bis oberdevonische Karbonate auf Blatt Weilburg (Rheinisches Schiefergebirge) und in Randgebieten: Initialstadien der Riffentwicklung auf Vulkanschwellen. *Geol. Jb. Hessen*, **120**, 77-97.

- BURRETT, C. F. (1972): Plate Tectonics and the Hercynian Orogeny. *Nature*, **239**, 155-157.
- BUTLER, R. W. H. (1982): The terminology of structures in thrust belts. *J. Struct. Geol.*, **4**, 239-246.
- CANON-TAPIA, E., WALKER, G. P. L. & HERRERO-BEREVERA, E. (1995): Magnetic fabric and flow direction in basaltic pahoehoe lava of Xitle volcano, Mexico. *J. Volcan. Geotherm. Res.*, **65**, 249-263.
- CARMICHAEL, R. S. (1989): Magnetic Properties of Minerals and Rocks. In: R. S. CARMICHAEL (ed.), Practical Handbook of Physical Properties of Rocks and Minerals. CRC, USA, 299-356.
- CHAPPLE, W. M. (1978): Mechanics of thin skinned fold-and-thrust belt. *Bull. Geol. Soc. Am.*, **89**, 1189-1198.
- CLOOS, E. (1947): Oolite deformation in the south mountain fold, Maryland. *Bull. Geol. Soc. Am.*, **58**, 843-918.
- COCK, L. R. M. & FORTEY, R. A. (1982): Faunal evidence for oceanic separations in the Palaeozoic of Britain. *J. Geol. Soc. London*, **139**, 465-478.
- COGNÉ, J.-P. (1988): Strain, magnetic fabric and Paleomagnetism of the deformed Red beds of the Pont-Rean formation, Brittany. *J. Geophys. Res.*, **93**, 13673-13687.
- COISH, R. A., BRAMLEY, A., GAVIGAN, T. & MASINTER, R. (1991): Progressive changes in volcanism during lapetan rifting: comparisons with the East African Rift-Red Sea system. *Geology*, **19**, 1021-1024.
- COWARD, M. P. (1976): Strain within ductile shear zones. *Tectonophysics*, **34**, 181-197.
- COWARD, M. P. (1994): Inversion Tectonics. In: P. L. HANCOCK (ed.), Continental Deformation. Pergamon, Oxford, 289-304.
- COWARD, M. P., GILLERIST, R. & TRUDGILL, B. (1991): Extensional structures and their tectonic inversion in the Western Alps. In: A. M. ROBERTS, G. YIELDING & B. FREEMAN, (ed.), The geometry of Normal faults. *Geol. Soc. Spec. Public. London*, **56**, 93-112.
- DAVIS, G. A. (1988): Rapid upward transport of mid-crustal mylonitic gneisses in the footwall of a Miocene detachment fault, Whipple Mountains, southwestern California. *Geol. Rundsch.*, **77**, 191-209.
- DAVIS, G. A., LISTER, G. S. & REYNOLDS, S. J. (1986): Structural evolution of the Whipple and South Mountains shear zones, southwestern United States. *Geology*, **14**, 7-10.
- DE WALL, H. (1991): Die Gefüge der Paragneise in der KTB-Vorbohrung und ihr Einfluss auf gesteinsphysikalische Eigenschaften. *Diss., Geol.-Paläont. Inst., Univ. Göttingen*, 129 p.
- DEWEY, J. F., PITMAN W. C., RYAN, W. B. F. & BONNIN, J. (1973): Plate Tectonics and the Evolution of the Alpine System. *Bull. Geol. Soc. Am.*, **84**, 3137-3180.
- DIETERICH, J. H. (1969): Origin of cleavage in folded rocks. *Am. J. Sci.*, **267**, 155-165.
- DITTMAR, U. & ONCKEN, O. (1992): Anatomie und Kinematik eines passiven varistischen Kontinentalrandes – zum Strukturbau des südwestlichen Rheinischen Schiefergebirges. *Frankf. Geowiss. Arb.*, **A11**, 34-37.
- DITTMAR, U., MEYER, W., ONCKEN, O., SCHIEVENBUSCH, T., WALTER, R. & WINTERFELD, C V. (1994): Strain partitioning across a fold and thrust belt: the Rhenish Massif, Mid-European Variscides. *J. Struct. Geol.*, **16**, 1335-1352.
- DIXON, T. H., IVINS, E. R. & FRANKLIN, B. J. (1989): Topographic and volcanic asymmetry around the red sea: Constraints on rift models. *Tectonics*, **8**, 1193-1216.
- DROZDZEWSKI, G., ENGEL, H., WOLF, R. & WREDE, V. (1985): Beiträge zur Tiefentektonik westdeutscher Steinkohlenlagerstätten. *Geol. L. - Amt Nordrhein-Westfalen (Krefeld)*, 235 p.
- DUNNET, D. (1969): A technique finite strain using elliptical particles. *Tectonophysics*, **7**, 117-136.

- DUNNET, D. & SIDDANS, A. W. B. (1971): Non-random sedimentary facies and their modification by strain. *Tectonophysics*, **12**, 307-325.
- DVORÁK, J. & HROUDA, F. (1972): The origin of tectonic structures in weakly metamorphosed sediments, as studied by magnetic anisotropy. *N. Jb. Geol. Paläont. Monatshefte*, **12**, 703-712.
- ELDHOLM, O. & MONTADERT, L. (1981): The main types of passive margins: an introduction, In: C3, 6 Geology of Continental Margins. 26C, *Congr. Geol. Intern. Paris*, **1980**, Colloque, 7-10.
- ELLIOTT, D. (1970): Deformation of finite strain and initial shape from deformed elliptical objects. *Bull. Geol. Soc. Am.*, **81**, 2221-2236.
- ELLWOOD, B. B. (1978): Flow and emplacement direction determined for selected basaltic bodies using magnetic anisotropy measurements. *Earth Planet. Sci. Letters*, **41**, 254-264.
- ELLWOOD, B. B. (1982): Estimates of flow direction for calc-alkaline welded tuffs and paleomagnetic data reliability from anisotropy of magnetic susceptibility measurements, Central San Juan Mountains, SW-Colorado. *Earth Planet. Sci. Letters*, **59**, 303-314.
- ELLWOOD, B. B. & LEDBETTER, M. T. (1977): Antarctic bottom water fluctuations in the Vema Channel: effects of velocity changes on particle alignment and size. *Earth Planet. Sci. Letters*, **35**, 189-198.
- ENGEL, W., FRANKE, W. & LANGENSTRASSEN, F. (1983): Palaeozoic Sedimentation in the Northern Branch of the Mid-European Variscides: Essay of an Interpretation. In: H. MARTIN & F. W. EDER (ed.), *Intracontinental Fold Belts*. Springer, Heidelberg, 9-42.
- ENGELDER, T. & GEISER, P. (1980): On the use of regional joint sets as trajectories of Paleostress fields during the development of the Appalachian Plateau, New York. *J. Geophys. Res.*, **85**, 6319-6341.
- ENGLAND, P. C. (1983): Some numerical investigations of large-scale continental deformation. In: K. J. HSÜ (ed.), *Mountains building processes*. Academic, London, 129-139.
- ERIKSSON, K. A. (1980): Hydrodynamic and Palaeographic interpretation of turbidite deposit from the Archean Fig Tree Group of the Barberton Mountain Land, South Africa. *Bull. Geol. Soc. Am.*, **91**, 21-26.
- ERSLEV, E. A. (1988): Normalised center-to-center strain analysis of packed aggregates. *J. Struct. Geol.*, **10**, 201-209.
- ERSLEV, E. A. & GE, H. (1990): Least-squares center-to-center and mean object ellipse fabric analysis. *J. Struct. Geol.*, **12**, 1047-1059.
- FLEUTY, M. J. (1964): The description of folds. *Proc. Geol. Assoc.*, **75**, 461-492.
- FLICK, H. (1977): Geologie und Petrographie der Keratophyre des Lahn-Dill-Gebietes (südliches Rheinisches Schiefergebirge). *Clausth. Geol. Abh.*, **26**, 1-231.
- FLICK, H. (1978): Die chemischen Parameter der Keratophyre und Quarzkeratophyre des Lahn-Dill-Gebietes. *Z. dt. geol. Ges.*, **129**, 161-170.
- FLICK, H. (1979): Die Keratophyre und Quarzkeratophyre des Lahn-Dill-Gebietes. Petrographische Charakteristik und geologische Verbreitung. *Geol. Jb. Hessen*, **107**, 27-43.
- FLICK, H. & NESBOR, H. D. (1988): Der Vulkanismus in der Lahnmulde. *Jber. Mitt. Oberrhein. Geol. Ver.*, N. F. **70**, 411-475.
- FLICK, H., PFEFFERKORN, H. W. & SCHMIDT, J. (1988): Presence of Land-Plants on a Volcanic island in a Devonian sea (Rhenish Mountains, West Germany). *Review of Palaeobotany and Palynology*, **56**, 177-181.
- FLICK, H., NESBOR, H. D. & BEHNISCH, R. (1990): Iron ore of the Lahn-Dill type formed by diagenetic seeping of pyroclastic sequences, a case study on the schalstein section at Gänsberg (Weilburg). *Geol. Rundsch.*, **79**, 401-415.

- FLICK, H., LIPPERT, H.-J., NESBOR, H. D. & REQUADT, H. (1998): Geologie des Lahn-Dill-Gebietes: Eine Übersicht. *Jb. Nass. Ver. Naturk.*, SB.1, 9-31.
- FLINN, D. (1962): On folding during three-dimensional progressive deformation. *Q. J. Geol. Soc. London*, **118**, 385-433.
- FLINN, D. (1978): Construction and computation of three-dimensional progressive deformations. *J. Geol. Soc. London*, **135**, 291-305.
- FLÖTTMANN, TH. & ONCKEN, O. (1992): Constraints on the evolution of the Mid German Crystalline Rise: A study of outcrops west of the river Rhine. *Geol. Rundsch.*, **81**, 515-543.
- FLOYD, P. A. (1982): Chemical variation in Hercynian Basalts relative to plate tectonics. *J. Geol. Soc. London*, **139**, 505-520.
- FLOYD, P. A. (1995): III.B.3 Igneous Activity. In: R. D. DALLMEYER, W. FRANKE & K. WEBER (ed.), Pre-Permian Geology of Central and Eastern Europe. Springer, Heidelberg, 59-81.
- FRANKE, W. (1989A): Variscan plate tectonics in central Europe: Current ideas and open questions. *Tectonophysics*, **169**, 221-228.
- FRANKE, W. (1989B): Tectonostratigraphic units in the Variscan belt of central Europe. In: R. D. DALLMEYER (ed.), Terranes in the Circum-Atlantic Paleozoic Orogens. *Geol. Soc. Am. Spec. Paper*, **230**, 67-90.
- FRANKE, W. & ONCKEN, O. (1990): Geodynamic evolution of the North Central Variscides - a comic strip. In: R. FREEMAN, P. GIESE & S. MÜLLER (ed.), The European Geotraverse: Integrative studies, results from the 5th Study Centre 26.3.-7.4.1990. European Science Foundation, Strassbourg, 187-194.
- FRANKE, W. & WALLISER, O. H. (1983): 'Pelagic' carbonates in the Variscan Belt: their sedimentary and tectonic environments. In: H. MARTIN & F. W. EDER (ed.), Intracontinental Fold Belts. Springer, Heidelberg, 77-92.
- FRANKE, W., EDER, W., ENGEL, W. & LANGENSTRASSEN, F. (1978): Main aspect of geosynclinal sedimentation in the Rhenohercynian zone. *Z. dt. geol. Ges.*, **129**, 201-216.
- FRANKE, W., BORTFELD, R. K., BRIX, M., DROZDZEWSKI, G., DÜRBAUM, H. J., GIESE, P., JANOTH, W., JÖDICKE, H., REICHERT, CHR., SCHERP, A., SCHMOLL, J., THOMAS, R., THÜNKER, M., WEBER, K., WIESNER, M. G., & WONG, H. K. (1990): Crustal structure of the Rhenish Massif: results of deep seismic reflection lines DECORP2-North and 2-North-Q. *Geol. Rundsch.*, **79**, 523-566.
- FRY, N. (1979): Random point distribution and strain measurement in rocks. *Tectonophysics*, **60**, 89-105.
- FULLER, M. D. (1963): Magnetic anisotropy and paleomagnetism. *J. Geophys. Res.*, **68**, 293-309.
- GEOFYZIKA BRNO (1981): Instruction Manual for Magnetic Susceptibility Bridge - Kappabridge Kly-2. 63 p., *Geofyziky Brno (CZ)*.
- GHOSH, S. K. (1966): Experimental tests of buckling folds in relation to strain ellipsoid in simple shear deformations. *Tectonophysics*, **3**, 169-185.
- GHOSH, S. K. (1993): Structural Geology: Fundamentals and Modern Developments. 598 p., Pergamon, Oxford.
- GIESE, U., KATZUNG, G., WALTER, R. & WEBER, J. (1997): The Caledonian deformation of the Brabant Massif and the Early Palaeozoic in northeast Germany: Compared. *Geol. Mag.*, **134**, 637-652.
- GLEN, J. M. G., RENNE, P. R., MILNER, S. C. & COE, R. S. (1997): Magma flow inferred from anisotropy of magnetic susceptibility in the coastal Parana-Elendeka igneous province: Evidence for rifting before flood volcanism. *Geology*, **25**, 1131-1134.
- GOLDSTEIN, A. G. (1980): Magnetic susceptibility anisotropy of mylonites from the Lake Char mylonite zone, southeastern New England. *Tectonophysics*, **66**, 197-211.

- GRAHAM, J. W. (1949): The stability and significance of magnetism in sedimentary rocks. *J. Geophys. Res.*, **54**, 131-167.
- GRAHAM, J. W. (1954): Magnetic susceptibility, an unexploited element of petrofabric. *Bull. Geol. Soc. Am.*, **65**, 1257-258.
- GRAHAM, J. W. (1966): Significance of magnetic anisotropy in Appalachian Sedimentary rocks. In: J. S. STEINHART & T. J. SMITH (ed.), *The Earth Beneath the continents*. Am. Geophys. Union Monograph, 10, Washington, 627-648.
- GRANAR, L. (1958): Magnetic measurements on Swedish varved sediments. *Arkiv. F. Geofysik*, **3**, 1-40.
- GREIM, G. (1887): Die Diabascontactmetamorphose bei Weilburg an der Lahn. *Diss. Universität Giessen*, 31 p.
- GRÖSSER, J. & DÖRR, W. (1986): MOR-Typ-Basalte im östlichen Rheinischen Schiefergebirge. *N. Jb. Geol. Pläont. Mh.*, **12**, 705-722.
- GUTSCHER, M.-A., KUKOWSKI, N., MALAVIELLE, J. & LALLEMAND, S. (1996): Cyclical behaviour of thrust wedges: Insights from high basal friction sand box experiments. *Geology*, **24**, 135-136.
- HANCOCK, P. L., DUNNE, W. M. & TRINGHAM, M. E. (1983): Variscan Deformation in Southwest Wales. In: P. L. HANCOCK (ed.), *The Variscan Fold Belt in the British Isles*. Adam Hilger, Bristol, 47-73.
- HANNA, S. S. & FRY, N. (1979): A Comparison of methods of strain determination in rocks from southwest Dyfed (Pembrokeshire) and adjacent areas. *J. Struct. Geol.*, **1**, 155-162.
- HATCHER, R. D. (1988): Basement-cover relationships in the Appalachian-Caledonian-Variscan orogen: mid-Devonian (end of Acadian orogeny) to end of Permian. In: A. L. HARRIS & D. J. FETTES (ed.), *The Caledonian-Appalachian orogen*. *Geol. Soc. Spec. Public. London*, **38**, 507-514.
- HELLER, F. (1973): Magnetic anisotropy of granitic rocks of the Bergell massif (Switzerland). *Earth Planet. Sci. Letters*, **20**, 180-188.
- HERBIG, H.-G. (1998): The late Asbian transgression in the central European Culm basins (Late Viséan, cd III α). *Z. dt. geol. Ges.*, **149**, 39-58.
- HILLS, E. S. (1972): *Elements of Structural Geology*. 502 p., Chapman & Hall, London.
- HIRT, A. M., LOWRIE, W., CLENDENEN, W. S. & KLIGFIELD, R. (1988): The correlation of magnetic anisotropy with strain in the Chelmsford formation of the Sudbury Basin, Ontario. *Tectonophysics*, **145**, 177-184.
- HOLST, T. B. (1982): The role of initial fabric on strain determination from deformed ellipsoidal objects. *Tectonophysics*, **82**, 329-350.
- HOUSEN, B. A., TOBIN, H. J., LABAUME, P., LEITCH, E. C. & MALTMAN, A. J. (1996): Strain decoupling across the décollement of the Barbados accretionary prism. *Geology*, **24**, 127-130.
- HROUDA, F. (1976): The origin of cleavage in the light of magnetic anisotropy investigations. *Phys. Earth Planet. Inter.*, **13**, 132-142.
- HROUDA, F. (1978): The magnetic fabric in some folds. *Phys. Earth Planet. Inter.*, **17**, 89-97.
- HROUDA, F. (1979): The strain interpretation of magnetic anisotropy in rocks of the Nizky Jeseník Mountains (Czechoslovakia). *Sb. Geol. Ved Vžitá Geofyz.*, **16**, 27-62.
- HROUDA, F. (1982): Magnetic anisotropy of rocks and its application in Geology and Geophysics. *Geophys. Surv.*, **5**, 37-82.
- HROUDA, F. & HRUSKOVA, L. (1990): On the detection of weak strain parallel on the bedding by magnetic anisotropy: A mathematical model study. *Stud. Geophys. Geod.*, **34**, 327-341.
- HROUDA, F., JANÁK, F. & REJL, L. (1978): Magnetic anisotropy and ductile deformation of rocks of progressive regional metamorphism. *Gerlands Beitr. Geophys.*, **78**, 126-134.

- HROUDA, F., JANÁK, F., REJL, L. & WEISS, J. (1971): The use of the magnetic susceptibility anisotropy for estimating the ferromagnetic mineral fabrics of metamorphic rocks. *Geol. Rundsch.*, **60**, 1124-1142.
- HSU, T. C. (1966): The characteristics of coaxial and non-coaxial strain paths. *J. Strain Analysis*, **1**, 216-222.
- ILLIES, J. H. & GREINER, G. (1978): Rhinegraben and the Alpine system. *Bull. Geol. Soc. Am.*, **89**, 770-782.
- ILLIES, J. H. & FUCHS, K. (1983): Plateau-Uplift of the Rhenish Massif - Introductory remarks. In: K. FUCHS, K. VON GEHLEN, H. MÄLZER, H. MURAWSKI & A. SEMMEL (ed.), Plateau Uplift: The Rhenish Shield - A case History. Springer, Berlin, 1-8.
- INGLES, J. (1983): Theoretical strain patterns in ductile zones simultaneously undergoing heterogeneous simple shear and bulk shortening. *J. Struct. Geol.*, **5**, 369-381.
- JÄGER, M. (1993): Geologische Kartierung des Weiltals zwischen Ernsthäusen und Freienfels in der mittleren Lahnmulde (Südöstliches Rheinisches Schiefergebirge). *Diplomkartier.*, *Geol.-Paläont. Inst., Univ. Heidelberg*, 88 p.
- JÄGER, M. (1996): Fazieskorrelierung in den Vulkaniklastiten des Schalstein-Hauptsattels bei Ernsthäusen (Mittlere Lahnmulde). *Diplomarbeit, Geol.-Paläont. Inst., Univ. Heidelberg*, 145 p.
- JANÁK, F. (1972): Magnetic susceptibility anisotropy of various rock types and its significance for geophysics and geology. *Geophys. Prospect.*, **20**, 375-384.
- JEFFREY, G. B. (1922): The motion of ellipsoidal particles immersed in a viscous fluid. *Proc. R. Soc. A.*, **102**, 161-179.
- JELINEK, V. (1977): The statistical theory of measuring anisotropy of magnetic susceptibility of rocks and its application. *Geofyzika, Brno*, 1-88.
- JELINEK, V. (1980): Kappabridge KLY-2. A precision Laboratory Bridge for Measuring Magnetic Susceptibility of Rocks (Including Anisotropy). Leaflet, *Geofyzika, Brno*.
- JELINEK, V. (1981): Characterization of the magnetic fabric of rocks. *Tectonophysics*, **79**, 63-67.
- JUCKENACK, C. (1990): Beitrag der Anisotropie der magnetischen Suszeptibilität (AMS) für Struktur- und Gefügeuntersuchungen von Metamorphiten: Einzelbeispiele und regionale Anwendung im Spessart-Kristallin. *Diss., Geol.-Paläont. Inst., Univ. Göttingen*, 176 p.
- KEGEL, W. (1922): Abriß der Geologie der Lahnmulde. Erläuterungen zu einer von JOHANNES AHLBURG hinterlassenen Übersichtskarte und Profildarstellung der Lahnmulde. *Abh. Preuß. Geol. L.-Amt, N. F.*, **86**, 1-81.
- KHAN, M. A. (1962): The anisotropy of magnetic susceptibility of some igneous and metamorphic rocks. *J. Geophys. Res.*, **67**, 2873-2885.
- KLIGFIELD, R., LOWRIE, W. & DAIZIEL, I. W. D. (1977): Magnetic susceptibility anisotropy as a strain indicator in the Sudbury Basin, Ontario. *Tectonophysics*, **40**, 287-308.
- KLIGFIELD, R.; OWENS, W. H. & LOWRIE, W. (1981): Magnetic susceptibility anisotropy, strain and progressive deformation in Permian sediments from the Maritime Alps, (France). *Earth Planet. Sci. Letters*, **55**, 181-189.
- KLIGFIELD, R., LOWRIE, W. & PFIFFNER, O. A. (1982): Magnetic properties of deformed oolitic limestones from the Swiss Alps: The correlation of magnetic anisotropy and strain. *Eclogae Geol. Helv.*, **75**, 127-157.
- KNIGHT, M. D. & WALKER, G. P. L. (1988): Magma flow directions in dykes of the Koolan Complex, Oahu, determined from magnetic fabric studies. *J. Geophys. Res.*, **93**, 4308-4319.
- KÖNIGSWALD, W. v. & MEYER, W. (Hrsg), (1994): Erdgeschichte im Rheinland. Fossilien und Gesteinen aus 400 Millionen Jahren. 239S., München.

- KOLOFIKOVA, O. (1976): Geological interpretations of magnetic properties of basalts: Examples of the Chibsky les Lava flow of the Velky Roudny volcano (Nizky Jesenik). *Cas. Min. Geol.*, **21**, 387-396, (in Czech).
- KOSSMAT, F. (1927): Gliederung des variszischen Gebirgsbaues. *Abh. Sächs. Geol. L-Amt*, **1**, 1-39.
- KREBS, W. (1971): Devonian Reef Limestones in the Eastern Rhenish Schiefergebirge, Sedimentology of parts of central Europe. *Guidebook, VIII. International Sedimentology Congress 1971.*, 45-71.
- LALLEMAND, S. SCHNÜRLE, P. & MATAVIEILLE, J. (1994): Coulomb theory applied to accretionary and non-accretionary wedges: Possible causes for tectonic erosion and/or frontal accretion. *J. Geophys. Res.*, **99**, 12033-12055.
- LANGENSTRASSEN, F. (1983): Neritic Sedimentation of the Lower and Middle Devonian in the Rheinische Schiefergebirge, East of the River Rhine. In: H. MARTIN & F. W. EDER (ed.), *Intracontinental Fold Belts*. Springer, Heidelberg, 43-76.
- LANGHEINRICH, G. (1976): Verformungsanalyse im Rhenoherynikum. *Geotekt. Forsch.*, **51**, 1-127.
- LEEDER, M. R. (1988): Devonian-Carboniferous river systems and sediment dispersal from the orogenic belts and cratons of NW Europe. In: A. L. HARRIS & D. J. FETTES (ed.), *The Caledonian-Appalachian Orogen*. *Geol. Soc. Spec. Public. London*, **38**, 549-558.
- LEEDER, M. R. & GAWTHORPE, R. L. (1987): Sedimentary models for extensional tilt-block/half-graben basins. *Geol. Soc. Spec. Public. London*, **28**, 139-152.
- LE GALL, B. (1992): The deep structure of the Ardennes Variscan thrust belt from structural and ECORS seismic data. *J. Struct. Geol.*, **14**, 5531-5546.
- LE THEOFF, B. (1979): Non-coaxial deformation of elliptical particles. *Tectonophysics*, **53**, T7-T13.
- LEMOINE, M., TRICART, P. & BOILLOT, G. (1987): Ultramafic and gabbroic ocean floor of the Ligurian Tethys (Alps, Cosica, Appennines): In search of a model. *Geology*, **15**, 622-625.
- LIPPERT, H.-J., HENTSCHEL, VON H. & RABIEN, A. (1970): Bl. 5215 Dillenburg. *Erläuterungen zur Geologischen Karte von Hessen, 1:25000*, 550 p.
- LISLE, R. J. (1984): Strain continuities within the Seve-Köli Nappe Complex, Scandinavian Caledonides. *J. Struct. Geol.*, **6**, 101-110.
- LISLE, R. J. (1985): *Geological strain analysis: A manual for the Rf/Ø Method*. 99 p., Pergamon, Oxford.
- LISTER, G. S. & DAVIS, G. (1989): The origin of metamorphic core complexes and detachment faults formed during Tertiary continental extension in the northern Colorado River region, U. S. A.. *J. Struct. Geol.*, **11**, 65-94.
- LISTER, G. S., ETHERIDGE, M. A. & SYMONDS, P. A. (1986): Detachment faulting and the evolution of passive continental margins. *Geology*, **14**, 246-250.
- LORENZ, V. & NICHOLLS I. A. (1984): Plate and Intraplate processes of Hercynian Europe during the Late Palaeozoic. *Tectonophysics*, **107**, 25-56.
- LORENZ, V. (1976): Formation of Hercynian Subplates, possible causes and consequences. *Nature*, **262**, 374-377.
- LOWRIE, W. (1989): Magnetic analysis of rock fabric. In: D. E. JAMES (ed.), *The Encyclopedia of solid Earth Geophysics*. Van Nostrand Reinhold, New York, 689-706.
- MACDONALD, W. D., PALMER, H.C. & HAYATSU, A. (1992): Egan range volcanic complex, Nevada: Geochronology, Paleomagnetism and Magnetic fabrics. *Phys. Earth Planet. Inter.*, **74**, 109-126.
- MALTMAN, A. J., BYRNE, T., KARIG, D. E. & LALLEMAND, S. (1993): Deformation at the toe of an active accretionary prism: Synopsis of results from ODP leg 131, Nankai, SW Japan. *J. Struct. Geol.*, **15**, 949-964.

- MAZZOLI, S. (1995): Strain analysis in Jurassic argillites of the Monte Sirino area (Lagonegro Zone, Southern Apennines, Italy) and implications for deformation path in pelitic rocks. *Geol. Rundsch.*, **84**, 781-793.
- MAZZOLI, S. & CARNEMOLLA, S. (1993): Effects of the superposition of compaction and tectonic strain during folding of a multilayer sequence-model and observations. *J. Struct. Geol.*, **15**, 277-291.
- MCCABE, C., JACKSON, M. J. & ELLWOOD, B. B. (1985): Magnetic anisotropy in the Trenton limestone: Result of a new technique anisotropy and anhysteretic susceptibility. *Geophys. Res. Letters*, **12**, 333-336.
- MCCLAY, K. R. & ELLIS, P. G. (1987): Geometries of extensional fault system developed in model experiments. *Geology*, **15**, 341-344.
- MCCLAY, K. R. & BUCHANAN, P. G. (1992): Thrust faults in inverted extensional basins. In: K. R. MCCLAY (ed.), *Thrust Tectonics*. Chapman & Hall, London, 93-104.
- MCKERROW, W. S. & ZIEGLER, A. M. (1972): Paleozoic oceans. *Nature Phys. Sci.*, **240**, 92-94.
- MEISL, S. (1990): Metavolcanic rocks in the 'Northern Phyllite Zone' at the southern margin of the Rheno-hercynian belt. In: W. FRANKE (ed.), *Mid-German Crystalline Rise and Rheinisches Schiefergebirge: Field Guide*. Int. Conf. Paleozoic Orogens in Central Europe 1990, Göttingen-Giessen, 25-42.
- MEISSNER, R., BARTELTSEN, H. & MURAWSKI, H. (1981): Thin-skinned tectonics in the northern Rhenish Massif. *Nature*, **290**, 399-401.
- MEYER, K. (1981): Geochemische Untersuchungen an Spiliten, Pikriten, Quarzkeratophyren und Keratophyren des Rheinoherzynikums. *Diss., Geol.-Paläont. Inst., Univ. Göttingen*, 121 p.
- MEYER, W. & STETS, J. (1975): Das Rheinprofil zwischen Bonn and Bingen. *Z. dt. Geol. Ges.*, **126**, 15-29.
- MEYER, W., ALBERS, H. J., BERNERS, H. P., GEHLEN, K.V., GLATTHAAR, D., LÖHNERTZ, W., PFEFFER, K. H., SCHNÜTGEN, A., WIENECKE, K. & ZAKOSEK, H. (1983): Pre-Quaternary Uplift in the Central part of the Rhenish Massif. In: K. FUCHS, K. VON GEHLEN, H. MÄLZER, H. MURAWSKI & A. SEMMEL (ed.), *Plateau Uplift: The Rhenish Shield - A case History*. Springer, Berlin, 39-46.
- MILTON, N. J. (1980): Determination of the strain ellipsoid from measurements on any three sections. *Tectonophysics*, **64**, T19-T27.
- MITCHELL, A. H. & READING, H. G. (1969): Continental margins, geosynclines and ocean floor spreading. *J. Geol.*, **77**, 629-646.
- MOE, A. (1998): Neotectonic movements in the Rheinisches Schiefergebirge (Germany) and possible block rotation. *Zbl. Geol. Paläont.*, **1998 Teil I**, Heft 1/2, 81-92.
- MOORE, E. M. & TWISS, R. J. (1995): *Tectonics*. 415 p., W. H. Freeman, New York,
- MORLEY, C. K. (1988): Out-of-sequence thrusts. *Tectonics*, **7**, 539-561.
- MOSHER, S. (1987): Pressure-solution deformation of the Purgatory conglomerate, Rhode Island (USA): quantification of volume change, real strains and sedimentary shape factor. *J. Struct. Geol.*, **9**, 224-232.
- MÜLLERRIED, F. (1921): Klüfte, Harnische und Tektonik der Dinkelberge und des Basler Tafeljuras. *Verh. Naturhist. Med. Ver. Heidelberg*, **15**, 1-46.
- NADAI, A. (1963): *Theory of flow and fracture of solids*. vol. 2., 705 p., McGraw-Hill, New York.
- NAGATA, T. (1961): *Rock Magnetism*. 350 p., 2nd ed., Maruzen, Tokyo.
- NESBOR, H. D. (1987): Die doleritischen Spilite der Lahnmulde (Rheinisches Schiefergebirge) - Regionale Geologie und geotektonische Stellung. *Diss., Geol.-Paläont. Inst., Univ. Heidelberg*, 163 p.

- NESBOR, H. D. (1988): Petrographie, Geochemie und geotektonische Stellung der doleritischen Spilitite der Lahnmulde (Rheinisches Schiefergebirge). *Heidelberger Geowiss. Abh.*, **20**, 137-197.
- NESBOR, H. D. & FLICK, H. (1987A): Faziesentwicklung der basischen Pyroklastite (Schalstein) im Devon der Lahnmulde (südliches Rheinisches Schiefergebirge). *Heidelberger Geowiss. Abh.*, **8**, 175-177.
- NESBOR, H. D. & FLICK, H. (1987B): Faziesgebunde Überschiebungstektonik in der Lahnmulde (Rheinisches Schiefergebirge). *Z. dt. geol. Ges.*, **138**, 121-130.
- NESBOR, H. D. & FLICK, H. (1988): Das Schalstein Profil vom Gänsberg bei Weilburg. Aufbau und fazielle Entwicklung einer submarinen pyroklastischen Abfolge im Devon der Lahnmulde (Rheinisches Schiefergebirge). *Geol. Jb. Hessen*, **116**, 189-205.
- NESBOR, H. D., BUGGISCH, W., FLICK, H., HORN, M. & LIPPERT, H.-J. (1993): Vulkanismus im Devon des Rhenohercynikums, Fazielle und paläogeographische Entwicklung vulkanisch geprägter mariner Becken am Beispiel des Lahn-Dill-Gebietes. *Geol. Abh. Hessen*, **98**, 3-87.
- NICOLAS, A. (1972): Was the Hercynian Orogenic Belt of Europe of the Andean type? *Nature*, **236**, 221-223.
- NICOLAS, A. (1987): Principles of Rock deformation. 208 p., D. Reidel, Tokyo.
- OCZLON, M. S. (1992): Gondwana and Laurussia before and during the Variscan Orogeny in Europe and Related Areas. *Heidelberger Geowissenschaft. Abh.*, **53**, 1-56.
- OCZLON, M. S. (1993): Palaeogeographic and Metamorphic Evolution of the Ligerian Belt in Europe. In: R. A. GAYER, R. O. GREILING & A. K. VOGEL (ed.), Rhenohercynian and Subvariscan Fold Belts. Vieweg, Wiesbaden, 83-130.
- OGAWA, Y. (1982): Tectonics of some forearc fold belts in and around the arc-arc crossing area in central Japan. In: J. K. LEGGETT (ed.), Trench-Forearc Geology: sedimentation and tectonics on modern and ancient active plate margins. *Geol. Soc. Spec. Public. London*, **10**, 49-61.
- ONCKEN, O (1988): Geometrie und Kinematik der Taunuskammüberschiebung. Beitrag zur Diskussion des Deckenproblems im südlichen Schiefergebirge. *Geol. Rundsch.*, **77**, 551-575.
- ONCKEN, O (1989): Geometrie, Deformationsmechanismen und Kinematik großer Strörungzonen der hohen Kruste (Beispiel Rheinisches Schiefergebirge). *Geotekt. Forsch.*, **73**, 1-215.
- ONCKEN, O. (1997): Transformation of a magmatic arc and an orogenic root during oblique collision and its cosequences for the evolution of the European Variscides (Mid-German crystalline Rise). *Geol. Rundsch.*, **86**, 2-20.
- ONCKEN, O & WEBER, K. (1995): III.B.2 Structure. In: R. D. DALLMEYER, W. FRANKE & K. WEBER (ed.), Pre-Permian Geology of Central and Eastern Europe. Springer, Heidelberg, 50-58.
- ONCKEN, O, WINTERFELD, C. VON & DTTMAR, U. (1999): Accretion of a rifted passive margin: The Late Paleozoic Rhenohercynian fold and thrust belt (Middle European Variscides). *Tectonics*, **18**, 75-91.
- OWENS, W. H. (1974A): Mathematical model studies on factor affecting the magnetic anisotropy of deformed rocks. *Tectonophysics*, **24**, 115-131.
- OWENS, W. H. (1974B): Representation of finite strain state by three-axis planar diagrams. *Bull. Geol. Soc. Am.*, **85**, 307-310.
- PALMER, H. C., MACDONALD, W. D. & HAYATSU, A. (1991): Magnetic, structural and geochronologic evidence bearing on volcanic sources and oligocene deformation of ashflow tuff, northeast Nevada. *J. Geophys. Res.*, **96**, 2185-2202.
- PASSCHIER, C. W. (1997): The fabric attractor. *J. Struct. Geol.*, **19**, 113-127.
- PAULY, E. (1958): Das Devon der Südwestlichen Lahnmulde und ihrer Randgebiete. *Abh. Hess. L.-Amt Bodenforsch.*, **25**, 1-138.

- PEREKALINA, T. V. (1981): Variscan volcanism of central and western Europe. In: H. J. ZWART & U. F. DORNSIEPEN (ed.), *The Variscan Orogen of Europe. Geol. Mijnbouw*, **60**, 17-21.
- PHILLIPS, F. C. (1962): The study of small scale structures in the Variscan Fold Belt. In: K. COE (ed.), *Some aspects of the Variscan Fold Belt. Inter. Uni. Geol. Cong., 9th, Exeter*, 109-128.
- PICKERING, K. T. & SMITH, A. G. (1995): Arcs and backarc basins in the Early Paleozoic Iapetus Ocean. *The Island Arc*, **4**, 1-67.
- PISCIOTTO, K. A., TAMAKI, K., ALLAN, J. F., ALEXANDROVICH, J. M., BARNES, D. A., CRAMP, A., JOLIVET, L., KAWKA, O. E., KOIZUMI, I., KURAMOTO, S. I., LANGSETH, M. G., MCEVOY, J., MEREDITH, J. A., MERTZ, K. A., MURRAY, R., STEWART, K. P., TADA, R., THY, P., VIGLIOTTI, L., WHITE, L. D., WIPPERN, J. J. M., YAMASHITA, S., INGLE, J. C., SUYEHIRO, K., VON BREYMAN, M. T., BRISTOW, J. S., BURCKLE, L. H., CHARVET, J., CRAGG, B. A., DE MENOCAL, P. B., DUNBAR, R. B., FOLLM, K. B., GRIFFIN, J. R., GRIMM, K. A., HAMANO, Y., HIRATA, N., HOLLER, P., ISAACS, C. M., KATO, M., KETTLER, R. M., KHERADYAR, T., KRUMSIEK, K. A. O., LING, H. Y., MASUMOTO, R., MUZA, J. P., PARKES, R. J., POUCKET, A., SCOTT, S. D., STEIN, R., & STURZ, A. A. (1990): Ocean drilling Program; evolution of the Japan Sea. *Nature (London)*, **346**, 18-20.
- PLATT, J. P. (1986): Dynamics of orogenic wedges and the uplift of high-pressure metamorphic rocks. *Bull. Geol. Soc. Am.*, **97**, 1037-1053.
- PRICE, N. J. (1981): *Fault and Joint development in Brittle and Semi-brittle rock*. 176 p., Pergamon, Oxford.
- QUADE, H. (1976): Genetic problems and environmental features of volcano-sedimentary iron-ore deposits of the Lahn-Dill type. In: K. H. WOLF (ed.), *Handbook of strata-bond and stratiform ore deposits*. Elsevier, Amsterdam, **Chap. 6.**, 255-294.
- RABIEN, A. (1956): Zur Stratigraphie und Fazies des Oberdevons in der Waldecker Hauptmulde. *Abh. hess. L.-Amt Bodenforsch.*, **16**, 1-83.
- RAMBERG, H. (1963): Evolution of Drag Folds. *Geol. Mag.*, **100**, 97-106.
- RAMBERG, H. (1975): Particle paths, displacement and progressive strain applicable to rocks. *Tectonophysics*, **28**, 1-37.
- RAMBERG, H. (1987): Drag Folds. In: C. K. SEYFERT (ed.), *The Encyclopedia of Structural Geology and Plate Tectonics*. Van Nostrand Reinhold, New York, 206-207.
- RAMSAY, J. G. (1967): *Folding and Fracturing of Rocks*. 568 p., McGraw-Hill, New York.
- RAMSAY, J. G. & WOOD, D. S. (1973): The geometric effects of volume change during deformation processes. *Tectonophysics*, **16**, 263-277.
- RAMSAY, J. G. & HUBER, M. I. (1983A): *The Techniques of Modern Structural Geology Vol. 1. Strain analysis*. 307 p., Academic, London.
- RAMSAY, J. G. & HUBER, M. I. (1983B): *The Techniques of Modern Structural Geology Vol. 2. Folds and Fractures*. 308-700, Academic, London.
- RAST, N. & SKEHAN, J. W. S. J. (1983): The Evolution of the Avalonian Plate. *Tectonophysics*, **100**, 257-286.
- RAST, N. (1983): Variscan Orogeny. In: P. L. HANCOCK (ed.), *The Variscan Fold Belt in the British Isles*. Adam Hilger, Bristol, 1-19.
- RAST, N. (1988): Tectonic implications of the timing of the Variscan orogeny. In: A. L. HARRIS & D. J. FETTES (ed.), *The Caledonian-Appalachian Orogen. Geol. Soc. Spec. Public. London*, **38**, 585-595.
- RATHORE, J. S. (1979): Magnetic susceptibility anisotropy in the Cambrian Slate Belt of North Wales and correlation with strain. *Tectonophysics*, **53**, 83-97.
- RAVNÅS R. & STEEL, R. J. (1997): Contrasting styles of late Jurassic syn-rift turbidite sedimentation: A comparative study of the Magnus and Oseberg areas, northern North Sea. *Marine Petrol. Geol.*, **14**, 417-449.

- REES, A. I. (1968): The production of preferred orientation in a concentrated dispersion of elongated and flattened grains. *J. Geol.*, **76**, 457-465.
- REES, A. I. (1979): The orientation of grains in a sheared dispersion. *Tectonophysics*, **55**, 275-287.
- REQUADT, H. (1990): Blatt 5613 Schaumburg. 2 Aufl. *Erl. Geol. Kt. Rheinld.-Pfalz 1:25000*, 212 p.
- RIETSCHEL, S. (1966): Die Geologie des mittleren Lahntroges, Stratigraphie und Fazies des Mitteldevons, Oberdevons und Unterkarbons bei Weilburg und Usingen (Lahnmulde und Taunus, Rheinisches Schiefergebirge). *Abh. Senckenb. naturf. Ges.*, **509**, 1-58.
- RIETSCHEL, S. & STRIBRNY, B. (1979): Zur Geologie und Stratigraphie der Hochweiser Mulde (Bl. Usingen, östlicher Taunus, Rheinisches Schiefergebirge). *Geol. Jb. Hessen*, **107**, 13-25.
- ROCHETTE, P. (1987): Magnetic susceptibility of the rock matrix related to magnetic fabric studies. *J. Struct. Geol.*, **9**, 1015-1020.
- ROCHETTE, P. (1988): Inverse magnetic fabric in carbonate bearing rocks. *Earth Planet. Sci. Letters*, **90**, 229-237.
- ROCHETTE, P., JACKSON, M. & AUBOURY, C. (1992): Rock magnetism and the interpretation of Anisotropy of Magnetic Susceptibility. *Reviews of Geophys.*, **30**, 209-226.
- ROCHETTE, P., JENATTON, L., DUPUY, C., BOUDIER, F. & REUBER, I. (1991): Emplacement mode of basaltic dykes in the Oman ophiolite: Evidences from magnetic anisotropy with reference to geochemical studies. In: T.J. PETERS, A. NICOLAS & R. G. COLEMAN (ed.), *Ophiolite Genesis and the evolution of the Oceanic Lithosphere*. Kluwer, Dordrecht, 55-82.
- RÖDER, D. (1960): Ulmen-Gruppe in sandiges Fazies (Unter-Devon, Rheinisches Schiefergebirge). *Abh. Hess. L.-Amt. Bodenforsch.*, **31**, 1-66.
- RODGERS, J. (1988): Fourth time-slice: mid-Devonian to Permian synthesis. In: A. L. HARRIS & D. J. FETTES (ed.), *The Caledonian-Appalachian Orogen*. *Geol. Soc. Spec. Public. London*, **38**, 621-626.
- RUTTEN, M. G. (1955): Schistosity in the Rhenic massif and the Ardennes. *Geol. Mijnbouw*, **17**, 104-110.
- SANDERSON, D. J. (1976): The superposition of compaction and plain strain. *Tectonophysics*, **30**, 35-54.
- SANDERSON, D. J. (1979): The transition from upright to recumbent folding in the Variscan fold belt of southwest England: A model based on the kinematics of simple shear. *J. Struct. Geol.*, **1**, 171-180.
- SAWKINS, F. J. & BURKE, K. (1980): Extensional Tectonics and Mid-Paleozoic Massive Sulfide Occurrences in Europe. *Geol. Rundsch.*, **69**, 349-360.
- SCHLEUNIGER, K. (1989): Geologische Kartierung in der Mittleren Lahnmulde nordlich von Weilburg (Rheinisches Schiefergebirge). *Diplomkart., Geol.-Paläont. Inst., Univ. Heidelberg*, 50 p.
- SCHLEUNIGER, K. (1991): Submariner basischer Vulkanismus im Devon (Givet/Adorf) der Mittleren Lahnmulde: Fazielle Untersuchungen an einer effusiven/vulkaniklastischen Abfolge (Weilburg/Südöstliches Rheinisches Schiefergebirge). *Diplomarbeit, Geol. -Paläont. Inst., Univ. Heidelberg*, 87 p.
- SCHÖNENBERG, R. (1956) mit einem Beitrag von GIESE, P.: Oberdevonische Tektonik und kulmischer Magmatismus im nordöstlichen Dilltrog. *Geol. Jb.*, **71**, 595-616.
- SCHWERDTNER, W. M. (1973) A scale problem in paleo-strain analysis. *Tectonophysics*, **16**, 47-54.
- SINGH, J. (NOW RATHORE, J.), SANDERSON, D. J. & TARLING, D. H. (1975): The magnetic susceptibility anisotropy of deformed rocks from North Cornwall, England. *Tectonophysics*, **27**, 141-153.
- SMITH, A. G. (1996): Some aspect of the Phanerozoic paleogeographic evolution of Europe. *Z. dt. geol. Ges.*, **147**, 147-168.
- SOLLE, G. (1960): Synsedimentäre Bruchtektonik im Südwest-Teil der rheinischen Geosynklinale im epirogenen Stadium. *Notizbl. Hess. L.-amt Bodenforsch.*, **88**, 343-360.

- STAUDIGEL, H., GEE, J., TAUXE, L. & VARGA, R. J. (1992): Shallow intrusive directions of sheeted dykes in the Troodos ophiolite: Anisotropy of magnetic susceptibility and structural data. *Geology*, **20**, 841-844.
- STILLE, H. (1924): Grundfragen der vergleichen der Tektonik. 322 p., Gebrueder Borntrager, Berlin.
- STILLE, H. (1951): Das Mitteleuropäische variszische Grundgebirge im Bilde des gesamteuropäischen. *Beihefte Geologisches Jahrbuch*, **2**, 138 p.
- SUESS, E. (1888): Das Antlitz der Erde. Band **2**, 703 p., Tempsky.
- TARLING, D. H. (1983): Palaeomagnetism. 379 p., Chapman & Hall, London.
- TARLING, D. H. & HROUDA, F. (1993): The magnetic anisotropy of rocks. 212 p., Chapman & Hall, London.
- THORBURY, W. D. (1980): Principles of Geomorphology. 618 p., John Wiley & Sons, New York.
- TIKOFF, B. & FOSSEN, H. (1995): The limitation of three-dimensional kinematic vorticity analysis. *J. Struct. Geol.*, **17**, 1771-1784.
- TRUESDELL, C. (1953): Two measures of vorticity. *J. Rational Mech. Anal.*, **2**, 173-217.
- TURNER, J. F. & WEISS, L. E. (1963): Structural analysis of metamorphic Tectonites. 545 p., McGraw-Hill, New York.
- TWISS, R. J. & MOORES, E. M. (1992): Structural Geology. 532 p., W. H. Freeman, New York.
- VERGA, R. J. (1993): Rocky mountain foreland uplift: Products of rotating stress field or strain partitioning. *Geology*, **21**, 1115-1118.
- WALKER, R. G. (1992): Turbidites and submarine fans. In: R. G. WALKER & N. P. JAMES (ed.), *Facies Models: response to sea level change*. Geological Association of Canada, Quebec, 239-263.
- WALLISER, O. H. (1981): The geosynclinal development of the Rheinisches Schiefergebirge (Rhenohercynian zone of the Variscides; Germany). In: H. J. ZWART & U. F. DORNSIEPEN (ed.), *The Variscan Orogen in Europe*. *Geol. Mijnbouw*, **60**, 89-96.
- WALTER, R. (1995) mit beiträgen von GIESE, P., WALTHER, H. W. & DILL, H. G.: *Geologie von Mitteleuropa*. 566 p, E. Schweizerbart'sche Verlagsbuchhandlung, Stuttgart.
- WEBER, K. (1981A): Kinematic and metamorphic aspects of cleavage formation in very-low grade metamorphic slates. *Tectonophysics*, **78**, 291-306.
- WEBER, K. (1981B): The Structural Development of the Rheinische Schiefergebirge. In: H. J. ZWART & U. F. DORNSIEPEN (ed.), *The Variscan Orogen in Europe*. *Geol. Mijnbouw*, **60**, 149-159.
- WEBER, K. (1984): Variscan events: early Palaeozoic continental rift metamorphism and late Palaeozoic crustal storting. In: D. H. W. HUTTON & D. J. SANDERSON (ed.), *Variscan Tectonics of the North Atlantic Region*. *Geol. Soc. Spec. Public. London*, **14**, 3-22..
- WERNER, W. (1989): Synsedimentary Faulting and Sediment-Hosted Submarine-Hydrothermal Mineralization in the Late Palaeozoic Rhenish Basin (Germany). *Geotekt. Forsch.*, **71**, 1-305.
- WERNICKE, B. (1981): Low-angle normal faults in the Basin and Range province: nappe tectonics in an extending orogen. *Nature*, **291**, 645-648.
- WERNICKE, B. (1985): Uniform sense normal simple shear of the continental lithosphere. *Can. J. Earth Sci.*, **22**, 108-125.
- WERNICKE, B. & BURCHFIEL (1982): Modes of extensional tectonics. *J. Struct. Geol.*, **4**, 105-115.
- WHITNEY, J. A. & STORMER, J. C. (1983): Igneous sulfides in the Fish Canyon Tuff and the role of sulfur in calc-alkaline magmas. *Geology*, **11**, 99-102.
- WHITTEN, E. H. T. (1966): Structural Geology of Folded Rocks. 663 p., Rand McNally, Chigaco.
- WIGNALL, P. B. (1991): Model for transgressive black shales? *Geology*, **19**, 167-170.

-
- WILLIAMS, G. D. & CHAPMAN, T. J. (1983): Strains developed in the hanging wall of thrusts due to their slip/propagation rate: a dislocation model. *J. Struct. Geol.*, **5**, 563-571.
- WILSON, G. (1982): Introduction to Small-scale Geological Structures. 128 p., George Allen & Unwin, London.
- WOOD, D. S. & HOLM, P. E. (1980): Quantitative analysis of strain heterogeneity as a function of temperature and strain rate. *Tectonophysics*, **66**, 1-14.
- WURSTER, V. P. (1988): Das varistische Gebirge - eine Überlegungsfigur. *Geol. Rundsch.*, **77**, 771-775.
- ZINGG, T. (1935): Beitrag zur Schotteranalyse. *Schweiz. Mineral. Petrog. Mitt.*, **15**, 39-140.
- ZIEGLER, P. A. (1989): Evolution of Laurussia. 102S., Kluwer, London.

APPENDIX

Appendix-A

Sample list-1 for Anisotropy of Magnetic Susceptibility measurement

No.	Sample No.	Type of rock	Bulk Magnetic Susceptibility		Orientation	Remarks
			10 ⁻³ SI			
			Sample test	Insitu test		
1	LF1	lapillituff	0.55-0.63	0.50-0.68	135, 55	
2	LF2	lava	0.43-0.59	0.29-0.48	s-030, 10	
3	LF3	lava	0.37-1.38	0.38-0.71	155, 47	
4	LF4	lava	1.11-2.78	1.50-3.05	s-180, 43	
5	LF5	lapillituff	0.44-0.69	1.20-2.32	130, 45	
6	LF6	lava	0.58-0.74	3.70-19.7	135, 42	
7	LF7	lapillituff	0.55-0.74	0.73-0.93	135, 42	
8	WF1	lapillituff	0.33-0.44	0.35-0.46	130, 43	
9	WF2	ash tuff	0.44-0.66	0.23-0.67	155, 25	
10	WF3	lapillituff	0.19-0.21	0.19-0.26	130, 53	
11	WF4	pillow lava	0.29-0.49	0.22-0.55	130, 51	
12	WF4A	lapillituff			135, 46	
13	WF5	lapillituff	0.23-0.36	0.34-0.40	135, 41	
14	WF6	lapillituff	1.91-2.96	1.52-2.96	130, 51	
15	WF7	lapillituff with crystal	0.39-0.43	0.37-0.46	160, 51	
16	WF8	lava	0.51-0.66	0.42-0.68	130, 31	
17	WF9	lapillituff	0.40-0.46	0.40-0.46	s-160, 60	
18	WF10	lapillituff (laminated)	0.50-0.64	0.43-0.64	125, 36	
19	WF11	lapillituff	0.35-0.43	0.28-0.44	s-140, 68	
20	WF12	lava	4.75-8.45	13.6-22.7	s-160, 54	
21	WF13	lava			s-180, 55	
22	FG1	lapillituff	0.39-0.56	0.39-0.56	s-038, 35	
23	FG2	ash tuff	0.33-0.51	0.39-0.57	130, 45	
24	FG3	lava	0.43-0.61	0.33-0.67	130, 45	
25	FG4	lapillituff	0.29-0.52	0.58-0.67	120, 38	
26	FG5	dyke	0.47-0.64	0.46-0.64	s-230, 47	
27	FG6	dyke	0.46-0.57	0.41-0.58	sj-170, 80	
28	FG7	lapillituff with epiclastics	4.81-9.74	5.70-17.8	120, 42	
			0.19-35.8 epiclastics			
29	FG8	lapillituff with crystal	0.39-0.46	0.19-0.57	125, 42	
30	FG9	lava (porphyry)	0.43-0.51	0.31-0.56	120, 34	
31	FG10	lapillituff with epiclastics	0.69-0.74	0.37-0.78	s-250, 48	
32	FG11	lapillituff with crystal	0.31-0.43	0.45-0.57	120, 54	
33	FG12	lava (porphyry)	0.37-0.47	0.33-0.50	s-180, 90	
34	FG13	lapillituff (epiclast. & cryst.)	0.39-0.53	0.34-0.56	142, 40	
35	FG14	lava (porphyry)	0.55-0.57	0.58-0.61	s-240, 87	
36	FG15	lava	0.27-0.44	0.36-1.03	s-165, 70	
37	FG16	lapillituff with epiclastics	0.35-0.55	0.40-0.56	150, 34	
38	FG17	lava	0.35-0.60	0.35-0.64	s-200, 76	
39	FG18	lava	0.33-0.35	0.46-0.54	s-200, 76	
40	FG19	lapillituff with epiclastics	0.74-1.24	0.95-1.26	s-130, 35	
41	FG20	dyke	0.48-0.55	0.46-0.59	s-270, 34	
42	FG21	dyke	0.37-0.51	0.46-0.60	s-190, 80	

43	FEA1	lava			s-150, 55
44	FEA11	lava			150, 55
45	FE1	fault plane (lava)	0.27-0.39	0.27-0.41	190, 73
46	FE2	l.st	0.22-0.26	0.16-0.24	150, 42
47	FE3	lava (mandel)	17.0-23.1	22.4-33.6	s-150, 35
48	FEA4	lava (granulated)			135, 56
49	FE4	ash tuff	7.70-9.20	5.70-8.21	242, 62
50	FE5	lapillituff	0.98-1.60	1.40-1.80	140, 42
51	FE6	lava epiclastics	8.70-20.4	9.40-21.5	s-205, 72
52	FE7	lapillituff	0.40-0.45	0.41-0.46	142, 46
53	FE8	lapillituff like pillow	4.50-18.0	5.80-19.6	145, 42
54	FE9	lava	0.32-0.46	0.36-0.50	s-130, 53
55	FE10	lava	0.23-0.56	0.32-0.62	s-070, 30
56	FE11	ash tuff	0.15-0.19	0.16-0.19	s0-100, 54
57	FE12	lapillituff (ash)	0.28-1.25	0.29-1.30	s-180, 40
58	FE13	lapillituff (ash)			s0-050, 25
59	FE14	lapillituff	0.24-0.30	0.29-0.30	140, 41
60	FE15	lava pillow	5.80-8.90	7.40-9.20	s-235, 60
61	S1	lapillituff			160, 46
62	BH1	lapillituff			s0-135, 51
63	BH2	lava (mandel)			s-080, 72
64	L1	lava pillow			135, 35
65	L2	lapillituff			s-180, 60
66	L3	lava pillow			s-052, 67
67	K1	lapillituff			s0-290, 15

N.B.

s = surface of exposure

sj = joint surface

s0 = bedding

Anisotropy of Magnetic Susceptibility measurement of sample list-1														
No.	Sample No	Km	L	F	P	P'	T	q	Kmax	Kmax-D/I	Kint	Kint-D/I	Kmin	Kmin-D/I
1	LF1.1.1	615.80	1.024	1.076	1.102	1.106	0.492	0.291	1.0401	160,33	1.0157	62,13	0.9442	314,54
2	LF1.2.1	578.40	1.022	1.067	1.091	1.094	0.472	0.304	1.0363	157,27	1.0135	58,18	0.9502	298,57
3	LF1.3.1	573.00	1.024	1.065	1.090	1.094	0.432	0.331	1.0368	164,28	1.0124	61,22	0.9508	299,53
4	LF1.4.1	583.40	1.026	1.075	1.103	1.107	0.459	0.313	1.0413	170,30	1.0149	68,20	0.9438	310,53
5	LF1.5.1	597.60	1.025	1.072	1.099	1.103	0.464	0.309	1.0395	167,32	1.0145	67,16	0.9460	314,54
6	LF2.1.2	637.50	1.024	1.010	1.034	1.035	-0.407	1.085	1.0191	71,58	0.9954	229,30	0.9855	325,10
7	LF2.2.1	676.80	1.030	1.008	1.038	1.040	-0.599	1.332	1.0223	69,62	0.9926	235,28	0.9851	328,6
8	LF2.2.2	686.60	1.033	1.009	1.042	1.045	-0.558	1.275	1.0248	72,62	0.9922	253,28	0.9830	162,0
9	LF2.3.1	676.70	1.026	1.006	1.030	1.032	-0.626	1.369	1.0177	71,62	0.9939	236,27	0.9884	329,6
10	LF2.3.2	675.20	1.023	1.011	1.034	1.034	-0.356	1.026	1.0186	102,64	0.9961	260,24	0.9854	354,9
11	LF3.1.1	435.50	1.010	1.016	1.026	1.026	0.207	0.495	1.0119	65,73	1.0018	309,7	0.9864	217,15
12	LF3.1.2	462.50	1.002	1.024	1.026	1.029	0.859	0.073	1.0091	77,70	1.0073	297,15	0.9835	204,12
13	LF3.2.1	544.20	1.011	1.021	1.032	1.033	0.315	0.413	1.0142	96,65	1.0033	293,25	0.9825	200,6
14	LF3.2.2	550.50	1.001	1.026	1.027	1.031	0.941	0.030	1.0091	335,88	1.0083	110,1	0.9826	200,1
15	LF3.2.3	568.20	1.009	1.020	1.029	1.030	0.374	0.371	1.0127	102,37	1.0036	308,50	0.9837	202,13
16	LF3.3.3	534.80	1.008	1.022	1.030	1.031	0.478	0.300	1.0125	110,52	1.0047	308,37	0.9828	211,9
17	LF4.1.1	3045.00	1.020	1.039	1.060	1.061	0.298	0.426	1.0262	210,14	1.0058	101,54	0.9681	309,33
18	LF4.1.2	2590.00	1.018	1.037	1.055	1.056	0.336	0.398	1.0237	207,22	1.0060	91,48	0.9703	313,34
19	LF4.2.1	3046.00	1.016	1.068	1.085	1.090	0.600	0.222	1.0322	193,28	1.0161	79,37	0.9517	310,40
20	LF4.3.1	4284.00	1.017	1.042	1.060	1.062	0.399	0.354	1.0253	210,15	1.0078	106,42	0.9669	315,44
21	LF4.3.2	2854.00	1.014	1.035	1.050	1.051	0.417	0.341	1.0208	209,17	1.0067	102,43	0.9725	315,42
22	LF5.1.1	1212.00	1.021	1.085	1.109	1.115	0.575	0.238	1.0412	213,12	1.0195	114,39	0.9393	317,49
23	LF5.1.2	1110.00	1.018	1.081	1.101	1.108	0.610	0.216	1.0380	208,16	1.0194	105,37	0.9426	317,48
24	LF5.2.1	1113.00	1.017	1.081	1.099	1.106	0.630	0.204	1.0369	204,27	1.0196	96,31	0.9434	326,47
25	LF5.2.2	1086.00	1.012	1.075	1.088	1.095	0.708	0.157	1.0317	206,25	1.0196	98,32	0.9486	326,47
26	LF5.3.2	913.50	1.016	1.070	1.086	1.092	0.614	0.214	1.0326	215,19	1.0168	108,41	0.9506	323,43

27	LF6.2.1	838.00	1.009	1.056	1.065	1.070	0.710	0.156	1.0238	183,2	1.0148	92,26	0.9614	277,64
28	LF6.2.2	815.00	1.005	1.048	1.053	1.059	0.810	0.100	1.0188	169,7	1.0139	75,25	0.9674	273,64
29	LF6.3.1	809.80	1.010	1.055	1.065	1.070	0.672	0.179	1.0244	178,4	1.0141	86,24	0.9615	278,66
30	LF6.3.2	755.20	1.004	1.044	1.048	1.053	0.818	0.095	1.0170	188,1	1.0127	97,24	0.9703	280,66
31	LF6.3.3	801.00	1.006	1.045	1.051	1.056	0.758	0.129	1.0184	174,6	1.0125	81,27	0.9691	275,63
32	LF7.1.1	1063.00	1.018	1.109	1.129	1.140	0.692	0.167	1.0459	41,1	1.0275	132,37	0.9266	309,53
33	LF7.2.1	997.20	1.021	1.095	1.118	1.126	0.616	0.212	1.0437	43,1	1.0226	134,38	0.9337	311,52
34	LF7.2.2	951.50	1.022	1.107	1.131	1.140	0.634	0.201	1.0477	45,4	1.0256	138,37	0.9267	310,53
35	LF7.3.1	942.80	1.026	1.092	1.120	1.126	0.525	0.270	1.0463	217,4	1.0196	124,35	0.9341	313,55
36	LF7.4.1	959.20	1.019	1.119	1.140	1.153	0.691	0.167	1.0497	41,2	1.0298	133,39	0.9205	309,51
37	LF7.5.1	949.20	1.023	1.099	1.124	1.132	0.586	0.231	1.0466	215,5	1.0226	122,34	0.9308	312,55
38	WF1.1.1	515.40	1.005	1.067	1.072	1.081	0.845	0.081	1.0248	228,2	1.0194	137,25	0.9558	322,65
39	WF1.1.2	436.90	1.003	1.057	1.060	1.068	0.886	0.059	1.0205	220,4	1.0172	128,25	0.9623	318,65
40	WF1.1.3	497.30	1.009	1.048	1.057	1.061	0.673	0.178	1.0214	212,9	1.0124	118,24	0.9663	321,64
41	WF1.4.1	539.20	1.003	1.065	1.068	1.078	0.911	0.046	1.0228	48,1	1.0199	139,24	0.9573	316,66
42	WF1.4.2	455.00	1.003	1.052	1.056	1.063	0.872	0.066	1.0191	199,14	1.0156	102,26	0.9653	314,60
43	WF1.4.3	395.00	1.004	1.059	1.063	1.070	0.872	0.066	1.0213	71,15	1.0175	169,26	0.9612	314,60
44	WF2.2.1	628.60	1.015	1.050	1.066	1.069	0.533	0.264	1.0260	88,19	1.0112	181,8	0.9628	292,69
45	WF2.2.2	511.30	1.016	1.050	1.067	1.059	0.488	0.293	1.0269	94,19	1.0104	187,8	0.9627	300,69
46	WF2.4.1	707.70	1.025	1.049	1.075	1.076	0.315	0.414	1.0323	81,21	1.0076	173,6	0.9602	277,68
47	WF2.4.2	585.50	1.016	1.049	1.065	1.068	0.497	0.287	1.0263	90,22	1.0104	184,8	0.9633	293,66
48	WF2.4.3	464.20	1.011	1.056	1.067	1.072	0.650	0.192	1.0253	98,22	1.0140	192,11	0.9606	306,65
49	WF2.4.4	395.80	1.016	1.049	1.065	1.068	0.501	0.285	1.0262	87,18	1.0105	182,16	0.9633	311,65
50	WF3.1.1	290.70	1.007	1.048	1.055	1.060	0.724	0.149	1.0203	83,41	1.0129	201,28	0.9668	313,36
51	WF3.1.2	284.60	1.008	1.048	1.056	1.061	0.715	0.153	1.0206	75,35	1.0129	195,36	0.9665	316,35
52	WF3.1.3	316.60	1.007	1.049	1.056	1.061	0.729	0.145	1.0206	105,50	1.0132	212,14	0.9662	313,36
53	WF3.1.4	307.70	1.007	1.049	1.057	1.062	0.726	0.147	1.0207	94,47	1.0132	209,21	0.9660	315,35
54	WF3.4.1	312.10	1.007	1.053	1.061	1.066	0.757	0.129	1.0218	92,43	1.0147	206,24	0.9635	315,38
55	WF3.4.2	379.90	1.006	1.049	1.055	1.060	0.787	0.113	1.0195	86,46	1.0138	206,26	0.9667	315,33
56	WF3.4.3	335.60	1.011	1.053	1.066	1.070	0.633	0.202	1.0249	85,41	1.0133	202,27	0.9618	314,37
57	WF4.1.1	570.00	1.021	1.022	1.043	1.043	0.008	0.660	1.0208	44,25	1.0001	145,22	0.9791	271,55

58	WF4.1.2	574.70	1.017	1.022	1.040	1.040	0.119	0.565	1.0187	47,26	1.0015	148,23	0.9798	274,54
59	WF4.3.1	620.30	1.017	1.023	1.040	1.040	0.149	0.540	1.0185	51,28	1.0019	155,23	0.9796	278,52
60	WF4.3.2	623.20	1.015	1.026	1.042	1.042	0.247	0.464	1.0187	44,22	1.0034	147,30	0.9779	284,51
61	WF4.4.1	536.30	1.015	1.027	1.042	1.043	0.263	0.452	1.0187	56,28	1.0036	160,25	0.9777	284,51
62	WF4.4.2	571.20	1.015	1.025	1.040	1.041	0.219	0.485	1.0183	52,27	1.0029	158,28	0.9788	286,49
63	WF4A.2.1	494.10	1.009	1.019	1.029	1.029	0.354	0.385	1.0124	240,10	1.0033	144,31	0.9842	345,57
64	WF4A.2.2	640.40	1.015	1.026	1.041	1.042	0.251	0.461	1.0184	244,4	1.0034	152,28	0.9783	341,62
65	WF4A.2.3	654.40	1.014	1.034	1.048	1.050	0.405	0.350	1.0203	245,2	1.0063	154,28	0.9734	339,62
66	WF4A.3.1	561.00	1.012	1.025	1.038	1.038	0.347	0.390	1.0163	211,40	1.0043	98,25	0.9795	345,40
67	WF4A.3.2	623.80	1.014	1.028	1.043	1.044	0.311	0.416	1.0189	209,38	1.0044	202,21	0.9768	349,45
68	WF4A.3.3	604.70	1.012	1.029	1.041	1.042	0.385	0.363	1.0176	217,33	1.0052	104,32	0.9773	341,41
69	WF5.1.1	500.10	1.006	1.009	1.015	1.016	0.215	0.489	1.0071	113,25	1.0011	209,12	0.9918	323,61
70	WF5.1.2	588.40	1.014	1.012	1.027	1.027	-0.085	0.744	1.0136	107,26	0.9993	215,32	0.9872	346,46
71	WF5.2.1	481.60	1.006	1.012	1.018	1.018	0.348	0.392	1.0077	116,29	1.0020	216,18	0.9903	333,55
72	WF5.3.1	491.20	1.009	1.016	1.025	1.025	0.246	0.464	1.0113	103,16	1.0020	199,21	0.9867	338,63
73	WF5.3.2	488.90	1.005	1.013	1.018	1.019	0.472	0.304	1.0076	105,25	1.0028	212,32	0.9896	345,47
74	WF6.1.1	2768.00	1.004	1.097	1.102	1.116	0.916	0.043	1.0331	173,51	1.0291	39,29	0.9377	295,23
75	WF6.2.3	3464.00	1.008	1.123	1.133	1.149	0.860	0.072	1.0435	46,43	1.0350	182,38	0.9214	292,24
76	WF6.4.1	2837.00	1.001	1.110	1.111	1.129	0.976	0.012	1.0350	195,7	1.0338	92,62	0.9312	289,27
77	WF6.4.2	2891.00	1.005	1.111	1.116	1.132	0.909	0.046	1.0376	26,13	1.0327	140,60	0.9296	289,26
78	WF6.6.1	3038.00	1.003	1.111	1.114	1.131	0.950	0.025	1.0363	58,46	1.0336	177,25	0.9300	284,34
79	WF.6.6.2	3351.00	1.003	1.133	1.137	1.157	0.946	0.027	1.0429	40,33	1.0395	160,38	0.9175	283,35
80	WF6.6.3	3264.00	1.003	1.115	1.119	1.137	0.940	0.030	1.0379	104,55	1.0346	14,0	0.9275	283,35
81	WF7.1.1	563.40	1.032	1.070	1.105	1.107	0.337	0.397	1.0439	189,7	1.0111	96,20	0.9450	296,69
82	WF7.1.2	570.90	1.031	1.068	1.102	1.104	0.340	0.395	1.0428	187,8	1.0109	94,17	0.9463	302,71
83	WF7.2.1	567.50	1.034	1.060	1.096	1.097	0.245	0.465	1.0418	188,12	1.0074	93,22	0.9508	305,64
84	WF7.2.2	557.50	1.032	1.066	1.100	1.102	0.322	0.408	1.0424	190,11	1.0102	95,23	0.9474	304,64
85	WF7.3.1	548.50	1.033	1.057	1.091	1.092	0.247	0.464	1.0399	183,11	1.0072	89,21	0.9530	300,66
86	WF7.3.2	558.00	1.032	1.067	1.102	1.104	0.321	0.409	1.0431	187,8	1.0103	93,22	0.9466	296,66
87	WF8.1.3	692.00	1.012	1.042	1.054	1.057	0.547	0.255	1.0215	188,25	1.0096	85,26	0.9690	316,53
88	WF8.3.1	745.40	1.012	1.035	1.047	1.049	0.469	0.306	1.0195	184,25	1.0072	83,21	0.9733	319,56

89	WF8.3.2	627.50	1.010	1.035	1.046	1.048	0.537	0.262	1.0183	200,19	1.0080	98,31	0.9737	316,52
90	WF8.4.1	732.80	1.010	1.036	1.047	1.049	0.539	0.260	1.0186	194,22	1.0081	94,25	0.9733	321,56
91	WF8.4.2	1185.00	1.008	1.018	1.025	1.026	0.390	0.360	1.0109	183,28	1.0032	79,24	0.9859	351,51
92	WF9.1.1	548.30	1.025	1.059	1.085	1.087	0.385	0.363	1.0354	67,17	1.0104	168,32	0.9542	313,53
93	WF9.1.2	608.30	1.029	1.065	1.096	1.098	0.358	0.382	1.0401	56,9	1.0109	152,35	0.9490	314,53
94	WF9.2.1	580.30	1.027	1.065	1.094	1.096	0.393	0.358	1.0387	66,17	1.0117	166,31	0.9497	312,54
95	WF9.2.2	667.40	1.027	1.071	1.100	1.104	0.429	0.333	1.0406	60,12	1.0135	158,33	0.9459	314,54
96	WF9.4.1	625.00	1.024	1.050	1.075	1.077	0.334	0.400	1.0321	65,18	1.0081	165,28	0.9598	306,56
97	WF9.4.2	625.70	1.024	1.069	1.095	1.099	0.453	0.317	1.0383	61,12	1.0136	159,35	0.9480	314,53
98	WF10.1.1	622.90	1.029	1.077	1.108	1.112	0.426	0.335	1.0438	29,5	1.0145	122,32	0.9417	291,58
99	WF10.1.2	680.40	1.032	1.073	1.107	1.110	0.362	0.380	1.0444	32,9	1.0122	127,29	0.9435	288,59
100	WF10.2.1	665.20	1.032	1.068	1.102	1.104	0.329	0.403	1.0429	29,9	1.0106	124,32	0.9466	285,57
101	WF10.3.1	700.70	1.028	1.076	1.107	1.110	0.429	0.333	1.0430	31,9	1.0144	124,31	0.9426	293,59
102	WF10.4.1	709.00	1.027	1.077	1.105	1.109	0.455	0.315	1.0421	32,6	1.0151	125,29	0.9429	292,6
103	WF10.5.1	695.00	1.031	1.070	1.103	1.106	0.364	0.378	1.0429	31,1	1.0429	126,3	0.9453	285,58
104	WF11.1.1	579.80	1.014	1.045	1.059	1.062	0.510	0.279	1.0237	41,3	1.0097	136,58	0.9666	310,32
105	WF11.1.2	581.20	1.015	1.050	1.066	1.069	0.514	0.277	1.0262	43,6	1.0108	142,57	0.9630	309,32
106	WF11.2.1	581.70	1.013	1.045	1.058	1.061	0.548	0.255	1.0231	49,11	1.0103	155,56	0.9666	312,32
107	WF11.2.2	594.60	1.016	1.042	1.059	1.060	0.423	0.337	1.0243	221,3	1.0080	127,57	0.9677	313,33
108	WF11.4.1	604.70	1.013	1.051	1.064	1.068	0.585	0.231	1.0247	221,2	1.0120	128,58	0.9633	313,32
109	WF11.4.2	588.70	1.013	1.053	1.067	1.071	0.590	0.228	1.0258	217,5	1.0126	119,57	0.9619	310,32
110	WF12.1.1	14950.00	1.010	1.018	1.028	1.029	0.300	0.424	1.0125	79,10	1.0028	176,33	0.9847	334,55
111	WF12.1.2	9143.00	1.002	1.010	1.013	1.013	0.624	0.208	1.0050	99,26	1.0026	213,41	0.9924	347,38
112	WF12.2.1	11280.00	1.004	1.012	1.015	1.016	0.525	0.270	1.0062	197,31	1.0026	85,33	0.9912	319,42
113	WF12.2.2	8192.00	1.007	1.012	1.019	1.020	0.229	0.478	1.0089	144,32	1.0015	241,12	0.9896	350,55
114	WF12.3.1	5454.00	1.008	1.007	1.015	1.015	-0.124	0.782	1.0077	329,71	0.9994	190,15	0.9929	97,12
115	WF12.3.2	5650.00	1.013	1.014	1.027	1.027	0.051	0.622	1.0132	322,53	1.0005	159,36	0.9863	63,8
116	WF13.1.1	730.60	1.016	1.046	1.063	1.065	0.456	0.314	1.0257	245,0	1.0092	155,49	0.9651	336,41
117	WF13.3.1	751.30	1.017	1.045	1.062	1.064	0.434	0.329	1.0257	65,0	1.0087	156,61	0.9656	335,29
118	WF13.3.2	778.10	1.022	1.030	1.053	1.053	0.139	0.549	1.0244	62,5	1.0024	159,54	0.9732	329,35
119	WF13.3.3	823.10	1.017	1.045	1.062	1.065	0.432	0.331	1.0258	69,6	1.0087	168,58	0.9655	335,31

120	WF13.4.1	720.60	1.019	1.043	1.063	1.064	0.381	0.366	1.0264	70,5	1.0077	166,51	0.9660	226,38
121	WF13.4.3	839.20	1.024	1.041	1.066	1.067	0.244	0.466	1.0292	69,3	1.0052	164,61	0.9656	338,28
122	FG1.1.1	695.10	1.025	1.026	1.051	1.051	0.008	0.660	1.0249	211,32	1.0001	96,34	0.9750	332,40
123	FG1.1.2	721.00	1.026	1.026	1.051	1.051	-0.057	0.719	1.0251	209,29	0.9991	95,36	0.9758	326,40
124	FG1.2.3	730.40	1.027	1.021	1.049	1.049	-0.134	0.792	1.0250	214,27	0.9979	103,36	0.9771	332,43
125	FG1.3.1	663.10	1.027	1.019	1.046	1.047	-0.181	0.838	1.0241	211,26	0.9973	98,39	0.9786	325,40
126	FG1.3.2	714.10	1.032	1.016	1.048	1.049	-0.338	1.006	1.0261	207,26	0.9947	92,40	0.9792	320,39
127	FG2.2.2	647.70	1.035	1.045	1.082	1.082	0.110	0.572	1.0377	28,20	1.0029	134,39	0.9594	277,45
128	FG2.3.1	692.30	1.038	1.045	1.085	1.085	0.054	0.620	1.0399	27,16	1.0015	130,39	0.9586	279,47
129	FG2.3.2	700.20	1.037	1.048	1.087	1.087	0.102	0.579	1.0400	27,20	1.0028	134,39	0.9572	276,44
130	FG2.3.3	660.20	1.034	1.044	1.079	1.080	0.102	0.579	1.0369	27,18	1.0026	133,41	0.9605	280,44
131	FG2.4.1	612.00	1.035	1.042	1.078	1.078	0.065	0.610	1.0368	32,23	1.0016	144,41	0.9616	281,41
132	FG3.1.1	771.30	1.011	1.031	1.043	1.044	0.447	0.321	1.0177	53,7	1.0062	149,38	0.9761	315,51
133	FG3.1.2	830.90	1.011	1.035	1.046	1.048	0.517	0.275	1.0186	50,3	1.0077	142,39	0.9737	316,51
134	FG3.2.2	855.30	1.016	1.028	1.044	1.045	0.271	0.446	1.0196	222,4	1.0039	128,44	0.9765	316,46
135	FG3.3.1	894.90	1.016	1.037	1.054	1.055	0.371	0.373	1.0230	41,3	1.0065	134,44	0.9705	307,46
136	FG3.3.2	861.80	1.010	1.032	1.043	1.044	0.516	0.275	1.0172	49,2	1.0071	141,39	0.9757	317,51
137	FG4.1.1	826.10	1.032	1.004	1.036	1.040	-0.803	1.642	1.0226	198,25	0.9904	290,5	0.9869	30,64
138	FG4.2.1	904.60	1.028	1.016	1.044	1.045	-0.295	0.958	1.0240	189,32	0.9957	80,27	0.9803	319,46
139	FG4.3.1	759.70	1.028	1.014	1.043	1.044	-0.328	0.994	1.0235	185,2	0.9954	91,63	0.9811	276,27
140	FG4.4.1	888.50	1.032	1.004	1.036	1.039	-0.772	1.591	1.0222	211,17	0.9909	306,15	0.9869	75,67
141	FG4.5.1	931.10	1.035	1.012	1.047	1.049	-0.487	1.184	1.0268	201,24	0.9925	99,26	0.9807	328,53
142	FG5.1.1	809.70	1.018	1.042	1.061	1.063	0.391	0.359	1.0257	345,0	1.0077	255,42	0.9666	75,48
143	FG5.1.2	872.10	1.013	1.051	1.065	1.069	0.573	0.239	1.0254	326,15	1.0120	225,36	0.9626	75,50
144	FG5.2.1	819.20	1.005	1.036	1.041	1.045	0.742	0.138	1.0151	343,9	1.0100	244,45	0.9749	81,43
145	FG5.2.2	831.60	1.012	1.042	1.055	1.057	0.553	0.252	1.0215	322,25	1.0097	215,33	0.9687	81,47
146	FG5.3.1	786.40	1.010	1.036	1.046	1.049	0.555	0.250	1.0183	336,12	1.0083	235,41	0.9734	79,46
147	FG6.1.1	652.70	1.012	1.034	1.047	1.049	0.459	0.313	1.0194	204,25	1.0070	65,59	0.9736	303,18
148	FG6.3.1	661.90	1.012	1.025	1.037	1.038	0.359	0.382	1.0160	197,36	1.0044	53,48	0.9797	301,19
149	FG6.4.1	676.20	1.011	1.029	1.041	1.042	0.428	0.334	1.0172	197,32	1.0057	56,51	0.9771	300,19

150	FG6.5.1	632.70	1.011	1.034	1.044	1.046	0.510	0.279	1.0180	204,23	1.0074	74,57	0.9747	304,22
151	FG7.1.1	6081.00	1.017	1.103	1.122	1.132	0.693	0.166	1.0435	26,7	1.0261	126,55	0.9304	291,34
152	FG7.2.1	10200.00	1.012	1.074	1.087	1.094	0.695	0.165	1.0317	21,8	1.0191	121,52	0.9491	285,37
153	FG7.2.2	6658.00	1.018	1.077	1.097	1.103	0.603	0.220	1.0365	20,5	1.0184	116,54	0.9451	287,35
154	FG7.3.1	44130.00	1.006	1.018	1.024	1.025	0.517	0.275	1.0096	179,42	1.0040	54,33	0.9863	301,31
155	FG7.3.2	25990.00	1.016	1.056	1.073	1.076	0.535	0.263	1.0287	199,1	1.0124	108,54	0.9589	289,36
156	FG7.3.3	13820.00	1.019	1.084	1.105	1.112	0.601	0.222	1.0395	31,10	1.0198	137,56	0.9407	294,32
157	FG8.1.1	540.00	1.036	1.062	1.100	1.101	0.241	0.468	1.0434	232,3	1.0076	139,44	0.9490	325,46
158	FG8.2.1	581.90	1.037	1.060	1.099	1.100	0.213	0.490	1.0438	230,3	1.0067	137,42	0.9495	324,48
159	FG8.3.1	681.30	1.032	1.067	1.101	1.103	0.321	0.409	1.0428	227,9	1.0103	129,41	0.9469	327,48
160	FG8.3.2	565.50	1.035	1.062	1.099	1.100	0.254	0.459	1.0430	226,9	1.0079	127,44	0.9490	325,45
161	FG8.4.1	669.50	1.030	1.072	1.104	1.107	0.381	0.366	1.0429	227,9	1.0125	129,40	0.9447	327,48
162	FG9.1.1	795.70	1.035	1.041	1.078	1.078	0.054	0.620	1.0367	185,15	1.0013	87,28	0.9619	300,58
163	FG9.1.2	783.40	1.031	1.038	1.071	1.071	0.076	0.601	1.0333	184,18	1.0017	85,25	0.9650	305,58
164	FG9.2.1	666.00	1.023	1.035	1.058	1.059	0.195	0.504	1.0264	189,15	1.0037	90,30	0.9699	303,56
165	FG9.2.2	727.60	1.026	1.034	1.061	1.061	0.107	0.575	1.0287	189,15	1.0021	90,30	0.9692	302,56
166	FG9.2.3	700.90	1.023	1.039	1.062	1.063	0.247	0.464	1.0277	188,14	1.0050	90,29	0.9673	301,57
167	FG10.1.1	1060.00	1.021	1.042	1.063	1.065	0.310	0.417	1.0275	197,42	1.0063	78,28	0.9662	326,35
168	FG10.1.2	1055.00	1.022	1.037	1.060	1.061	0.248	0.463	1.0267	201,42	1.0048	78,31	0.9685	326,32
169	FG10.2.1	1099.00	1.020	1.044	1.064	1.066	0.361	0.380	1.0272	201,44	1.0074	79,29	0.9654	329,33
170	FG10.2.2	1058.00	1.019	1.043	1.063	1.064	0.359	0.382	1.0267	209,44	1.0072	81,33	0.9661	331,28
171	FG10.3.1	1050.00	1.022	1.042	1.066	1.067	0.290	0.431	1.0286	198,39	1.0061	79,31	0.9652	323,35
172	FG11.2.1	645.90	1.033	1.031	1.065	1.065	-0.038	0.701	1.0320	200,13	0.9992	88,58	0.9688	297,28
173	FG11.2.2	652.70	1.034	1.040	1.075	1.075	0.068	0.608	1.0352	200,12	1.0016	90,59	0.9631	297,28
174	FG11.2.3	624.10	1.033	1.033	1.067	1.067	-0.025	0.689	1.0329	202,11	0.9995	92,60	0.9677	298,27
175	FG11.3.1	771.10	1.034	1.044	1.079	1.079	0.102	0.579	1.0366	208,15	1.0026	89,61	0.9608	305,24
176	FG11.3.2	597.20	1.033	1.037	1.072	1.072	0.038	0.633	1.0342	207,14	1.0009	90,61	0.9649	304,25
177	FG12.1.1	470.80	1.017	1.036	1.054	1.055	0.349	0.389	1.0231	233,18	1.0061	109,61	0.9709	331,22
178	FG12.1.2	505.90	1.011	1.040	1.051	1.054	0.544	0.257	1.0204	226,23	1.0090	98,56	0.9705	327,24
179	FG12.2.1	508.20	1.018	1.033	1.052	1.053	0.270	0.447	1.0230	214,43	1.0045	91,31	0.9725	339,32

180	FG12.2.2	568.70	1.013	1.037	1.050	1.052	0.467	0.307	1.0205	211,42	1.0076	91,29	0.9720	339,34
181	FG12.3.1	524.00	1.018	1.034	1.053	1.053	0.283	0.437	1.0231	231,27	1.0048	94,55	0.9720	332,2
182	FG12.3.2	470.90	1.016	1.032	1.048	1.049	0.321	0.409	1.0210	232,24	1.0050	97,58	0.9740	331,20
183	FG13.1.1	655.80	1.036	1.046	1.084	1.084	0.092	0.587	1.0389	185,22	1.0025	277,3	0.9586	13,67
184	FG13.2.1	433.50	1.018	1.024	1.043	1.043	0.136	0.551	1.0200	188,24	1.0019	279,2	0.9781	13,66
185	FG13.3.1	510.60	1.024	1.030	1.054	1.054	0.101	0.580	1.0253	185,18	1.0018	275,3	0.9729	14,72
186	FG13.4.1	645.30	1.023	1.041	1.066	1.066	0.261	0.453	1.0289	187,15	1.0055	278,3	0.9656	18,75
187	FG13.4.2	702.50	1.025	1.062	1.089	1.092	0.405	0.350	1.0366	180,18	1.0114	89,1	0.9520	358,72
189	FG14.2.1	694.40	1.009	1.047	1.057	1.061	0.656	0.188	1.0216	68,4	1.0121	163,48	0.9663	335,41
190	FG14.2.2	655.90	1.012	1.043	1.056	1.059	0.539	0.261	1.0224	69,6	1.0098	166,47	0.9679	334,42
191	FG14.3.1	660.40	1.008	1.052	1.060	1.065	0.724	0.148	1.0219	72,8	1.0139	169,42	0.9642	334,47
192	FG14.3.2	640.00	1.007	1.046	1.053	1.058	0.713	0.154	1.0197	71,3	1.0123	163,42	0.9680	338,47
193	FG14.3.3	705.60	1.011	1.044	1.055	1.058	0.593	0.227	1.0214	245,2	1.0105	154,40	0.9681	337,50
194	FG15.1.1	739.70	1.011	1.039	1.050	1.053	0.550	0.254	1.0200	168,53	1.0090	71,5	0.9710	337,36
195	FG15.1.2	672.40	1.006	1.034	1.040	1.043	0.672	0.178	1.0152	185,48	1.0088	76,16	0.9760	334,37
196	FG15.2.1	776.00	1.008	1.039	1.047	1.050	0.649	0.192	1.0178	169,51	1.0098	72,6	0.9723	338,39
197	FG15.2.2	565.90	1.009	1.037	1.046	1.049	0.616	0.213	1.0178	193,46	1.0092	82,18	0.9730	338,38
198	FG15.3.2	573.20	1.015	1.022	1.038	1.038	0.178	0.517	1.0175	156,43	1.0022	64,2	0.9803	332,47
199	FG16.1.1	774.30	1.012	1.070	1.083	1.090	0.692	0.167	1.0305	169,40	1.0183	67,14	0.9512	321,47
200	FG16.1.2	749.50	1.011	1.062	1.073	1.079	0.689	0.169	1.0270	156,39	1.0161	62,5	0.9568	325,50
201	FG16.2.2	692.10	1.011	1.060	1.072	1.077	0.664	0.183	1.0267	154,41	1.0152	57,8	0.9581	319,48
202	FG16.4.1	719.10	1.011	1.059	1.071	1.077	0.665	0.183	1.0266	154,42	1.0152	56,8	0.9582	317,47
203	FG16.4.2	751.90	1.011	1.064	1.076	1.082	0.688	0.169	1.0278	161,42	1.0166	61,11	0.9556	320,46
204	FG17.1.1	648.60	1.003	1.016	1.019	1.020	0.698	0.163	1.0072	172,52	1.0043	62,15	0.9885	321,34
205	FG17.1.2	1125.00	1.006	1.015	1.022	1.023	0.400	0.353	1.0094	196,29	1.0029	77,41	0.9877	309,35
206	FG17.2.1	792.90	1.002	1.020	1.023	1.025	0.778	0.117	1.0083	199,17	1.0058	86,51	0.9859	301,33
207	FG17.2.2	1122.00	1.011	1.020	1.031	1.032	0.259	0.454	1.0141	204,20	1.0027	93,45	0.9832	311,38
208	FG17.3.1	557.30	1.009	1.019	1.028	1.028	0.340	0.396	1.0122	203,39	1.0031	83,31	0.9847	328,35
109	FG17.3.2	576.80	1.007	1.020	1.027	1.028	0.478	0.300	1.0111	204,35	1.0042	87,33	0.9846	327,38
210	FG18.1.1	446.70	1.017	1.026	1.043	1.044	0.204	0.497	1.0197	211,34	1.0029	104,23	0.9775	346,47

241	FE1.1.1	627.90	1.011	1.011	1.022	1.022	0.024	0.646	1.0109	106,0	1.0002	196,51	0.9890	16,39
242	FE1.2.1	523.00	1.008	1.012	1.020	1.020	0.163	0.530	1.0093	278,19	1.0011	161,53	0.9896	20,30
243	FE1.2.2	911.70	1.013	1.044	1.058	1.060	0.514	0.277	1.0231	274,17	1.0096	171,35	0.9673	25,50
244	FE1.3.1	483.60	1.008	1.020	1.028	1.029	0.441	0.325	1.0119	276,33	1.0041	143,46	0.9841	24,25
245	FE2.1.1	447.10	1.002	1.014	1.016	1.017	0.800	0.105	1.0057	197,18	1.0042	290,8	0.9901	44,70
246	FE2.1.2	446.40	1.004	1.006	1.010	1.010	0.161	0.531	1.0046	176,7	1.0005	269,23	0.9949	69,66
247	FE2.1.3	420.20	1.002	1.006	1.008	1.009	0.558	0.248	1.0033	267,42	1.0015	50,42	0.9952	159,20
248	FE2.2.1	430.40	1.004	1.014	1.019	1.020	0.513	0.277	1.0077	263,29	1.0032	171,3	0.9892	75,61
249	FE2.2.2	405.60	1.002	1.013	1.015	1.017	0.737	0.141	1.0057	331,21	1.0037	234,19	0.9906	105,62
250	FE2.2.3	388.50	1.006	1.005	1.011	1.011	-0.043	0.705	1.0054	249,5	0.9998	339,1	0.9948	82,84
251	FE3.1.1	33490.00	1.019	1.085	1.106	1.113	0.610	0.216	1.0397	24,36	1.0202	159,44	0.9401	275,24
252	FE3.1.2	31730.00	1.029	1.099	1.131	1.137	0.516	0.276	1.0503	27,36	1.0209	162,44	0.9288	278,24
253	FE3.2.1	30170.00	1.017	1.081	1.099	1.106	0.635	0.201	1.0368	25,37	1.0198	158,42	0.9434	274,26
254	FE3.3.1	28480.00	1.010	1.084	1.094	1.104	0.778	0.117	1.0329	26,38	1.0231	151,37	0.9440	268,31
255	FE3.3.2	26920.00	1.012	1.083	1.096	1.105	0.732	0.143	1.0343	16,32	1.0221	143,44	0.9436	265,29
256	FE3.4.1	23050.00	1.009	1.084	1.094	1.104	0.786	0.113	1.0327	42,57	1.0232	177,25	0.9441	277,21
257	FEA4.1.1	31430.00	1.014	1.115	1.132	1.145	0.755	0.131	1.0455	21,27	1.0306	197,47	0.9239	325,28
258	FEA4.1.2	56460.00	1.026	1.179	1.209	1.229	0.712	0.155	1.0706	85,42	1.0440	218,37	0.8854	329,26
259	FEA4.2.1	23290.00	1.023	1.131	1.157	1.170	0.669	0.180	1.0556	93,47	1.0319	223,31	0.9125	330,26
260	FEA4.3.1	24330.00	1.027	1.120	1.150	1.160	0.602	0.221	1.0550	80,38	1.0276	210,40	0.9174	326,28
261	FEA4.4.1	27820.00	1.023	1.125	1.151	1.163	0.658	0.187	1.0539	66,29	1.0303	198,50	0.9158	321,25
262	FE4.1.1	11090.00	1.068	1.162	1.241	1.247	0.346	0.391	1.0939	314,12	1.0245	209,51	0.8817	53,36
263	FE4.2.1	11750.00	1.036	1.095	1.134	1.138	0.417	0.342	1.0536	318,9	1.0173	214,56	0.9292	54,32
264	FE4.3.1	9899.00	1.018	1.051	1.070	1.073	0.454	0.316	1.0286	320,12	1.0102	213,55	0.9612	58,32
265	FE4.4.1	11150.00	1.015	1.058	1.074	1.078	0.564	0.245	1.0287	319,11	1.0133	213,54	0.9581	56,34
266	FE4.5.1	11390.00	1.015	1.048	1.065	1.067	0.498	0.287	1.0259	327,2	1.0103	234,59	0.9637	58,31
267	FE5.1.1	1677.00	1.027	1.043	1.072	1.072	0.211	0.491	1.0320	195,32	1.0048	85,28	0.9631	323,45
268	FE5.1.2	1395.00	1.026	1.054	1.081	1.082	0.331	0.401	1.0343	205,20	1.0085	98,39	0.9572	316,44
269	FE5.2.1	2000.00	1.026	1.051	1.077	1.079	0.306	0.420	1.0334	38,1	1.0076	129,48	0.9591	307,42
270	FE5.2.2	1703.00	1.028	1.032	1.061	1.061	0.043	0.629	1.0293	213,15	1.0009	113,33	0.9699	324,53
271	FE5.3.1	2025.00	1.034	1.031	1.066	1.066	-0.047	0.709	1.0325	227,14	0.9990	118,54	0.9685	326,33

272	FE5.3.2	1546.00	1.028	1.040	1.070	1.070	0.152	0.538	1.0318	216,15	1.0034	106,52	0.9648	316,34
273	FE6.1.1	8106.00	1.024	1.020	1.045	1.045	-0.085	0.745	1.0224	339,62	0.9988	125,24	0.9788	222,14
274	FE6.1.2	7569.00	1.056	1.033	1.091	1.092	-0.268	0.928	1.0475	2,60	0.9922	268,2	0.9603	177,30
275	FE6.2.1	5437.00	1.033	1.027	1.061	1.061	-0.122	0.780	1.0307	320,51	0.9976	130,38	0.9717	224,5
276	FE6.2.2	7852.00	1.058	1.047	1.108	1.108	-0.119	0.777	1.0533	345,58	0.9959	252,2	0.9508	161,32
277	FE6.2.3	14540.00	1.062	1.034	1.098	1.099	-0.309	0.973	1.0516	339,55	0.9904	246,2	0.9580	154,35
278	FE7.1.1	656.20	1.018	1.100	1.120	1.129	0.668	0.181	1.0434	200,9	1.0248	103,32	0.9318	304,56
279	FE7.1.2	684.40	1.021	1.102	1.125	1.134	0.629	0.204	1.0459	204,9	1.0244	108,33	0.9297	306,55
280	FE7.2.1	684.60	1.018	1.101	1.121	1.130	0.677	0.176	1.0435	202,10	1.0253	106,32	0.9312	307,56
281	FE7.2.2	681.60	1.017	1.099	1.118	1.128	0.676	0.176	1.0427	199,13	1.0248	101,31	0.9325	308,56
282	FE7.4.1	683.30	1.019	1.102	1.123	1.133	0.658	0.187	1.0447	201,11	1.0251	104,31	0.9302	309,57
283	FE7.4.2	660.00	1.020	1.098	1.119	1.128	0.637	0.199	1.0438	200,13	1.0236	102,31	0.9326	310,56
284	FE8.1.1	27490.00	1.020	1.084	1.106	1.112	0.587	0.230	1.0400	97,45	1.0195	205,17	0.9405	310,40
285	FE8.1.2	31160.00	1.025	1.076	1.103	1.107	0.482	0.297	1.0406	100,45	1.0156	208,17	0.9438	313,40
286	FE8.2.1	25520.00	1.020	1.081	1.103	1.110	0.573	0.239	1.0394	101,49	1.0186	210,16	0.9420	312,37
287	FE8.2.2	28250.00	1.025	1.081	1.109	1.114	0.501	0.285	1.0425	105,49	1.0170	216,17	0.9404	319,36
288	FE8.4.1	22470.00	1.021	1.086	1.109	1.115	0.577	0.236	1.0412	113,14	1.0196	23,2	0.9392	285,76
289	FE8.4.2	27100.00	1.022	1.084	1.107	1.113	0.557	0.249	1.0411	104,50	1.0187	215,17	0.9402	317,35
290	FE9.2.1	912.00	1.008	1.034	1.042	1.045	0.623	0.208	1.0162	150,42	1.0085	18,36	0.9752	267,26
291	FE9.2.2	1147.00	1.011	1.034	1.045	1.047	0.508	0.281	1.0182	149,56	1.0074	11,27	0.9744	271,19
292	FE9.2.3	791.20	1.004	1.020	1.025	1.026	0.659	0.187	1.0095	96,58	1.0053	1,3	0.9852	269,32
293	FE9.3.1	942.80	1.011	1.040	1.051	1.053	0.567	0.243	1.0199	174,44	1.0093	21,43	0.9708	278,14
294	FE9.3.2	1022.00	1.005	1.039	1.044	1.049	0.771	0.121	1.0160	141,68	1.0111	16,13	0.9729	282,18
295	FE9.3.3	876.80	1.005	1.019	1.025	1.026	0.569	0.241	1.0099	357,17	1.0046	145,70	0.9855	264,10
296	FE10.1.3	801.20	1.005	1.035	1.040	1.044	0.720	0.151	1.0149	222,5	1.0094	125,63	0.9756	315,27
297	FE10.2.0	762.70	1.004	1.035	1.039	1.043	0.806	0.102	1.0139	237,0	1.0103	146,64	0.9758	327,26
298	FE10.2.1	733.50	1.009	1.030	1.039	1.041	0.527	0.268	1.0157	214,43	1.0067	73,40	0.9776	324,21
300	FE10.2.2	663.00	1.010	1.029	1.039	1.040	0.491	0.292	1.0158	215,34	1.0062	78,48	0.9780	321,22
301	FE10.3.1	679.30	1.008	1.022	1.030	1.031	0.444	0.323	1.0127	198,43	1.0044	71,33	0.9829	320,29
302	FE10.3.2	636.40	1.004	1.032	1.035	1.039	0.789	0.111	1.0127	191,61	1.0091	58,21	0.9782	321,19

303	FE11.1.1	403.50	1.024	1.002	1.026	1.029	-0.871	1.757	1.0167	194,13	0.9925	296,42	0.9908	90,45
304	FE11.2.1	371.20	1.017	1.008	1.024	1.025	-0.380	1.053	1.0136	192,21	0.9970	298,37	0.9895	78,46
305	FE11.3.1	330.60	1.009	1.018	1.027	1.028	0.344	0.392	1.0118	179,18	1.0031	22,7	0.9851	272,7
306	FE11.4.1	307.10	1.002	1.021	1.024	1.026	0.793	0.109	1.0086	56,65	1.0062	172,12	0.9852	267,22
307	FE11.5.1	300.20	1.003	1.024	1.025	1.027	0.764	0.110	1.0088	76,64	1.0063	187,20	0.9854	276,23
308	FE12.1.1	709.10	1.009	1.016	1.025	1.025	0.269	0.447	1.0112	205,21	1.0022	110,13	0.9866	350,65
309	FE12.1.2	643.00	1.008	1.027	1.036	1.037	0.536	0.262	1.0143	219,19	1.0062	123,16	0.9794	355,64
310	FE12.2.1	647.90	1.009	1.027	1.036	1.038	0.513	0.277	1.0146	213,25	1.0060	118,12	0.9730	5,62
311	FE12.2.2	648.20	1.010	1.024	1.034	1.035	0.422	0.337	1.0143	214,24	1.0047	115,19	0.9810	351,59
312	FE12.2.3	693.50	1.011	1.032	1.042	1.044	0.484	0.296	1.0174	214,22	1.0067	115,21	0.9757	346,58
313	FE13.2.1	624.30	1.015	1.053	1.069	1.073	0.542	0.259	1.0273	96,33	1.0120	202,22	0.9607	316,48
314	FE13.2.2	627.40	1.012	1.058	1.071	1.076	0.643	0.196	1.0266	86,32	1.0145	192,24	0.9589	312,48
315	FE13.3.1	611.20	1.012	1.055	1.067	1.072	0.632	0.202	1.0256	91,35	1.0137	199,24	0.9608	315,45
316	FE13.3.2	704.20	1.018	1.056	1.074	1.078	0.494	0.290	1.0298	85,36	1.0118	194,25	0.9584	310,44
317	FE13.4.1	604.60	1.016	1.048	1.065	1.068	0.474	0.303	1.0264	104,35	1.0099	207,18	0.9636	320,50
318	FE13.4.2	635.70	1.014	1.053	1.067	1.071	0.570	0.241	1.0262	90,32	1.0123	195,24	0.9615	315,49
319	FE14.2.1	404.20	1.027	1.055	1.083	1.085	0.317	0.412	1.0356	127,42	1.0084	236,20	0.9560	345,41
320	FE14.2.3	347.90	1.025	1.053	1.079	1.081	0.328	0.404	1.0339	128,39	1.0083	237,22	0.9578	349,43
321	FE14.4.1	371.40	1.025	1.057	1.083	1.085	0.363	0.379	1.0349	125,42	1.0096	235,21	0.9555	345,41
322	FE14.4.2	384.00	1.029	1.057	1.088	1.089	0.301	0.424	1.0376	127,42	1.0084	237,21	0.9541	347,41
323	FE14.4.3	378.60	1.027	1.056	1.085	1.087	0.317	0.412	1.0363	128,39	1.0086	236,21	0.9551	348,44
324	FE15.1.1	17900.00	1.003	1.019	1.022	1.023	0.742	0.138	1.0080	209,39	1.0053	84,36	0.9868	238,31
325	FE15.2.1	22340.00	1.003	1.035	1.038	1.042	0.835	0.086	1.0134	221,20	1.0103	103,52	0.9763	324,31
326	FE15.3.1	19130.00	1.004	1.021	1.025	1.027	0.710	0.156	1.0094	206,24	1.0058	95,38	0.9848	320,42
327	FE15.4.1	14060.00	1.006	1.007	1.013	1.013	0.045	0.627	1.0066	165,18	1.0002	264,26	0.9932	43,57
328	FE15.5.1	15330.00	1.004	1.013	1.017	1.017	0.544	0.257	1.0068	168,48	1.0030	66,11	0.9903	326,40
329	FE15.5.2	13260.00	1.003	1.001	1.004	1.004	-0.508	1.210	1.0022	189,54	0.9994	291,9	0.9985	27,35
330	K1.2.1	3599.00	1.005	1.006	1.011	1.011	0.169	0.525	1.0052	347,0	1.0006	77,2	0.9942	245,88
331	K1.2.2	3988.00	1.006	1.004	1.010	1.010	-0.261	0.921	1.0054	1,1	0.9991	91,24	0.9954	269,66
332	K1.3.1	3109.00	1.004	1.006	1.010	1.010	0.160	0.532	1.0048	171,4	1.0005	81,6	0.9947	297,83
333	K1.3.2	3814.00	1.003	1.004	1.007	1.007	0.229	0.478	1.0033	15,13	1.0006	111,23	0.9961	258,64

334	K1.4.1	2671.00	1.003	1.004	1.008	1.008	0.132	0.555	1.0037	302,24	1.0003	211,1	0.9959	119,66
335	K1.4.2	3069.00	1.002	1.003	1.005	1.006	0.129	0.556	1.0026	313,22	1.0002	219,11	0.9971	105,65
336	BH1.1.1	85.40	1.003	1.039	1.043	1.048	0.849	0.079	1.0148	135,55	1.0117	225,0	0.9734	315,35
337	BH1.2.1	86.53	1.005	1.035	1.044	1.047	0.574	0.238	1.0175	165,50	1.0083	54,17	0.9742	312,35
338	BH1.2.2	85.77	1.006	1.043	1.049	1.054	0.748	0.135	1.0178	83,39	1.0118	197,28	0.9703	313,39
339	BH1.4.1	80.53	1.005	1.040	1.045	1.049	0.784	0.114	1.0161	135,53	1.0114	225,0	0.9725	315,37
340	BH1.4.2	95.13	1.006	1.041	1.047	1.052	0.756	0.130	1.0171	81,41	1.0115	200,29	0.9713	313,36
341	BH2.1.1	43280.00	1.002	1.029	1.031	1.035	0.846	0.080	1.0111	144,53	1.0087	246,9	0.9802	343,35
342	BH2.1.2	46030.00	1.003	1.029	1.032	1.035	0.813	0.098	1.0114	78,20	1.0084	191,47	0.9802	333,36
343	BH2.2.2	38310.00	1.009	1.047	1.057	1.061	0.668	0.181	1.0214	70,17	1.0122	193,60	0.9664	332,24
344	BH2.3.1	37980.00	1.022	1.029	1.052	1.052	0.113	0.569	1.0242	72,9	1.0019	177,57	0.9739	336,31
345	BH2.3.2	38650.00	1.022	1.034	1.057	1.057	0.202	0.498	1.0257	67,12	1.0037	186,67	0.9706	333,20
346	L1.1.1	12520.00	1.037	1.008	1.045	1.049	-0.657	1.415	1.0272	155,27	0.9902	59,11	0.9826	308,60
347	L1.2.1	16770.00	1.017	1.028	1.046	1.046	0.224	0.481	1.0206	173,27	1.0033	69,24	0.9760	304,52
348	L1.3.1	910.80	1.009	1.020	1.028	1.029	0.390	0.360	1.0122	162,43	1.0036	57,15	0.9842	313,43
349	L1.3.2	191.90	1.008	1.016	1.024	1.025	0.319	0.410	1.0108	158,28	1.0026	55,23	0.9867	292,53
350	L2.1.1	1143.00	1.030	1.085	1.117	1.122	0.450	0.319	1.0466	153,46	1.0165	245,5	0.9369	343,43
351	L2.2.1	960.60	1.011	1.076	1.088	1.096	0.726	0.147	1.0317	162,44	1.0202	252,0	0.9481	342,46
352	L2.3.1	999.60	1.011	1.086	1.098	1.108	0.752	0.132	1.0347	160,42	1.0232	251,1	0.9421	342,48
353	L2.4.1	938.30	1.013	1.088	1.102	1.111	0.725	0.147	1.0363	167,44	1.0232	73,3	0.9405	340,46
354	L3.2.1	10630.00	1.020	1.032	1.052	1.052	0.220	0.484	1.0234	42,9	1.0037	298,57	0.9728	138,32
355	L3.2.2	12060.00	1.021	1.024	1.045	1.045	0.052	0.621	1.0218	42,7	1.0008	301,55	0.9775	137,34
356	L3.3.1	7582.00	1.021	1.040	1.061	1.062	0.295	0.428	1.0267	42,15	1.0058	289,55	0.9675	141,31
357	L3.3.2	9422.00	1.020	1.025	1.046	1.046	0.085	0.593	1.0218	45,5	1.0013	309,54	0.9769	139,36
358	L3.4.1	4347.00	1.023	1.030	1.054	1.054	0.119	0.565	1.0252	47,10	1.0021	300,58	0.9727	143,30
359	L3.4.2	4427.00	1.022	1.031	1.054	1.054	0.147	0.542	1.0250	46,8	1.0026	303,58	0.9724	141,31
360	S1.1.1	600.50	1.040	1.072	1.115	1.117	0.256	0.457	1.0496	157,37	1.0093	265,22	0.9411	19,45
361	S1.1.2	528.70	1.051	1.038	1.091	1.091	-0.161	0.818	1.0460	159,38	0.9953	259,14	0.9587	6,49
362	S1.2.1	593.50	1.039	1.076	1.118	1.120	0.287	0.434	1.0501	169,36	1.0106	273,18	0.9393	24,48
363	S1.2.2	495.00	1.037	1.060	1.100	1.100	0.209	0.493	1.0440	164,36	1.0066	255,2	0.9494	347,54

364	S1.3.1	531.00	1.036	1.060	1.098	1.099	0.221	0.484	1.0431	172,36	1.0069	273,16	0.9500	23,50
365	S1.3.2	584.00	1.048	1.049	1.099	1.099	-0.009	0.675	1.0472	174,40	0.9997	278,16	0.9531	25,46
	N.B.													
	Km = mean susceptibility				Kmax, Kint, Kmin = principal susceptibility ellipsoid axes (Kmax = K1, Kint = K2, Kmin = K3)									
	L = magnetic lineation				D/I = magnetic declination and inclination									
	F = magnetic foliation				Kmax-D/I, Kint-D/I, Kmin-D/I = orientations of principal susceptibility ellipsoid axes									
	P = anisotropy degree													
	P' = corrected anisotropy degree													
	T = shape factor													
	q = q-factor for unconsolidated sediments													

Appendix-B

Sample list-2 for Anisotropy of Magnetic Susceptibility measurement

No.	Sample No.	Rock type	Exposure type	Orientation	Remarks
1	D1	mafic	dyke	130, 67	
2	D1.1	mafic	dyke	196, 67	
3	D1.2	mafic	dyke	020, 82	
4	D2	mafic	dyke	106, 40	
5	D3	mafic	dyke	165, 40	
6	D4	-	-	-	
7	D5	mafic	dyke	210, 62	
8	D5.1	mafic	dyke	228, 89	
9	D6	mafic	dyke	190, 79	
10	D7	mafic	dyke	240, 89	
11	D7.1	mafic	dyke	190, 58	
12	D8	mafic	dyke	145, 24	
13	D8A	mafic	dyke	360, 00	
14	D9	mafic	dyke	248, 70	
15	p1	basalt	pillow	168, 31	
16	p2	basalt	pillow	222, 88	
17	p3	basalt	pillow	175, 55	
18	ker1	trachyte	stock	080, 85	
19	ker2	trachyte	stock	105, 46	Frei.-Wein. road
20	f (Fürfurt)	basalt	lava	304, 76	
21	g (Gräveneck)	basalt	plug	035, 89	
22	al (Aldi)	mafic	dyke	144, 60	
23	l (Kubach L.st.)	limestone	sedimentary rock	360, 00	
24	wf (wasserwerk)	basalt	dyke/boss (lava)	182, 60	
25	la (Lack factory)	basalt	lava	180, 40	
26	905	basalt	lava	174, 80	Frei.-Ernsth. road

N.B.

Frei.-Wein. = Freienfels-Weinbach

Frei.-Ernsth. = Freienfels-Ernsthausen

Anisotropy of Magnetic Susceptibility measurement of dykes														
No.	SampleNo.	Km	L	F	P	P'	T	q	Kmax	Kmax-D/I	KInt	KInt-D/I	Kmin	Kmin-D/I
1	D1.1.1	632.80	1.015	1.028	1.044	1.045	0.285	0.435	1.0195	231,21	1.0041	117,47	0.9765	337,36
2	D1.1.2	644.60	1.017	1.034	1.052	1.053	0.333	0.400	1.0224	226,14	1.0056	121,47	0.9721	328,40
3	D1.2.1	652.60	1.017	1.025	1.042	1.042	0.172	0.052	1.0194	229,22	1.0024	112,49	0.9782	334,33
4	D1.2.2	651.00	1.015	1.032	1.048	1.049	0.346	0.391	1.0205	223,20	1.0054	111,45	0.9741	330,37
5	D1.3.1	624.70	1.019	1.031	1.051	1.051	0.227	0.479	1.0228	230,13	1.0037	126,46	0.9735	331,41
6	D1.3.2	691.20	1.016	1.034	1.051	1.052	0.351	0.387	1.0218	228,14	1.0058	123,44	0.9725	331,42
7	D1,1.1	747.00	1.009	1.039	1.048	1.051	0.623	0.208	1.0186	219,23	1.0097	106,43	0.9717	328,38
8	D1,1.2	733.50	1.013	1.042	1.055	1.058	0.051	0.282	1.0222	222,26	1.0090	109,38	0.9688	337,41
9	D1,1.3	725.70	1.012	1.043	1.056	1.059	0.558	0.248	1.0219	232,19	1.0100	124,40	0.9680	341,43
10	D1,2.1	768.30	1.013	1.033	1.047	1.049	0.415	0.343	1.0199	18,1	1.0064	287,44	0.9738	108,46
11	D1,2.2.1	1251.00	1.007	1.020	1.027	1.028	0.486	0.295	1.0112	6,7	1.0043	271,40	0.9844	104,49
12	D1,2.2.2	825.90	1.012	1.030	1.043	1.044	0.408	0.348	1.0181	15,1	1.0057	284,44	0.9762	107,46
13	D1,2.2.3	779.30	1.010	1.033	1.044	1.046	0.509	0.280	1.0178	204,1	1.0073	295,47	0.9750	113,43
14	D1,2.3.1	854.60	1.011	1.040	1.051	1.054	0.566	0.243	1.0201	21,2	1.0094	289,52	0.9705	112,38
15	D1,2.3.2	908.00	1.012	1.036	1.048	1.050	0.492	0.291	1.0196	18,3	1.0077	284,51	0.9727	110,39
16	D1,2.3.3	927.90	1.013	1.024	1.037	1.037	0.278	0.440	1.0164	15,6	1.0034	275,58	0.9802	109,31
17	D2.1	838.80	1.023	1.055	1.080	1.082	0.384	0.364	1.0334	215,26	1.0098	102,39	0.9568	330,40
18	D2.2	690.00	1.026	1.062	1.089	1.091	0.389	0.361	1.0368	214,26	1.0110	95,45	0.9522	323,34
19	D2.3	669.50	1.022	1.064	1.087	1.091	0.465	0.309	1.0350	207,30	1.0129	90,39	0.9521	323,37
20	D2.4	712.20	1.012	1.061	1.074	1.079	0.659	0.186	1.0276	232,8	1.0155	131,55	0.9569	327,34
21	D3.1.1	1689.00	1.006	1.018	1.024	1.025	0.523	0.271	1.0096	98,46	1.0041	339,25	0.9863	231,34
22	D3.1.2	2088.00	1.011	1.025	1.036	1.037	0.395	0.356	1.0152	88,54	1.0046	334,16	0.9802	234,31
23	D3.3.1	2696.00	1.008	1.032	1.041	1.043	0.572	0.240	1.0160	103,54	1.0075	341,21	0.9764	239,27
24	D3.3.2	3466.00	1.009	1.038	1.047	1.050	0.621	0.209	1.0181	80,64	1.0094	332,9	0.9725	238,24
25	D3.4.1	1866.00	1.007	1.022	1.029	1.030	0.532	0.265	1.0117	108,54	1.0050	344,22	0.9833	243,27

26	D3.4.2	2523.00	1.009	1.030	1.040	1.042	0.532	0.265	1.0159	119,55	1.0069	347,25	0.9772	246,23
27	D5.1.1	42100.00	1.039	1.040	1.081	1.081	-0.009	0.675	1.0391	104,61	0.9998	235,20	0.9611	333,20
28	D5.2.1	41320.00	1.032	1.024	1.057	1.058	-0.146	0.803	1.0293	98,57	0.9973	231,24	0.9734	331,21
29	D5.2.2	37070.00	1.024	1.037	1.062	1.062	0.198	0.502	1.0280	101,57	1.0040	244,27	0.9681	343,17
30	D5,1.1.1	36430.00	1.051	1.033	1.087	1.087	-0.228	0.887	1.0448	111,60	0.9937	253,25	0.9616	351,16
31	D5,1.1.2	43970.00	1.054	1.043	1.099	1.099	-0.133	0.790	1.0492	122,58	0.9958	255,23	0.9550	354,21
32	D5,1.2.1	34280.00	1.050	1.016	1.067	1.070	-0.517	1.221	1.0381	90,52	0.9888	253,37	0.9731	349,8
33	D5,1.2.2	47140.00	1.053	1.022	1.077	1.079	-0.416	1.095	1.0423	95,46	0.9897	238,37	0.9580	343,20
34	D5,1.2.3	42730.00	1.045	1.018	1.064	1.066	-0.436	1.120	1.0356	96,42	0.9910	224,34	0.9734	336,29
35	D6.1.1	602.10	1.027	1.003	1.030	1.033	-0.832	1.690	1.0188	153,41	0.9918	273,30	0.9894	26,35
36	D6.1.2	517.90	1.023	1.006	1.028	1.030	-0.605	1.341	1.0169	156,40	0.9943	272,29	0.9888	27,37
37	D6.2.1	669.80	1.030	1.006	1.036	1.039	-0.660	1.419	1.0218	147,41	0.9921	269,31	0.9861	22,33
38	D6.2.2	629.10	1.029	1.008	1.038	1.040	-0.553	1.269	1.0220	146,40	0.9932	268,33	0.9849	23,33
39	D6.3.1	694.10	1.028	1.009	1.037	1.038	-0.537	1.248	1.0213	146,41	0.9935	267,31	0.9851	21,33
40	D6.3.2	586.90	1.026	1.005	1.032	1.034	-0.662	1.422	1.0192	144,36	0.9930	262,33	0.9877	21,37
41	D7.1.1	782.80	1.024	1.043	1.068	1.069	0.264	0.451	1.0299	152,39	1.0058	242,0	0.9643	333,51
42	D7.1.2	803.00	1.025	1.037	1.064	1.064	0.176	0.519	1.0290	151,40	1.0036	243,2	0.9674	335,49
43	D7.2.1	804.90	1.021	1.045	1.067	1.069	0.349	0.389	1.0287	151,48	1.0076	60,1	0.9637	330,42
44	D7.2.2	792.60	1.023	1.044	1.067	1.068	0.297	0.426	1.0292	154,49	1.0064	245,1	0.9644	337,41
45	D7,1.1.1	526.50	1.004	1.014	1.018	1.019	0.507	0.281	1.0074	118,19	1.0030	253,65	0.9896	22,17
46	D7,1.1.2	691.90	1.009	1.024	1.034	1.035	0.430	0.332	1.0142	132,53	1.0047	279,32	0.9811	19,16
47	D7,1.1.3	679.30	1.010	1.025	1.035	1.036	0.425	0.336	1.0147	143,60	1.0048	284,25	0.9805	22,17
48	D8.1.1	38370.00	1.019	1.090	1.110	1.118	0.626	0.206	1.0409	295,2	1.0216	204,24	0.9375	30,66
49	D8.1.2	38170.00	1.028	1.111	1.142	1.151	0.563	0.245	1.0533	274,11	1.0246	179,22	0.9220	30,65
50	D8.2.1	28990.00	1.031	1.096	1.130	1.135	0.477	0.301	1.0507	287,4	1.0192	196,17	0.9301	31,72
51	D8.2.2	22300.00	1.029	1.102	1.135	1.142	0.520	0.273	1.0516	256,17	1.0216	162,15	0.9267	32,67
52	D8.3.1	30920.00	1.030	1.094	1.128	1.133	0.478	0.300	1.0500	250,6	1.0190	158,24	0.9310	354,65
53	D8.3.2	18720.00	1.039	1.087	1.129	1.132	0.345	0.392	1.0533	245,8	1.0138	152,19	0.9329	358,69

54	D8a.1.1	567.90	1.007	1.031	1.037	1.040	0.636	0.200	1.0144	31,8	1.0077	295,36	0.9779	132,53
55	D8a.1.2	572.30	1.007	1.035	1.043	1.046	0.640	0.198	1.0164	13,13	1.0089	275,30	0.9748	123,57
56	D8a.2.1	639.20	1.006	1.029	1.035	1.037	0.637	0.200	1.0135	221,0	1.0073	312,36	0.9792	130,54
57	D8a.2.2	585.80	1.007	1.029	1.036	1.039	0.585	0.232	1.0144	31,5	1.0070	298,34	0.9787	129,56
58	D8a.3.1	621.20	1.007	1.025	1.032	1.033	0.556	0.250	1.0127	39,5	1.0058	305,36	0.9815	136,53
59	D8a.3.2	531.00	1.004	1.028	1.032	1.035	0.733	0.143	1.0119	29,8	1.0077	295,29	0.9805	132,60
60	D9.1.1	846.70	1.016	1.019	1.035	1.035	0.066	0.609	1.0169	87,30	1.0008	190,20	0.9823	308,52
61	D9.1.2	789.70	1.004	1.028	1.032	1.035	0.743	0.137	1.0117	78,23	1.0077	179,24	0.9806	310,56
62	D9.2.1	754.80	1.009	1.027	1.036	1.038	0.510	0.279	1.0147	83,32	1.0060	195,31	0.9793	318,42
63	D9.2.2	745.40	1.009	1.026	1.036	1.037	0.471	0.300	1.0147	73,24	1.0055	184,39	0.9798	320,41
64	D9.3.1	687.90	1.012	1.023	1.036	1.036	0.290	0.431	1.0157	87,31	1.0034	192,23	0.9809	312,50
65	D9.3.2	796.10	1.007	1.027	1.034	1.036	0.580	0.234	1.0135	102,40	1.0065	207,18	0.9800	316,45
66	D9.3.3	772.40	1.007	1.027	1.034	1.036	0.587	0.231	1.0135	84,32	1.0066	193,27	0.9799	314,46
	N.B.													
Km, L, F, P, P', T, q, Kmax, Kmax-D/I, KInt, Kint-D/I, Kmin and Kmin-D/I are mentioned in appendix-A.														

Anisotropy of Magnetic Susceptibility measurement of pillow lavas														
No.	SampleNo.	Km	L	F	P	P'	T	q	Kmax	Kmax-D/I	KInt	KInt-D/I	Kmin	Kmin-D/I
1	p1.1.1	1811.00	1.015	1.012	1.027	1.027	-0.111	0.769	1.0139	117,35	0.9990	232,31	0.9870	352,39
2	p1.1.2	525.20	1.007	1.030	1.037	1.039	0.603	0.220	1.0145	220,35	1.0073	101,35	0.9782	341,36
3	p1.1.3	619.90	1.007	1.033	1.040	1.043	0.642	0.197	1.0154	225,32	1.0084	110,34	0.9763	346,40
4	p1.2.1	2392.00	1.019	1.006	1.025	1.026	-0.506	1.207	1.0145	111,36	0.9958	226,31	0.9897	345,39
5	p1.2.2	662.60	1.007	1.025	1.032	1.034	0.579	0.235	1.0127	131,51	1.0061	234,11	0.9812	333,36
6	p1.2.3	685.80	1.012	1.036	1.048	1.050	0.501	0.285	1.0193	215,37	1.0078	100,30	0.9729	342,39
7	p2.1.1	86290.00	1.008	1.048	1.056	1.061	0.717	0.152	1.0208	56,18	1.0130	152,30	0.9662	300,54
8	p2.1.2	82770.00	1.005	1.051	1.057	1.063	0.817	0.096	1.0199	43,8	1.0149	138,34	0.9653	301,55
9	p2.1.3	85110.00	1.015	1.047	1.063	1.065	0.487	0.294	1.0254	37,9	1.0098	133,32	0.9648	293,57
10	p2.2.1	84230.00	1.007	1.041	1.048	1.052	0.702	0.161	1.0179	43,12	1.0109	144,41	0.9711	300,47
11	p2.2.2	82120.00	1.013	1.040	1.053	1.055	0.486	0.295	1.0216	209,1	1.0084	118,39	0.9700	301,51
12	p3.1.1	23360.00	1.017	1.101	1.120	1.130	0.684	0.171	1.0432	78,5	1.0255	174,51	0.9313	344,39
13	p3.1.2	32450.00	1.014	1.058	1.073	1.078	0.592	0.227	1.0281	80,13	1.0138	182,43	0.9581	336,44
14	p3.1.3	34000.00	1.007	1.093	1.100	1.113	0.853	0.076	1.0338	131,42	1.0268	235,14	0.9394	339,44
15	p3.2.1	25330.00	1.019	1.110	1.131	1.142	0.677	0.176	1.0471	251,0	1.0274	161,45	0.9255	341,45
16	p3.2.2	31540.00	1.017	1.045	1.063	1.065	0.440	0.325	1.0258	70,3	1.0089	163,47	0.9653	337,43
17	p3.2.3	28560.00	1.003	1.072	1.075	1.085	0.914	0.044	1.0248	91,19	1.0218	197,38	0.9534	340,45
18	FE15.1.1	17900.00	1.003	1.019	1.022	1.023	0.742	0.138	1.0080	209,39	1.0053	84,36	0.9868	238,31
19	FE15.2.1	22340.00	1.003	1.035	1.038	1.042	0.835	0.086	1.0134	221,20	1.0103	103,52	0.9763	324,31
20	FE15.3.1	19130.00	1.004	1.021	1.025	1.027	0.710	0.156	1.0094	206,24	1.0058	95,38	0.9848	320,42
21	FE15.4.1	14060.00	1.006	1.007	1.013	1.013	0.045	0.627	1.0066	165,18	1.0002	264,26	0.9932	43,57
22	FE15.5.1	15330.00	1.004	1.013	1.017	1.017	0.544	0.257	1.0068	168,48	1.0030	66,11	0.9903	326,40
23	FE15.5.2	13260.00	1.003	1.001	1.004	1.004	-0.508	1.210	1.0022	189,54	0.9994	291,9	0.9985	27,35
24	L1.1.1	12520.00	1.037	1.008	1.045	1.049	-0.657	1.415	1.0272	155,27	0.9902	59,11	0.9826	308,60
25	L1.2.1	16770.00	1.017	1.028	1.046	1.046	0.224	0.481	1.0206	173,27	1.0033	69,24	0.9760	304,52

26	L1.3.1	910.80	1.009	1.020	1.028	1.029	0.390	0.360	1.0122	162,43	1.0036	57,15	0.9842	313,43
27	L1.3.2	191.90	1.008	1.016	1.024	1.025	0.319	0.410	1.0108	158,28	1.0026	55,23	0.9867	292,53
28	L3.2.1	10630.00	1.020	1.032	1.052	1.052	0.220	0.484	1.0234	42,9	1.0037	298,57	0.9728	138,32
29	L3.2.2	12060.00	1.021	1.024	1.045	1.045	0.052	0.621	1.0218	42,7	1.0008	301,55	0.9775	137,34
30	L3.3.1	7582.00	1.021	1.040	1.061	1.062	0.295	0.428	1.0267	42,15	1.0058	289,55	0.9675	141,31
31	L3.3.2	9422.00	1.020	1.025	1.046	1.046	0.085	0.593	1.0218	45,5	1.0013	309,54	0.9769	139,36
32	L3.4.1	4347.00	1.023	1.030	1.054	1.054	0.119	0.565	1.0252	47,10	1.0021	300,58	0.9727	143,30
33	L3.4.2	4427.00	1.022	1.031	1.054	1.054	0.147	0.542	1.0250	46,8	1.0026	303,58	0.9724	141,31
	N.B.													
	Km, L, F, P, P', T, q, Kmax, Kmax-D/I, KInt, Kint-D/I, Kmin and Kmin-D/I are mentioned in appendix-A.													

Anisotropy of Magnetic Susceptibility measurement of miscellaneous types														
No.	SampleNo.	Km	L	F	P	P'	T	q	Kmax	Kmax-D/I	Kint	Kint-D/I	Kmin	Kmin-D/I
1	ker1.1.1	311.80	1.003	1.003	1.006	1.006	0.073	0.603	1.0031	332,8	1.0002	65,18	0.9967	220,70
2	ker1.1.2	297.70	1.008	1.002	1.010	1.011	-0.621	1.362	1.0061	353,36	0.9979	247,20	0.9960	134,46
3	ker1.2.1	289.60	1.003	1.004	1.007	1.007	0.090	0.589	1.0036	9,45	1.0002	247,28	0.9962	138,32
4	ker1.2.2	283.30	1.002	1.004	1.006	1.006	0.432	0.331	1.0027	13,32	1.0009	264,26	0.9965	144,46
5	ker1.3.1	277.40	1.004	1.005	1.009	1.009	0.044	0.628	1.0043	291,1	1.0001	22,42	0.9956	199,48
6	ker1.3.2	271.70	1.009	1.003	1.012	1.012	-0.470	1.163	1.0069	306,9	0.9981	43,36	0.9950	204,52
7	ker2.1.1	183.60	1.002	1.005	1.007	1.007	0.466	0.308	1.0030	31,10	1.0011	128,36	0.9959	288,53
8	ker2.1.2	276.60	1.001	1.003	1.004	1.004	0.316	0.412	1.0018	121,54	1.0004	27,4	0.9978	294,36
9	ker2.2.1	254.10	1.001	1.002	1.003	1.003	0.402	0.351	1.0013	88,42	1.0004	199,21	0.9983	308,41
10	ker2.2.2	317.60	1.002	1.002	1.004	1.004	-0.183	0.840	1.0021	117,17	0.9998	215,22	0.9981	353,61
11	ker2.3.1	133.10	1.003	1.003	1.006	1.006	-0.102	0.760	1.0031	80,52	0.9998	178,6	0.9971	273,37
12	ker2.3.2	302.50	1.001	1.001	1.002	1.002	-0.305	0.969	1.0012	240,65	0.9998	76,24	0.9990	343,6
13	ker2.3.3	304.20	1.002	1.001	1.003	1.003	-0.317	0.981	1.0019	237,66	0.9996	106,16	0.9985	11,17
14	f1.1	10520.00	1.006	1.016	1.022	1.023	0.415	0.342	1.0095	278,17	1.0030	30,52	0.9875	176,33
15	f1.2	9516.00	1.009	1.014	1.023	1.023	0.235	0.473	1.0103	272,7	1.0017	13,59	0.9880	178,31
16	f2	8045.00	1.008	1.013	1.021	1.021	0.196	0.503	1.0097	268,14	1.0014	20,57	0.9889	169,29
17	g1.1.1	87880.00	1.021	1.051	1.073	1.076	0.400	0.353	1.0306	317,16	1.0094	141,74	0.9600	47,1
18	g1.1.2	54490.00	1.017	1.057	1.075	1.079	0.519	0.273	1.0298	314,57	1.0125	139,33	0.9577	48,2
19	g1.2.1	83440.00	1.029	1.048	1.078	1.079	0.219	0.485	1.0347	138,23	1.0055	305,67	0.9598	46,4
20	g1.2.2	70440.00	1.011	1.072	1.085	1.092	0.711	0.156	1.0307	137,24	1.0191	312,66	0.9502	46,2
21	g1.3.1	72010.00	1.043	1.036	1.080	1.081	-0.102	0.760	1.0400	138,2	0.9974	247,83	0.9626	48,7
22	g1.3.2	55250.00	1.022	1.067	1.090	1.094	0.491	0.291	1.0359	137,17	1.0141	335,72	0.9500	228,5
23	al1	8283.00	1.011	1.012	1.023	1.023	0.023	0.646	1.0113	85,11	1.0002	351,20	0.9885	202,66
24	al2.1	9240.00	1.023	1.008	1.031	1.032	-0.484	1.180	1.0177	61,21	0.9951	323,21	0.9872	192,60
25	al2.2	7740.00	1.023	1.011	1.034	1.035	-0.371	1.043	1.0190	53,21	0.9958	314,23	0.9852	181,59

Appendix-C

Sample list for Natural Remanent Magnetization measurement

No.	Sample No.	Type of rock	Orientation	Remarks
1	K1	lapillituff	s0-290, 15	
2	BH1	lapillituff	s0-135, 51	
3	BH2	lava (mandel)	s-080, 72	
4	L1	lava pillow	135, 35	
5	L2	lapillituff	s-180, 60	
6	L3	lava pillow	s-052, 67	
7	WF1	lapillituff	130, 43	
8	WF2	ash tuff	155, 25	
9	WF3	lapillituff	130, 53	
10	WF4	pillow lava	130, 51	
11	WF4A	lapillituff	135, 46	
12	WF5	lapillituff	135, 41	
13	WF6	lapillituff	130, 51	
14	WF7	lapillituff with crystal	160, 51	
15	WF8	lava	130, 31	
16	WF9	lapillituff	s-160, 60	
17	WF10	lapillituff (laminated)	125, 36	
18	WF11	lapillituff	s-140, 68	
19	WF12	lava	s-160, 54	
20	WF13	lava	s-180, 55	
21	FG1	lapillituff	s-038, 35	
22	FG2	ash tuff	130, 45	
23	FG3	lava	130, 45	
24	FG4	lapillituff	120, 38	
25	FG5	dyke	s-230, 47	
26	FG6	dyke	sj-170, 80	
27	FG7	lapillituff with epiclastics	120, 42	
28	FG8	lapillituff with crystal	125, 42	
29	FG9	lava (porphyry)	120, 34	
30	FG10	lapillituff with epiclastics	s-250, 48	
31	FG11	lapillituff with crystal	120, 54	
32	FG12	lava (porphyry)	s-180, 90	
33	FG13	lapillituff (epiclast. & cryst.)	142, 40	
34	FG14	lava (porphyry)	s-240, 87	
35	FG15	lava	s-165, 70	
36	FG16	lapillituff with epiclastics	150, 34	
37	FG17	lava	s-200, 76	
38	FG18	lava	s-200, 76	
39	FG19	lapillituff with epiclastics	s-130, 35	
40	FG20	dyke	s-270, 34	
41	FG21	dyke	s-190, 80	
42	FEA1	lava	s-150, 55	

43	FEA11	lava	150, 55
44	FE1	fault plane (lava)	190, 73
45	FE2	l.st	150, 42
46	FE3	lava (mandel)	s-150, 35
47	FEA4	lava (granulated)	135, 56
48	FE4	ash tuff	242, 62
49	FE5	lapillituff	140, 42
50	FE6	lava epiclastics	s-205, 72
51	FE7	lapillituff	142, 46
52	FE8	lapillituff like pillow	145, 42
53	FE9	lava	s-130, 53
54	FE10	lava	s-070, 30
55	FE11	ash tuff	s0-100, 54
56	FE12	lapillituff (ash)	s-180, 40
57	FE13	lapillituff (ash)	s0-050, 25
58	FE14	lapillituff	140, 41
59	FE15	lava pillow	s-235, 60
60	LF1	lapillituff	135, 55
61	LF2	lava	s-030, 10
62	LF3	lava	155, 47
63	LF4	lava	s-180, 43
64	LF5	lapillituff	130, 45
65	LF6	lava	135, 42
66	LF7	lapillituff	135, 42
67	S1	lapillituff	160, 46

N.B.

s = surface of exposure

sj = joint surface

s0 = bedding

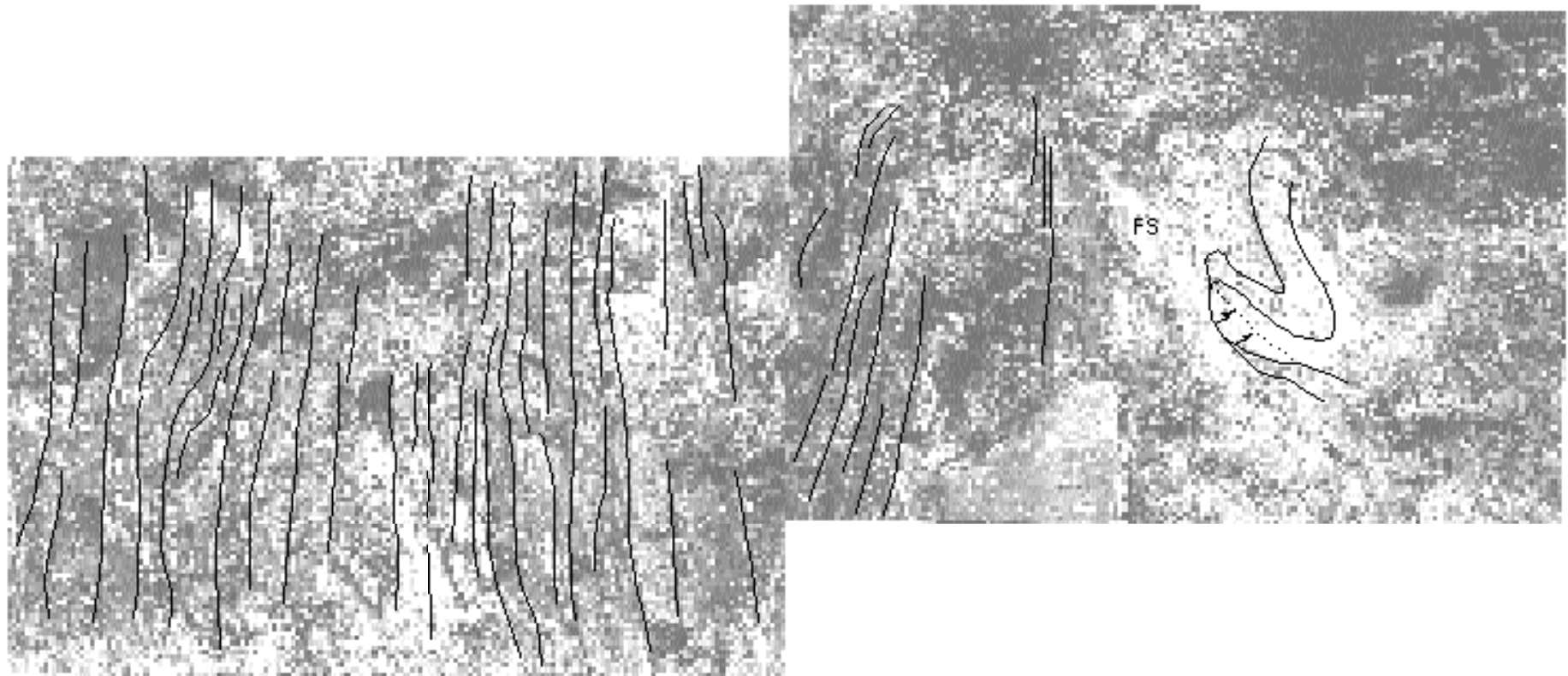
Magnetic intensity (mA/m) in Thermal Demagnetization (Natural Remanent Magnetization measurement)												
Sample No.	0°C	100°C	200°C	250°C	300°C	350°C	400°C	450°C	500°C	550°C	575°C	600°C
K1	7.01	9.54	8.08	16.58	27.44	7.62	2.58	2.26	3.99	8.99	2.67	1.06
BH1	0.77	1.22	0.80	0.46	0.29	0.24	0.23	0.13	0.08	0.59	0.40	0.19
BH2	739.06	572.29	340.74	184.96	154.87	194.51	177.57	183.02	170.37	216.79	164.62	9.11
L1	19.10	14.13	11.75	13.15	18.64	7.24	8.61	8.29	9.05	4.79	5.41	5.54
L2	37.23	40.00	24.62	25.29	30.90	10.82	32.10	2.84	9.98	6.30	9.09	3.23
L3	56.63	47.20	10.86	30.12	3.17	11.28	6.94	5.42	1.79	7.57	7.89	1.79
WF1	0.56	0.77	0.84	0.50	0.03	0.09	0.05	0.12	0.40	2.45	2.60	7.76
WF2	0.37	0.90	1.03	0.45	0.16	0.08	0.07	0.09	0.22	0.99	1.69	11.81
WF3	0.50	1.14	0.89	0.65	0.07	0.01	0.07	0.21	0.30	0.81	0.71	4.61
WF4	2.29	1.91	1.01	0.43	0.61	0.10	0.13	0.82	1.03	1.69	1.32	14.23
WF4A	0.40	0.53	1.63	0.68	0.03	0.02	0.17	0.36	1.75	7.37	10.60	89.67
WF5	1.43	1.97	0.79	0.52	0.21	0.13	0.41	15.30	106.22	182.90	203.91	399.68
WF6	66.49	55.56	24.69	23.74	21.53	19.54	30.17	17.90	7.47	35.42	7.08	6.71
WF7	0.44	1.33	0.62	0.49	0.06	0.03	0.12	0.13	2.45	2.00	1.56	11.07
WF8	4.47	4.59	3.17	4.86	3.38	3.95	3.27	2.71	2.36	4.75	6.87	4.37
WF9	2.07	3.45	0.38	0.34	0.34	0.15	0.30	0.53	0.55	0.82	1.26	4.41
WF10	0.82	0.70	0.90	0.14	0.10	0.06	0.10	0.26	1.10	1.85	4.60	8.81
Wf11	1.45	1.29	1.44	0.66	0.32	0.20	0.12	0.55	0.81	1.70	4.52	8.81
WF12	109.39	98.67	54.93	18.21	21.12	15.00	34.88	11.41	7.34	61.62	7.13	7.05
WF13	1.49	2.61	1.08	1.67	1.65	1.19	0.83	0.58	0.60	5.43	7.27	9.44
FG1	0.47	2.54	2.30	1.92	0.81	0.84	0.40	0.27	0.59	1.05	0.70	0.50
FG2	0.35	0.90	0.25	0.64	0.07	0.03	0.05	0.07	0.49	1.59	1.80	1.27
FG3	0.08	0.91	0.31	0.81	0.06	0.02	0.02	0.16	3.15	7.08	3.48	4.29
FG4	0.14	0.72	0.24	0.84	0.66	0.02	0.03	0.12	3.37	5.49	2.80	2.34
FG5	0.52	0.84	1.96	1.95	19.21	1.42	1.30	1.16	1.12	1.28	1.34	0.45
FG6	0.47	0.72	2.01	4.06	38.52	1.81	1.72	0.91	1.59	1.58	0.61	0.60
FG7	29.29	82.81	88.71	90.03	70.22	73.28	56.93	13.20	11.09	36.25	13.27	7.60
FG8	0.09	0.24	0.33	0.65	0.12	0.04	0.06	0.03	0.51	2.44	3.36	1.91

FG9	0.19	0.41	0.11	0.24	0.05	0.07	0.03	0.08	1.33	4.77	9.95	13.99
FG10	1.20	2.54	2.00	5.85	2.01	2.41	2.51	1.36	1.82	3.37	10.91	14.89
FG11	1.19	0.85	0.35	0.11	0.02	0.06	0.08	0.13	0.86	4.09	7.60	9.36
FG12	1.72	1.89	0.47	3.40	1.82	1.37	1.17	0.82	1.03	0.67	2.69	1.57
FG13	1.85	0.70	1.04	0.67	0.17	0.20	0.19	0.10	0.14	5.66	10.53	10.24
FG14	0.63	0.96	0.62	0.98	0.51	0.29	0.33	0.33	0.34	7.43	5.53	2.35
FG15	1.41	0.14	1.64	0.17	0.07	0.05	0.07	0.11	1.97	10.68	4.24	11.52
FG16	1.61	1.82	0.61	0.29	0.14	0.12	0.16	0.06	1.60	7.05	7.67	3.90
FG17	0.92	1.25	0.99	0.44	0.39	0.21	0.30	0.37	2.18	9.39	5.19	7.24
FG18	3.08	1.45	2.16	0.72	0.53	0.51	0.51	0.24	0.30	1.00	1.74	0.44
FG19	14.26	10.05	3.51	6.83	4.70	3.42	2.78	2.61	2.35	6.05	12.00	5.19
FG20	1.03	0.40	0.73	0.15	0.05	0.07	0.36	0.16	0.78	1.24	1.02	0.53
FG21	1.30	4.42	1.72	1.04	0.97	1.00	1.23	1.49	3.12	5.77	11.68	7.98
FEA1	493.14	408.99	189.59	101.52	240.10	99.87	244.70	273.78	254.50	288.02	344.07	152.57
FEA11	188.34	162.57	60.09	34.12	122.76	26.25	94.63	149.30	54.20	31.36	115.05	6.32
FE1	1.44	0.88	0.38	0.77	0.30	0.25	0.16	0.11	0.12	1.10	5.33	1.78
FE2	2.35	0.80	0.78	0.62	0.75	0.24	1.06	1.87	1.74	2.62	4.43	2.27
FE3	1630.38	1558.70	1180.12	938.32	854.63	653.68	531.09	317.30	197.33	99.54	133.74	58.12
FE4	112.20	94.63	52.08	238.87	19.71	28.34	2.04	8.68	6.79	53.22	20.17	8.75
FEA4	286.43	250.08	94.94	79.54	83.91	50.09	104.71	155.20	148.54	102.64	156.72	34.79
FE5	23.35	18.44	5.99	6.42	24.88	4.33	2.06	6.13	6.20	3.77	7.21	8.88
FE6	105.59	103.92	90.74	79.56	2.66	37.00	51.65	12.49	14.95	48.98	6.35	11.96
FE7	0.49	0.36	0.51	0.49	0.06	0.04	0.13	0.17	0.44	0.37	1.83	13.94
FE8	257.66	202.46	138.55	135.19	115.40	98.68	73.41	123.94	105.27	73.16	18.90	13.07
FE9	2.58	1.95	1.52	3.41	4.66	2.58	2.08	2.91	2.94	1.78	7.80	4.91
FE10	0.51	0.35	1.42	0.66	0.37	0.36	0.36	0.18	0.31	1.02	5.46	4.55
FE12	1.47	0.82	0.68	1.02	0.50	0.19	0.28	0.50	1.23	5.67	1.30	11.41
FE13	0.62	0.55	0.30	0.07	0.15	0.09	0.03	0.08	0.12	0.23	12.84	10.14
FE14	1.87	1.44	0.72	0.87	0.33	0.35	0.21	0.42	0.65	1.06	11.82	10.57
FE15	747.15	717.51	237.69	208.86	182.16	77.59	66.42	53.82	44.34	65.41	44.54	9.92
LF1	0.85	0.33	0.20	0.16	0.08	0.04	0.24	0.13	0.30	0.11	0.83	2.95
LF2	0.05	0.88	1.28	0.33	0.06	0.06	0.14	0.17	0.83	1.20	8.75	6.76

PLATES

NW

SE



Sketch of plate 1. (FS = fault surface)

NW

SE

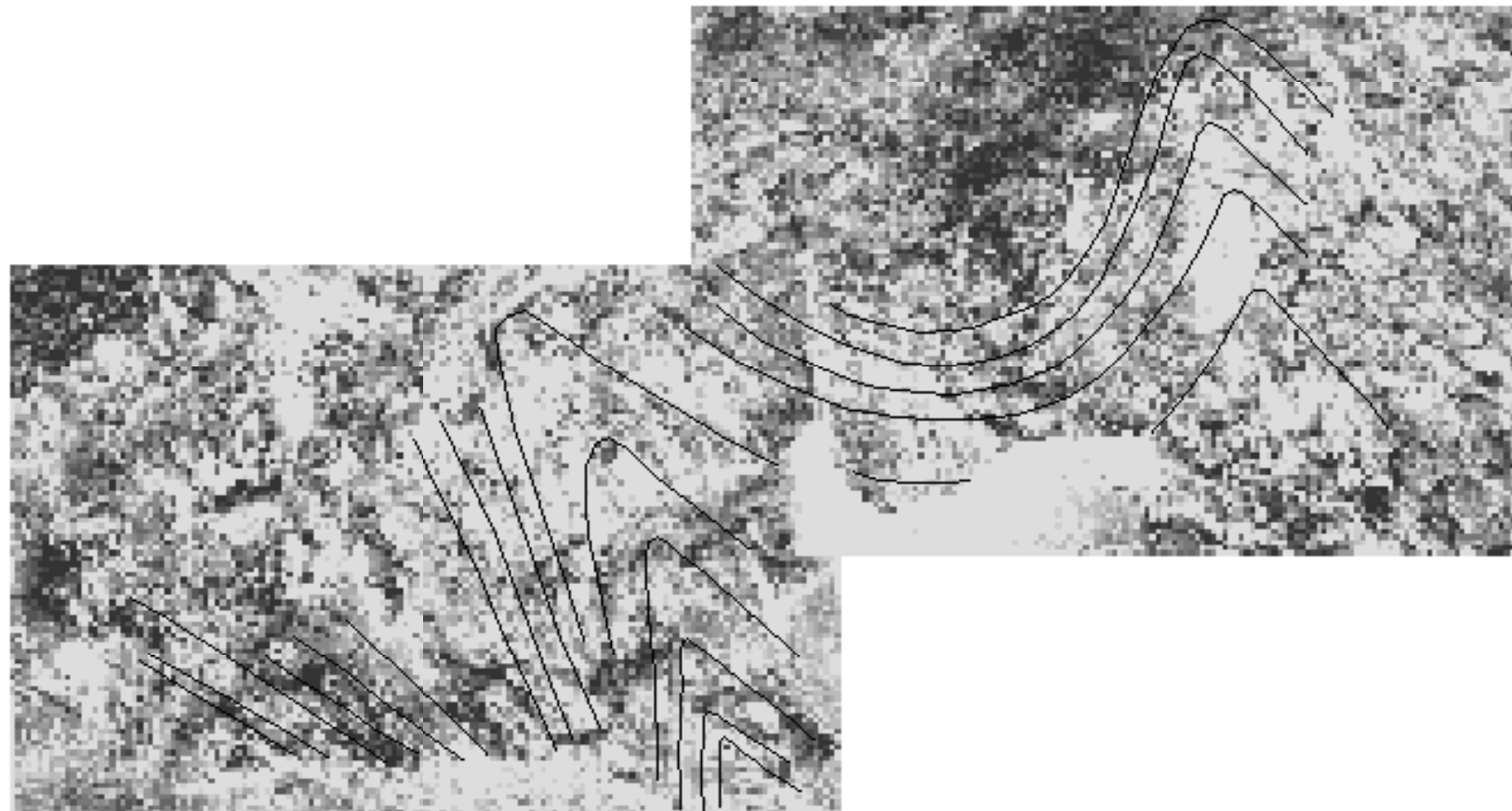


0 2 m

Plate 1. Fold development in the Kirschhofen syncline with vertical bedding in *Adorf-Plattenkalk* at the Zeppelifels, south-eastern part of the syncline.

NW

SE



Sketch of plate 2.

NW

SE

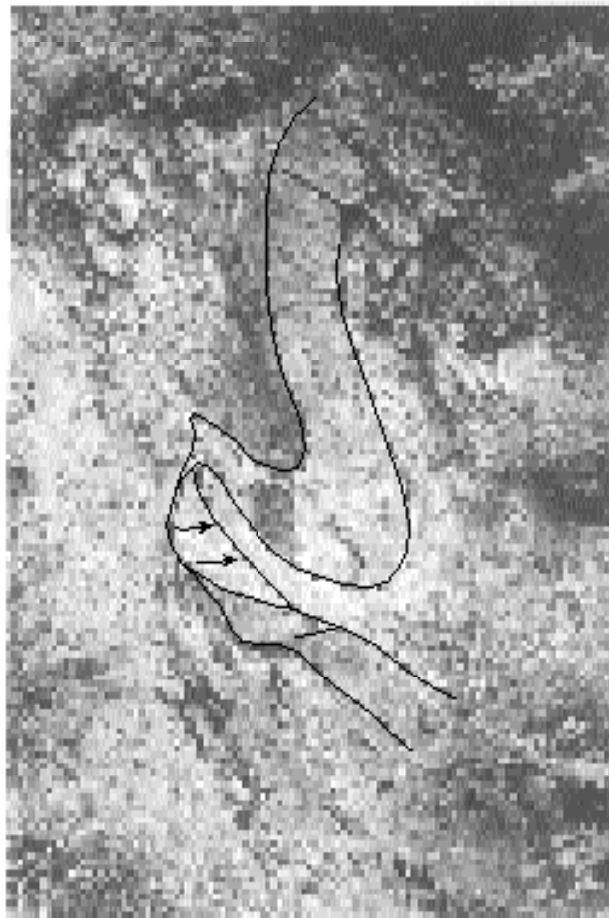


Plate 2. Fold development in the Kirschhofen syncline, continuation of Plate 1: disharmonic folding from SE to NW direction at the Zeppelinfels.

A.



B.



Sketch of plate 3.

A.

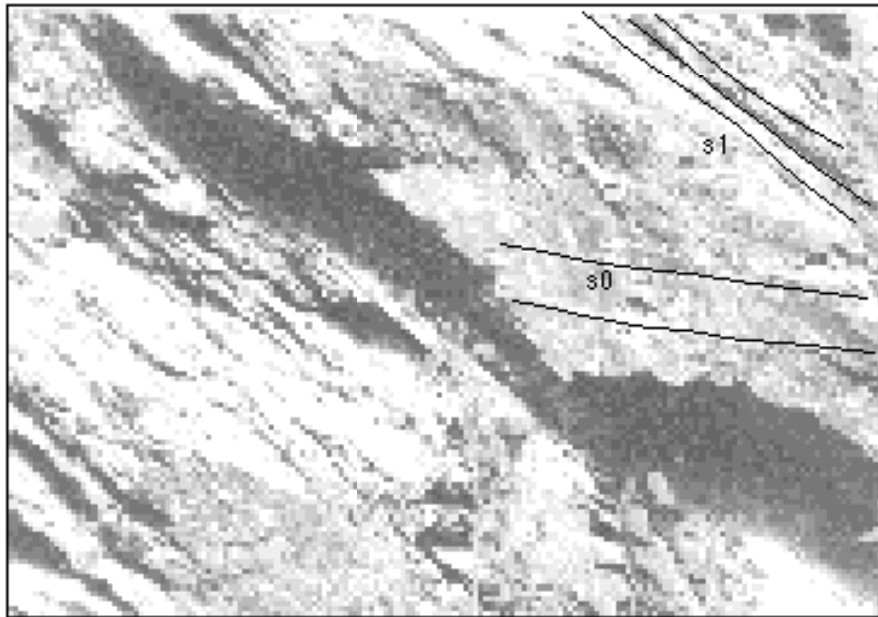


B.



Plate 3. The Kirschhofen syncline, continuation of Plate 2:
A: Upright fold (SW plunging) in *Kalkknotenschiefer* in the disharmonic fold at the road-cut of the Zeppelinfels. (arrow indicates upright fold axis)
B: Twisted fold in sandstone layer intercalating in slate at the road-cut at the Zeppelinfels.
(Both exposures are looking NE)

A



B



Sketch of plate 4. (P = Pillowlava)

A.



B.

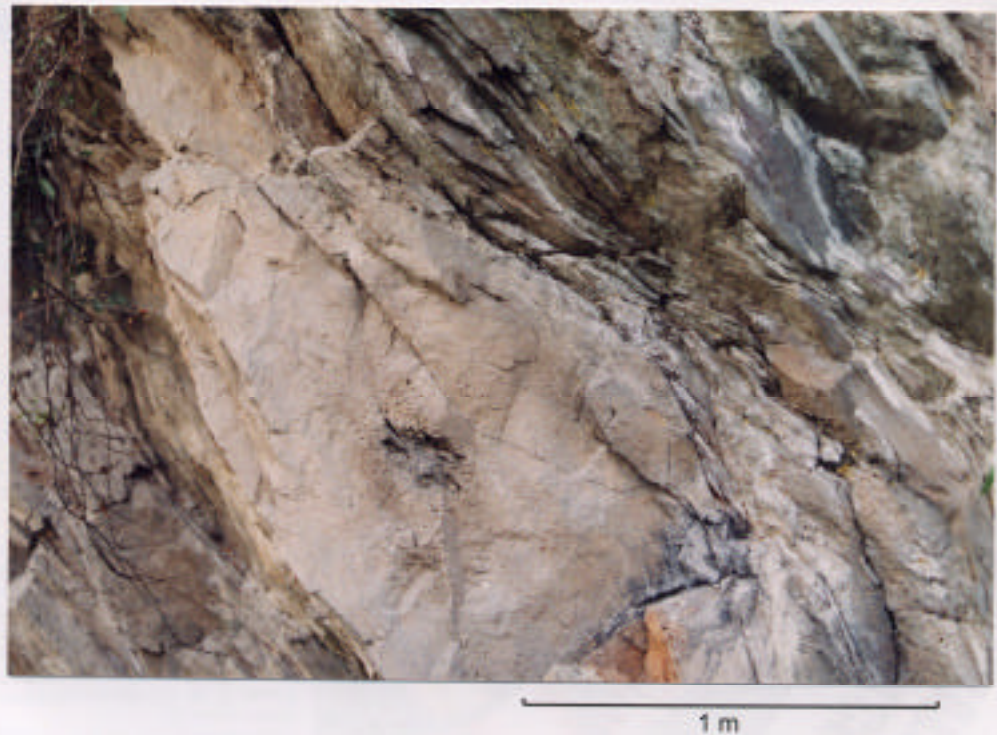


Plate 4. A: Relationship of bedding and s1-cleavage in lapillituff (*Schalstein*) at the road-cut between Guntersau and Freienfels (looking NE).
B: Pillow lava and s1-cleavage relationship at the road-cut between Freienfels and Weinbach (looking NE).



Plate 5. Undeformed pillow lava and its typical joint development at the road-cut near the Laimbach junction, Weital road (looking NE).

A.



B.



Sketch of plate 6.

A.



B.



Plate 6. s₂-cleavage development (kink folding) in lapillituff (*Schalstein*) near Freienfels (looking NE), (arrow indicates s₂-cleavage), (A) and in *Kalkknotenschiefer* at the road-cut, opposite of Ahausen in the Ahausen syncline (looking SW), (B).

A.

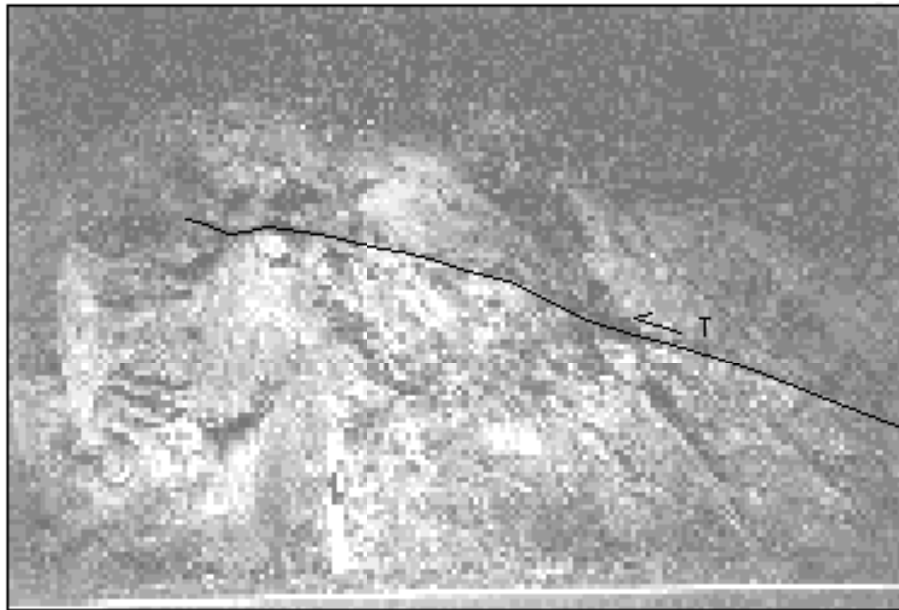


B.

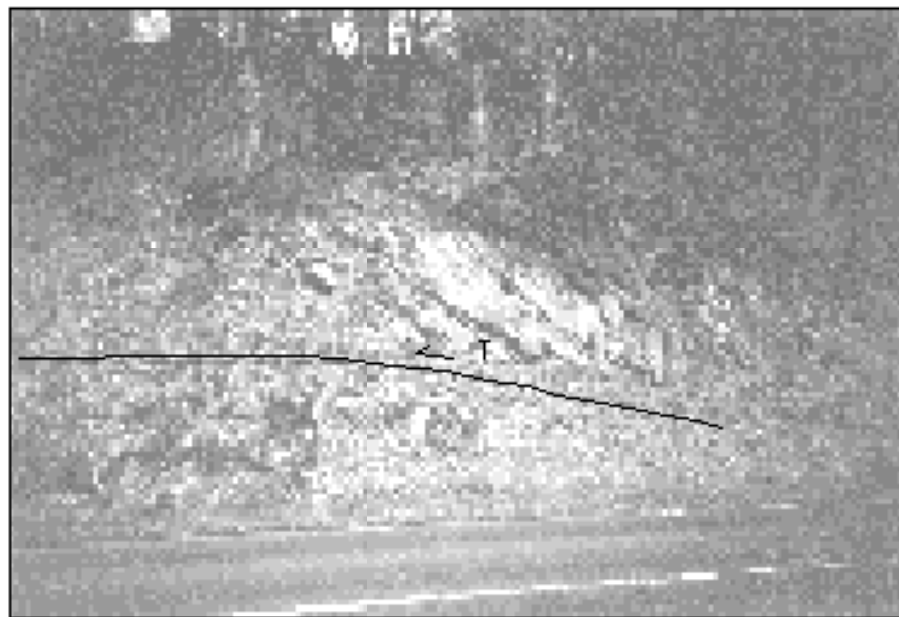


Plate 7. A: Non-sigmoidal right-stepped shear fracture in sheet flow lava near Freienfels (looking NE).
B: Sigmoidal tension gashes in conjugate alignments in sheet flow lava between Freienfels and Weinbach (looking SE).
(Both exposures in the Freienfels-Ernsthausen sub-area).

A.



B.



Sketch of plate 8. (T = overthrust plane)

A.



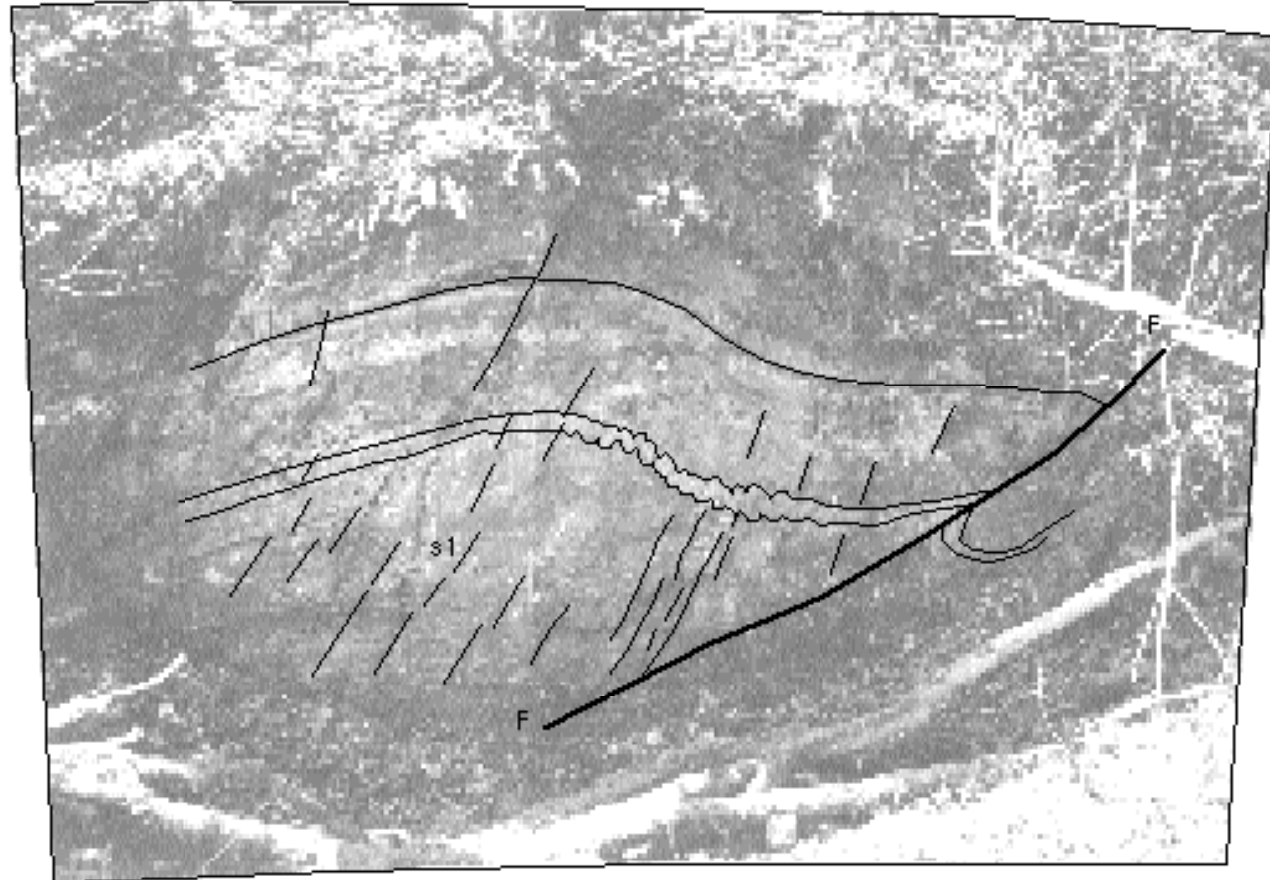
B.



Plate 8. A: Overthrust fault at Guntersau: Lapillituff (*Schalstein*) thrust over Adorf-Plattenkalk at the road-cut section (looking NE).
B: Overthrust fault at Freienfels: Lapillituff (*Schalstein*) thrust over reef limestone at the road-cut section (looking NE).
Both exposures indicate thrust front (deformation toe) of a local accretionary wedge with respect to the Guntersau-Freienfels half-graben basin (A) and the Freienfels-Ernsthausen half-graben basin (B).

SE

NW



Sketch of plate 9. (FF = Fault)

SE

NW



1 m

Plate 9. Thrust related folding with axial cleavage development at the old railroad-cut between Essershausen and Ernsthausen. Showing a small scale in-sequence thrust model with backlimb and forelimb thrust development.
General lithology: lapillituff and ashtuff alternations with intercalated calcareous laminations (after JÄGER 1996).



1 m



4 cm

Plate 10. *Kalkknoten* exposure in Adorf-Plattenkalk at the Zeppelifels in the Kirschhofen syncline (looking NE).

A.



1 m

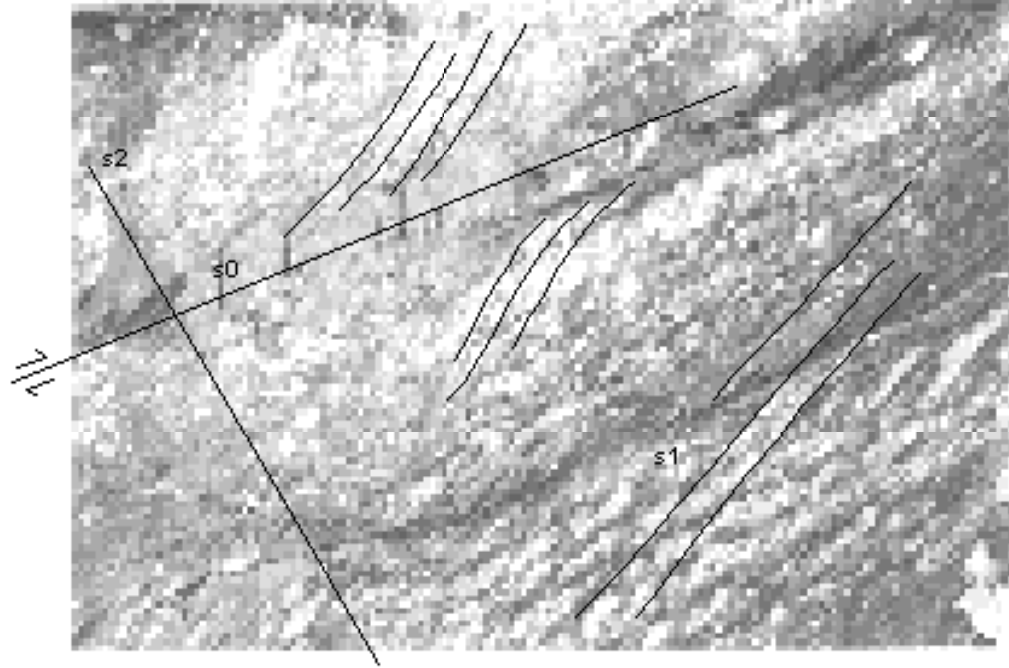
B.



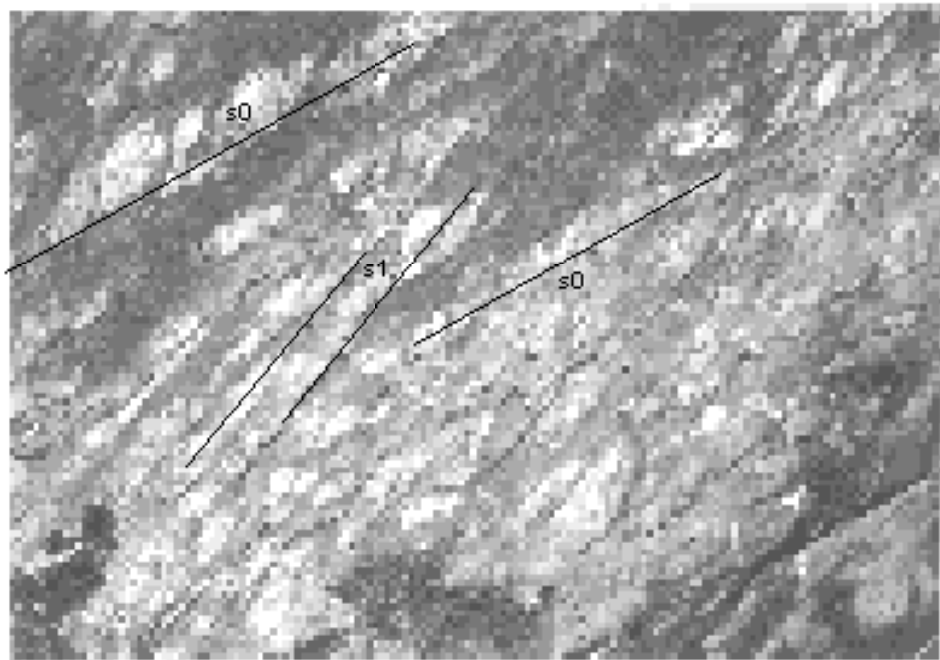
5 cm

Plate 11. Bedding and s1-cleavage development in *Kalkknotenschiefer* (A) and *Kalkknoten* lying in the s1-cleavage (B) at the road-cut, opposite of Ahausen in the Ahausen syncline (looking SW).

A.



B.



Sketch of plate 12.

A.



30 cm

B.



5 cm

- Plate 12. A. Progressive deformation as revealed in the *Kalkknotenschiefer* at the road-cut, opposite of Ahausen in the Ahausen syncline (looking SW).
1. Strain markers of *Kalkknoten* lying in the s1-cleavage.
 2. Shear movement (layer parallel shear) parallel to the bedding (s0) during the s1-cleavage formation and the s1-cleavage as a result of progressive movement with internal deformation by flexural flow.
 3. Kink folding: s2-cleavage superimposed on the s1-cleavage (s1-cleavage folding).
 4. Tension fractures perpendicular to bedding.
- B. Detail of *Kalkknotenschiefer* showing *Kalkknoten*: rotation by simple shear and preferred orientation by progressive simple shear movement (Looking SW).



Plate 13. Individual *Kalkknoten* for strain analysis of *Kalkknotenschiefer* from the Ahausen syncline.

A.



0 1 cm

B.



Plate 14. A: Lapillus as a strain marker embedded in lapillituff at the Guntersau-Freienfels sub-area.
B: Individual lapilli for strain analysis of the lapillituff at the Freienfels-Ernsthausen sub-area.



Plate 15. Metabasaltic conglomerate (JÄGER 1993): epiclastic lapillituff at the road-cut near Edelsberg junction in the Frelenfels-Ernsthausen sub-area (looking NE).

A.



B.



Sketch of plate 16. (d= dyke)

A.

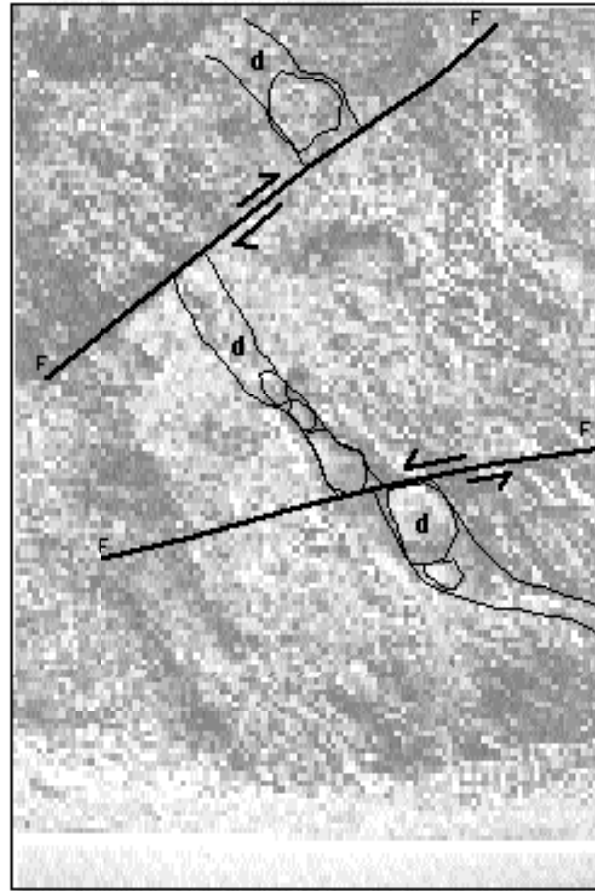


B.

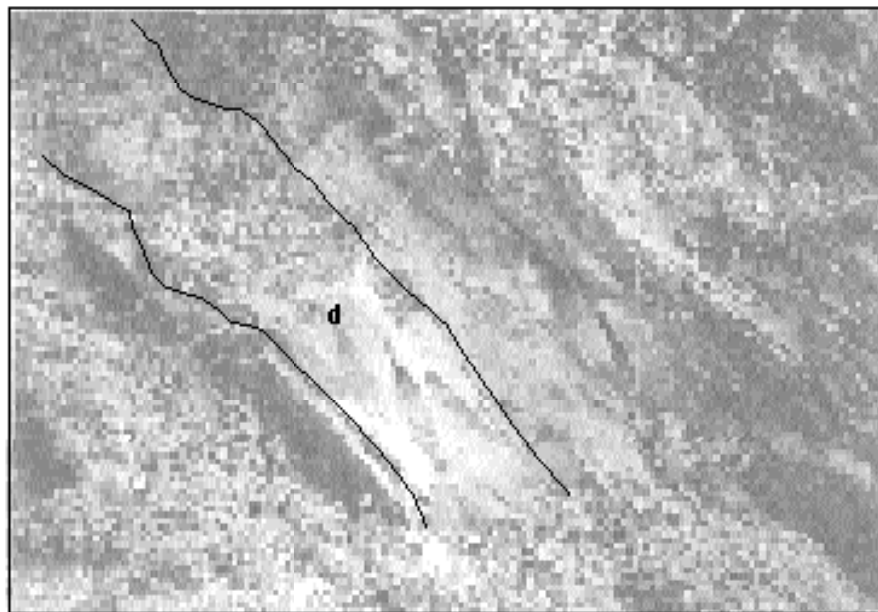


Plate 16. Metabasaltic dyke exposures at the road-cut between Guntersau and Freienfels (A) dyke D5 and (B) dyke D6 in Fig. 7-37. Both exposures are looking NE.

A.



B.



Sketch of plate 17. (d = dyke, FF = fault)

A.



B.



Plate 17. Metabasaltic dyke exposures at the road-cut between Guntersau and Freienfels (A) dyke D8a and (B) dyke D7 in Fig. 7-37. Both exposures are looking NE.

CIRRICULUM VITAE

CIRRICULUM VITAE

PERSONAL DATA

Name: Aung Moe
Date of Birth: 3 November 1954
Place of Birth: Taungdwingyi, Myanmar (Burma)
Sex: male
Nationality: Myanmar
Language: Myanmar (Mother tongue)
English (write/read/speak)
German (write/read/speak)

ACADEMIC CAREER

1971 to 1975 B.Sc (Geology), Yangon University, Myanmar.

Report: Geology of Paungdaw-Ngetmi area, East of Pyawbwe Township, Burma.

1976 to 1980 M.Sc (Geology) with Credit, Yangon University, Myanmar

Thesis: Petrology and structures of the rocks of Mount Popa area, Kyaukpadaung Township, Burma.

1985 to 1986 Lab-techniques study in Heidelberg University, Germany.

1995 to 2000 D.Sc (Structural Geology), Heidelberg University, Germany.

Thesis: Structural development of a volcanic sequence of the Lahn area during the Variscan orogeny in the Rhenohercynian belt (Germany).

PROFESSIONAL CAREER

10/95 to present D.Sc study in Heidelberg University, Germany

08/92 to 10/95 Geological Engineer, Soil & Foundation (Pte) Ltd, Singapore

01/92 to 08/92 Consultant Geologist, Sittoung Geoservices & Consultancy Ltd, Myanmar

05/89 to 01/92 Assistant lecturer, Geology Dept., Yangon University, Myanmar

09/80 to 05/89 Demonstrator, Geology Dept., Yangon University, Myanmar

01/79 to 09/80 Research Assistant, Applied Geology Dept., Yangon University, Myanmar

RESEARCH EXPERIENCE

Conferences

1. Moe, A. (1997) Neotectonic movement and Block rotation of Rheinische Schiefergebirge, Germany. (TSK-7 = Tectonics, Structures and Kristallin, Freiberg - Germany).
2. Moe, A. (1998) Deformation and Rf/Ø diagrams. (DGG150 = Deutschen Geologischen Gesellschaft, Berlin - Germany).
3. Moe, A. (1998) Variscan folding and its tectonic mechanism in Rheinische Schiefergebirge, Germany. (POCEEL = Paleozoic Orogenesis and Crustal evolution of the European Lithosphere, Prague - Czech).
4. Moe, A. (1999) Transtensional tectonics in Rhenohercynian zone during the Variscan orogeny: implications of folding and its strain characters. (EGS99 = European Geological Society, The Hague – The Netherlands)
5. Moe, A. and Flick, H. (1999) Observation of Thrust systems and its related Folding in inversion tectonics: a small scale 2-D model from Rhenohercynian. (TT99 = Thrust Tectonics 99, London – England)
6. Moe, A. (1999) Burma Plate and Sinoburmalaya (Shan) Plate collision style on the evidence of regional folded structure during the Carboniferous time. (Active subduction and collision in southeast Asia, Montpellier –France)
7. Moe, A. (1999) Plastic deformation and strain from lime nodules (Kalkknoten), Variscan of central Europe. (DMR1 = Deformation Mechanisms Rheology Microstructures, Neustadt – Germany)
8. Moe, A. (1999) Shear strain preserved in twinned amygdale calcite, Lahn syncline, Rheinische Schiefergebirge, Germany. (International Conference on Textures and Physical properties of rocks, Göttingen - Germany)

Publications

1. Moe, A. (1998) Neotectonic movements in the Rheinisches Schiefergebirge (Germany) and possible block rotation. *Zbl. Geol. Paläont.* **1998 Teil I**, H 1/2, 81-92.
2. Moe, A. (1999) Burma Plate and Sinoburmalaya (Shan) Plate collision style on the evidence of regional folded structure during the Carboniferous time. *Tectonophysics* (submitted)
3. Moe, A. (1999) Plastic deformation and strain from lime nodules (Kalkknoten), Variscan of central Europe. *Geol. Rundsch.* (submitted)
4. Moe, A. (1999) Variscan folding and its tectonic mechanism in the Rheinisches Schiefergebirge, Germany. *Tectonics* (submitted)
5. Moe, A. (1999) Transtensional tectonics in the Rhenohercynian zone during the Variscan orogeny: implications of folding and its strain characters. *Tectonophysics* (submitted)

Preparations

1. Moe, A. and Seeling, J., Deformation on some Cretaceous bivalves from the Sergipe basin, north-eastern Brazil: estimation of compactional strain. (2000)
2. Moe, A., Final closure of northern Burma and its Plate movement during the Miocene time: timing in Miocene tectonic movements. (2000)
3. Moe, A., Theoretical strain deformation in strain-ratio diagram (long-short axes ratio): implication of power-law flow. (2000)